Saving Oseberg
January 2013–September 2016

Technical Report

Part 1: Analyses and characterization of alum-treated wood without other additives

---

SAVING OSEBERG

UiO : Kulturhistorisk museum

Saving Oseberg January 2013–September 2016 Technical Report Part 1: Analyses and characterization of alum-treated wood without other additives

Jeannette Jacqueline Łucejko [1,2], Diego Tamburini[1,2] , Susan Braovac[3], Caitlin M. A. McQueen[3], Francesca Gambineri[4]

April 2017
University of Oslo – Museum of Cultural History
Project 000208 Saving Oseberg
Saksnummer 2017/6982

[1] *Department of Chemistry and Industrial Chemistry (DCCI), University of Pisa, via Moruzzi 13, I-56124 Pisa, Italy*
[2] *Institute for the Conservation and Promotion of Cultural Heritage (ICVBC), National Research Council, via Madonna del Piano 10, I- 50019, Sesto Fiorentino, Florence, Italy*
[3] *Department of Collection Management, Museum of Cultural History (KHM), University of Oslo, Postbox 6762 St. Olavs plass, 0130 Oslo, Norway*

[4] *Archa Laboratories Srl, via Tegulaia 10/A, I-56121 Pisa, Italy*

Table of Contents

1. Introduction

A major aim of SO-I was to increase our understanding of chemical, physical and morphological properties of alum-treated wood from the Oseberg find. This technical report summarizes the main experimental work undertaken during SO-I for alum-treated wood without addition of linseed oil. Alum salt – wood – linseed oil systems with and without metal additions are covered in *Technical Report Part 2: Analyses of samples from composite objects*.
Alum-treated wood proved to be challenging to investigate morphologically due to its extremely brittle nature. For example, wood identification could not be carried out on most samples, beyond identifying the type of pore-pattern observable under low magnification (diffuse porous, ring porous). Thus common techniques for investigating cell morphology, such as scanning electron microscopy (SEM) and light microscopy, were complemented by advanced imaging methods such as tomographic X-ray microscopy and neutron tomography.
Generally the chemical analyses investigated three avenues of inquiry:

- The extent to which the alum-treatment has contributed to increased deterioration after conservation in the early 1900s;
- The variability of condition observed among alum-treated woods from different objects;
- The variability in alum-rich and alum-poor zones.

The research reported here includes chemical analyses of both organic (for ex. wood) and inorganic compounds (for ex. alum) found in the wood using established methods in wood analysis, which require little sample material (microgram to milligram range): infrared analyses (IR), analytical pyrolysis (Py-GC/MS), X-ray diffraction (XRD), inductively coupled plasma optical emission spectroscopy (ICP-OES), energy dispersive spectroscopy (EDS), etc.
Challenges involved in elucidating the chemical state of preservation of the wood fraction were mainly related to the presence of appreciable amounts of inorganic compounds (mainly alum salt) in the samples, which interfered with some types of analysis. For instance, before infrared spectra could be interpreted, alum had to be removed (either through rinsing or by digital subtraction). The effect of high amounts of alum salt was also investigated in Py-GC/MS to ensure that they did not cause artefacts during the pyrolysis step. Using complementary analytical techniques (such as both infrared analyses and Py-GC/MS) was therefore important to clarify whether trends seen in one analysis were also observed in the other.
An important sub-topic of SO-I investigated the chemical differences on large alum-treated fragments from Oseberg which had alum rich (surface) and alum poor (core) zones. This was undertaken in a related but independent project, ArCo[1]. Here the physical and chemical effects of extreme RH cycling at 30°C ('artificial aging') were also investigated.

Results for morphological and chemical analyses of sound wood and untreated archaeological woods are presented in Sections 3.1 and 3.2, respectively. Section 3.3 reports the analysis results of Oseberg samples grouped by object number. Wood-water interactions were studied on a range of samples and are summarized in Section 3.4. Model Studies – Section 3.5 – presents the alum-treatment as it was applied to archaeological and fresh wood (aspen and birch) to better understand it. In these model experiments, samples were also impregnated with sulphuric acid solutions at pH 0, 1, 2, 3. Aging studies were undertaken on the birch samples. Section 3.6 presents preliminary results from investigations relating the visual state of preservation from a larger sample set of Oseberg wood to potentially relevant indicators (pH, colour, iron content and extent of wood oxidation as determined by infrared analyses).

[1] The Aging Study of Treated Composite Archaeological Waterlogged Artifacts, ArCo, was an EU-sponsored joint project initiative, which ran from 2014-2016 to investigate unstable salts in wood. The project involved laboratories in four countries: Norway, France, Italy and Denmark.

2. Materials and Methods

2.1 Sample Overview

The selection of Oseberg samples was based on a combination of what was available and which larger fragments could be sacrificed. Alum-treated Oseberg wood fragments that represented different physical states of preservation were chosen. Two samples of untreated woods from the Oseberg find served as references to compare with those which were alum-treated. One sample (oak from the Oseberg ship) represented woods which were in good condition upon excavation. The other (Oseberg Maple, animal head post) represented woods in poor condition upon excavation but which had not been treated with alum (i.e. represents an approximation of the alum-treated woods' condition today had they not been treated with alum). Other references included fresh woods, untreated archaeological woods which had been recently excavated, as well as wood treated with alum in the laboratory.

Table 1 presents samples from Oseberg (untreated and alum-treated), and reference samples (fresh and untreated archaeological) (Sections 3.1, 3.2, 3.3, 3.4).
Table 2 presents samples used in model experiments investigating the alum treatment in greater detail in the laboratory on aspen wood (fresh and archaeological) (Section 3.5.1).
Table 3 presents samples used in model experiments where alum-treated birch (fresh and archaeological) underwent aging (Section 3.5.2).
Table 4 presents Oseberg objects sampled for the study investigating relationships between colour and chemical composition (Section 3.6).

Table 1 Description of analysed archaeological and reference samples

Sample	Description	Genus	Analysis
	Alum-treated archaeological wood - Oseberg treated ca 1905-1912		
185-1, -2, -3, -4, -5 -6	Alum-treated wood from Oseberg (C55000/185-1904.204a). Was compared to fresh birch (*Betula* spp.). Fragments do not contain linseed oil or varnish, and have been sampled from the alum-rich layer. The fragments - which originally fit together - are in increasing state of visual deterioration as the fragment number progresses from 185-1 to 185-6. That is, the samples become increasingly darker and possess less cohesiveness of wood fabric. pH of all fragments ca 1.	diffuse porous	Imaging ICP-OES Py-GC/MS FTIR
Fragment-1	Alum-treated Oseberg wood from the 'work sled' (C55000/190-1904.229-232, sample ID 26.02.01_1). Sampled from the alum-rich region. Not treated with linseed oil. Was compared to fresh birch (*Betula* spp.). Surface is friable, and it is dark brown in colour.	diffuse porous	Imaging ICP-OES FTIR
Fragment-1A	Alum-treated Oseberg wood from the 'work sled' (C55000/190-1904.229-232, sample ID 21.03.05_1A). Not treated with linseed oil. Surface is friable, and it is dark brown in colour.	diffuse porous	RH
Fragment-5	Alum-treated Oseberg wood from the 'work sled' (C55000/190-1904.229-232, sample ID 26.02.01_5). Alum-treated, alum-washed out, freeze dried. Density after washing out alum ca 0.134 g/cm^3. Was identified to either birch or alder (light microscopy). Was compared to fresh birch (*Betula* spp.). Before washing, it was in similar condition to Fragment-1: surface is friable, and it is dark brown in colour.	birch/ alder	Imaging RH FTIR
Fragment-8	Alum-treated Oseberg wood from the 'work sled' (C55000/190-1904.229-232, Sample ID 26.02.01_8). Sampled from the alum-rich region. Not treated with linseed oil. Was compared to fresh birch (*Betula* spp.). This fragment is more friable and is darker brown than Fragment-1.	diffuse porous	RH ICP-OES FTIR
Fragment-9	Alum-treated Oseberg wood from the 'work sled' (C55000/190-1904.229-232, sample ID 26.02.01_9). Alum-treated, alum-washed out. Density after washing out alum 0.111 g/cm^3. Was identified to either birch or alder (light microscopy). Before washing, it was in similar condition to Fragment-1: surface is friable, and it is dark brown in colour.	birch/ alder	Light microscopy
250	Alum-treated Oseberg wood from a carved board (C55000-250/1904.27). Sampled from the alum-treated part avoiding contamination with linseed oil. Was compared to fresh birch (*Betula* spp.). It is in better visual condition than the alum-treated woods described above: it has better structural cohesion and is lighter in colour compared to Fragments-1, 5, 8.	diffuse porous	ICP-OES FTIR
229-Fragments: 1B, 1C, 1D and 5. AND 1B-AR, 1B-AP, 1C-AR, 1C-AP, 1D-AR, 1D-AP, 5-AR, 5-AP	Alum-treated wood from Oseberg (C55000/190-1904.229), without linseed oil or varnish. Were compared to fresh birch (*Betula* spp.). pH of all fragments ca 1. Analysed as part of the ArCo project. Material comprised of 4 fragments 5, 1B, 1C, 1D, which were exposed to artificial aging conditions for approximately seven months (details are in methods section). From each of these fragments, powder samples were collected from the “alum rich” - AR (close to the surface) and “alum poor”- AP (from the core) regions before and after aging, in order to investigate chemical differences between alum poor and alum rich regions.	diffuse porous	ArCo project

Table 1 Con't

Sample	Description	Genus	Analysis
	Alum+linseed oil treated archaeological wood - Oseberg treated ca 1905-1912		
3B	Alum and linseed oil-treated band from one of the large buckets (C55000/210-211-1904.298 or 301, Sample ID 21.03.05-3B). Identified in the Oseberg catalogue as 'ash'. It is ring porous. It is less saturated with linseed oil than the Sled sample. In good condition, with a solid consistency.	ring porous ash?	RH
Sled	Alum/linseed oil-treated Oseberg wood from one of the reconstructed sleds. Could not be identified further than 'diffuse porous'. It is more saturated with linseed oil than 3B, but its surface is not sticky. Appears to be in good condition.	diffuse porous	RH
	Hjortspring find - treated in the 1920s at the National Museum of Denmark (donated samples)		
Hjortspring branch	Alum/glycerol + linseed oil.	Diffuse porous	RH
	Alum-treated archaeological wood - Recently treated		
4B-alum-2009	Archaeological waterlogged aspen (*Populus* spp.) excavated in 2005 from Presterød, Tønsberg, Vestfold county and dated to the Viking Age. Treated with alum in 2009 (2:1 alum: water w/w, 24 hours, 90°C). Density before treatment 0.125 g/cm^3. Sampled from the alum-rich region. After treatment, it was visually in very good condition, although more brittle and paler than it was before treatment.	aspen	ICP-OES Py-GC/MS Alum in lab
Arch-1-alum-2012	Archaeological waterlogged birch *(Betula* spp.) excavated in the 1980s, unknown site, kept in a waterlogged state. Treated with alum in 2012 (2:1 alum: water w/w, 24 hours, 90°C). Density before treatment 0.233 g/cm^3. Sampled from alum-rich area. After treatment, it was visually in very good condition, although more brittle and paler than it was before treatment. Used in aging experiments.	birch	ICP-OES Aging
Arch-4-alum-2012	Archaeological waterlogged birch *(Betula* spp.) excavated in the 1980s, unknown site, kept in a waterlogged state. Treated with alum in 2012 (2:1 alum: water w/w, 40 hours, 90°C). Density before treatment 0.095 g/cm^3. Sampled from alum-rich area. After treatment, it was visually in very good condition, although more brittle and paler than it was before treatment. Used in aging experiments.	birch	ICP-AES Aging

Table 1 Con't

Sample	Description	Genus	Analysis
	Untreated archaeological wood		
Arch maple/ Oseberg maple (nr.124)	Maple (*Acer* spp.) sample from Oseberg, animal head post (C55000/124-1904.138) which was in poor condition upon excavation in 1904, that is, similar to the condition of the woods which were treated with alum. Due to certain circumstances, this object was destroyed before being treated, it was air-dried. It is not as powdery as the alum-treated woods from Oseberg, but it has a very soft consistency.	maple	Py-GC/MS FTIR
Arch oak/ Oseberg-ship	Oak (*Quercus* spp.) sample from the Oseberg ship (C55000/1) which was in relatively good condition upon excavation. It had withstood air drying after only receiving a surface coating of linseed oil and creosote at the excavation site, and is therefore considered 'untreated'. The wood was sampled below the surface, in order to avoid the surface treatment. Visually, it appears to be in very good condition today. Despite this, it has retained only about 30% of its strength (Hørte, Sund et al., 2006).	oak	RH ICP-OES Py-GC/MS
Archaeological birch/1	Birch (*Betula* spp.) excavated from an unknown site in the 1980s. Density 0.128 g/cm^3. It was found in a waterlogged state and was freeze dried.	birch	RH FTIR
Archeaological alder	Alder (*Alnus* spp.) excavated from Presterød, Tønsberg, Vestfold in 2005. Dated to the Viking Age. Density 0.143 g/cm^3. It was found in a waterlogged state and was air-dried.	alder	FTIR
Archaeological aspen/1	Aspen *(Populus* spp.) excavated from Presterød, Tønsberg, Vestfold county in 2005 and dated to the Viking Age. The sample was taken from the same branch as sample 4B-alum-2009. Density was 0.118 g/cm^3. It was found in a waterlogged state and was freeze dried. The freeze dried sample has a light colour, and may be handled, but it is not as strong as that which had been treated with alum. It is similar in consistency to sample 124noFe.	aspen	Py-GC/MS FTIR
Archaeological aspen/2	Aspen *(Populus* spp.) excavated from Presterød, Tønsberg, Vestfold county in 2005 and dated to the Viking Age. The sample was taken from the same branch as sample 4B-alum-2009. Density was 0.114 g/cm^3. It was found in a waterlogged state and was freeze dried. The freeze dried sample has a light colour, and may be handled, but it is not as strong as that which had been treated with alum. It is similar in consistency to sample 124noFe.	aspen	RH
	Fresh wood		
Diffuse porous	Maple *(Acer* spp.) (as reference for 124noFe); Aspen *(Populus* spp.) (as reference for 4B-2009 and Arch-aspen); Birch *(Betula* spp.) and Alder *(Alnus* spp.) as references for diffuse porous alum-treated Oseberg woods.	maple aspen birch alder	ICP-OES Py-GC/MS FTIR
Ring porous	Oak *(Quercus* spp.) (as reference for Oseberg-ship sample).	oak	ICP-OES Py-GC/MS

Table 2 Archaeological aspen used in model experiments investigating the alum treatment in laboratory. Table shows treatments, densities and pH after treatment. Results are described in Section 3.5.1 Model studies of alum in the laboratory.

Sample treatment		Density before treatment g/cm^3	Density after treatment g/cm^3	pH after treatment
Archaeological aspen				
0A	untreated*	0.127	--	--
0B	untreated	0.122	--	--
0C	untreated	0.129	--	--
0D	untreated	0.130	--	--
5A	untreated	0.118	--	--
5B	untreated	0.131	--	--
5C	untreated	0.121	--	--
5D	untreated	0.130	--	--
9A	untreated	0.119	--	--
9B	untreated	0.123	--	--
9C	untreated	0.130	--	--
9D	untreated	0.123	--	--
average density		**0.125**	--	--
AA-water-90C	immersed water, 90C 24 hrs, air-dried	0.125	--	5
AA-water-RT	immersed water, RT 24 hrs, air-dried	0.125	--	5
4A-2:1	alum solution 2:1 RT, 24 hrs, air-dried	0.125	--	4
6A-2:1	alum solution 2:1 RT, 24 hrs, air-dried	0.125	--	4
7A-4:1	alum solution 4:1 RT, 24 hrs, air-dried	0.125	--	4
8A-4:1	alum solution 4:1 RT, 24 hrs, air-dried	0.125	--	4
4B-2:1	alum solution 2:1 90C, 24 hrs, air-dried	0.125	0.724	3
6B-2:1	alum solution 2:1 90C, 24 hrs, air-dried	0.125	0.681	3
7B-4:1	alum solution 4:1 90C, 24 hrs, air-dried	0.125	0.746	3
8B-4:1	alum solution 4:1 90C, 24 hrs, air-dried	0.125	0.513	3
AA-pH 0-RT	Sulphuric acid treated, pH 0, RT, 24 hrs, air-dried	0.125	--	1
AA-pH 1-RT	Sulphuric acid treated, pH 1, RT, 24 hrs, air-dried	0.125	--	2
AA-pH 2-RT	Sulphuric acid treated, pH 2, RT, 24 hrs, air-dried	0.125	--	4.5
AA-pH 3-RT	Sulphuric acid treated, pH 3, RT, 24 hrs, air-dried	0.125	--	4.5
AA-pH 0-90	Sulphuric acid treated, pH 0, 90C, 24 hrs, air-dried	0.125	--	1
AA-pH 1-90	Sulphuric acid treated, pH 1, 90C, 24 hrs, air-dried	0.125	--	2.5
AA-pH 2-90	Sulphuric acid treated, pH 2, 90C, 24 hrs, air-dried	0.125	--	4
AA-pH 3-90	Sulphuric acid treated, pH 3, 90C, 24 hrs, air-dried	0.125	--	4.5

* All untreated samples were used to calculate density. Sampled for IR before drying (with heat).

Table 2, con't Fresh aspen used in model experiments investigating the alum treatment in laboratory. Table shows treatments, densities and pH after treatment. Results are described in Section 3.5.1 Model studies of alum in the laboratory.

	Sample treatment	Density before treatment g/cm^3	Density after treatment g/cm^3	pH after treatment
FA-density-1		0.450		
FA-density-2		0.421		
average density		**0.436**		
FA-ref-1	Air-dried, RT	0.436		
FA-ref-2	Air-dried at 90C 24 hrs	0.436		
FA-water-90C	immersed water, 90C 24 hrs,	0.436	-	4
FA-water-RT	immersed water, RT 24 hrs, air-dried	0.436	- -	4
FA-1-alum	alum solution 2:1 RT	0.436	0.511	4
FA-2-alum	alum solution 4:1 RT	0.436	0.494	4
FA-3-alum	alum solution 2:1 90	0.436	0.695	3
FA-4-alum	alum solution 4:1 90	0.436	0.619	3.5
FA-1-pH 0-RT	pH 0, RT, 24 hrs, air-dried	0.436	--	1
FA-2-pH 1-RT	pH 1, RT, 24 hrs, air-dried	0.436	--	2
FA-3-pH 2-RT	pH 2, RT, 24 hrs, air-dried	0.436	--	3-3.5
FA-4-pH 3-RT	pH 3, RT, 24 hrs, air-dried	0.436	-- --	4
FA-1-pH 0-90C	pH 0, 90C, 24 hrs, air-dried	0.436	--	1
FA-2-pH 1-90C	pH 1, 90C, 24 hrs, air-dried	0.436	--	2.5
FA-3-pH 2-90C	pH 2, 90C, 24 hrs, air-dried	0.436	--	3
FA-4-pH 3-90C	pH 3, 90C, 24 hrs, air-dried	0.436	--	4

Table 3 Aging studies. Sample overview. Those sampled for SEM analyses are indicated with an asterisk *. Described in Section 3.5.2

Sample	Aging temperature and RH used	dry bulk density (g/ml)	Max moisture content (%)
	FRESH BIRCH		
Freeze dried			
Fresh FD-1*	RT, 60% RH	0.534	112
Fresh FD-3	RT, 60% RH	0.534	112
Fresh FD-2*	50C 60% RH	0.534	112
Fresh FD-4	50C 60% RH	0.534	112
Alum 24 hours 90C			
Fresh alum-1*	RT, 60% RH	0.534	112
Fresh alum-3	RT, 60% RH	0.534	112
Fresh alum-2*	50C 60% RH	0.534	112
Fresh alum-4	50C 60% RH	0.534	112
Sulphuric acid pH2 24 hours 90C			
Fresh sulf-1*	RT, 60% RH	0.534	112
Fresh sulf-3	RT, 60% RH	0.534	112
Fresh sulf-2*	50C 60% RH	0.534	112
Fresh sulf-4	50C 60% RH	0.534	112
	ARCHEAOLOGICAL BIRCH		
Freeze dried			
Arch-3 (VIII-2)*	RT, 60% RH	0.154	580
Arch-11 (V-6)	RT, 60% RH	0.107	866
Arch-6 (III-2)	50C 60% RH	0.128	713
Arch-10 (VIII-3)*	50C 60% RH	0.084	1131
Alum 40 hours 90C			
Arch-2 (V-5)-1	RT, 60% RH	0.090	1004
Arch-7 (VI-2)*	RT, 60% RH	0.150	599
Arch-2 (V-5)-2	50C 60% RH	0.090	1004
Arch-4 (II-2)*	50C 60% RH	0.095	988
Arch-5 (VIIII-4)	50C 60% RH	0.126	716
Arch-14 (V-7)	50C 60% RH	0.214	403
Alum 24 hours 90C			
Arch-9 (VII-4)-1	RT, 60% RH	0.103	906
Arch-12 (VII-7)*	RT, 60% RH	0.117	785
Arch-1 (DR 49/A46)*	50C 60% RH	0.233	361
Arch-8 (V-I)	50C 60% RH	0.086	1101
Arch-9 (VII-4)-2	50C 60% RH	0.103	906
Arch-13 (VII-2)	50C 60% RH	0.107	870
Sulphuric acid pH2 at 24 hours, 90C			
Arch-18 (VIIII-1)	RT, 60% RH	0.189	463
Arch-19 (VIIII-3)*	RT, 60% RH	0.094	1002
Arch-16 (DR 186D-DR67)*	50C 60% RH	0.113	824
Arch-17 (IV-1)	50C 60% RH	0.094	996

Table 4 Oseberg objects sampled for the study investigating relationships between visual state of preservation and colour- and chemical information. Results are described in Section 3.6.

Sample name/object number	Type of treatment
C55000_185-1904.204a-fragment-1-average	alum
C55000_185-1904.204a-fragment-2-average	alum
C55000_185-1904.204a-fragment-3-average	alum
C55000_190-1904.229-eske2av2-fragment-1-average	alum
C55000_190-1904.229-eske2av2-fragment-2-average	alum
C55000_190-1904.229-eske2av2-fragment-3-average	alum
C55000_190-1904.229-eske2av2-fragment-4-average	alum
C55000_190-1904.229-eske2av2-fragment-5-average	alum
C55000_190-1904.229-eske2av2-fragment-6-average	alum
C55000_190-1904.229-eske2av2-fragment-7-average	alum
C55000_206-1904.290a-fragment-1-average	alum
C55000_206-1904.290a-fragment-2-average	alum
C55000_206-1904.290a-fragment-3-average	alum
C55000_206-1904.290a-fragment-4-average	alum
C55000_206-1904.290a-fragment-5-average	alum
C55000_206-1904.290a-fragment-6-average	alum
C55000_206-1904.290a-fragment-7-average	alum
C55000_206-1904.290e-fragment-1-average	alum
C55000_206-1904.290e-fragment-2-average	alum
C55000_206-1904.290e-fragment-3-average	alum
C55000_206-1904.290e-fragment-4-average	alum
C55000_206-1904.290e-fragment-5-average	alum
C55000_206-1904.290e-fragment-6-average	alum
C55000_206-1904.290e-fragment-7-average	alum
C55000_206-1904.290e-fragment-8-average	alum
C55000_275-1904.112-cdef-fragment-3a-average	alum
C55000_275-1904.112-cdef-fragment-4-average	alum
C55000_296-OXVa-fragment-1-bag 2/23-top-average	alum
C55000_296-OXVa-fragment-2-bag 4/23-top-average	alum
C55000_296-OXVa-fragment-3-bottom tray-average	alum
C55000_296-OXVa-fragment-4-bottom tray-average	alum
C55000_296-OXVb-average	alum
C55000_197-1904.260-average	alum+linseed oil
C55000_197-1904.261b-average	alum+linseed oil
C55000_198-1904.263-eske3av3-average	alum+linseed oil
C55000_207-1904.291a-average eske 2 av 2	alum+linseed oil
C55000_207-1904.291a-eske 1 av 2-average	alum+linseed oil
C55000_207-1904.291b-average	alum+linseed oil
C55000_258_1904.54b-average	alum+linseed oil
C55000_279-1904.170a-h-fragment-1-average	alum+linseed oil
C55000_279-1904.170a-h-fragment-2-average	alum+linseed oil
C55000_279-1904.170a-h-fragment-3a-average	alum+linseed oil
C55000_279-1904.170a-h-fragment-3b-average	alum+linseed oil
C55000_279-1904.170a-h-fragment-4-average	alum+linseed oil
C55000_410-1904.206-207b-eske3av3-fragment-1-average	alum+linseed oil
C55000_410-1904.206-207b-eske3av3-fragment-3-average	alum+linseed oil
C55000_410-1904.206-207b-eske3av3-fragment-4-average	alum+linseed oil
C55000_410-1904.206-207b-eske3av3-fragment-5-average	alum+linseed oil
C55000_410-1904.206-207b-eske3av3-fragment-6-average	alum+linseed oil
C55000_203-1904.283b-fragment-2-average	alum+linseed oil+varnish
C55000_250_1904.27-fragment-2-average	alum+linseed oil+varnish
C55000_250_1904.27-fragment-1-average	alum+linseed oil+varnish

2.2 Analytical techniques and experimental conditions

Below are listed the analytical techniques which were employed to characterize the organic and inorganic components of the wood samples. Table 5 presents the types of chemical analyses undertaken on 'major' samples and is a cross-reference for Table 1.

- Light microscopy
- pH measurements
- Scanning Electron Microscopy with Energy Dispersive X-ray analysis (**SEM-EDX**): observation of the morphology of wood surface and elemental analysis;
- Inductively Coupled Plasma Optical Emission Spectroscopy (**ICP-OES**): quantitative determination of the elemental composition;
- Ionic-Conductivity Liquid-Chromatography (**IC-LC**): quantitative determination of anions;
- X-ray diffraction (**XRD**): identification of mineral composition;
- Fourier Transform Infrared Spectroscopy (**FTIR**): analysis at molecular level of inorganic and organic components of wood; in some cases data was interpreted with the help of principal component analysis (**PCA**).
- Nuclear Magnetic Resonance (**NMR**) relaxometry: assessment of free and bound water in alum-treated samples
- **NMR** for chemical characterization of wood
- Gel permeation chromatography (**GPC)** for analysis of polymer molecular weight.
- Analytical pyrolysis coupled with gas chromatography and mass spectrometry (**Py-GC/MS**): analysis at molecular level of organic components of wood;
- **GC-MS**
- **HPLS-Q-ToF-MS**
- X-ray and neutron tomography

Table 5 Chemical analyses carried out on Oseberg samples (not all results are shown in this report).

Object	Fragment	Sample	SEM-EDS	ICP-OES	IC-LC	XRD	FT-IR	NMR-time resolved	Py-GC/MS	LC-MS	tomography	Colour measurement	NMR spectroscopy	GPC
185		185-1	√	√		√	√		√		√	√		√
		185-2	√	√		√	√		√		√	√		√
		185-3	√	√		√	√		√		√	√		√
		185-4	√	√		√	√		√		√	√		√
		185-5	√	√		√	√		√		√	√		√
		185-6	√	√		√	√		√			√		√
229	5	5-AR	√	√	√	√	√	√	√					
		5-AP	√	√	√	√	√	√	√					
	1B	1B-AR	√	√	√	√	√		√					
		1B-AP	√	√	√	√	√		√					
	1C	1C-AR	√	√	√	√	√		√					
		1C-AP	√	√	√	√	√		√					
	1D	1D-AR	√	√	√	√	√	√	√					
		1D-AP	√	√	√	√	√	√	√					
	5-alum removed		√				√				√		√	√
Arch-oak (Oseberg ship)	Dendro-9								√				√	√
Arch-maple 124 (Oseberg animal head)							√		√					√

Light microscopy: Wood identification of the alum-treated woods was challenging due to the difficulty of obtaining good quality thin sample slices. Very few alum-treated samples were possible to identify by transmission light microscopy. Samples were otherwise classified according to their pore-distribution pattern. Alum-treated woods are mainly diffuse porous types.

pH measurements: Surface pH measurements were taken of sampled fragments from the objects by applying damp pH strips with slight pressure.

SEM-EDX: Analyses were performed at the Museum of Cultural History, University of Oslo, Norway on all samples using a FEI Quanta 450 Scanning Electron Microscope coupled with an Oxford X-MaxN 50mm2 detector or a JEOL JSM-840 scanning electron microscope, using a voltage of 20 kV (the JEOL required that samples were sputtered with carbon). The other parameters (spot size, pressure, and working distance) were modified depending on the sample. Samples analysed under high vacuum were sputtered using carbon before observation, with the aim to obtain information on the morphology of the samples and elemental distribution.

Tomographic imaging

Both neutron and X-ray tomographic imaging were undertaken at the Paul Scherrer Institute, Villingen, Switzerland.

Synchrotron X-ray tomographic microscopy

The TOMCAT beamline is located at the X02DA port of SLS which receives photons from a 2.9 Tesla superbending magnet [1]. The X-ray energy used for the samples ranged between 10-15 keV at 400 mA, and exposure time between 200-500 ms, depending on the inorganic content of samples. The number of projections was between 1400 and 1800, over a rotation range of 180˚. Typical acquisition times were thus in the order of 15 minutes. The scintillator-CCD camera used was PCO2000 with 2048x2048 pixels, and a LAG:Ce scintillation layer, 20 µm thick. Three different objectives were used: 4x, 10x and 20x. Sample sizes were dependent on the magnification used, and ranged from less than 1 mm in diameter (spatial resolution 1 micron) for the 20x objective, up to 3 mm diameter (spatial resolution 3.8 microns) for the 4x objective [2]. Samples were mounted onto their holders using beeswax.

Neutron tomographic imaging

Neutron tomography was carried out at both NEUTRA and ICON facilities at the SINQ neutron source. At NEUTRA, images were recorded with thermal neutrons (wavelength ca 1.2 Ångstom, room temperature). Samples for neutron tomography were placed at Position 2, where it is possible to accommodate dimensions up to ca 20 cm in length at a resolution of 85 microns per pixel (voxel). At the ICON facility, samples were imaged at Position 2 (sample sizes up to ca 1-1.5 cm^3). ICON uses cold neutrons for imaging, which means they are less energetic than thermal neutrons (wavelength ca 1.8 Ångstrom) and thus generate images of enhanced contrast relative to those obtained by thermal neutrons [3]. The resolution at ICON (13.5 microns per pixel (voxel)) is higher than that at NEUTRA, however, the ICON set-up at Position 2 requires smaller samples (Table 2). Transmission data were recorded by CCD cameras equipped with scintillation foils. At NEUTRA, an Andor DV434 1024 Pixel camera, with a Lanex scintillator was used. At ICON, the Andor DW436 2048 Pixel camera had a 10 µm Gadox scintillator. At ICON, the exposure time was 150s, with 360° rotation and 375 projections. At NEUTRA exposure time was 80s, with 360° rotation and 625 projections. Thus tomography took up to 15 hours per run.

Data reconstruction and evaluation

The calibration and transformation of transmission data into transverse slices from both neutron and X-ray sources were carried out by specialized software programs at the respective facilities. Tomographic data (image stacks) were studied in 2D using the public domain Java image processing program *ImageJ*.The software used to render 3D-reconstructions was *VGstudio MAX 2.1*®, from Volume Graphics GmbH, Heidelberg, Germany.

ICP-OES Two different instruments were used.

1. Some analyses were performed at the Analytics Laboratory, Leibniz Institute for New Materials (INM), Saarbrücken, Germany. Samples were mineralised using 4 mL nitric acid (≥ 65% HNO3), 1 mL hydrofluoric acid (50% HF), 1 mL hydrogen peroxide (30% H2O2) and 1 mL pure water. The samples were digested in a microwave (Anton Paar) at 200°C for 2 hours. After cooling to room temperature, ultra-pure water was added to the digested solutions to 50 mL. The instrument used was ICP-OES Ultima 2, Horiba Jobin Yvon. Elements analysed included Aluminum (Al), Calcium (Ca), Copper (Cu), Iron (Fe), Potassium (K), Magnesium (Mg), Manganese (Mn) and Zinc (Zn).
2. Analyses undertaken within the ArCo project were performed by Archa Srl Laboratory, Pisa, Italy. After micro-wave assisted mineralisation of the samples using 4:1 = HNO3 65%: H2O2 10%, the concentration of Ag, Al, As, Sb, Ba, Be, B, Cd, Ca, Cr, Co, Cu, Fe, Li, Pb, Mg, Mn, Mo, Ni, Se, Si, Sn, V, Zn, K, Na, Ti, S, Hg were measured. The instrument was an Optima 5300 DV, Perkin-Elmer (**Figure 1**).

IC-Conductivity analysis:
Analyses were performed by Archa Srl Laboratory, Pisa, Italy. The concentrations of the anions fluorides, formates, acetates, chlorides, bromides, nitrates, phosphates, sulphates were determined after a ultrasonic assisted water extraction (60°C – 30 min) and filtration of the samples. The instrument was a Dionex ICS-1000 (Thermo Scientific).

ARCHA Laboratories: analyses were performed following a SPECIFIC analytical protocol. Each sample was divided into two sub-samples: Sub-Sample 1 was subjected to elemental analysis by ICP-OES. Sub-Sample 2 was extracted in water at 60°C for 30 minutes, using ultrasound (US); then the eluate was analysed by IC-LC to detect anions, whereas the solid residue was subjected to elemental analysis by ICP-OES, to detect elements present in salts insoluble in water. The protocol is showed in Figure 1

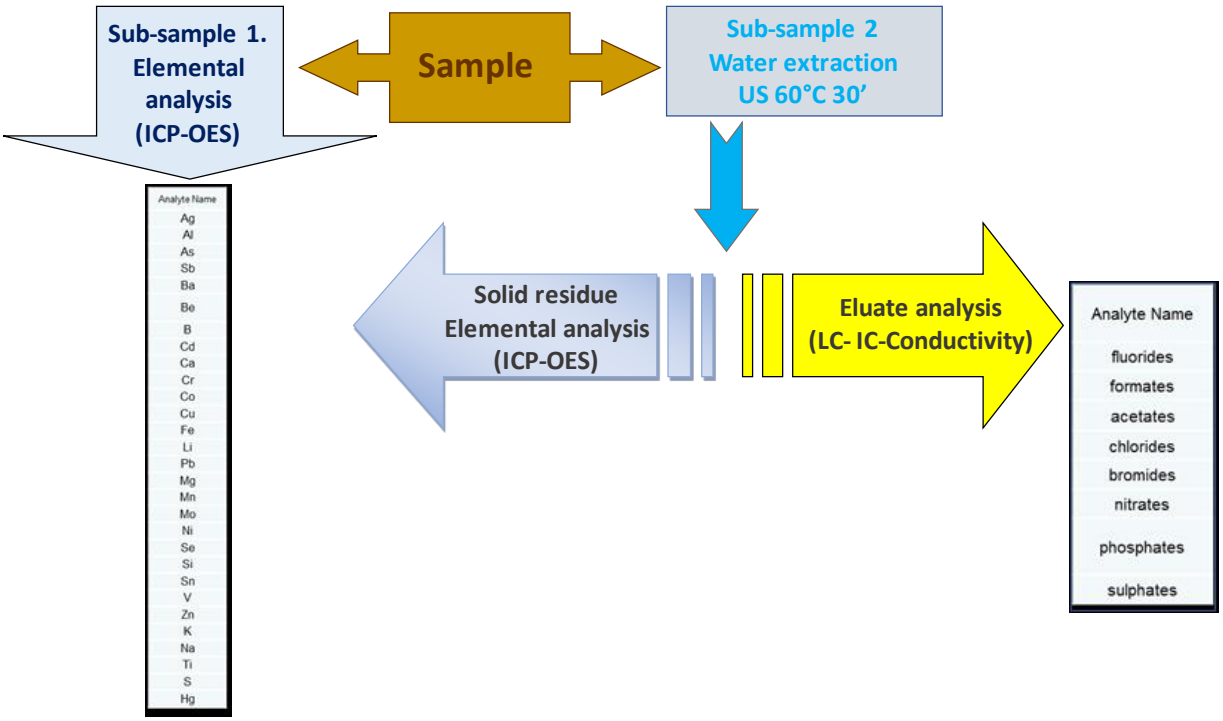

Figure 1 ICP-OES and IC-LC protocol analysis scheme performed at the ARCHA Laboratories.

As regards ICP-OES analyses, after micro-wave assisted mineralisation of the samples using 4:1 = HNO_3 65%: H_2O_2 10%, the concentration of Ag, Al, As, Sb, Ba, Be, B, Cd, Ca, Cr, Co, Cu, Fe, Li, Pb, Mg, Mn, Mo, Ni, Se, Si, Sn, V, Zn, K, Na, Ti, S, Hg were measured. The instrument was an Optima 5300 DV, Perkin-Elmer. Metals were detected on a calibration line with 5 points

at concentration from 50 to 5000 µg/L. Titanium and, sulphur on a line from 100 to 10000 µg/L; mercury was read on a calibration line from 5 to 20 µg/L.
As regards IC-LC analyses, the water extracts were filtered by cellulose nitrate membrane of 0.45 µm. Anions such as fluorides, formates, acetates, chlorides, bromides, nitrates, phosphates and sulphates were determined using using a Dionex ICS-1000 (Thermo Scientific).The concentrations were read on calibration line with 5 point at concentrations that vary from 0,1 to 1 mg/L for fluorides and bromides; from 1 to 10 mg/L for chlorides, nitrates, phosphates and sulphates.

XRD: analysis was carried at the Museum of Cultural History, University of Oslo, Norway using PANalytical diffractometer Empyrean Series 2 with radiation CuKα1 =1.54 Å, operating at 45 kV, 40 mA, 2θ range 8–70°, step size 0.03°, time per step 5000 s, equipped with a PIXcel1D-Medipix3 RTMS detector, and High Score data acquisition and interpretation software. A zero background sample holder was used. Crystalline phases were identified using the ICDD database

Some analysis was also carried out with the support of Dr. Emma Cantisani at the Institute for Conservation and Valorization of Cultural Heritage, Florence, Italy, using a PANalytical diffractometer X'Pert PRO with radiation CuKα1 = 1.545 Å, operating at 40 kV, 30 mA, 2θ range 3–70° step size 0.02°, -time per step 50 s, scan rate 0.04°/s, equipped with X'Celerator RTMS (Real Time Multiple Strip) X-ray detection technology, an High Score data acquisition and interpretation software. A zero background sample holder was used. Crystalline phases were identified using the ICDD database.

GPC analyses[2] [4] were performed on a Waters 600 E liquid chromatography connected to a HP1040 ultraviolet UV detector set at 240 nm or 280 nm for benzoylated and acetylated samples respectively. The injection port was a Rheodyne loop valve equipped with a 20 µL loop. The GP-column system was composed by a sequence of an Agilent PL gel 5 µm, 500 Å and an Agilent PL gel 5 µm, 104 Å [sic?: or 10^4 Å?]. The solvent used was tetrahydrofuran (Fluka 99.8%). PL Polymer Standards of Polystyrene from Polymer Laboratories were used for calibration. The peak molecular weight M_p is defined as the molecular weight of the species with maximum absorbance. M_p values reported are the average of three replicate analyses (M_p: ±100 g mol^{-1}, P = 0.05, n=3). Acetylated and benzoylated samples were dissolved in THF (1 mg/mL) and passed through a 0.45 µm GH Acrodisc syringe filter and analyzed at a flow rate of 1 mL/min.

2D-HSQC-NMR Analyses[2] [4]: Two-dimensional *Heteronuclear Single Quantum Coherence* spectra were run in DMSO-d_6 on acetylated wood samples. The inverse detected ^{1}H-^{13}C correlation spectra were measured on a Varian Mercury 400 MHz NMR instrument at 308 K. The spectral width was set at 5 kHz in F2 and 25 kHz in F1. Altogether 128 transients in 256 time increments were collected. The polarization transfer delay was set at the assumed coupling of 140 Hz and a relaxation delay of 2 s was used. The spectra were processed using Π/2 shifted squared sinebell functions in both dimensions before Fourier transformation.

NMR relaxometry: Analyses were undertaken under the guidance of Prof. Eddy Walther Hansen, Department of Chemistry, University of Oslo. The instrument was Maran Ultra NMR operating at 0.5 T. The sample was packed in a 10 mm NMR tube and placed in the NMR instrument. The temperature was set to 35 °C (±1 °C) and equilibrated for 10 min before starting the measurements. Spin-lattice and spin-spin relaxation measurements were performed using Inversion Recovery and CPMG sequences respectively; free induction decay (FID) was

[2] Additional information for this method was also added from the following unpublished document: Luca Zoia, Diego Tamburini, Marco Orlandi, Jeannette Jacqueline Łucejko, Anika Salanti, Eeva-Liisa Tolppa, Francesca Modugno, Maria Perla Colombini, *Integrated Approach for the Chemical Characterization of the Whole Wall Cell Materials: Application to Archaeological Woods*, version sent to Oslo 30.09.15.

recorded using Solid-echo pulse sequence for different values of τ, in order to obtain information about water content and its state (free, bound, mobile...). Analyses were performed on dried samples after reaching the humidity equilibrium with the environment.

Raman microscopy: Raman spectra were recorded at the Museum of Cultural History, University of Oslo. Raman spectra were recorded for all samples without linseed oil. Those with linseed oil showed too much background fluorescence to see other peaks. Mapping was performed with a Renishaw inVia Raman microscope, using a 488 nm laser. Laser power, exposure time and the number of accumulations were modified depending on the sample.

FTIR: Spectra in ATR mode were recorded at the Museum of Cultural History, University of Oslo on a Thermo Fischer FTIR spectrometer (Nicolet iS50). 64 scans and 4 cm^{-1} resolution were adopted. The range was 4000-400 cm^{-1}. ATR-FTIR analyses of 185-series and model experiments (described in Sections 3.3 and 3.5, respectively) were undertaken at the Dept. of Conservation Studies, University of Oslo on a Perkin Elmer Spectrum One ATR-FTIR unit, with a ZnSe/diamond hybrid crystal, a resolution of 4 cm^{-1} and a range between 4000-650 cm^{-1}. Most samples were analyzed in triplicate.
IR microscopy was performed on all wood samples using conventional IR radiation (using the above instrument) and/or synchrotron radiation (SR). SR-FTIR, was carried out at the IRIS beamline at the BESSY II synchrotron facility, Helmholtz-Zentrum Berlin Germany, using a Nicolet Nexus 870 spectrometer. Samples were compressed in a diamond cell and micro-infrared spectroscopy (μFTIR) performed using a Nicolet Continuum FTIR microscope. Spectra were recorded in transmittance mode with a spectral resolution of 4 cm-1, within the range 4000-650 cm-1 and 4000-800 cm-1 for conventional and synchrotron radiation, respectively. Each spectrum in a map was recorded with 128 scans and, spot analyses were recorded with 256 scans.
Principal component (PC) analyses of selected IR spectra were undertaken using the Unscrambler X 10.3 software (Camo Software AS) after they were baseline corrected and normalized at 1505 cm^{-1}. Band heights in spectra were measured using the Perkin Elmer Spectrum software on baseline corrected and normalized spectra (normalized to 1505 cm^{-1}). Table 6 gives infrared assignments for wood and potassium aluminum sulphate salts.

Table 6 Infrared band assignments for wood and alum salt.

Band (cm^{-1})	Assignment	Reference
3645-3620	Free OH	[5]
3570-3450	valence vibration of H-bonded OH-groups (intramolecular)	[5]
3345	alum, crystal water	[6]
3400-3200	valence vibration of H-bonded OH-groups	[5]
3000-2842	C-H stretch in methyl and methylene groups	[5]
2840-2835	methoxyl C-H stretching	[5]
2888	alum, crystal water	[6]
2455	alum, crystal water	[6]
1730-1725	C=O valence vibration of acetyl- or COOH-groups	[5]
1738-1709	C=O stretch in unconjugated ketones, carbonyls and in ester groups (frequently of carbohydrate origin..mainly hemicelluloses);	[5]
1700	conjugated aldehydes and carboxylic acids absorb around and below 1700	[5]
1675-1655	C=O stretch: in conjugated p-substituted aryl ketones; strong electronegative substituents lower the wavenumber	[5]
1646	conjugated C=O groups, mainly originating from lignin	[7]
1635	adsorbed water	[5]
1605-1593	aromatic skeletal vibrations plus C=O stretch; S>G; G-condensed > G-etherified	[5]
1615	alum ?	
1610	Aromatic skeletal vibration plus C=O stretch, hardwood	[8]
1605	carboxylate groups; C=C	[9]
1600-1595	lignin, xylan (O-groups)	[9]
1587	conjugated C-O	
1515-1505	aromatic skeletal vibrations; G>S	[5]

1470-1455	CH2 of pyran ring symmetric scissoring; OH plane deformation vibration	[5]
1470-1460	C-H deformations: asymmetric in -CH3 and -CH2-	[5]
1450	C-H deformation in lignin and carbohydrates; CH3, CH2, benzene ring vibration in lignin	[10]
1430	HOC in plane bending of alcohol groups	[5]
1430-1422, 1417	Aromatic skeletal vibrations combined with C-H in-plane deformation (lignin and carbohydrates)	[5]
1400	cellulose	[9]
1375-1374	CH deformation vibration	[5]
1370-1365	aliphatic C-H stretch in CH3, but not not methoxyl groups	[5]
1365-1335	OH plane deformation vibration	[5]
1363	C-H bending vibration in cellulose and hemicelluloses	[10]
1330-1325	phenolic OH: S ring plus G ring condensed: (ie G-ring substituted in pos. 5)	[5]
1319	C-H vibration in cellulose; C1-O in syringyl derivatives	[10]
1315	C-O syringyl ring (hardwood)	[8]
1282-1277	CH-deformation	[5]
1270-1266	C-O Guaiacyl ring plus C=O stretch	[5, 8]
1235-1225	OH plane deformation, also COOH	[5]
1226	syringyl ring; C-O stretch in lignin and xylan	[10]
1230-1221	C-C plus C-O plus C=O stretch lignin and xylan; C-O og guaiacyl ring, hardwoods; G-condensed > G-etherified	[5]
1230	lignin, C=O in xylan	[9]
1218	C-O of guaiacyl ring, hardwoods	[8]
1190	alum sulfate stretch	[6]
1166	C=O in ester groups (conj.)	[11]

Table 6 con't Infrared band assignments for wood and alum salt.

Band (cm^{-1})	Assignment	Reference
1162-1125	C-O-C asymmetric valence vibration in cellulose and hemicelluloses	[5]
1140	aromatic C-H in-plane deformation; typical for G units; whereby G-condensed > G-etherified plus secondary alcohols plus C=O stretch	[5]
1128-1125	aromatic C-H in-plane deformation; typical for S units; plus secondary alcohols plus C=O stretch	[12]
1120-1115	asymmetric in-phase ring stretching, C-C and C-O stretching; aromatic skeletal: C-C stretch; O-H association band in cellulose and hemicelluloses	[5]
1113	Guaiacyl C-H and syringyl C-H (hardwoods).	[8]
1110-1107	ring asymmetric valence vibration	[5]
1082/1093	alum sulfate stretch	[6]
1059/1063	alum sulfate stretch	[6]
1086	C-O deformation in secondary alcohols and aliphatic ethers	[5]
1040-1030	C-alkyl-O ether vibrations in guaiacol	[5]
1035-1030	aromatic C-H in-plane deformation G>S; plus C-O deformation in primary alcohols; plus C=O stretch (unconj.)	[5]
1026, 1024	C-O stretch in cellulose and hemicelluloses; C-O of primary alcohol, guaiacyl C-H, hardwood	[8]
996-985	C-O valence vibration	[5])
990-966	-HC=CH- out-of-plane deformation (trans)	[3]
976-970	alum sulfate stretch	[6]
967	C-O stretch	[9]
930-925	Pyran ring vibration	[5]
925-915	C-H out-of-plane; aromatic	[5]
913/921	alum, 'trivalent water' (attached to aluminum ion)	[6]
912	C-H out of plane	[8]
898-892	C-H deformation in cellulose; C1 group frequency in cellulose and hemicelluloses	[9]
872, 870	glucomannan, mannose	[9]
858-853	C-H out-of-plane in position 2, 5 and 6 of G units	[5]
835-834	C-H out-of-plane in position 2 and 6 of S, and in all positions of hydroxyphenylpropane units	[11]
832-817	C-H out-of-plane in positions 2, 5 and 6 of G units	[3]
814, 805	glucomannan	[9]
800	pyran vibration	[5]
690	alum, 'trivalent water' (attached to aluminum ion)	[6]

Py-GC/MS: Analytical pyrolysis was performed at DCCI, Pisa using 1,1,1,3,3,3-hexamethyldisilazane (HMDS, chemical purity 99.9%, Sigma Aldrich Inc., USA) as a silylation agent for the *in situ* thermally assisted derivatisation of pyrolysis products. The instrumentation consisted of a Multi-Shot Pyrolyzer® EGA/PY-3030D (Frontier Lab) connected to a gas chromatograph 6890 Agilent (USA) equipped with an HP-5MS fused silica capillary column (stationary phase 5% diphenyl and 95% dimethyl-polysiloxane, 30 m x 0.25 mm i.d., Hewlett Packard, USA) and with a deactivated silica pre-column (2 m x 0.32 mm i.d., Agilent J&W, USA).
Before instrumental analysis the samples were dried in the oven for 24 hours at 50-60 °C, after that they were ground with a ball mill in order to homogenize.
After analysis, the compounds were identified by comparing their mass spectra with spectra reported in the Wiley and NIST libraries or in the literature [13, 14]. The areas were normalized for each sample, and the data from three replicates were averaged and expressed as percentages, in order to calculate the relative amount of wood components and evaluate the degradation state.

EGA-MS: Analyses were performed at DCCI, Pisa. The same EGA/Py-3030D apparatus described above was used, with the only difference being that the GC was equipped with a deactivated and uncoated stainless steel transfer tube (UADTM-2.5N, 0.15mm i.d.×2.5m length, Frontier Lab). A program temperature was chosen for the micro-furnace chamber: initial temperature 50°C; 20°C min-1 up to 200°C; 8°C min-1 up to 500°C; 20°C min-1 up to 700°C. Analyses were performed under a helium flow (1mL min-1) with a split ratio 1:20. The micro-furnace interface temperature was kept at 100°C higher than the furnace temperature until the maximum value of 300°C. The inlet temperature was 280°C. The chromatographic oven was kept at 300°C. A total of 0.5 mg of sample was put into a stainless steel cup and inserted into the micro-furnace. The sample underwent a thermal decomposition in inert atmosphere over the chosen heating range and evolved gaseous compounds were directly ionised and analysed as a function of time. The result is a total ion thermogram (TIT) corresponding to the volatile pyrolysis products evolved in the temperature range.
The mass spectra obtained by this kind of analysis are the sum of all the mass spectra of all the pyrolysis products in the analyzed samples. Thus each fragment ion may be present in more than one pyrolysis product and identification is crucial for a correct interpretation. (Table) summarizes the attribution of the most abundant peaks derived from the pyrolysis of wood components according to the literature [15].

The AMDIS library of mass spectra: The AMDIS (Automated Mass spectral Deconvolution and Identification System) software is part of the full NIST MS Database package. The library build using this software was used to recognise the mass spectra of the pyrolysis products obtained for analysed wooden samples and the areas of chromatographic peaks of identified compounds were integrated.

Table 7 Molecular assignment of the most abundant observed m/z values in the mass spectra of lignin, lignin monomers and polysaccharides. C – carbohydrates; L – lignin; G – guaiacyl-lignin; S – syringyl-lignin

m/z	Molecular origin	Wood component	Ref
55	dihydrofuranone; methyl-dihydrofuranone; 2-hydroxy-3-methyl-2-cyclopenten-1-one; 5,6-dihydropyran-2,5-dione; methyldihydropyranone	C	[16-19]
57	(4H)-methyltetrahydrofuran-3-one; 2-methyl-3-hydroxy-2,3-dihydrofuran; tetrahydrofuran-3-one	C	[16-18]
60	1,6-anhydro-β-D-glucopyranose (levoglucosan)	C	[16-19]
65	present in many pyrolysis products of both carbohydrates and lignin*	C/L	[16-18]
69	2-methoxy-2,5-dihydrofuran; 2,4-dihydropyran-3-one; 3-(hydroxymethyl)furan; 2,3-dihydro-5-methylfuran-2-one; methyldihydropyranone; 3-hydroxy-2-methyl-2-cyclopenten-1-one; 3-methyltetrahydrofuran-2,4-dione; dimethyldihydropyranone; 5-hydroxymethyl-2-tetrahydrofuraldehyde-3-one; 2-hydroxymethyl-2,3-dihydro- pyran-4-	C	[16-19]

	one; 5-hydroxymethyl-2-furaldehyde		
73	1,6-anhydro-β-D-glucopyranose (levoglucosan); 1,6-anhydro- β-D-glucofuranose	C	[16-19]
77	present in many pyrolysis products of both carbohydrates and lignin*	C/L	[16-18]
81	2-methylfuran, 2-(hydroxymethyl)furan, 5-hydroxymethyl-2-furaldehyde, 2,5-dimethylfuran	C	[16-19]
85	(5-)acetyltetrahydrofuran-2-one; 5-hydroxymethyl-2-tetrahydro-furaldehyde-3-one; 3,5-dihydroxy-2-methyl-(4H)- pyran-4-one	C	[16-18]
91	alkylbenzenes	L	[17]
94	phenol	L	[16-18, 20]
96	2-furaldehyde; 2,5-dimethylfuran	C	[16-19]
98	3-(hydroxymethyl)furan; 2-(hydroxymethyl)furan; 2,3-dihydro-5-methylfuran-2-one; 2,4-dihydropyran-3-one; 3-hydroxy-6-methyl-(2H)-pyran-2-one; 3-hydroxy-2-methyl-(4H)-pyran-4-one	C	[16-19]
107	alkylphenols	L	[17, 20]
110	1,2-dihydroxybenzene; 1,4-dihydroxybenzene; 5-methyl-2-furaldehyde; 2-acetylfuran	C/L	[16-19]
112	3-hydroxy-2-methyl-2-cyclopenten-1-one; 2-hydroxy-3-methyl-2-cyclopenten-1-one; methyldihydropyranone; 5,6-dihydropyran-2,5-dione	C	[16-19]
114	4-hydroxy-5,6-dihydro-(2H)-pyran-2-one; 2-hydroxymethylene-tetrahydrofuran-3-one; 3-methyltetrahydrofuran-2,4-dione	C	[16-19]
123	4-methylcatechol; 4-methylguaiacol; dihydrocaffeic acid*	L	[17-20]
124	guaiacol; 4-methylcatechol; coniferyl alcohol;	G	[17-21]
126	3-hydroxy-6-methyl-(2H)-pyran-2-one; 3-hydroxy-2-methyl-(4H)-pyran-4-one; dimethyldihydropyranones; 5-hydroxymethyl-2-furaldehyde; 2-furoic acid methyl ester	C	[16-19]
137	4-ethylguaiacol; 4- propylguaiacol; coniferyl alcohol*; dihydroconiferyl alcohol; guaiacylacetone, homovanillin	G	[17-21]
138	4-methylguaiacol	G	[17-21]
144	5-hydroxymethyl-2-tetrahydro- furaldehyde-3-one, 1,4:3,6-dianhydro-α-D-gluco-pyranose, 1,4-dideoxy-D-glycero-hex-1-enopyranos-3-ulose	C	[16-18]
150	4-vinylguaiacol	G	[17-21]
151	vanillin*; acetovanillone*; vanillic acid methyl ester; propiovanillone;guaiacyl vinyl ketone; vanillic acid*	G	[17-21]
152	4-ethylguaiacol; vanillin*; coniferyl alcohol*	G	[17-21]
154	syringol	S	[17-21]
164	eugenol; isoeugenol (*E* and *Z*); p-coumaric acid;	G	[17-21]
166	acetovanillone*; 4-propylguaiacol	G	[17-20]
167	4-ethylsyringol; 4-propylsyringol; sinapyl alcohol*; dihydrosinapyl alcohol; syringylacetone	S	[17-21]
168	vanillic acid*; 4-methylsyringol	G/S	[17-21]
178	coniferylaldehyde*	G	[17-21]
180	coniferyl alcohol*, 4-vinylsyringol; guaiacylacetone; propiovanillone	G/S	[17-21]
181	syringaldehyde*; acetosyringone*; syringic acid methyl ester; propiosyringone; syringyl vinyl ketone; syringic acid*	S	[17-21]
182	4-ethylsyringol; syringaldehyde*; dihydroconiferyl alcohol; vanillic acid methyl ester; dihydrocaffeic acid*; sinapyl alcohol*	S/G	[17-20]
194	4-(1-propenyl)syringol, 4-(2-propenyl)syringol (*E* and *Z*); 4-allylsyringol; ferulic acid*;	S	[17-21]
196	acetosyringone*; 4-propylsyringol	S	[17-21]
198	syringic acid*	S	[17-21]
208	sinapylaldehyde*	S	[17-21]
210	sinapyl alcohol*; syringylacetone; propiosyringone	S	[17-21]
212	dihydrosinapyl alcohol; syringic acid methyl ester	S	[17-20]
272	stilbene-type dimer	G-G dimer	[20, 21]
302	stilbene-type dimer	G-S dimer	[20, 21]
332	stilbene-type dimer	S-S dimer	[20, 21]
358	β-resinol type dimer	G-G dimer	[20, 21]
388	β-resinol type dimer	G-S dimer	[20, 21]
418	β-resinol type dimer	S-S dimer	[20, 21]

ArCo project setup Three of four fragments (5, 1C, 1D) had lost parts of their surfaces at some point after conservation with alum in the early 1900s, exposing the inner alum-rich core.

Thus it was possible to sample both alum-rich (surface) and alum-poor (core) zones before aging. Fragment 1B was also sampled in this way, even though we were less certain of the presence of distinct alum-rich and alum-poor zones (due to its slightly smaller dimensions). It was included as it had the poorest state of preservation of this set (very dark brown wood, little structural integrity such spontaneous loss of material occurred). The samples were aged for approximately 7 months in Denmark, as described under 'Artificial aging I'. After aging, fragments were sent to the University of Pisa to evaluate whether chemical changes during aging were induced by the co-presence of inorganic compounds. It is important to consider that the whole wood fragments were put into the climatic chamber and new samples were taken from the fragments after aging. Consequently, the samples before and after aging did not correspond exactly to the same spot of the fragment, although the same criteria were adopted for sampling. Since the variability of a complex heterogeneous system such as treated archaeological wood is high, the interpretation of the results after aging focused on significant differences only, with respect to non-aged samples, whereas minor differences were neglected. Methods used in ArCo included Py(HMDS)-GC/MS, FT-IR, SEM-EDX, XRD, ICP-OES, IC conductivity, most of which were applied before and after aging.

Artificial aging I. As a part of the ArCo study whole alum-treated fragments 5, 1B, 1C, 1D were exposed to artificial aging for approximately seven months (Oct. 2014 to May 2015) in a climate chamber at the Department of Conservation of the National Museum of Denmark (Brede, Denmark): the temperature was held at 30°C and the relative humidity cycled between 30% and 80% in 12 hour intervals.

Artificial aging II. Fresh birch and archaeological birch were treated with 2:1 parts alum : water by weight and by sulphuric acid at pH2 at 90C for 24 hours (and also for 40 hours for alum treatments on archaeological birch). Freeze dried samples of both fresh and archaeological woods served as controls. The sample overview is given in **Table 3.** After treatment all samples were divided into 2 groups: Aging (kept at 50C, 60% RH for 370 days) and Ambient (control group, kept at RT, 60% RH for 370 days). Colour measurements and infrared spectra were taken of samples at regular intervals. Two archaeological samples were analysed by ICP-OES-Procedure 1. Samples were also examined by SEM before and after aging, where the same spot was analyzed.

Colour measurement (Sections 3.5.2 and 3.6) was carried out using a Konica Minolta CM-700d handheld spectrophotometer, using the CIELAB (L*a*b*) colour space. Measurement diameter was 4 mm. The initial colour readings were taken after conditioning treated samples at 60% RH and room temperature for two weeks. The absolute change in colour, ΔE*, was calculated from the difference in coordinates L*, a*, b* from initial coordinates taken before aging. Human visual perception can distinguish colour change in ΔE*-values above approximately 3 [22]. The formula used to calculate ΔE is given below:

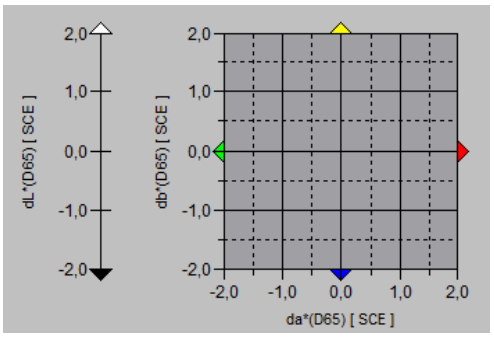

$$\Delta E^* = (\Delta L^{*2} + \Delta a^{*2} + \Delta b^{*2})^{1/2}$$

Moisture adsorption experiments (Section 3.4) were carried out at 20°C in a climate chamber (Termaks Series KB 8000FL, Bergen, Norway) at 30%, 40%, 50%, 60%, 70% and 75% RH. The water content was calculated from the equilibrium mass recorded at each step (RH_n-$RH_{initial}$), divided by the acclimatized starting weight at 30% RH ($RH_{initial}$):

$$\% \text{ moisture content} = \frac{(\text{mass at } RH_n - \text{mass at } RH_{initial})}{\text{mass at } RH_{initial}} \times 100\ \%$$

As experiments were only partly completed the weight gain due to water adsorption was normalized against the equilibrium mass at 30% RH. Despite the fact that experimental results represented only moisture uptake and results were not normalized to the dry wood mass, relative trends could nonetheless be observed.

GC-MS for the identification of free fatty acids profile GC/MS instrumentation consisted of an Agilent Technologies 6890N Gas Chromatograph coupled with a 5975 Mass Selective Detector single-quadrupole mass spectrometer. Samples were injected in splitless mode at 280 °C. GC separation was performed on a fused silica capillary column HP-5MS (J&W Scientific, Agilent Technologies, stationary phase 5% diphenyl-95% dimethyl-polysiloxane, 30 m length, 0.25 mm i.d., 0.25 µm film thickness). Chromatographic conditions were: initial temperature 80°C, 2 min isothermal, 10 °C/min up to 200°C, 4 min isothermal for the separation of unsaturated C18 fatty acids and their isomers, 6 °C/min up to 280°C, 40 minutes isothermal. The helium (purity 99.9995%) gas flow was set in constant flow mode at 1.2 mL/min. MS parameters: electron impact ionization (EI, 70 eV) in positive mode; ion source temperature 230°C; scan range 50-700 m/z; interface temperature 280°C. The injection volume was 2 µL.

High performance liquid chromatography/mass spectrometry for the identification of the triglyceride profile of lipids HPLC–ESI-Q-ToF analyses were carried out using a 1200 InfinityHPLC, coupled with a Quadrupole-Time of Flight tandem mass spec-trometer 6530 Infinity Q-ToF detector by a Jet Stream ESI interface(Agilent Technologies, U.S.A.).
The HPLC conditions were: Poroshell 120 EC-C18 column(3.0 mm × 50 mm, 2.7 µm particle size) with a Zorbax eclipse plusC-18 guard column (4.6 mm × 12.5 mm, 5 µm particle size); a flowrate of 0.3 mL min−1, an injection volume of 1 µL and a column temperature of 45◦C. Separation was achieved using a gradientof methanol (eluent A) and iso-propanol (eluent B). The elutiongradient was programmed as follows: 90% A for 5 min, followedby a linear gradient to 90% B in 25 min, then held for 5 min. Re-equilibration time for each analysis was 10 min.The ESI operating conditions were: drying gas (N2, purity>98%): 350◦C and 10 L min−1; capillary voltage 4.5 kV; nebulizergas 35 psig; sheath gas (N2, purity >98%): 375◦C and 11 L min−1.High resolution MS and MS/MS spectra were acquired in positivemode in the range 100–1700 m/z. The fragmentor was kept at 200 V,nozzle voltage 1000 V, skimmer 65 V, octapole RF 750 V, and thecollision energy for the MS/MS experiments was set at 50 V. Thecollision gas was nitrogen (purity 99.999%). The data were collectedby auto MS/MS acquisition with an MS scan rate of 1.03 spectra s−1and an MS/MS scan rate of 1.05 spectra s−1; only one precursor wasacquired per cycle (relative threshold 0.010%).

Analytical procedure for HPLC and GC-MS analyses: ~5 mg of each sample was subjected to extraction assisted by microwaves in a microwave oven Ethos One (Milestone, U.S.A.) (power 600 W), with 300 µL of a chloroform-hexane (3:2) mixture at 80°C for 25 min. The extracts were dried under a nitrogen stream, diluted with 600 µL of elution mixture, and filtered on a 0.45 µm PTFE filter (Grace Davison Discovery Sciences, U.S.A.) just before injection.
For the GC/MS analysis of samples, ~2-3 mg of the extract were subjected to microwaves assisted saponification (power 200 W) with 300 µL of KOH in EtOH 10% wt at 80 °C for 60 min. In order to maximize the extraction yield, two solvents were used: the neutral compounds were extracted with n-hexane (400 µL for three times); the residual solution was acidified with hydrochloric acid (6 M) and then carboxylic acids were extracted with diethyl ether (400 µL, three times). The two extracts (neutral + acidic fraction) were combined for GC/MS analysis in order to analyze them in a single chromatographic run, evaporated to dryness under nitrogen stream, and subjected to derivatization with 20 µL of N,O bistrimethyl-silyltrifluoroacetamide (BSTFA), 150 µL of iso-octane and 5 µL of tridecanoic acid solution (IS2) at 60 °C for 30 min. 5 µL of hexadecane solution (IS1) were added just before injection.

GC/MS Quantitative analysis: Quantitative analysis was performed using calibration curves calculated on the basis of selected ion monitoring (SIM) chromatograms: the selected ions for the SIM acquisition were: lauric acid m/z 117;257, suberic acid m/z 169;303, azelaic acid m/z

149;317, myristic acid m/z 117;285, sebacic acid m/z 149;331, palmitic acid m/z 117;313, oleic acid m/z 117;339, stearic acid m/z 117;341.
HPLC-EIS-Q-ToF quantitation, relative abundances were calculated on the basis of extract ion chromatograms, considering the isotopic distribution of the molecular species, and normalized to 100%.

3. Results

3.1. Sound wood

Py-GC/MS

Samples from sound wood were used as a reference for the interpretation of the data obtained from the analysis of archaeological wood samples.
Figure 2 shows the chromatographic profile obtained for sound oak wood sample. The peak identification is reported in Table 8.

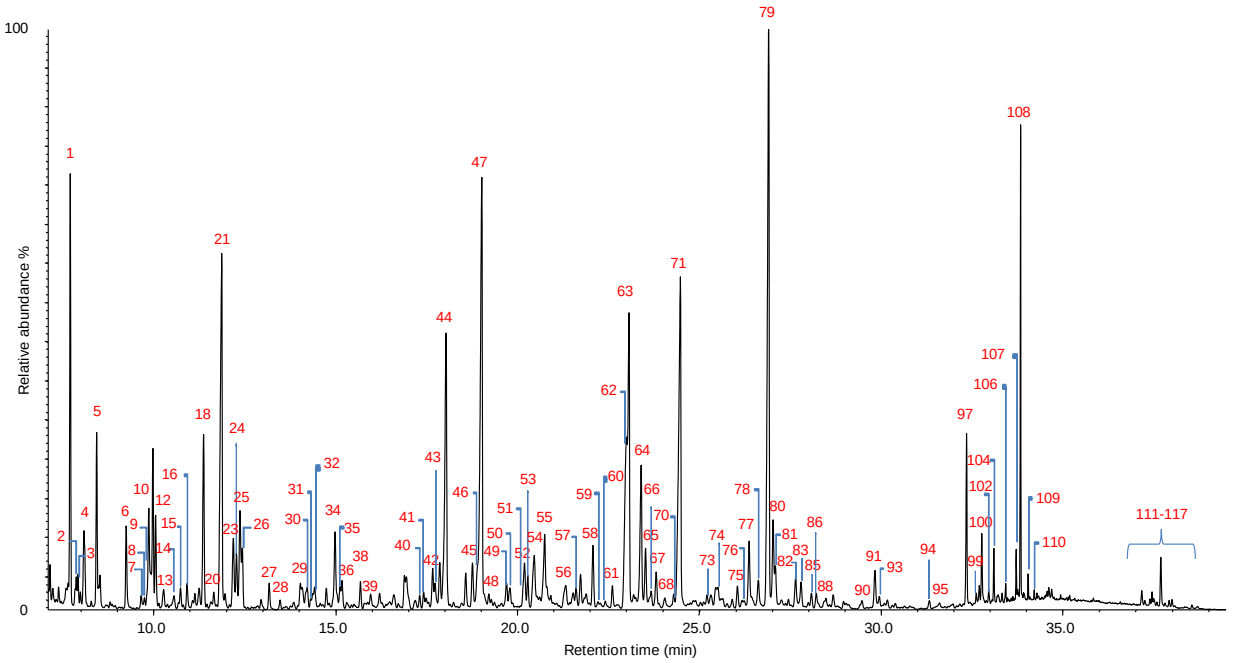

Figure 2 Pyrograms obtained by the Py(HMDS)-GC/MS analyses of oak wood reference sample. Numbers refer to compound numbers given in Table 8.

Table 8 reports a list of the 117 identified compounds. Some pyrolysis products are marked as “unknown”. In fact, the molecular structures of these pyrolysis products were not disclosed. Nevertheless, the analysis of holocellulose and lignin references allowed to attribute these pyrolysis products to the corresponding wood component, thus enabling these compounds to be used for further considerations.

Table 8 List of wood pyrolysis products identified by Py(HMDS)-GC/MS. H=Holocellulose, L=Lignin, G=Guaiacyl lignin, S=Syringyl lignin.

N°	Compound	m/z	Origin	Category
1	1,2-dihydroxyethane (2TMS)	73,103,147,191	H/L	Small molecules
2	2-hydroxymethylfuran (TMS)	53, 73, 81, 111, 125, 142, 155, 170	H	Furans
3	phenol (TMS)	75, 151, 166	L	Others
4	2-hydroxypropanoic acid (2TMS)	73, 117, 147, 190	H/L	Small molecules
5	2-hydroxyacetic acid (2TMS)	73, 147, 177, 205	H/L	Small molecules
6	1-hydroxy-1-cyclopenten-3-one (TMS)	53, 73, 81, 101, 111, 127, 155, 169	H	Cyclopentenones
7	3-hydroxymethylfuran (TMS)	53, 75, 81, 111, 125, 142, 155, 170	H	Furans
8	o-cresol (TMS)	73, 91, 135, 149, 165, 180	L	Others
9	2-furancarboxylic acid (TMS)	73, 95, 125, 169, 184	H	Furans
10	unknown holocellulose I	73, 152, 167	H	Others
11	m-cresol (TMS)	73, 91, 165, 180	L	Others
12	2-hydroxy-1-cyclopenten-3-one (TMS)	53, 73, 81, 101, 111, 127, 155, 170	H	Cyclopentenones
13	p-cresol (TMS)	73, 91, 165, 180	L	Others
14	3-hydroxy-(2H)-pyran-2-one (TMS)	75, 95, 125, 151, 169, 184	H	Pyranones
15	unknown holocellulose II	59, 73, 85, 101, 115, 131, 159	H	Others
16	unknown holocellulose III	73, 85, 103, 115, 129, 145, 173, 188	H	Others
17	*Z*-2,3-dihydroxycyclopent-2-enone (TMS)	59, 73, 115, 143, 171, 186	H	Cyclopentenones
18	*E*-2,3-dihydroxycyclopent-2-enone (TMS)	75, 101, 143, 171, 186	H	Cyclopentenones
19	1,2-dihydroxybenzene (TMS)	75, 91, 136, 151, 167, 182	H	Hydroxybenzenes
20	3-hydroxy-(4H)-pyran-4-one (TMS)	75, 95, 139, 151, 169, 184	H	Pyranones
21	5-hydroxy-(2H)-pyran-4(3H)-one (TMS)	59, 75, 101, 129, 143, 171, 186	H	Pyranones
22	2-hydroxymethyl-3-methy-2-cyclopentenone (TMS)	73, 103, 129, 173, 183, 198	H	Cyclopentenones
23	1-hydroxy-2-methyl-1-cyclopenten-3-one (TMS)	73, 97, 125, 139, 169, 184	H	Cyclopentenones
24	1-methy-2-hydroxy-1-cyclopenten-3-one (TMS)	73, 97, 125, 139, 169, 184	H	Cyclopentenones
25	1,3-dihydroxyacetone (2TMS)	73, 103, 147, 189, 219	H	Small molecules
26	guaiacol (TMS)	73, 151, 166, 181, 196	G	Short chain
27	unknown holocellulose IV	73, 217, 232	H	Others
28	3-hydroxy-6-methyl-(2H)-pyran-2-one (TMS)	73, 109, 139, 168, 183, 198	H	Pyranones
29	unknown holocellulose V	73, 101, 116, 131, 173	H	Others
30	2-methyl-3-hydroxy-(4H)-pyran-4-one (TMS)	73, 101, 153, 183, 198	H	Pyranones
31	2-methyl-3-hydroxymethyl-2-cyclopentenone (TMS)	73, 103, 129, 173, 183, 198	H	Cyclopentenones
32	2,3-dihydrofuran-2,3-diol (2TMS)	73, 147, 231, 246	H	Furans
33	2-furylhydroxymethylketone (TMS)	73, 81, 103, 125, 183, 198	H	Furans
34	5-hydroxymethyl-2-furaldehyde (TMS)	73, 81, 109, 111, 139, 169, 183, 198	H	Furans
35	4-methylguaiacol (TMS)	73, 149, 180, 195, 210	G	Short chain
36	1,2-dihydroxybenzene (2TMS)	73, 151, 239, 254	H	Hydroxybenzenes
37	2-hydroxymethyl-2,3-dihydropyran-4-one (TMS)	73, 142, 170, 185, 200	H	Pyranones
38	1,4:3,6-dianhydro-α-D-glucopyranose (TMS)	73, 103, 129, 155, 170, 171, 186	H	Anhydrosugars
39	Z-2,3-dihydroxycyclopent-2-enone (2TMS)	73, 147, 230, 243, 258	H	Cyclopentenones
40	4-methylcatechol (2TMS)	73,180, 253, 268	G	Demethylated/demethoxylated
41	4-ethylguaiacol (TMS)	73, 149, 179, 194, 209, 224	G	Short chain
42	syringol (TMS)	73, 153, 181, 196, 211, 226	S	Short chain
43	1,4-dihydroxybenzene (2TMS)	73, 112, 239, 354	H	Hydroxybenzenes
44	arabinofuranose (4TMS)	73, 147, 217, 230	H	Anhydrosugars

45	4-vinylguaiacol (TMS)	73, 162, 177, 192, 207, 222	G	Short chain
46	3-hydroxy-2-hydroxymethyl-2-cyclopentenone (2TMS)	73, 147, 257, 272	H	Cyclopentenones
47	*E*-2,3-dihydroxycyclopent-2-enone (2TMS)	73, 147, 243, 258	H	Cyclopentenones
48	4-ethylcatechol (2TMS)	73, 147, 179, 231, 267, 282	G	Demethylated/demethoxylated
49	3-hydroxy-2-(hydroxymethyl)cyclopenta-2,4-dienone (2TMS)	73, 147, 255, 270	H	Cyclopentenones
50	eugenol (TMS)	73, 147, 179, 206, 221, 236	G	Long chain
51	4-methylsyringol (TMS)	73, 167, 210, 225, 240	S	Short chain
52	3-methoxy-1,2-benzenediol (2TMS)	73, 153, 254, 269, 284	S	Demethylated/demethoxylated
53	3,5-dihydroxy-2-methyl-(4H)-pyran-4-one (2TMS)	73, 128, 147, 183, 271, 286	H	Pyranones
54	1,6-anhydro-β-D-glucopyranose (TMS at position 4)	73, 103, 117, 129, 145, 155, 171	H	Anhydrosugars
55	1,6-anhydro-β-D-glucopyranose (TMS at position 2)	73, 101, 116, 129, 132, 145, 155, 171	H	Anhydrosugars
56	*Z*-isoeugenol (TMS)	73, 179, 206, 221, 236	G	Long chain
57	vanillin (TMS)	73, 194, 209, 224	G	Carbonyl
58	1,2,3-trihydroxybenzene (3TMS)	73, 133, 147, 239, 327, 342	H	Hydroxybenzenes
59	5-methyl-3-methoxy-1,2-benzenediol (2TMS)	73, 151, 210, 253, 268, 283, 298	S	Demethylated/demethoxylated
60	4-ethylsyringol (TMS)	73, 191, 209, 224, 239, 254	S	Short chain
61	*E*-isoeugenol (TMS)	73, 179, 206, 221, 236	G	Long chain
62	1,4-anhydro-D-galactopyranose (2TMS)	73, 101, 116, 129, 145, 155, 171, 217	H	Anhydrosugars
63	1,6-anhydro-D-galactopyranose (2TMS)	73, 101, 116, 129, 145, 189, 204, 217	H	Anhydrosugars
64	2-hydroxymethyl-5-hydroxy-2,3-dihydro-(4H)-pyran-4-one (2TMS)	73, 129, 147, 155, 183, 273, 288	H	Pyranones
65	4-vinylsyringol (TMS)	73, 179, 222, 237, 252	S	Short chain
66	1,4-anhydro-D-glucopyranose (2TMS at position 2,4)	73, 101, 116, 129, 155, 191, 204, 217	H	Anhydrosugars
67	1,2,4-trihydroxybenzene (3TMS)	73, 133, 147, 239, 327, 342	H	Hydroxybenzenes
68	acetovanillone (TMS)	73, 193, 208, 223, 238	G	Carbonyl
69	4-hydroxybenzoic acid (2TMS)	73, 147, 193, 223, 267, 282	L	Acids
70	4-propenylsyringol (TMS)	73, 205, 236, 251, 266	S	Long chain
71	1,6-anhydro-β-D-glucopyranose (2TMS at position 2,4)	73, 101, 116, 129, 155, 191, 204, 217	H	Anhydrosugars
72	vanillic acid methyl ester (TMS)	73, 193, 224, 239, 254	G	Esters
73	5-vinyl-3-methoxy-1,2-benzenediol (2TMS)	73, 147, 179, 222, 280, 295, 310	S	Demethylated/demethoxylated
74	*Z*-4-isopropenylsyringol	73, 205, 236, 251, 266	S	Long chain
75	1,4-anydro-D-galactopyranose (3TMS)	73, 129, 147, 191, 204, 217, 243, 332	H	Anhydrosugars
76	unknown lignin I	73, 147, 193, 239, 313, 401, 416	L	Others
77	syringaldehyde (TMS)	73, 224, 239, 254	S	Carbonyl
78	2,3,5-trihydroxy-4H-pyran-4-one (3TMS)	73, 147, 239, 255, 270, 330, 345, 360	H	Pyranones
79	1,6-anhydro-β-D-glucopyranose (3TMS)	73, 129, 147, 191, 204, 217, 243, 333	H	Anhydrosugars
80	1,4-anhydro-D-glucopyranose (3TMS)	73, 129, 147, 191, 204, 217, 243, 332	H	Anhydrosugars
81	*E*-4-isopropenylsyringol (TMS)	73, 205, 236, 251, 266	S	Long chain
82	1,6-anhydro-β-D-glucofuranose (3TMS)	73, 129, 147, 191, 204, 217, 243, 319	H	Anhydrosugars
83	unknown lignin II	73, 179, 217,342, 358, 415, 430	L	Others
84	unknown lignin III	73, 147, 193, 239, 313, 401, 416	L	Others
85	vanillic acid (2TMS)	73, 253, 282, 297, 312	G	Acids
86	acetosyringone (TMS)	73, 223, 238, 253, 268	S	Carbonyl
87	5-propyl-3-methoxy-1,2-benzenediol (2TMS)	73, 147, 179, 209, 296, 311,	S	Demethylated/demethoxyla

		326		ted
88	coumaryl alcohol (2 TMS)	73, 189, 205, 267, 279, 294	G	Demethylated/demethoxylated
89	syringic acid methyl ester (TMS)	73, 223, 254, 269, 284	S	Esters
90	vanillylpropanol (2TMS)	73, 179, 206, 221, 236, 311, 326	G	Long chain
91	*Z*-coniferyl alcohol (2 TMS)	73, 204, 252, 293, 309, 324	G	Monomers
92	4-hydroxy-3,5-dimethoxycinnamic acid methyl ester (TMS)	73, 147, 179, 222, 280, 295, 310	S	Esters
93	coniferylaldehyde (TMS)	73, 192, 220, 235, 250	G	Carbonyl
94	trihydroxycinnamyl alcohol (3TMS)	73, 147, 210, 254, 368, 383, 398	S	Demethylated/demethoxylated
95	syringic acid (2TMS)	73, 253, 297, 312, 327, 342	S	Acids
96	unknown lignin IV	73, 179, 209, 237, 280, 310, 325, 340	L	Others
97	*E*-coniferyl alcohol(2 TMS)	73, 204, 235, 293, 309, 324	G	Monomers
98	3,4-dihydroxy-5-methoxybenzoic acid (3TMS)	73, 137, 147, 223, 253, 297, 385, 400	S	Acids
99	syringylpropanol (2TMS)	73, 210, 240, 341, 356	S	Long chain
100	*Z*-sinapyl alcohol (2TMS)	73, 234, 323, 339, 354	S	Monomers
101	unknown lignin V	73, 179, 209, 237, 280, 310, 325, 340	L	Others
102	3,4-dihydroxycinnamyl alcohol (3TMS)	73, 205, 293, 355, 382	G	Demethylated/demethoxylated
103	trihydroxycinnamyl alcohol I (3TMS)	73, 147, 210, 254, 368, 383, 398	S	Demethylated/demethoxylated
104	sinapylaldehyde (TMS)	73, 222, 250, 265, 280	S	Carbonyl
105	trihydroxycinnamyl alcohol II (3TMS)	73, 147, 210, 254, 368, 383, 398	S	Demethylated/demethoxylated
106	*Z*-2-methoxy-3,4-dihydroxycinnamyl alcohol (3TMS)	73, 235, 323, 385, 412	S	Demethylated/demethoxylated
107	synapyl alcohol (TMS)	73, 234, 251, 267, 282	S	Monomers
108	*E*-sinapyl alcohol (2TMS)	73, 234, 323, 339, 354	S	Monomers
109	*E*-2-methoxy-3,4-dihydroxycinnamyl alcohol (3TMS)	73, 235, 323, 385, 412	S	Demethylated/demethoxylated
110	unknown lignin VI	73, 147, 196, 253, 355, 370	L	Others
111	unknown anhydrosugar I (dimer)	73, 103, 117, 147, 177, 189, 303, 347	H	Anhydrosugars
112	unknown anhydrosugar II (dimer)	73, 103, 117, 129, 147, 204, 217, 361	H	Anhydrosugars
113	unknown anhydrosugar III (dimer)	73, 117, 129, 147, 204, 217, 223, 361	H	Anhydrosugars
114	unknown anhydrosugar IV (dimer)	73, 117, 129, 147, 204, 217, 243, 273	H	Anhydrosugars
115	unknown anhydrosugar V (dimer)	73, 117, 129, 147, 190, 204, 347, 352	H	Anhydrosugars
116	unknown anhydrosugar VI (dimer)	73, 117, 129, 147, 204, 217, 289, 361	H	Anhydrosugars
117	unknown anhydrosugar VII (dimer)	73, 117, 129, 147, 204, 217, 289, 361	H	Anhydrosugars

The evaluation of the degradation state of wood is always based on a comparison between archaeological and sound wood of the same genus. One of the most widely accepted parameters to estimate wet archaeological wood preservation is the ratio between holocellulose (H) and lignin (L) content: the differences between the H/L ratio obtained for sound and archaeological wood of the same genus can be used to estimate the extent of degradation [23, 24]. Estimation of the content of wood components using pyrolysis coupled with gas chromatography and mass spectrometry is obtained by integrating selected chromatographic peak areas. To calculate the pyrolytic H/L ratio, the peak areas are normalised with respect to sum of the areas of all peaks considered, obtaining a percentage value for each peak. The sum of the percentage areas of holocellulose pyrolysis products is then calculated as well as for lignin pyrolysis products, and the ratio between these two values is the pyrolytic H/L ratio. The calculation and the interpretation of results are based on three important assumptions:

- the pyrolytic H/L ratio does not express the exact content of holocellulose of lignin, but just an estimation of it;
- the values cannot be used as absolute values but their validity and usefulness is related to the comparison with the value obtained from a sound wood of the same species. Since the calculations are performed in the same way for sound and degraded wood, the pyrolytic H/L ratio is consequently reliable to evaluate degradation.

For the sound reference wood samples, the pyrolytic H/L ratios were listed in Table 9 below.

Table 9 H/L ratios calculated for the reference wood samples

	Sound Alder	Sound Aspen	Sound Birch	Sound Maple	Sound Oak
H/L	1.77	2.02	3.13	1.39	3.72
SD	0.04	0.04	0.39	0.12	0.21

The results showed that the H/L ratios of sound woods ranged from 3.72 to 1.39, depending on the wood genus.

In order to investigate the alterations of the single biopolymers more in detail we considered the various pyrolysis reaction pathways undergone by lignin and carbohydrates [25].

Five categories were selected for holocellulose pyrolysis products: furans, cyclopentenones, pyranones, hydroxybenzenes and anhydrosugars. Seven categories were selected for lignin pyrolysis products: short side chain aromatic compounds (guaiacyl and syringyl units with up to C2 alkyl substituent on the aromatic ring), long side chain compounds (guaiacyl and syringyl units with C3 alkyl substituent on the aromatic ring), monomers (coniferyl and sinapyl alcohols, which show an unaltered side chain), carbonyl compounds (guaiacyl and syringyl units containing aldehyde and ketone functionalities), carboxyl compounds (guaiacyl and syringyl units containing acid and ester functionalities), demethylated compounds (guaiacyl and syringyl units in which one or more methyl groups were removed from the methoxy substituents) and others.

In fact, during the pyrolysis of lignin, the formation of the monomers (coniferyl and sinapyl alcohols) is the first pyrolytic reaction, due to the predominant initial cleavage of the β-ether bonds among the various phenylpropane units. Reactions involving conversion/alteration of the side-chain and the methoxy substituents on the aromatic ring are secondary reactions, which lead to the formation of guaiacyl and syringyl units with shorter side chains and different functionalities [26-29]. Wood pyrolysis products divided into categories are presented in Table 8, while in Figures 3 and 4 are shown the distributions of lignin and holocellulose pyrolysis products respectively, expressed as percentages in the samples of reference wood. The monomers are the more abundant products in the sound wood and varied from 44% in the alder, 38% in the birch and maple to 32% in the aspen and oak. The acids are less abundant, around 3-4% except for the Aspen – 10%. The particularity of the aspen wood is that we found together with the usual acids as vanilic and syringic also the p-hydroxy benzoic acid, not present in the other species.

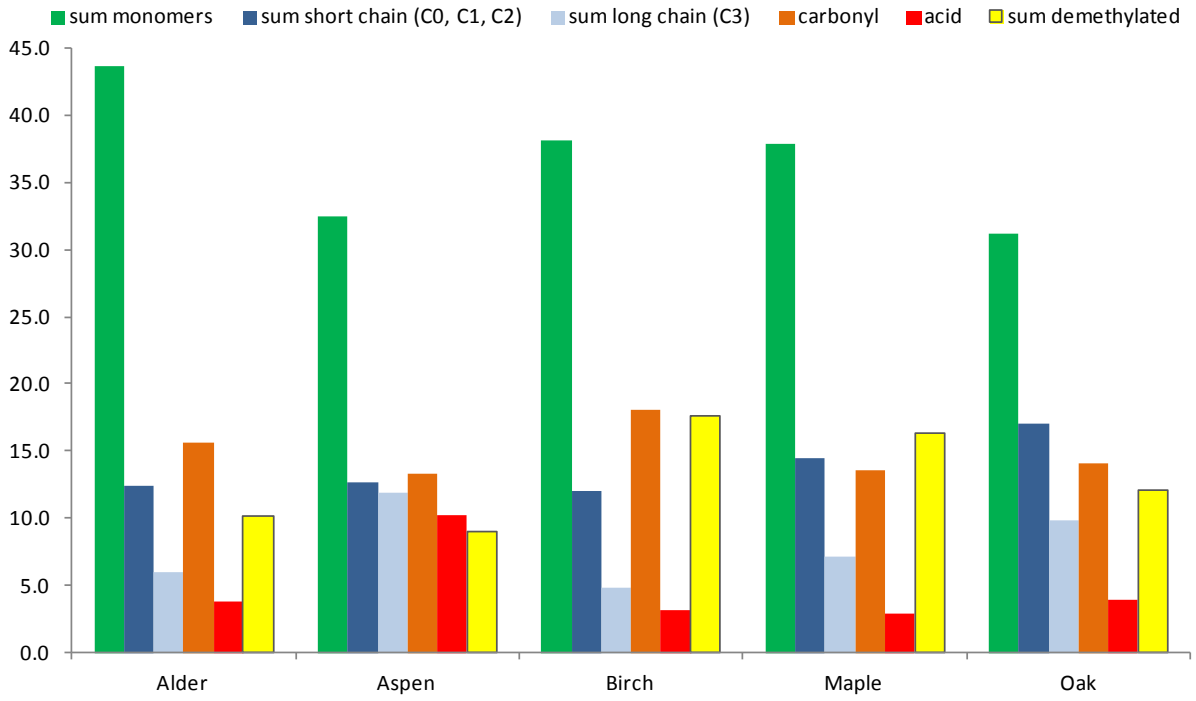

Figure 3 Distribution of categories of lignin pyrolysis products expressed as percentages in the samples of reference wood samples.

Also the compounds with long chain (3 carbon atoms) as eugenol, propyl syringol, vanillylpropanol and syringilpropanol and carbonyl compounds (vanillin, acetovanillone, synapylaldehyde, acetosyringone, coniferylaldehyde and syringaldehyde) are more abundant in sound aspen than in the other species.

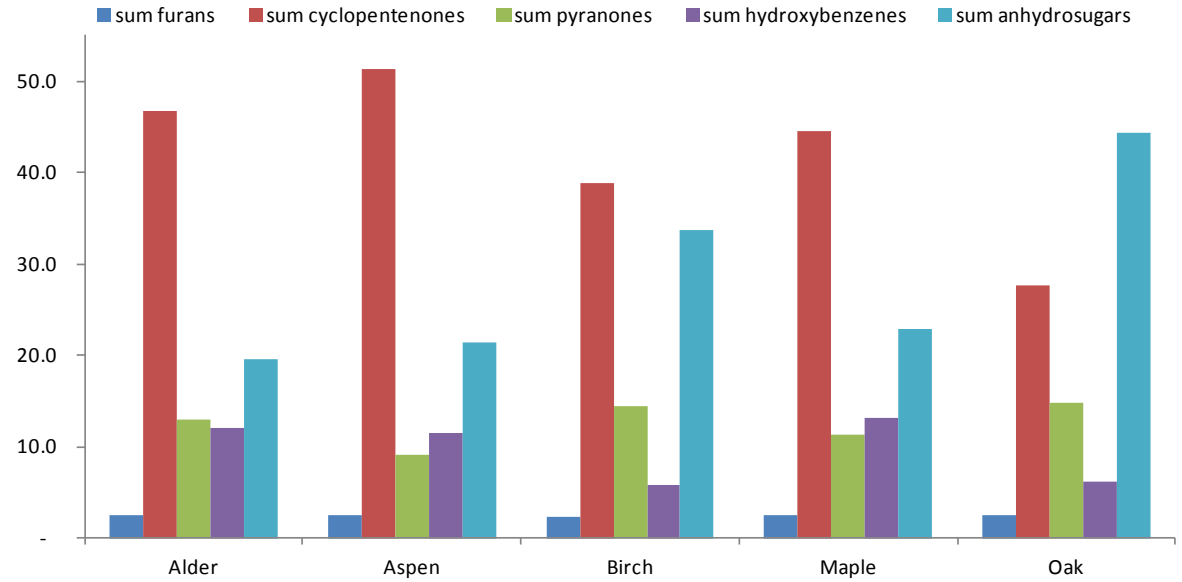

Figure 4 Distribution of categories of holocellulose pyrolysis products expressed as percentages in the samples of reference wood samples.

Regarding holocellulose pyrolysis products (Figure 4), the most different distribution of categorized pyrolysis products can be observed for the oak wood. Generally, The most abundant in sound wood are the group of cyclopentenones, the second group more abundant

are anhydrosugars, while in the oak wood contrary to the other species the anhydrosugars are the higher than cyclopentenones.

Infrared analyses sound wood

Four fresh diffuse porous hardwoods were compared: maple, aspen, birch and alder. Figure 5 shows that the four diffuse porous woods do not exhibit great differences in their spectra – their relative band intensities and assignments are almost identical. Therefore the spectrum for birch has been chosen to be discussed in detail.

The main bands usually attributed to pure carbohydrates occur at: 1733, 1371, 1157 and 897 cm^{-1}, which are distinct in undeteriorated woods. The bands assigned to lignin occur at 1592 and 1504 cm^{-1} and are due to aromatic skeletal vibrations, with the band at 1592 cm^{-1} also containing signals for C=O stretches. A minor, broad band at ca 1642 cm^{-1} is attributed to adsorbed water's OH stretches and conjugated carbonyl stretches for carbohydrates.

All other bands, 1460, 1423, 1327, 1237 and 1031 cm^{-1} are combination bands, that is they contain information from both lignin and carbohydrates. Assignments are described in more detail in Table 6.

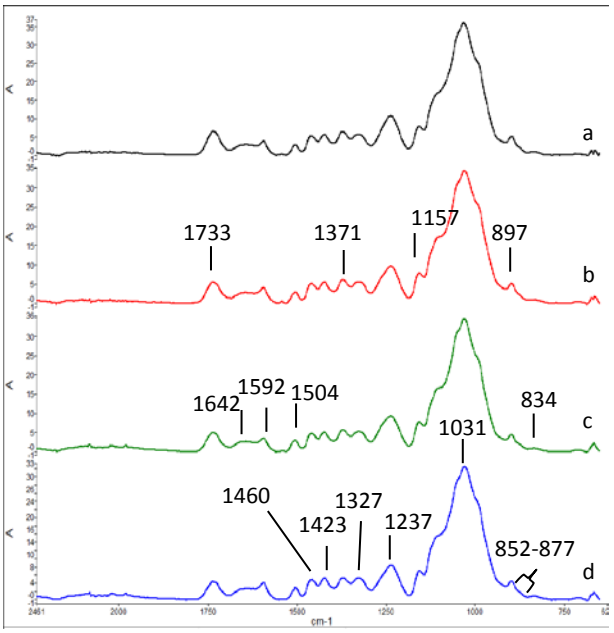

Figure 5 Spectra from fresh diffuse porous woods: a) birch b) aspen c) alder d) maple

3.2. Untreated archaeological wood

Bacterial degradation during burial reduces the mass of wood, as shown in Figure 6 below, comparing sound wood with archaeological wood. The brighter images (greater attenuation of X-rays) obtained from the wood cells from fresh birch indicated the presence of more wood mass relative to the archaeological sample. Figure 7 shows the 3D-reconstruction of the neutron image.

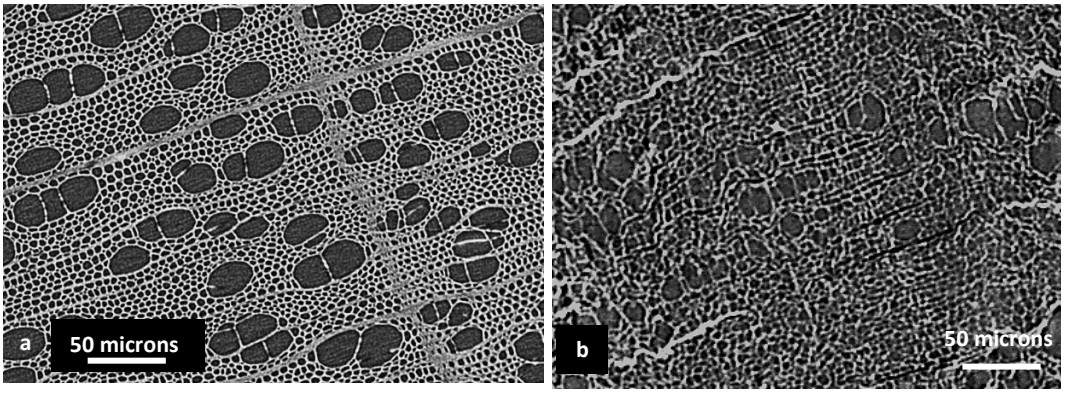

Figure 6 Both images were taken at the same X-ray exposure, TOMCAT. a) Fresh birch; b) Archaeological aspen. The greater attenuation in the fresh birch (the image is brighter) indicates a greater wood density, and hence better state of preservation.

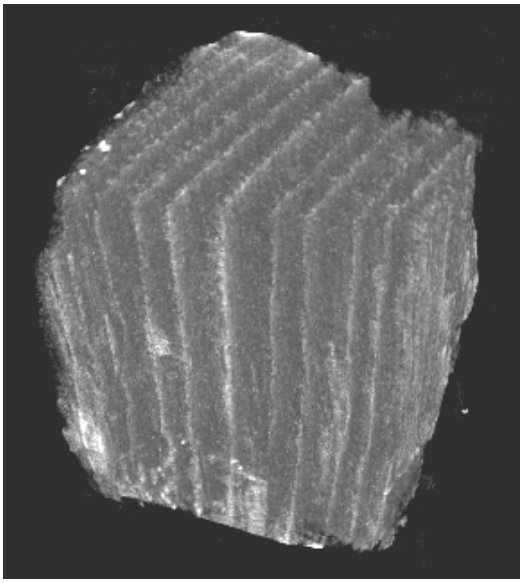

Figure 7 Reconstructed 3D neutron-image (at ICON) of untreated, freeze dried archaeologocial aspen. Growth rings are shown as the bright lines. Sample size was ca 12 mm^3.

Py-GC/MS

Two non-alum-treated samples from Oseberg collection were analysed, one from Oseberg ship (arch-oak wood) and the other from the animal head post nr. 124 (arch-maple wood). One archaeological aspen sample excavated from the site Presterød, Tønsberg, Vestfold county, in 2005 and dated to the Viking Age were also analysed. In Table 10 the pyrolytic H/L ratios were listed.

Table 10 H/L ratios calculated for untreated archaeological wood samples

	Arch-aspen	Arch-maple	Arch-oak
H/L	0.19	0.53	2.32
SD	0.02	0.02	0.20

Results obtained for the untreated archaeological oak sample (Arch-oak) from the Oseberg ship showed a quite high H/L ratio 2.32. The comparison of this value with the H/L ratio of sound oak wood (3.72) indicated a loss of holocellulose of around 10%, suggesting a very good state of preservation of analysed fragment. Arch-maple and Arch-aspen showed H/L ratios 0.53 and 0.19 respectively, which, when compared to the values obtained for the corresponding sound woods (1.39 and 2.02 respectively), were indicative of an extensive loss of carbohydrates.

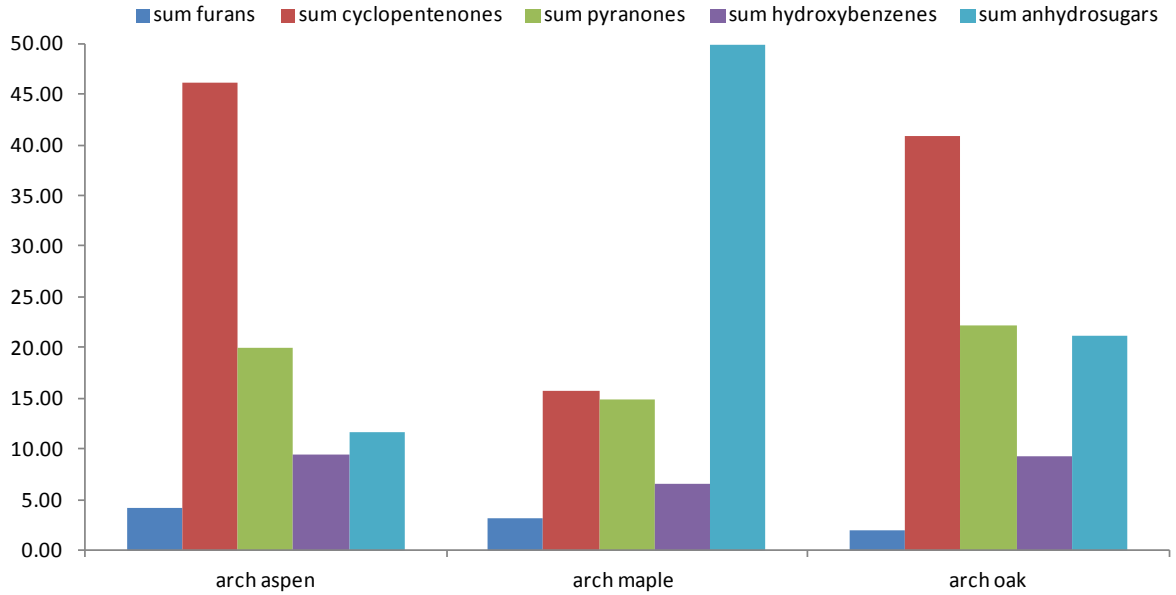

Figure 8 Distribution of categories of holocellulose pyrolysis products expressed as percentages in the samples of archaeological wood samples NOT treated with alum.

When we analyse the distribution of holocellulose categories (Figure 8) of less degraded from oak wood we observed the decrease of anhydrosugars with respect to the sound wood (Figure 4), while other categories remain unchanged. Archaeological wood from the object 124 (arch-maple) present the quite changed the distribution of holocellulose categories, in particular very high abundant of anhydrosugars, normally increased when the polymers as cellulose and hemicelluloses are partially depolymerised. Very strange behaviour is observed for the aspen wood sample. Despite most degraded among them (very low H/L ratio) it presents distribution of holocellulose categories very similar to that of sound wood (Figure 4). This behaviour is significant and due not only to the depolymerisation of holocellulose but also to the loss of wooden material.

Regarding the lignin degradation state. For the untreated archaeological woods (Figure 9), Arch-oak (from the Oseberg ship) showed a distribution of lignin pyrolysis products almost identical to that obtained for sound oak, confirming the good chemical state of preservation of this sample. This was also reflected in its physical condition, which retained a high structural integrity despite the fact that it possessed only ≈30% of its bending strength relative to sound oak [30]. Arch-maple (sample 124) showed a decrease in monomers and an increase in short chain and acidic compounds relative to sound maple. This indicated that lignin degradation processes, such as depolymerisation and oxidation occurred in this sample to a moderate extent [25]. The observed deterioration was likely due to a combination of degradation initiated during burial period with alteration occurred post-excavation. Arch-aspen did not show significant differences in lignin distribution with respect to sound aspen, except for a slight increase in carbonyl compounds.

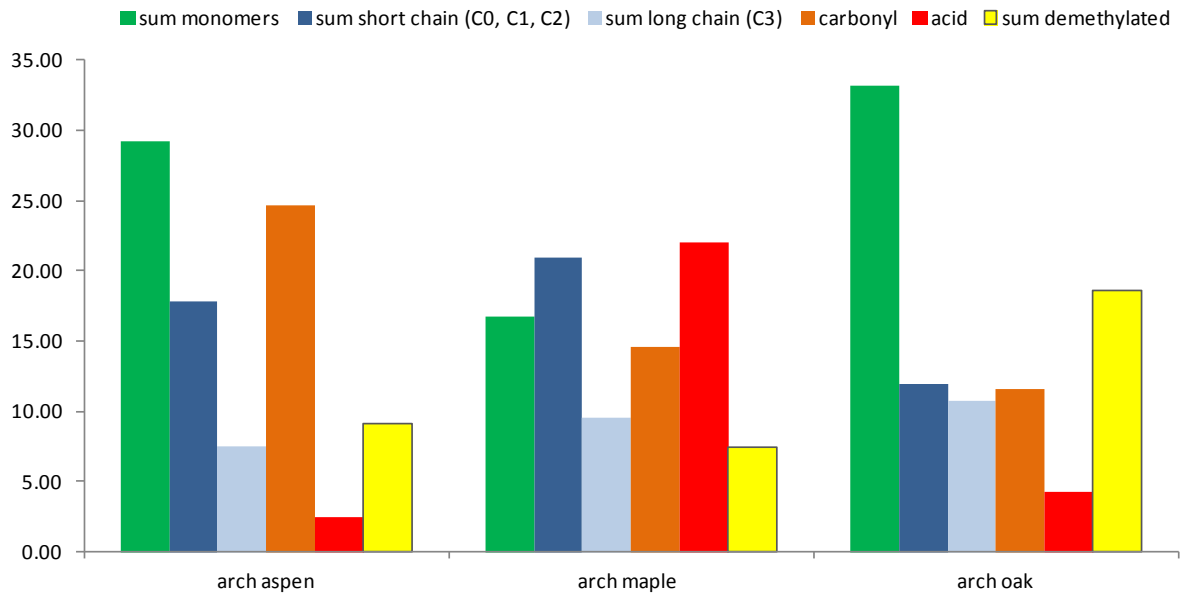

Figure 9 Distribution of categories of lignin pyrolysis products expressed as percentages in the samples of archaeological wood samples NOT treated with alum.

Infrared analyses

Figure 10 illustrates infrared spectra of untreated diffuse porous archaeological woods, showing that they have undergone similar deterioration trends. Untreated archaeological samples are generally characterized by changes due to loss of holocellulose relative to sound wood, demonstrated in reduced band intensities at 1733, 1371, 1156 and 897 cm^{-1} in deteriorated wood (Figure 11). The resulting decrease in holocellulose content causes the enhancement of lignin bands at 1594, 1506 cm^{-1} and the emergence of new bands at 1266, 1220 and 1120 cm^{-1}.
Although bands at 1031 cm^{-1} and 1122 cm^{-1} contain signals from both carbohydrate and lignin, it appears as though signals from lignin dominate band 1122 cm^{-1} and those from carbohydrate dominate the band at 1031 cm^{-1}. It should be noted that in the archaeological birch sample, the height of the band at 1031 cm^{-1} is greater than that at 1122 cm^{-1}. The height-ratio from these two bands (1123/1030) appears to increase with visible deterioration, a trend especially apparent in heavily degraded woods, as will be shown later.
Figure 12 clearly shows that the Oseberg maple has undergone greater deterioration than the archaeological birch. This is reflected in the broadening of the region assigned to carbonyl groups (1650-1775 cm^{-1}) as well as in the increase in the band height ratio 1121/1028, relative to archaeological birch. The higher amount of oxidized compounds in the Oseberg sample may be attributed either to the fact that its original condition differed greatly from that of the archaeological birch, or it may be related to its natural aging 100 years after excavation in a 'normal' museum environment.

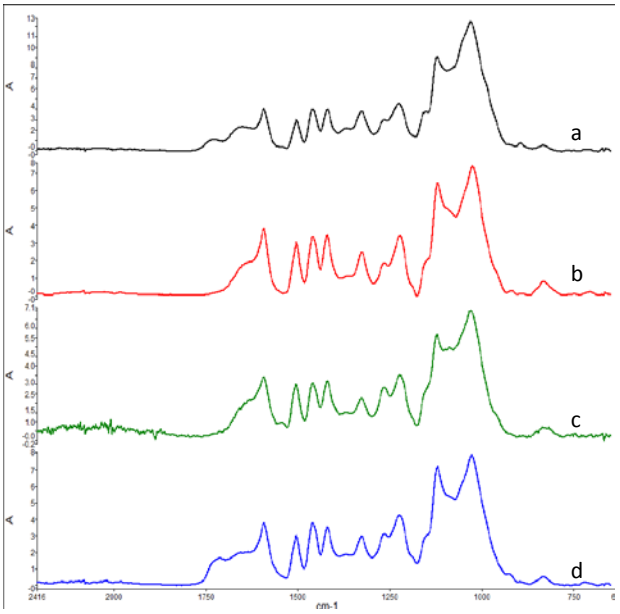

Figure 10 Spectra from untreated archaeological woods: All had been recently excavated except for the sample from Oseberg a) birch b) aspen c) alder d) maple (Oseberg, nr. 124)

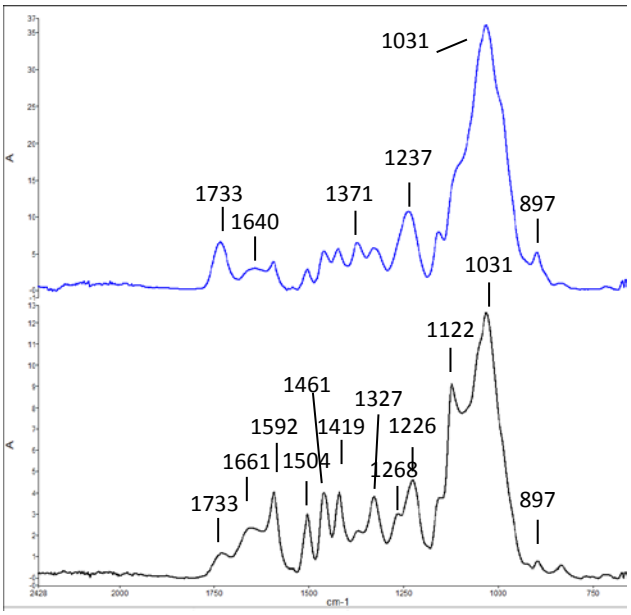

Figure 11 Fingerprint region of fresh birch (top) and archaeological birch (below).

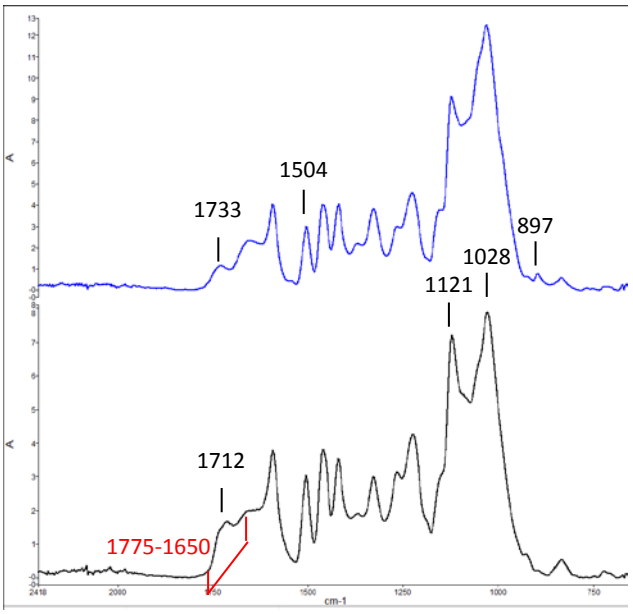

Figure 12 Fingerprint region of archaeological birch (top) and the untreated Oseberg sample (nr. 124, maple) (below).

3.3 Alum-treated wood

3.3.1 Archaeological wood treated with alum in 2009

This sample – archeological aspen treated with alum in 2009 (4B-alum-2009) – was a part of the model studies of alum-treated wood, which is presented in Section 3.5.1. Here results of analytical pyrolysis, undertaken 5 years after its alum treatment are presented. This sample serves as a reference representing the 'intial condition' of the Oseberg samples when first conserved (or short term effects of the alum treatment). This is a valid comparison, based on past descriptions of freshly treated woods with alum (pale, hard, heavy), which are similar to that obtained in 2009 [31].
The alum treatment was performed by heating a concentrated solution of alum salt to 90°C. The waterlogged wood fragment was immersed in the bath for 24 hours. The concentration used was 2:1 alum-water (w/w), according to the Oseberg records [31].

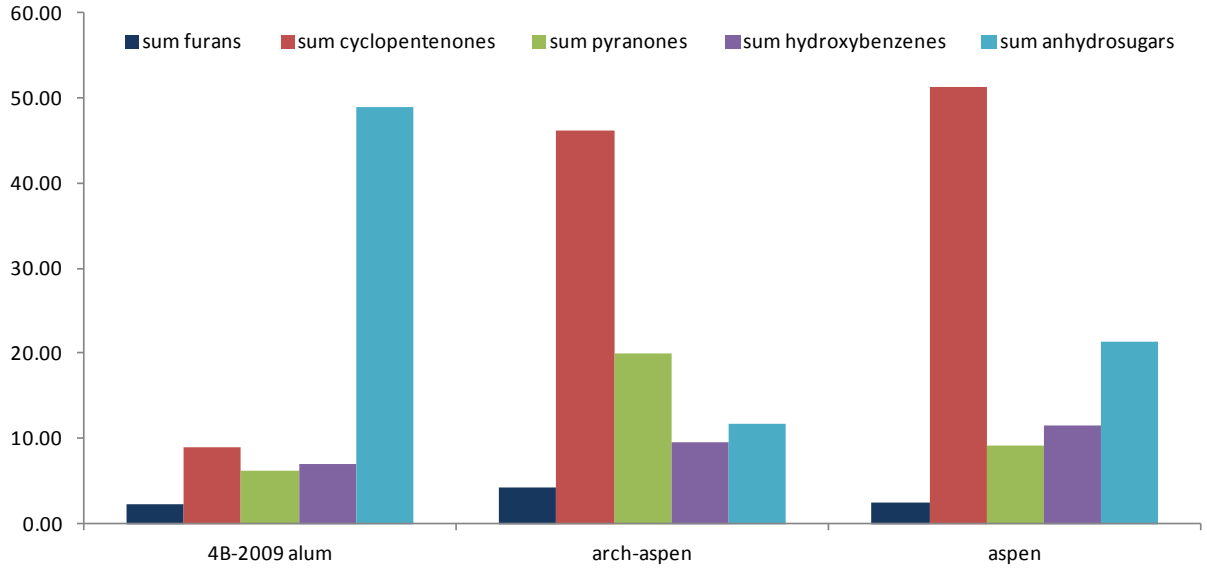

Figure 13 Distribution of categories of holocellulose pyrolysis products expressed as percentages in the samples of archaeological aspen treated with alum, untreated archaeological aspen and sound aspen samples.

The archaeological aspen sample treated with alum in 2009 showed an H/L ratio significantly higher (0.49) than the untreated arch-aspen (0.19). This difference between two samples, sampled from the same piece of wood before and after treatment, is probably due to the extractive procedure of wet alum treatment, which washes away altered part of material. (Lignin is insoluble in water, while solubility of vanillic acid 1500 mg/L (at 14 °C), syringic acid 5780 mg/L (at 25 °C) in water)
Despite lower values of H/L showed that the sample of untreated archaeological wood was more degraded, the more altered polymer structure can be observed for the alum-treated wood (Figure 13). We observe very low abundance of cyclopentenones ( ) with respect to the sound wood samples and at the same time increased abundance of anhydrosugars ( ), contrary to the untreated wood which shows the profile very similar to the sound aspen.

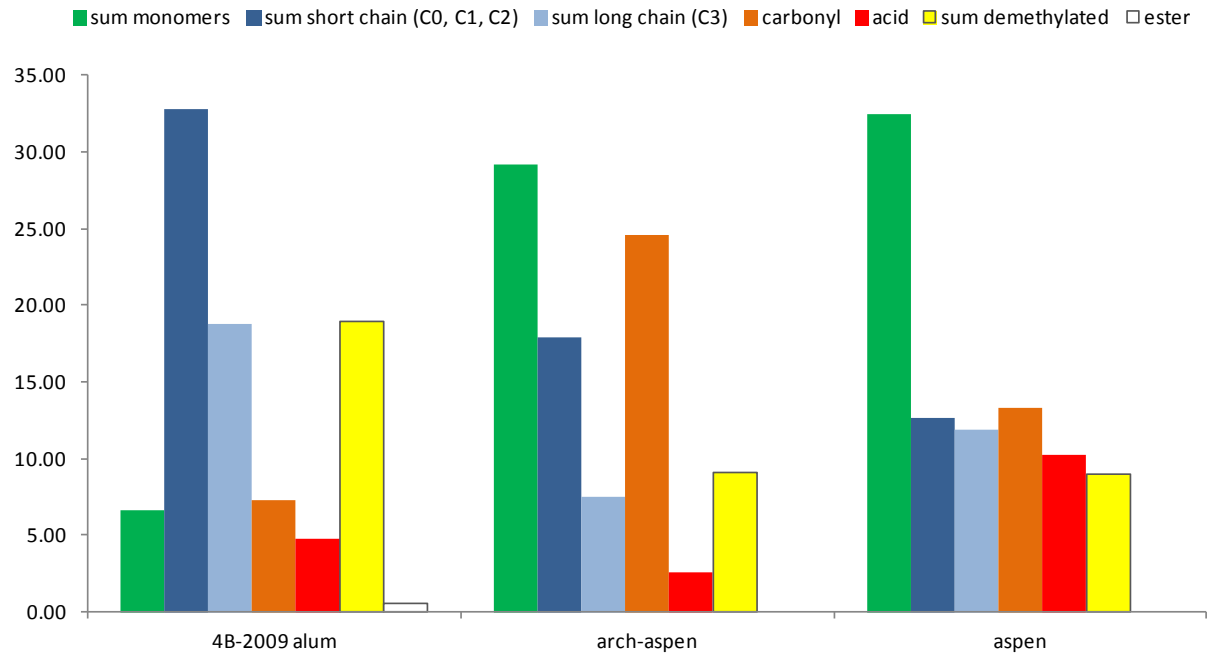

Figure 14 Distribution of categories of lignin pyrolysis products expressed as percentages in the samples of archaeological treated with alum, archaeological untreated and sound wood samples.

From lignin point of view (Figure 14) alum treatment induce depolymerisation processes observed from increasing of components with shorter side chain ( ) together with demetylated/demethoxylated pyrolysis products ( ) with respect to untreated archaeological wood sample. The presence of higher abundance of carbonyl pyrolysis products ( ) in untreated sample with respect to alum-treated is probably due to alum treatment, in particular the acidic components, together with the other molecular fragments were partially extracted (physically) during the procedure (wet procedure) in sample "4B-2009 alum".

3.3.2 Oseberg's 185-series

Six archaeological wood samples from the Oseberg find treated with alum salts some time during the period 1905-12 were collected from six slices which originally fit together in a weaving loom. They were named the '185-series' and were numbered from 185-1 to -6. This object had fallen apart (Figure 15) at some point before or after its treatment and had an interesting variability in condition: slice 185-1 was in best visual condition while 185-6 was in worst condition: increasing darkening and decreasing structural integrity from samples 185-1 to -6. Microscopic observations allowed to establish that the wood was diffuse porous, likely birch or alder.

Figure 15 Archaeological alum-treated samples from the 185 series

X-ray tomographic microscopy and Neutron tomography

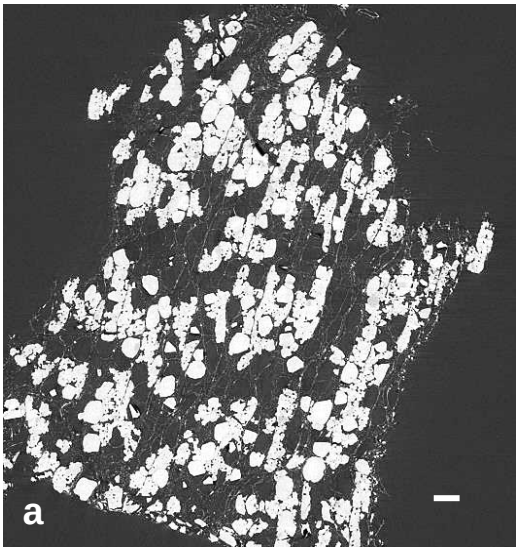

X-ray tomographic microscopy images show structural changes to the wood caused by the alum treatment, the distribution of alum salts and their association with the remaining wood. Less X-ray attenuation by wood indicates a higher state of decay for 185-5 (Figure 16c) than in either 0185-1 and 184-4 (Figures 16a, b, respt.). Localized differences in X-ray attenuation (density) were observed in the alum salts – both in discrete regions and along the edges of the salt crystals, which indicates either that post-conservation change had taken place in the salt, or that different types of salts had initially been deposited in the wood during the alum treatment. However the bulk of the salts observed by X-ray tomography had uniform densities, which indicates that it is most likely 'alum'. Figure 17 shows the reconstructed 3D X-ray images of 185-1 and -5.

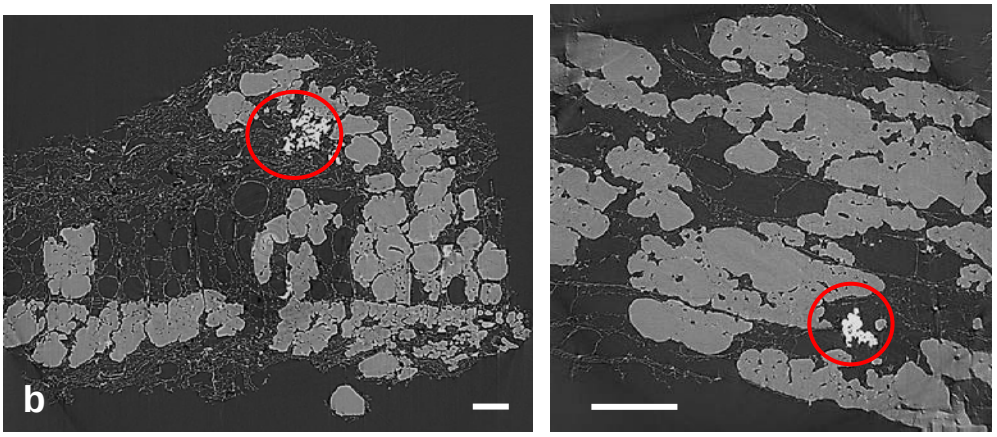

Figure 16 Three different samples recorded at TOMCAT using three different objectives: a) 185-1 at 4x; b) 185-4 10x; c) 185-5 20x. Imaging parameters were similar (between 15-18 KeV). Alum salts are white/grey. Attenuation of alum salts or other inorganic compounds differs in some regions are shown by circled areas, where it is denser (brighter). If originating from alum, it indicates chemical modification, formed either through natural aging or initial deposition. The bars show 50 microns.

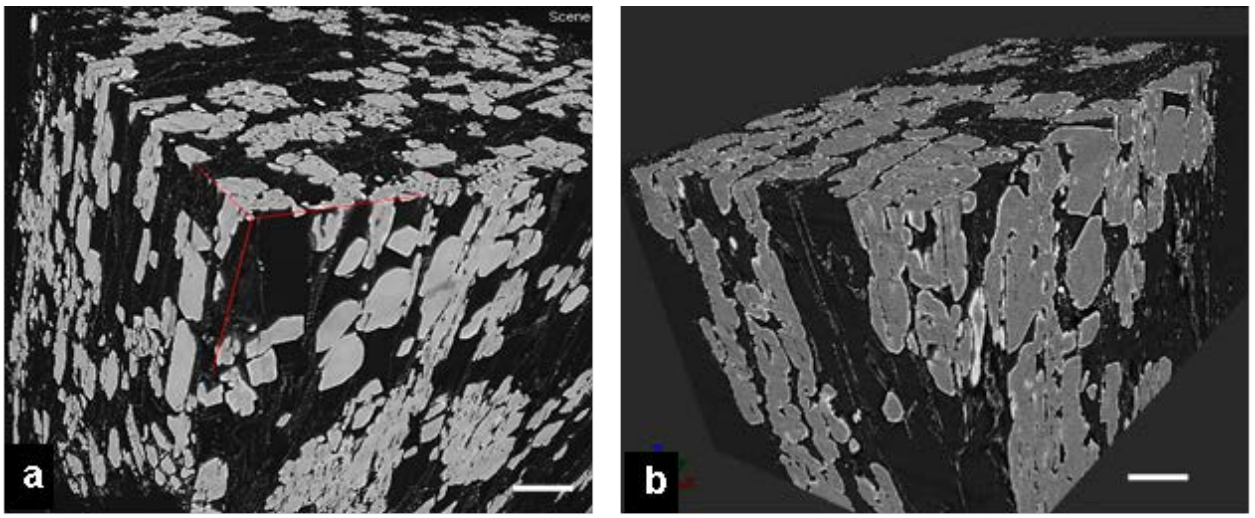

Figure 17 3D-reconstructions of Xray data show the uneven distribution of alum salts. a) 185-1, 4x objective and b) 185-5, 20x objective. Alum salts have been deposited in vessel elements and fibres. (NB: Filters used to process image a) resulted in lightening the alum salts). Bars show 50 microns.

Neutron images demonstrated the distribution of alum salts on a larger scale than that with X-ray tomographic microscopy. Neutron images revealed voids and cracks in samples, as well as the major elements of wood structure, such as growth rings. Thus, neutron imaging complements the information obtained from X-rays, regarding material properties but also in length-scale (Figure 18).

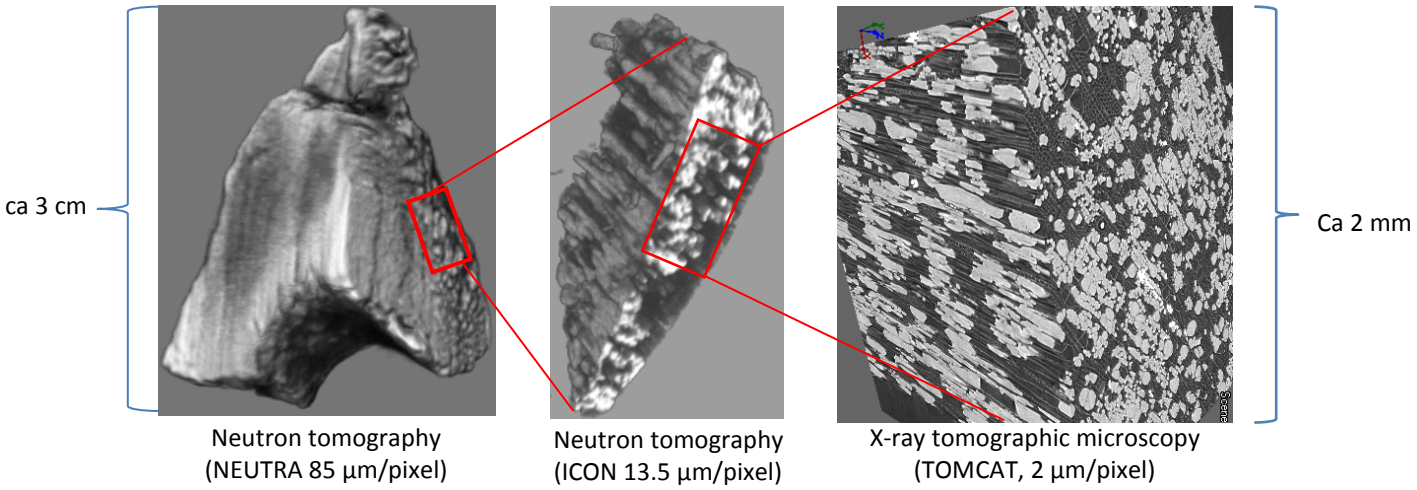

Figure 18 3D-reconstructions of alum-treated Fragment-4 at different length scales.

Scanning electron microscopy

SEM provided surface images of the 185 series at 500x and 1500x, shown in Figures 19 and 20. Due to their high extent of deterioration it was difficult to prepare high-quality samples such that they could be investigated at higher magnifications. SEM images show that the secondary cell walls in the 185-series are highly degraded: it is either missing (185-1) (Figure 19), or completely detached and shrunken (185-4) (Figure 20). The middle lamella appears to be the main part of the cell wall system that survived in samples 185-1 to -6. In sample 185-6, the lignin-rich cell corners also underwent deterioration. On the macro-scale, samples in the 185-series differed visually in both colour and material integrity – with increasing darkness and deterioration from 185-1 to -6. However these differences were not clearly distinguishable with the SEM. The uneven distribution of alum salts was evident in the SEM, where regions of undeformed cells containing alum were adjacent to areas of collapse, where no alum was present. Alum had mainly been deposited in vessel elements, but also in fibres. EDS analyses showed uneven distribution of Al, K and S across a wood cell containing an alum crystal in 185-1 (Figure 21). In sample 185-6 (most degraded of all in the series) there were few alum crystals, and the deposited crust mainly contained K and S (Figure 21).

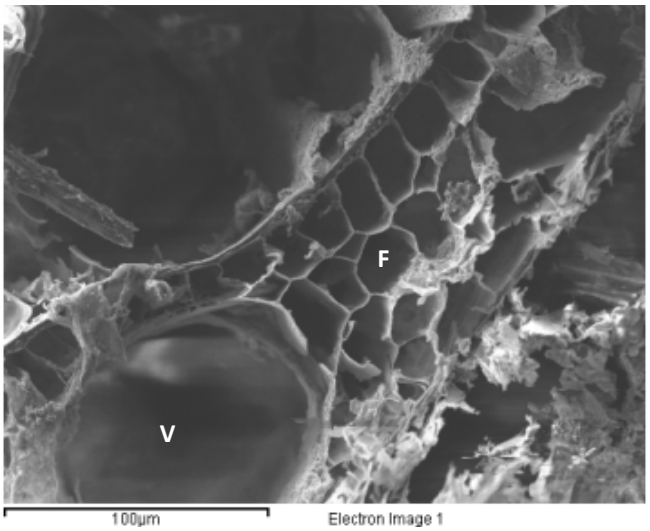

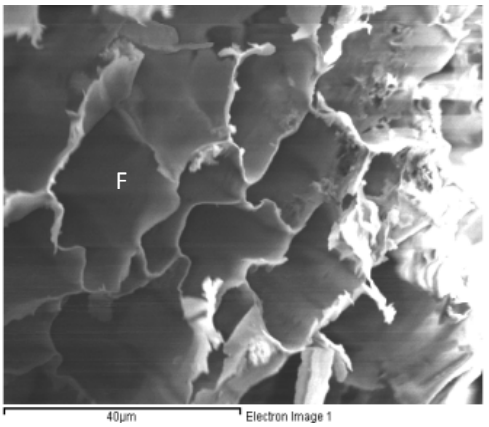

185-1

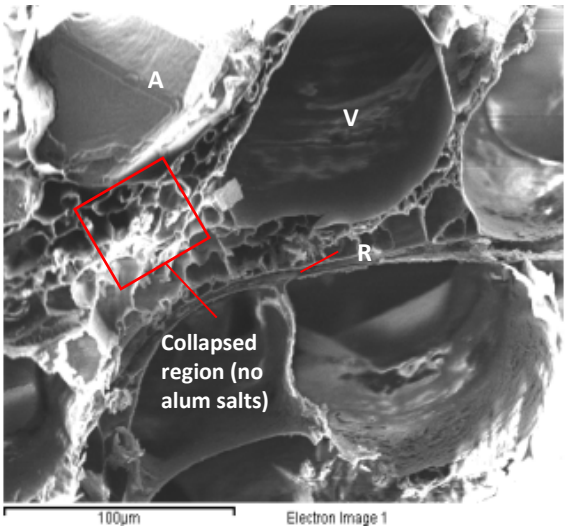

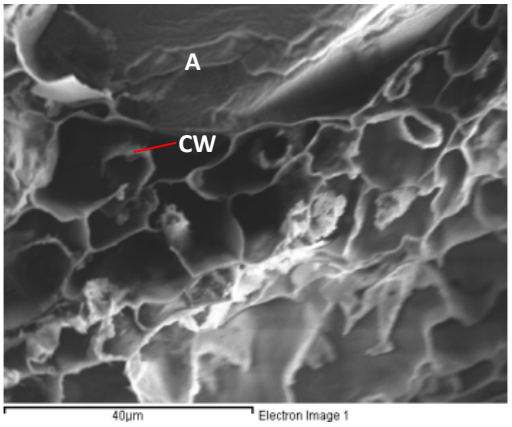

185-2

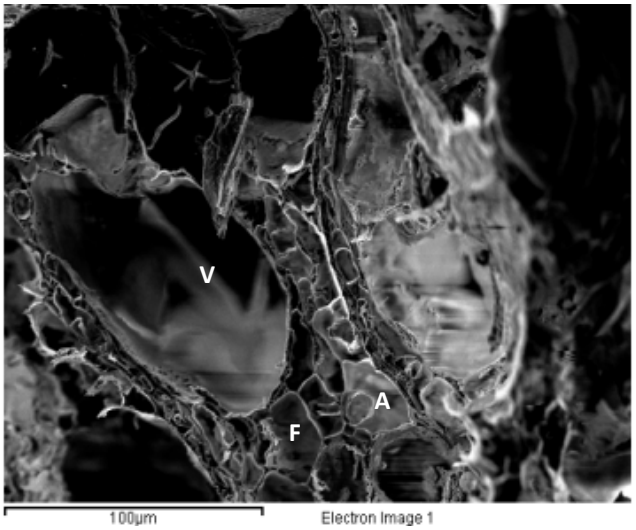

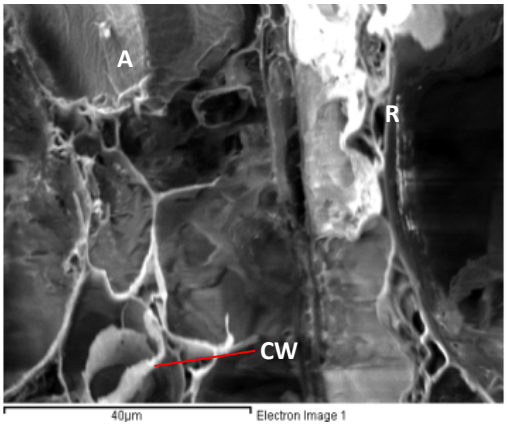

185-3

Figure 19 SEM images of 185-1, (top), 185-2 (middle) and 185-3 (bottom), at 500x and at 1500x magnification. Main features are labelled: V = vessel element; F = fibre; A = alum; CW = cell wall in fibre; R = ray cell;

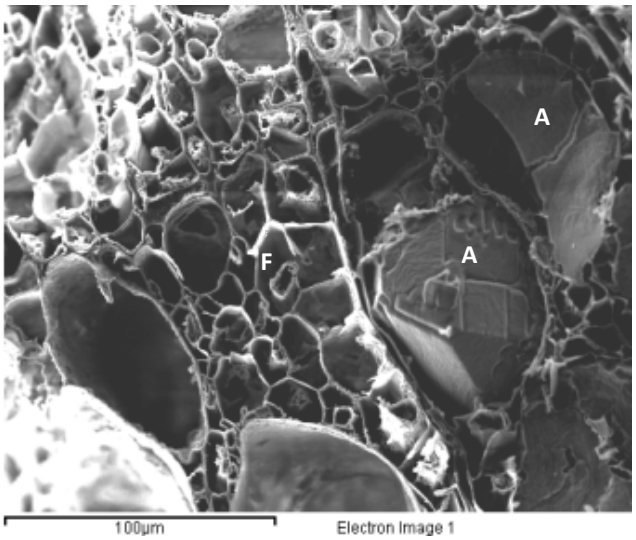

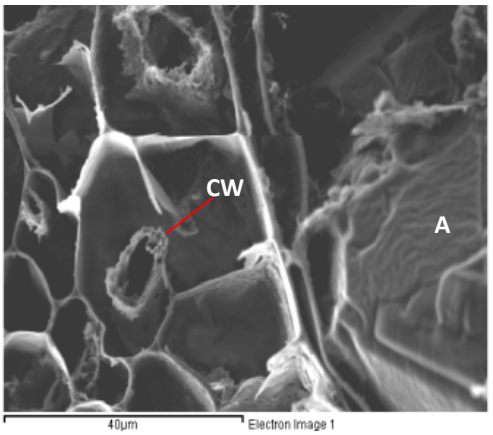

185-4

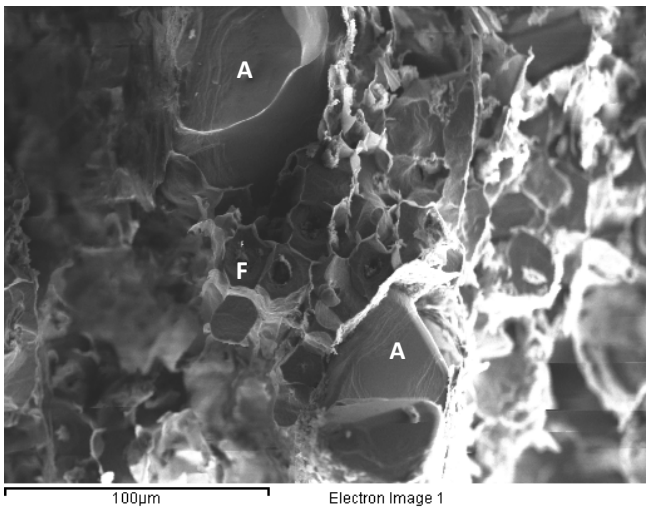

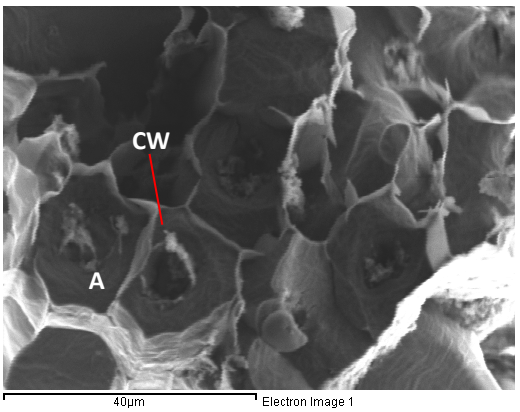

185-5

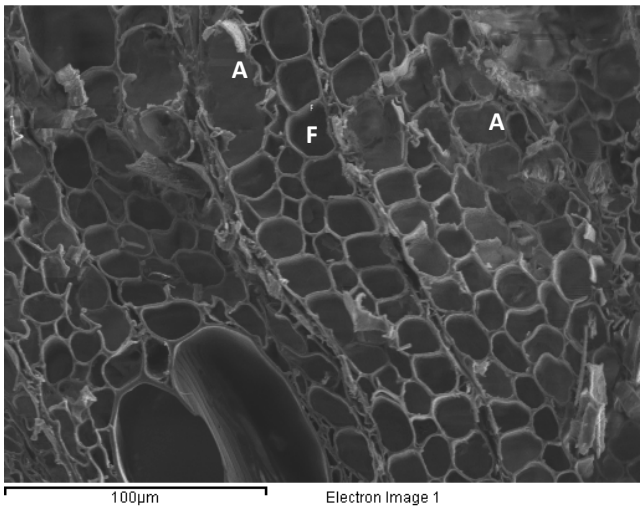

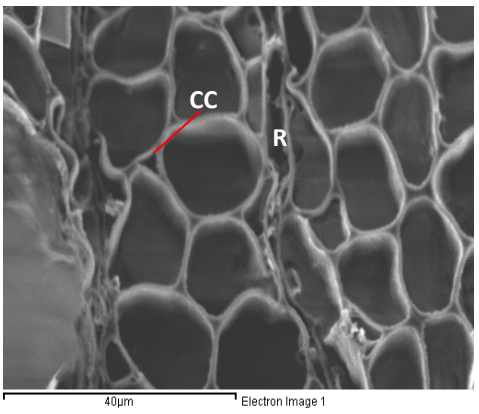

185-6

Figure 20 SEM images of 185-4 (top), 185-5 (middle) and 185-6 (bottom) at 500x and at 1500x magnification. Main features are **labelled**: V = vessel element; F = fibre; A = alum; CW= cell wall in fibre; R = ray cell; CC = cell corner;

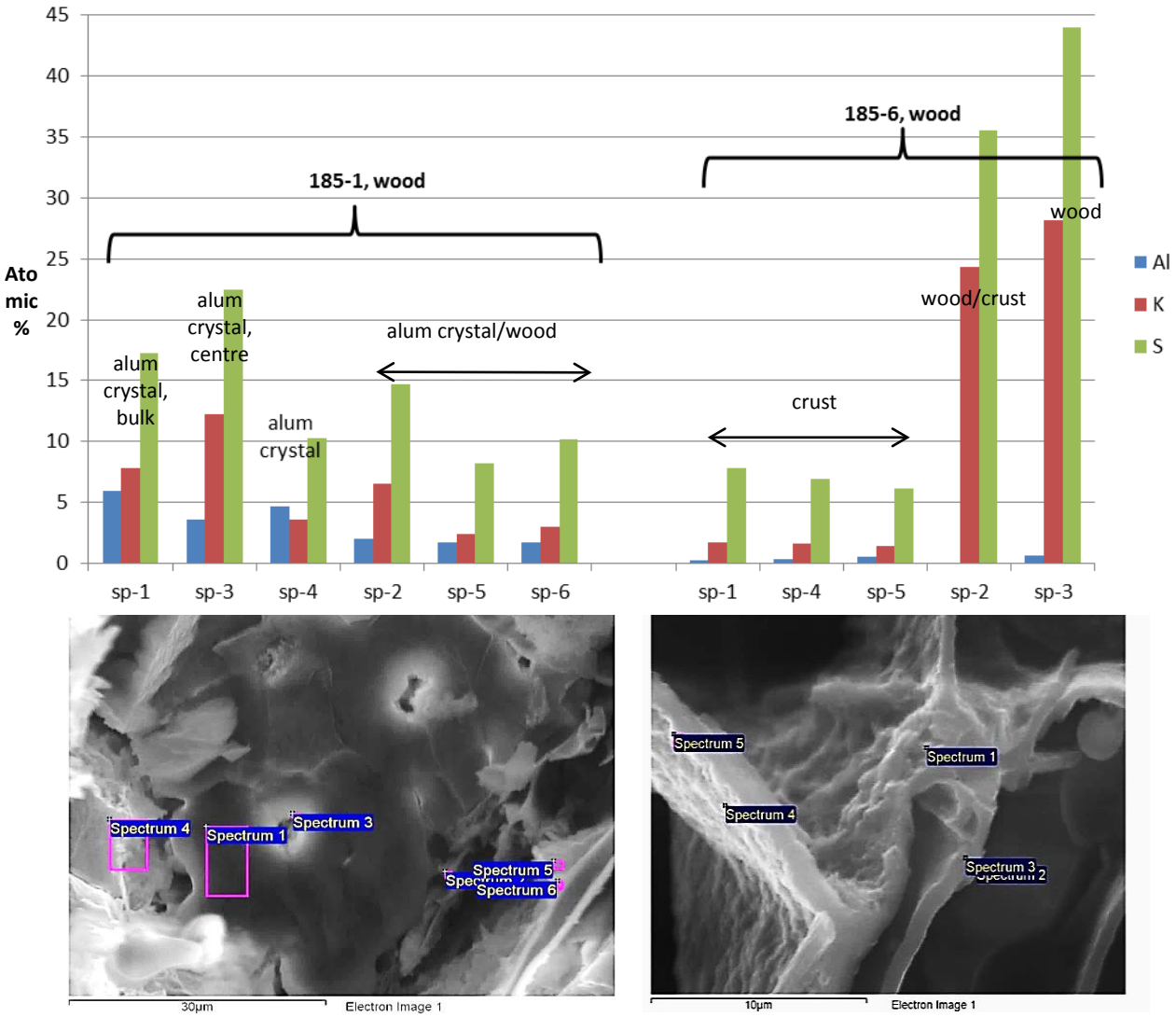

Figure 21 Atomic % of Al, K and S displayed graphically for 185-1 and 185-6.

Py-GC/MS

The results for six alum-treated archaeological samples, referred to as 185 series, were compared to those obtained for two untreated archaeological samples from the same burial environment, one archaeological sample alum-treated in 2009 and its untreated counterpart and five sound wood samples.

Figure 22 compares the chromatographic profiles obtained for sound birch, and archaeological alum-treated sample (185-6).

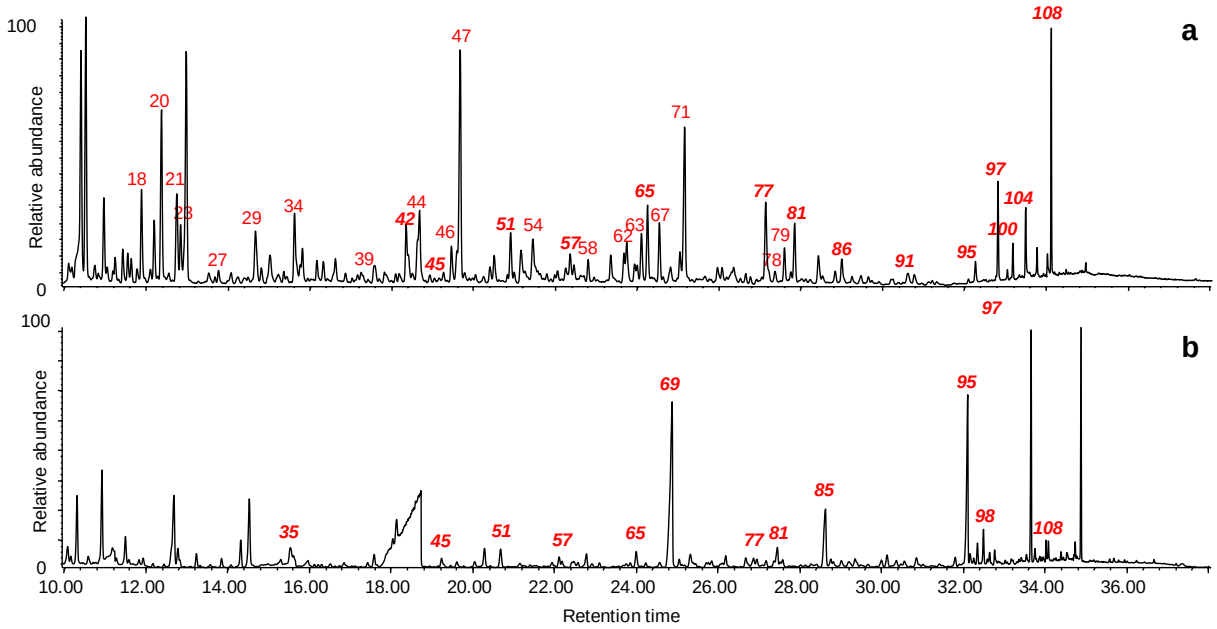

Figure 22 Py(HMDS)-GC/MS chromatographic profiles of a) sound birch and b) archaeological alum-treated sample 185-6. Peak labeling refers to compound numbers in Table 8.

From a qualitative point of view the chromatographic profile of sound birch was dominated by holocellulose pyrolysis products (#47, 71) and lignin monomers (#97, 108). For sample 185-6 holocellulose pyrolysis products were almost absent and lignin pyrolysis products containing acidic functionalities (#69, 85, 95) were the most abundant.

The H/L ratio was calculated for the samples of series 185 and archaeological aspen wood treated in 2009, and the standard deviation for three replicates was calculated as well (Table 11).

Table 11 H/L ratios calculated for the archaeological alum-treated wood samples

	Sound alder	Sound birch	185-1	185-2	185-3	185-4	185-5	185-6
H/L	1.77	3.13	0.26	0.17	0.17	0.03	0.05	0.03
SD	0.04	0.39	0.09	0.03	0.02	0.00	0.01	0.01

The Oseberg samples from the 185-series generally showed a very low H/L ratio, which decreased from 185-1 to -6, reaching values around 0 for samples 185-4, 5, and 6. This was indicative of an almost complete loss of the polysaccharide component in these samples.

As already illustrated, the H/L ratio can be a good indicator for comparing the general state of preservation of moderately deteriorated archaeological woods relative to their sound counterparts [23, 32]

However, the H/L ratio failed to reflect the visual and chemical variation in the states of preservation of the highly deteriorated archaeological samples, by not significantly differentiating the archaeological samples among each other. In fact, in the 185-series, the general low amount of polysaccharide components coupled with an extensive deteriorated lignin network contributed to H/L values which were unexpectedly similar to each other and to some untreated archaeological samples, despite the differences in their structural integrities.

In order to investigate changes in wood components in more detail and understand how wood degradation can affect the formation of primary and secondary lignin pyrolysis products we divided pyrolysis products into categories as described in chapter 3.1 and listed in Table 8.
The sum of the peak areas of the pyrolysis products assigned to each category was calculated and expressed as a percentage with respect to the total abundance of the respective wood component (holocellulose or lignin), in order to evaluate differences in the relative abundances unaffected by the total amount of the wood components in the samples.
According to this categorisation Figure 23 shows distribution of lignin pyrolysis products expressed as percentages in the analysed samples.
Despite the sound woods belonged to different genera, the distribution into categories of their lignin pyrolysis products gave very similar profiles. Under the analytical conditions used, monomers constituted 30-40% of all the lignin pyrolysis products, long chain compounds 5-10%, short chain compounds 10-15%, carbonyl compounds ca. 15%, carboxyl compounds 3-5% and demethylated/demethoxylated compounds 15-20%.
For the Oseberg samples treated with alum in the early 1900s, differences relative to sound birch and alder were remarkable (the identification of the species was not certain for these samples, thus they were compared to both birch and alder): the relative amount of carboxyl compounds highly increased. In fact, the chromatographic profiles showed that generally p-hydroxybenzoic, vanillic and syringic acids (#69, 85, 95) were the most abundant pyrolysis products (Figure 22). Lignin monomers had very low abundance, while the remaining lignin pyrolysis products were mainly composed of short chain compounds. Degradation of lignin in archaeological wood can be accompanied by oxidation with a consequent increase in carbonyl and carboxyl functionalities [32-34], but an increase of acids to such extent has never been previously observed in archaeological wood. Additionally, p-hydroxy benzoic acid has not been previously reported as a lignin break-down product in naturally aged archaeological samples analysed using this method [32, 35]. P-hydroxybenzoic acid is reported to be a characteristic component of aspen lignin, which forms some terminal ester and ether linkages with the macromolecule [36, 37]. In fact, a low abundance of this compound was detected in sound aspen wood, likely originating from the cleavage of terminal ester and ether bonds under pyrolytic conditions. *P*-hydroxy benzoic acid was not detected among the pyrolysis products of other sound woods. Its presence is often detected in lignin extracted in industrial processes (acidolysis, hydrolysis, etc.) with the aim to separate it from the holocellulose fraction [38, 39]. In these processes lignin is often exposed to oxidising conditions which promote the formation of significant amounts of carbonyl and carboxyl compounds, such as vanillin, syringaldehyde, vanillic acid and syringic acid [40, 41]. Thus, the results herein obtained suggested that the archaeological woods from the alum-treated Oseberg samples were exposed to extreme oxidising conditions and the specific formation of p-hydroxybenzoic acid was likely the result of a combination of reactions, including β-O-4'-cleavage, demethoxylation and side-chain cleavage coupled with oxidation. In addition, a trend was observed within the 185-series, where the amount of acid pyrolysis products was similar in samples 185-1, -2, and -3, whereas it was significantly higher in samples 185-4, -5, and -6. This highlighted an increase in oxidation from sample 185-1 to sample 185-6 and was in agreement with the visual state of preservation of these samples, where 185-1, -2, and -3 were lighter in colour and the wood fabric possessed greater structural integrity than in samples 185-4, -5, and -6.

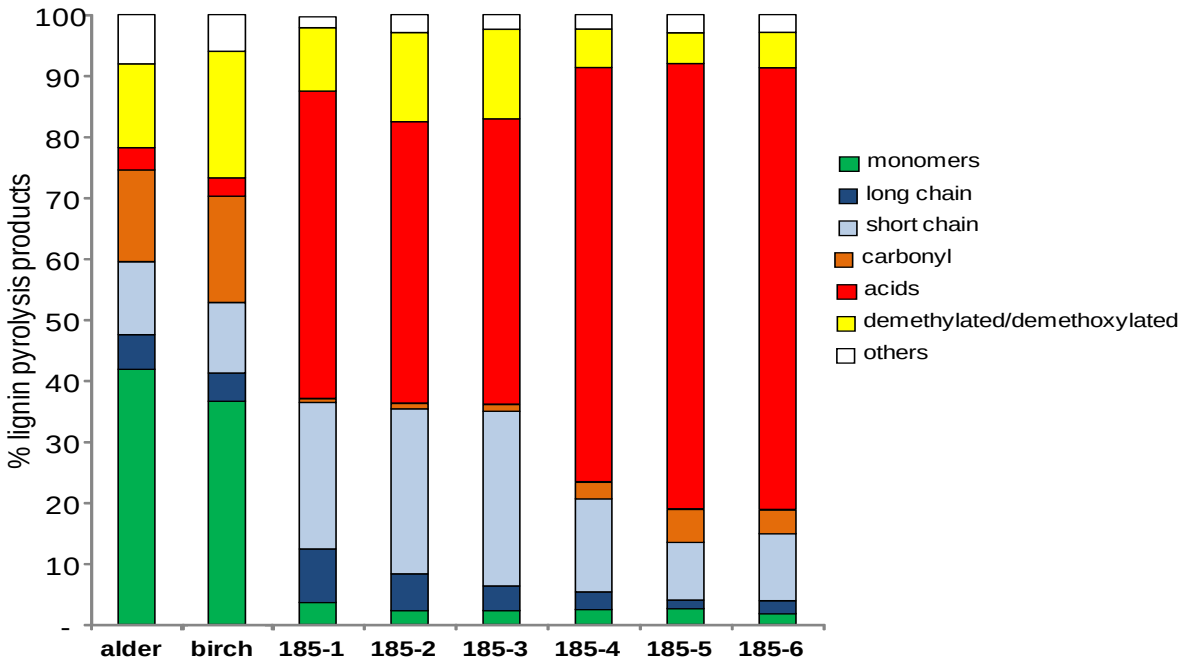

Figure 23 Distribution of categories of lignin pyrolysis products expressed as percentages in the samples of reference and archaeological treated and untreated wood samples.

ICP-OES results

Adopting the conditions described in section 2.1 (point 1), the amount of some inorganic elements was quantitatively evaluated by ICP-OES. These analyses were performed at the Analytics Laboratory, Leibniz Institute for New Materials (INM), Saarbrücken, Germany. The concentrations of various inorganic elements found in the samples of 185-series are summarised in Table 12. Analysis of fresh birch wood was included for comparison.

Table 12 Concentration of elements determined by ICP-OES in the Oseberg samples of 185-series (mmol/100g ± standard deviation determined in nine replicates).

	Al	K	Ca	Fe	Cu	Zn
185-1	25 ± 1	185 ± 7	0.06 ± 0.02	0.13 ± 0.00	0.21 ± 0.00	1.07 ± 0.01
185-2	23.6 ± 0.2	164 ± 7	0.16 ± 0.01	0.11 ± 0.00	0.20 ± 0.00	0.88 ± 0.02
185-3	23.6 ± 0.3	195 ± 7	0.39 ± 0.01	0.43 ± 0.01	0.66 ± 0.00	3.82 ± 0.09
185-4	21.3 ± 0.3	199 ± 8	0.43 ± 0.02	0.60 ± 0.01	0.96 ± 0.01	0.67 ± 0.03
185-5	38.3 ± 0.1	184 ± 6	0.00 ± 0.00	0.47 ± 0.02	0.56 ± 0.00	1.59 ± 0.02
185-6	31.2 ± 0.1	153 ± 4	0.00 ± 0.00	0.59 ± 0.01	0.63 ± 0.01	3.21 ± 0.04
Fresh birch	-	-	0.97 ± 0.02	0.00 ± 0.00	0.00 ± 0.00	0.04 ± 0.01

All the samples contained high levels of Al and K, due to the alum treatment, while the presence of copper and iron might be due to proximity to corroding brass and iron pieces, either in the object itself or in the soil in which it was buried. Copper vats were also used during alum treatment. Significant levels of zinc were probably due to wet storage of the objects in zinc vats prior to conservation.

Potassium levels were consistently higher than aluminium in all samples (Table 12), with K:Al ratios varying from approximately 5:1 to 9:1, despite the fact that these elements have a 1:1 ratio in alum ($KAl(SO_4)_2 \cdot 12H_2O$). This could be due to precipitation of insoluble monomeric and polymeric aluminium-hydroxide containing compounds in the treatment baths, as these are known to form in aqueous solution as a result of hydrolysis of hexa-aquo aluminium(III) species [42]. Such precipitates, which were identified as alunite ($KAl_3(SO_4)_2(OH)_6$), were formed during heating of alum solutions [43]. The variation between the K/Al ratios did not obviously correlate

with the degree of degradation of the fragments. However, the Al content partially correlated with poor preservation condition, as assessed by the sum of acid pyrolysis products (Figure 24). This could suggest some relationship between degradation and Al content. One possible explanation is that the aluminium was initially present as an alum salt deposit, which decomposed over time to produce sulphuric acid that diffused into the local wood environment. Alternatively, it is possible that Al(III) itself could have a detrimental effect on the wood, as suggested by some literature reporting that Al(III) can accelerate degradation of cellulose in paper [44, 45].

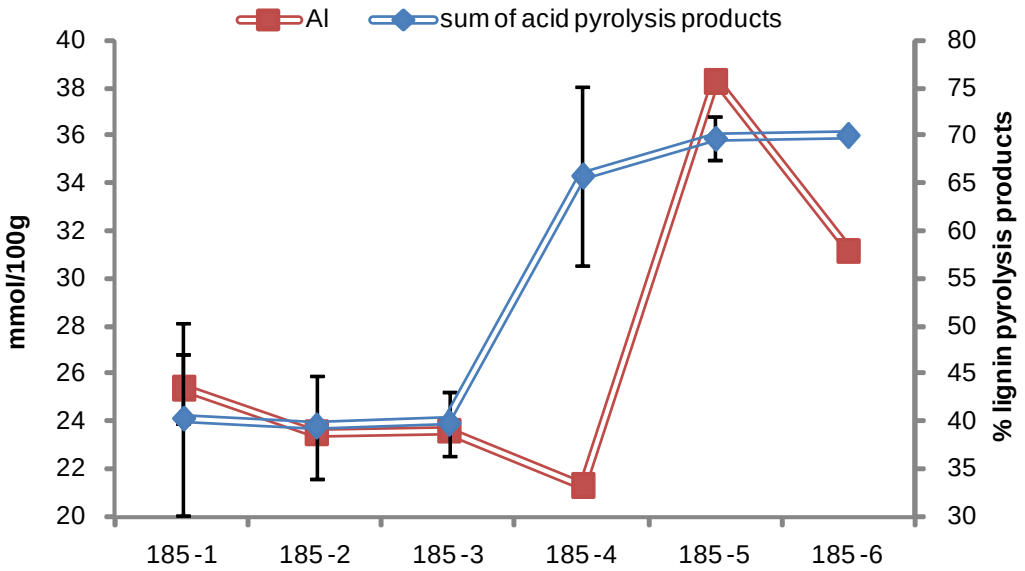

Figure 24 Correlation between Al content and the sum of acid lignin pyrolysis products in Oseberg samples of 185-series.

It was considered that the variability in the state of preservation of the 185-series might also be related to other inorganic elements. We noted that Zn was the most abundant element detected after K and Al. However, to our knowledge there is no literature suggesting a role of Zn in wood degradation have been reported so far. Moreover, no correlation between the content of Zn and the extent of wood degradation was found for these samples.

The concentrations of iron and copper were low relative to Al, K and even Zn. However, the iron concentration correlated closely with the visual/physical features of the fragments and with the results obtained by Py(HMDS)-GC/MS. The fact that Fe and Cu can act as catalysts in Fenton degradation of wood [46, 47] means that small amounts of these elements can still be quite harmful for wood. Iron-catalysed degradation tends to be efficient under acidic conditions, while copper-catalysed Fenton processes are inhibited in the presence of oxygen at acidic pH [48], well explaining the results obtained. Figure 25 compares plots of the iron content in the 185-series to the sum of acidic pyrolysis products. The Pearson's correlation coefficient r between iron concentration and the percentage sum of acid pyrolysis products was 0.81.

In addition, it was interesting to note that, among the fragments containing higher iron levels, those containing also significant levels of calcium were less degraded than those containing a low level of calcium, which might suggest inhibition of iron-catalysed degradation in the presence of calcium. Figure 26 shows a plot of iron concentrations in the 185-series after subtracting calcium concentrations, to illustrate this trend. The Pearson's correlation coefficient *r* for the difference between iron concentration and calcium concentration and the percentage sum of acidic pyrolysis products was 0.88, thus proving an increase in correlation between Py and ICP results when both iron and calcium were considered.

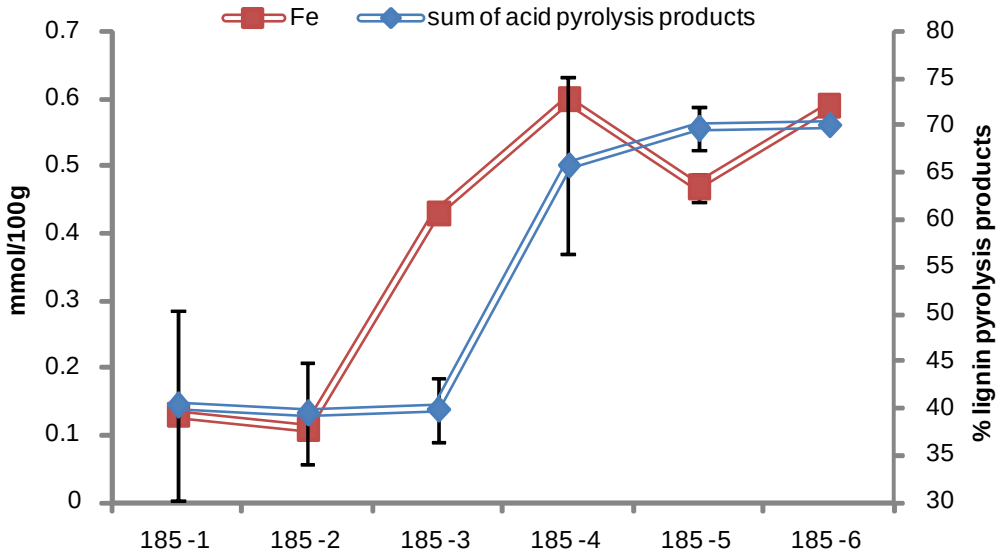

Figure 25 Correlation between Fe content and the sum of acid lignin pyrolysis products in Oseberg samples of 185-series.

Although the literature reports little information about the combined effect of iron and calcium on wood degradation, one study has noted an inhibiting effect of calcium salts on brown rot fungal degradation of wood [49]. This was proposed to be due to the calcium ion forming crystals with oxalate anions, which assist the supply of Fe(III) for Fenton chemistry by solubilising iron from insoluble iron (hydr)oxide forms. The calcium thereby indirectly limits the availability of iron. Although in this case the oxalate comes from oxalic acid excreted by the fungus, there is evidence that oxalic acid can be produced during oxidative degradation of wood without fungal infestation [50, 51], thus it is conceivable that similar indirect interactions between calcium and iron could have occurred in the 185-series. We note here that when samples from the 185-series were analysed for oxalic acid, the levels were below the limit of detection of 0.3 mg/g (Gunnar Almkvist, personal communication), so if it is present it is in low concentrations. Furthermore, it would be unsurprising if oxalic acid had also been degraded by the oxidizing conditions that have affected the lignin. It was also speculated that this trend could be due to basic calcium salts partially neutralising the acidity in the wood, reducing the effectiveness of iron-catalysed Fenton processes. However, 185-series fragments were all found to have a highly acidic pH of around 1, so it is unlikely that any significant degree of neutralisation occurred. In any case, complementary analyses to determine the types of compounds the iron and calcium comprise could help elucidate the mechanism behind this relationship.

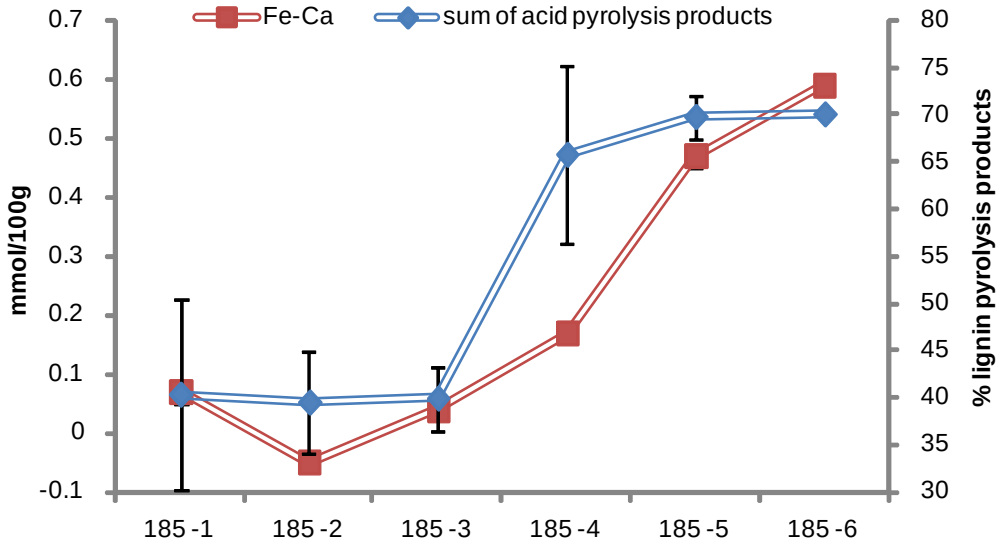

Figure 26 Correlation between the difference between Fe and Ca concentration and the sum of acid lignin pyrolysis products in Oseberg samples of 185-series.

Infrared analyses

Alum salt interference with infrared spectra

FTIR spectra (range 4000-650 cm^{-1}) of alum-treated wood showed significant interferences by alum salts, almost completely overshadowing information from the wood especially in the fingerprint region (Figure 27). This is due to the strong bands associated with the sulfate group in alum at 1190, 1082 and 1059 cm^{-1} and a less intense band at 974 cm^{-1} (bands due to crystal water are located at 3345, 2888, 2455 and 913 cm^{-1}.

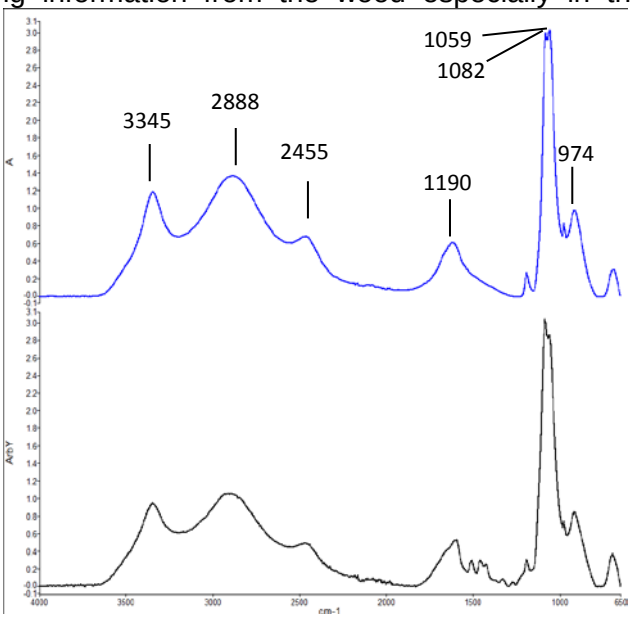

Figure 27 Spectra of alum salt (top) and alum-treated wood from Oseberg (185-3) where alum had not been removed (below).

Alum-treated samples were therefore rinsed three times in distilled water prior to infrared analyses. This procedure also removed some of the water-soluble fractions from the sample, which coloured the wash water a brownish-yellow after some hours of immersion. Figure 28 shows the spectrum for the residue from 185-3, along with the unrinsed and rinsed spectra from the same sample. The residue is very similar to the spectrum of the rinsed 185-3 sample, indicating that small fractions of wood were removed along with the alum and that washing enabled selective removal of different components due to differences in solubilities (i.e. not all bands in the residue existed in the same proportions as in the washed sample). For the residue of 185-3 (Figure 28) the oxidized region (1650-1800 cm^{-1}) had higher absorbance than in the washed sample. The band at 1030 cm^{-1} was lower in the residue than in the washed sample, indicating it was not affected as much as that at 1122 cm^{-1}. This means that bands at 1122 and 1700 cm^{-1} are likely lower in the washed sample than they should be.

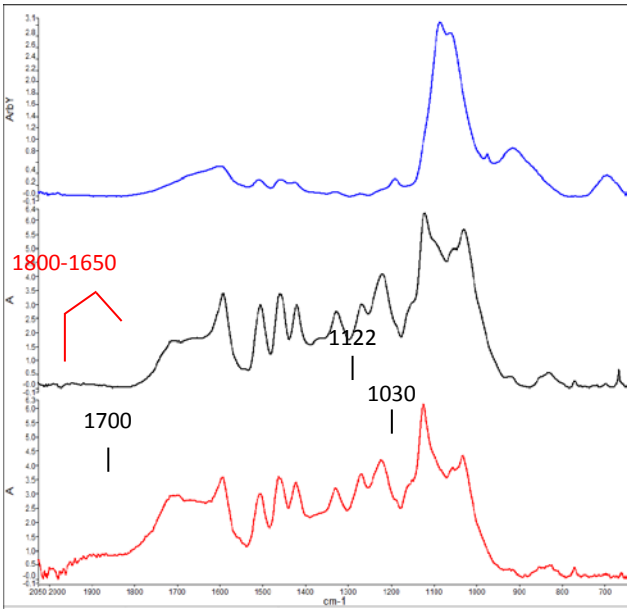

Figure 28 Spectra of alum-treated wood from Oseberg (185-3) where alum had not been removed (top), sample 185-3 after removal of alum salts (middle) and residues from the last wash of sample 185-3 (bottom). The residue shows that the main compounds rinsed out were oxidation products at 1700 cm^{-1}. Also compounds associated with the band at 1122 cm^{-1} were removed to a lesser degree.

The spectrum from alum salt was also digitally subtracted from the alum-treated wood spectra (after normalization to 1058 cm^{-1}) in an attempt to remove the interferences from sulfates. However the information in the resulting spectra was not consistent, as it changed with extent of degradation of the sample. This is illustrated in Figure 29 where the subtracted spectrum of the more deteriorated sample 185-6 contains far less information about wood. It would also make it more difficult to compare this sample to other archaeological woods. In Section 3.3.3, alum subtraction was performed by normalizing at 575 cm^{-1}, with better results (the lower limit of the instrument was at 400 cm-1). As the lower limit for this instrument was higher (650 cm^{-1}), it could not be normalized at 575 cm^{-1}.

Therefore despite the drawbacks, rinsing was used in IR analyses of the Oseberg woods presented in this section.

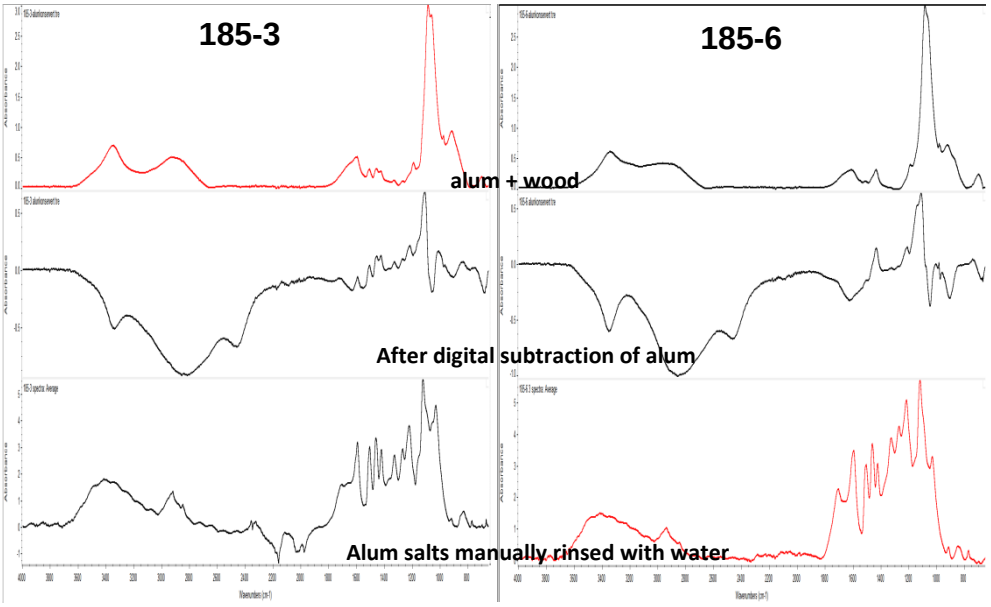

Figure 29 Comparison of spectra containing both wood and alum (top) and the result after subtracting from the spectrum of alum salt (middle). The wood spectra after rinsing with water to remove alum salts are shown on the bottom. The set on the left are spectra from 185-3 and on the right are spectra from the more degraded 185-6. The digitally subtracted spectra (middle) contain less information than those on the bottom, which are also more comparable to other archaeological woods.

Rinsed IR spectra

The IR spectrum of 185-1 (Figure. 30) shows it has become highly depleted in its carbohydrate content, resulting in the enhancement of bands due to lignin in its spectrum. Lignin bands were also broad, indicating that it had undergone structural changes. The spectrum also showed an increase in acidic oxidation products which are mainly attributed to lignin. These observations are confirmed by Py-GC/MS. In fact spectra of Oseberg alum-treated wood and Klason lignin (the dark brown residue remaining after dissolving most carbohydrates (and the acid-soluble fractions of lignin) from extractive-free wood powder using 72% sulphuric acid [52]) are very similar, implying that the spectrum of 185-1 generally contains signals from lignin. Bands normally attributed to signals from both lignin and carbohydrates, may therefore be assumed to be dominated by lignin for 185-1 and other heavily deteriorated alum-treated woods.

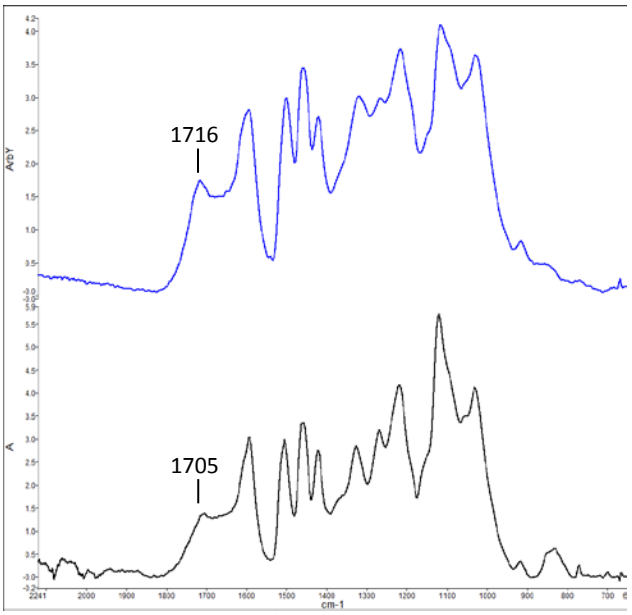

Figure 30 Fingerprint region of Klason lignin isolated from the well-preserved Oseberg ship (Oak) (top) and the alum-treated Oseberg sample (185-1, birch/alder?) (below). Although the spectra originate from different woods, the strong resemblance indicates that the majority of the bands in 185-1 are from lignin.

Sample 185-1 was also compared with the untreated Oseberg maple, which was in a similar poor condition upon recovery in the early 1900s (but had remained untreated) in order to investigate the cumulative deterioration in 185-1 since its treatment with alum (Figure 31). Distinct chemical changes in the alum-treated sample were apparent. The alum-treated wood was severely depleted of carbohydrate and showed signs of lignin deterioration. Both samples

showed signals in the range 1650-1800 cm^{-1} from carbonyl groups, indicating oxidation of wood polymers has occurred. The oxidation products observed in the Oseberg maple, which is in a better state of visual preservation, likely has originated from both carbohydrate and lignin, while in 185-1 these products are mainly derived from lignin. The alum-treated sample had a higher band height ratio 1122/1030 than the untreated sample, also indicating a higher degree of deterioration.

The IR spectra from all six slices from the 185-series are shown in Figure 32.
Generally the bands at 1030 and 1122 cm^{-1} and in the region spanning 1650-1800 cm^{-1} are most affected in all samples. However spectra also highlight differences. The samples may be classified into two groups, one including 185-1,2,3 and the second including 185-4,5,6. Specifically, 185-4,5,6 has greater intensities in the region between 1650 and 1800 cm^{-1} which demonstrate an increase in oxidation products for these samples. This is confirmed by Py-GC/MS.
Also, the ratios of band heights 1122/1030 are lower for 185-1,2,3 than for 185-4,5,6. All of this points towards a better state of preservation for 185-1,2,3.
These two groups also mirror the visual state of preservation of the wood polymers, where the first group (185-1,2,3) has a lighter colour and relatively greater structural integrity than the woods in the second group (185-4,5,6), although both groups are extensively deteriorated relative to untreated archaeological woods. Darkening of wood may be attributed to an increase in condensation of the lignin units or an increase in oxidation products, both of which enable greater absorption at wavelengths in the visible region of the electromagnetic spectrum [53, 54].

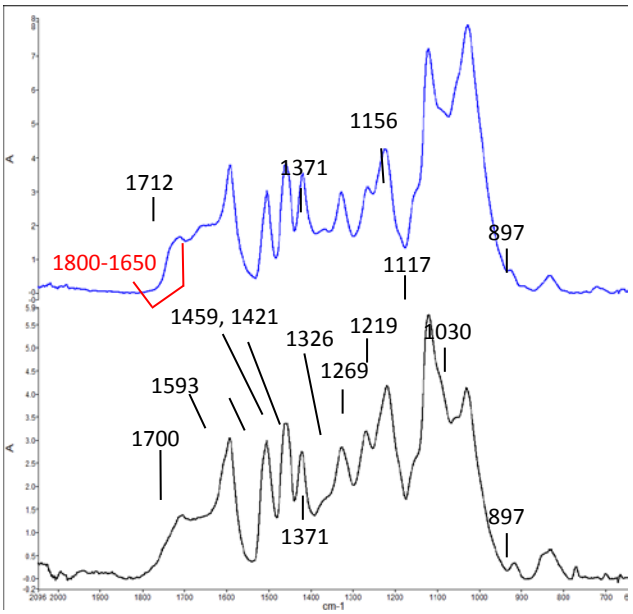

Figure 31 Fingerprint region of the untreated Oseberg sample (nr. 124, maple) (top) and the alum-treated Oseberg sample (185-1, birch/alder?) (below). The greatest differences occur at bands 1117 and 1030 cm^{-1}.

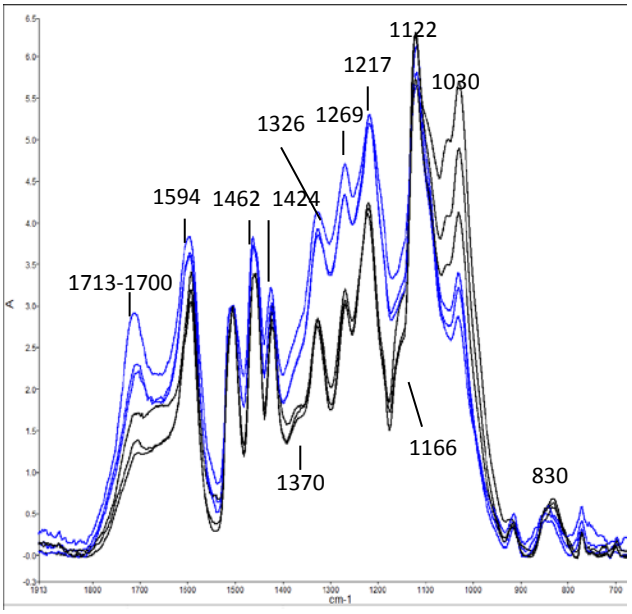

Figure 32 Fingerprint region of the 185-series, slices 1 to 6. The spectra are overlaid to demonstrate their differences. The spectra show two distinct groups regarding the state of preservation of the wood polymers: black curves are for 185-1, -2, -3 and blue curves are for 185-4, -5, -6.

Principal component (PC) analysis of IR spectra
To elucidate possible deterioration trends, IR spectra from the 185-series were compared to those from other alum-treated woods from Oseberg, untreated archaeological woods and fresh woods by principal component analysis (Figure 33). The PC1 axis represents increasing carbohydrate content along its positive direction, showing the expected greater carbohydrate content in fresh woods than in archaeological woods. All alum-treated samples had lower carbohydrate contents than untreated archaeological woods.
The PC2 axis shows increasing carbonyl content in the samples in its positive direction. For fresh woods the carbonyl content is mainly associated with hemicelluloses. Of the untreated

archaeological woods, those that were recently excavated (alder, aspen) are located below the fresh woods on the PC2 axis due to lower amounts of hemicelluloses and their position on the negative side of PC2 indicates low amounts of oxidized products. The untreated sample from Oseberg (maple) is located at approximately the same level as fresh maple, not due to retention of hemicellulose but rather due to increased oxidation of remaining polymers (of lignin and carbohydrate origin). Two distinct groups of alum-treated woods are apparent: those which are less oxidized (185-1, 2, 3, Fragment-5 and nr. 250) and those which are more oxidized (185-4, 5, 6, Fragments-1, -1A, and -8). The groups in the PCA analysis correspond very well to their visual state of preservation.

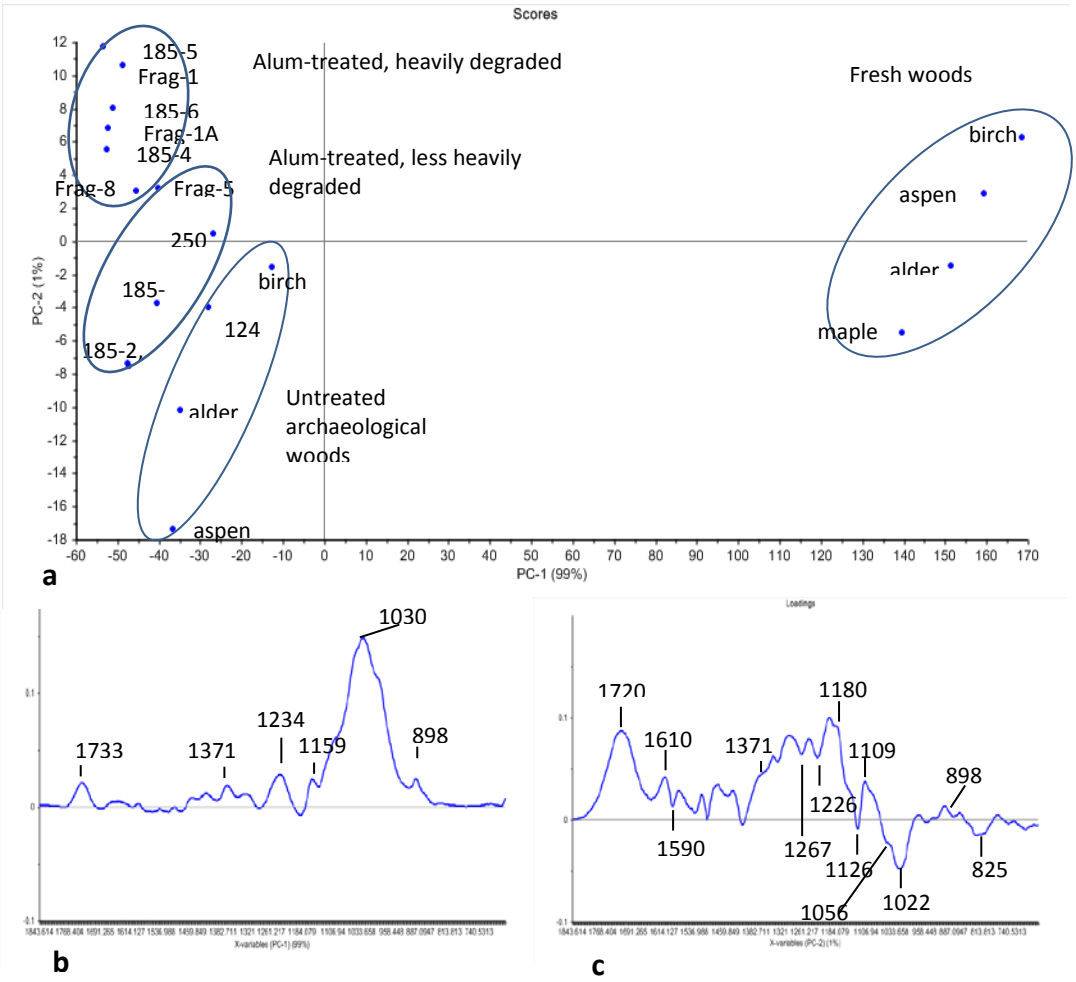

Figure 33 PCA of archaeological woods and fresh woods. a) score plot; b) loading PC1; c) loading PC2.

Band height ratios from infrared spectra

In the spectra of alum-treated woods, there were two bands which consistently showed greatest change relative to each other: at 1122 and 1030 cm^{-1}. Knowing that Py-GC/MS had identified increasing amounts of acidic products in woods of greater deterioration, it seemed reasonable to compare the change in these band heights with that at around 1700 cm^{-1}. Figure 34 shows the band height ratio 1700/1030 plotted against 1122/1030.

The graph shows increasing oxidation (1700/1030) with increasing carbohydrate and/or lignin degradation (1122/1030). Despite the fact that some wood components are rinsed away with alum salts (as discussed previously), the regression line shows a very good correlation (R^2=0.90). Similar clusters to those obtained by PC-analysis are also evident: untreated woods have lowest oxidation (1122/1030 less than 1), less-degraded alum-treated woods have moderate oxidation (1122/1030 values between 1-1.4) and heavily degraded alum-treated woods are highly oxidized (1122/1030 values over 1.4).

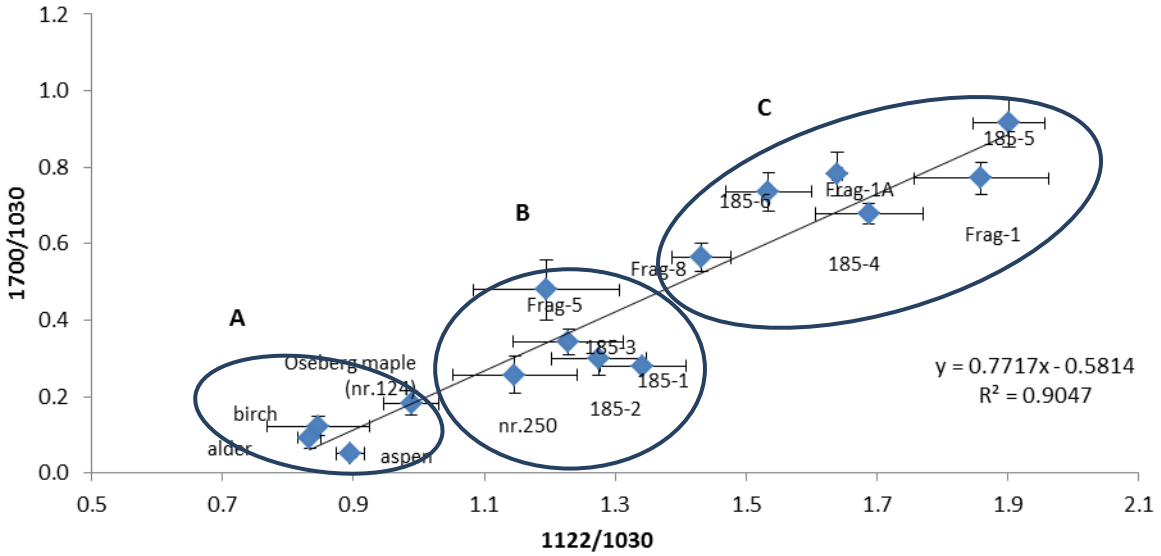

Figure 34 Scatter plot of band height ratios from archaeological woods, 1700/1030 vs 1122/1030. A good correlation (R^2=0.90) indicates that oxidation increases with deterioration (reduction) at 1030 cm^{-1}. Group A includes untreated archaeological woods, low levels of oxidation; Group B includes the alum-treated, less heavily degraded, medium levels of oxidation; Group C includes alum-treated, heavily degraded, high levels of oxidation.

Although this trend must be verified by analyzing a greater number of samples, it proves to be a promising way of quickly classifying spectra from archaeological woods in various states of preservation. If further work shows that the visual condition (such as changes in colour, wood consistency, etc.) can be consistently related to the state of chemical preservation obtained from spectral data, FTIR may prove to be a useful tool during storage surveys. For example, small samples may be taken from selected objects during surveys, and band height comparisons, together with visual data may allow for a more objective classification of the condition of objects in preparation for retreatment. This was in fact investigated in more depth, and is presented in Section 3.6.

GPC and 2D-HSQC NMR spectroscopy

- Samples were solubilized in ionic liquid and derivatized with benzoyl chloride or acetyl chloride, such that the wood became soluble in organic solvent
- Small sample (1-2 mg) only benzoylated and submitted to GPC
- Biggest sample (at least 20 mg) also acetylated and submitted to 2D-HSQC
- Benzoylated GPC: molecular weight distribution of entire wood
- 2D-HSQC: chemical structure of entire wood
- Oseberg ship oak (dendro 9): very good chemical structure (GPC and 2D-HSQC)
- 185-series: degradation trend from 1 to 6 (medium to strong degradation)
- 185-4-AR outlier
- Frag-5 (Oseberg, alum washed out): strong degradation
- 124untr(Oseberg maple, animal head): medium degradation

Results are shown in Figures 35-38.

See further details in: Zoia, L., A. Salanti, and M. Orlandi. *Application of Ionic Liquids for the Chemical Characterization of Archaeological Woods from Oseberg*. in *18th ISWFPC, International Symposium on Wood, Fiber and Pulping Chemistry*. 2015. Vienna, Austria: BOKU, Dept of Chemistry.

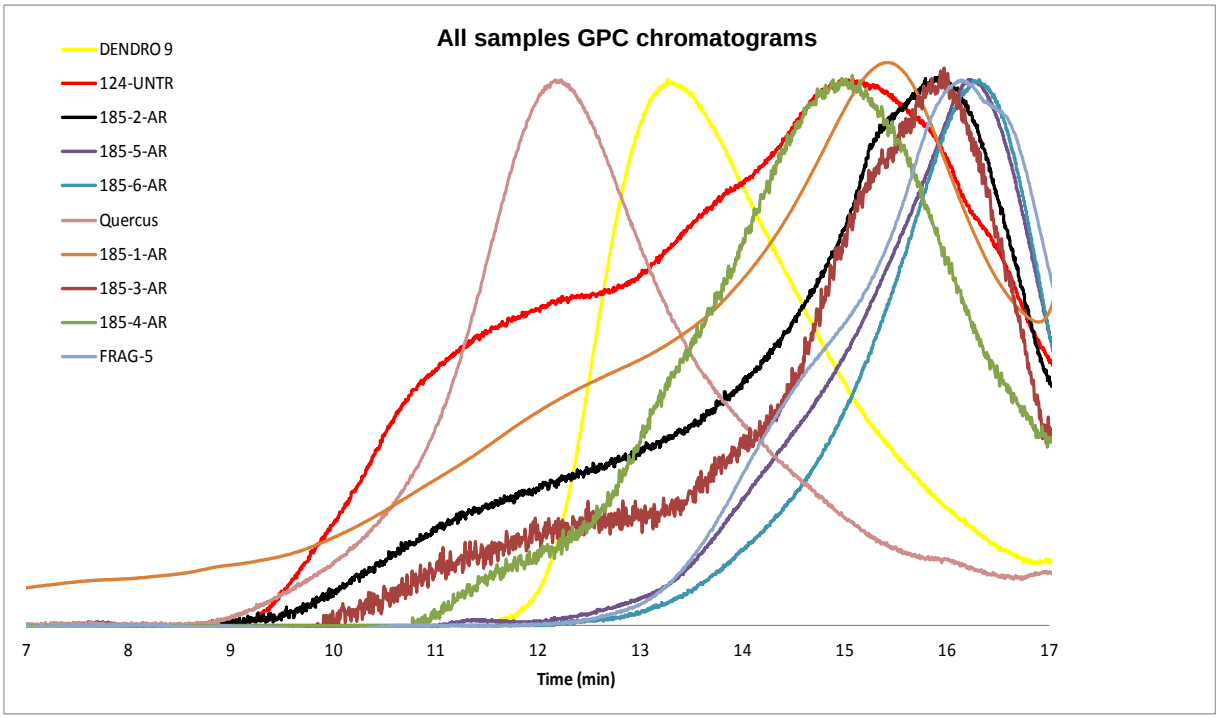

Figure 35 GPC chromatograms of all samples.

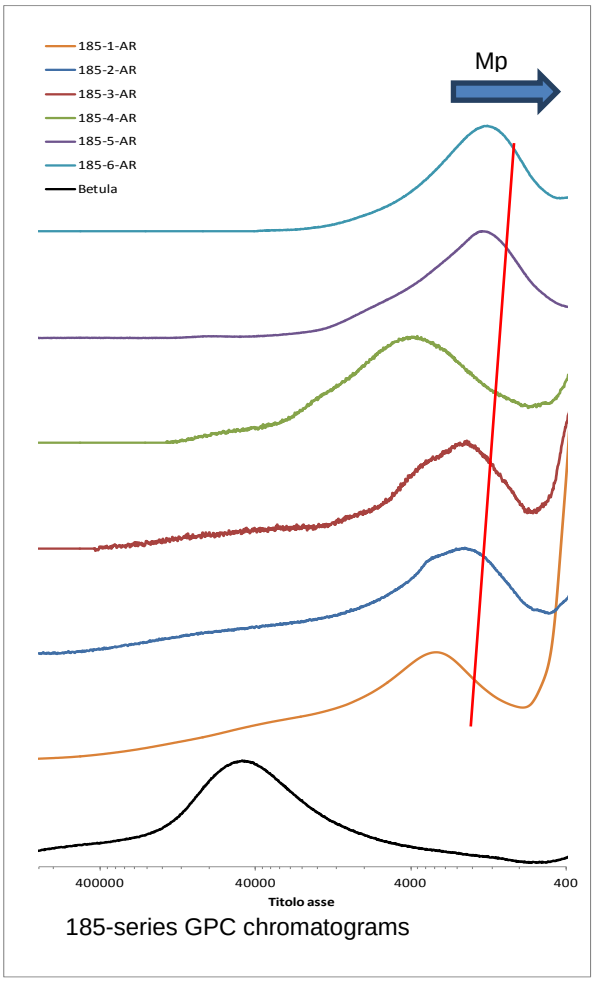

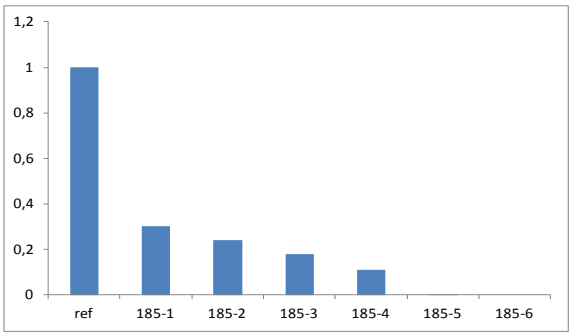

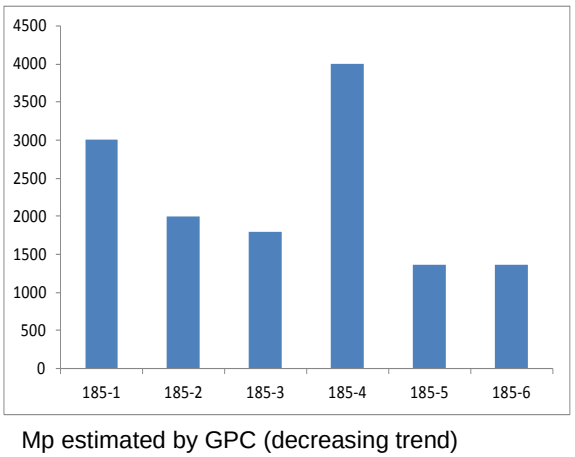

Figure 36 a) GPC chromatograms of 185-series relative to fresh birch (betula), b) Relative cellulose content estimated by GPC, c) Molecular weight (Mp) estimated by GPC.

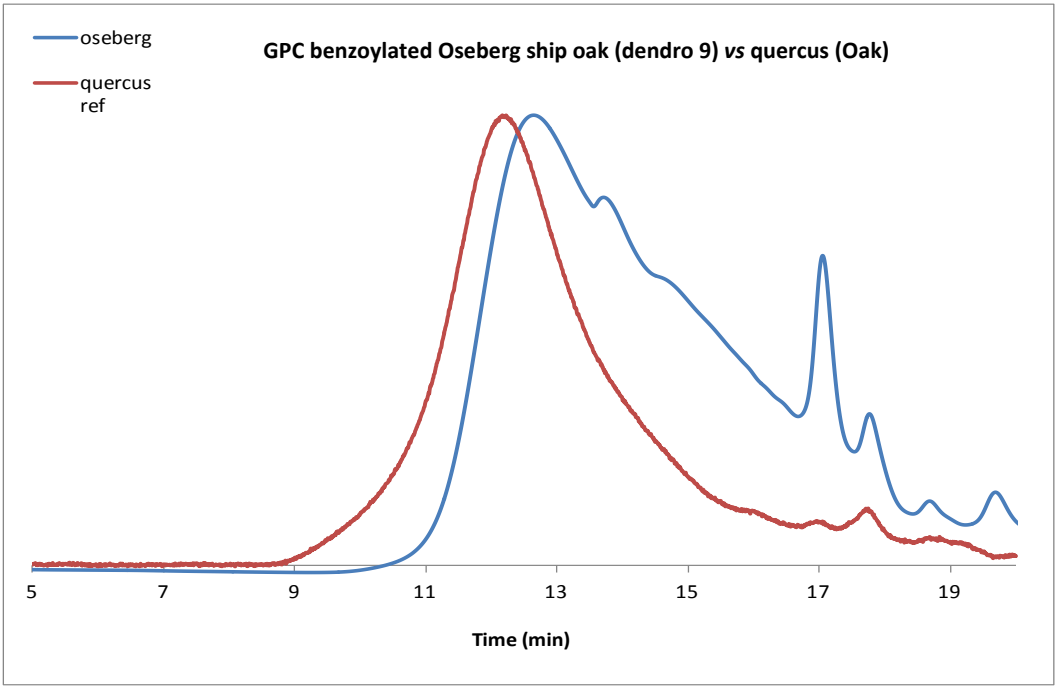

Figure 37 GPC chromatograms of Oseberg ship oak relative to fresh oak (quercus).

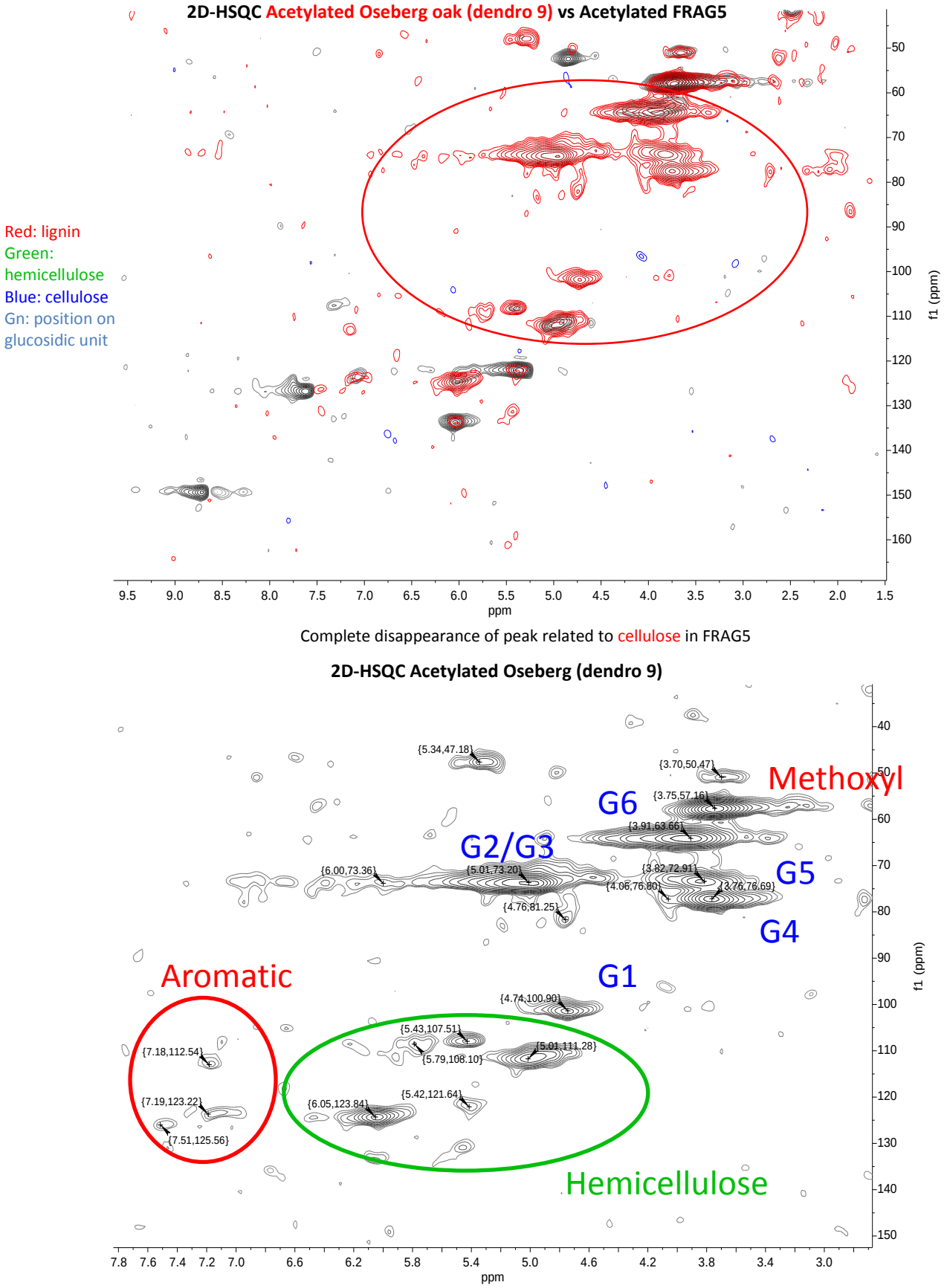

Figure 38 2D-NMR (HSQC) of a) Oseberg ship oak and b) Oseberg ship oak and Oseberg Fragment 5, which was alum-treated, but recently alum was removed by washing followed by freezed drying.

3.3.3 ArCo Project Simple sled '229'

Eight archaeological samples were taken from four alum-treated fragments (Figure 39). For each fragment two samples were taken from two regions "alum rich" – AR, close to the surface – and "alum poor" – AP, from the core. The samples: 1B-AP, 1B-AR, 1C-AP, 1C-AR, 1D-AP, 1D-AR, 5-AP and 5-AR were investigated.

These investigations aimed to:

- highlight differences in the chemical composition between the surface and the core of these wood fragments;
- investigate the effects of artificial aging on both the organic and inorganic components.

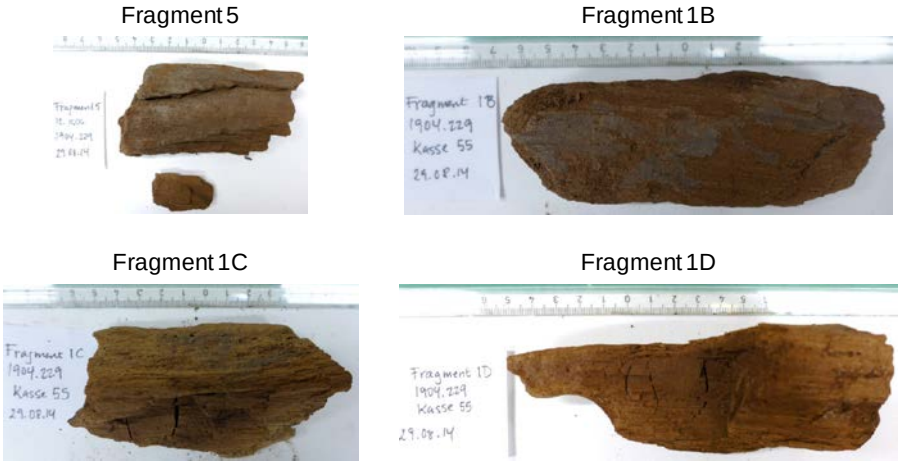

Figure 39 Archaeological alum-treated samples from simple sled '229'

SEM investigations

Samples **1C-AP, 1C-AR, 1D-AP** and **1D-AR** were examined by SEM recording images at high magnification (from 250x to 1500x). EDS spectra and elemental mapping were acquired in different areas. The experimental conditions are described in section 2.1.

To better evaluate SEM images of archaeological samples, Figure 40 shows an undegraded oak wood sample.

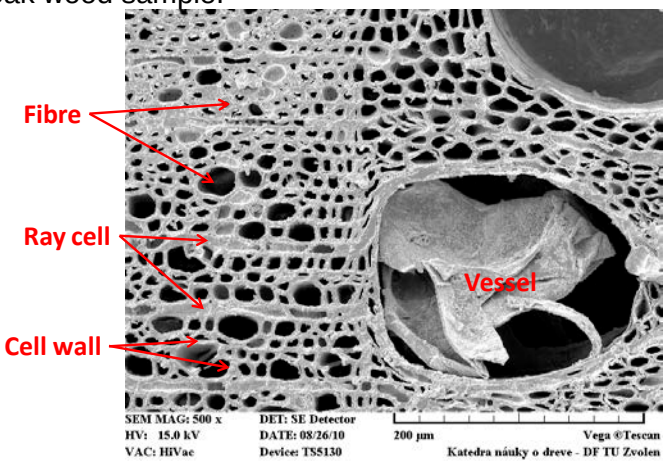

Figure 40 SEM image of sound oak wood

Alum poor samples

In Figure 41 SEM images for samples 1C and 1D from alum poor region are shown.

For both samples the thickness of the cell walls appeared very reduced with respect to sound wood, suggesting a depletion of carbohydrates. The middle lamella appeared to be the only part of the cell wall which survived. In sample **1C-AP** a partial collapse/shrinkage of wood cell walls was evident. The structure of sample **1D-AP** appeared to be in slightly better condition. Nevertheless, the images clearly show the difficulties in obtaining good cross sections from sample 1D-AP because of its very poor structural integrity.

Figure 42 shows the EDS spectra for the two samples. A series of spectra were acquired in different spots, but no significant differences were noticed.

The spectra highlighted the presence of S and K as major elements. No Al was observed for alum poor region.

To investigate the distribution of these elements some mappings were acquired. Figures 43 and 44 show the mappings of two selected areas for the two alum poor samples.

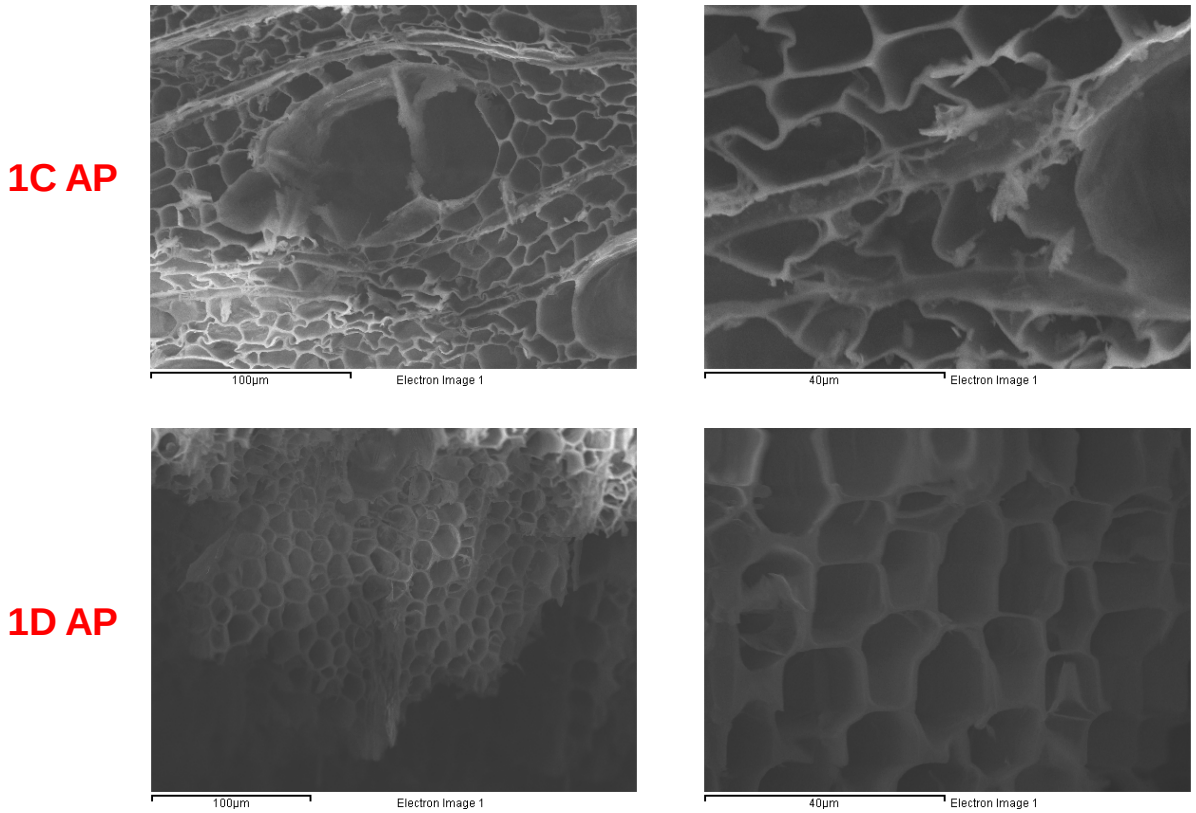

Figure 41 SEM images of AP samples. Left: 500x magnification, right: 1500x magnification.

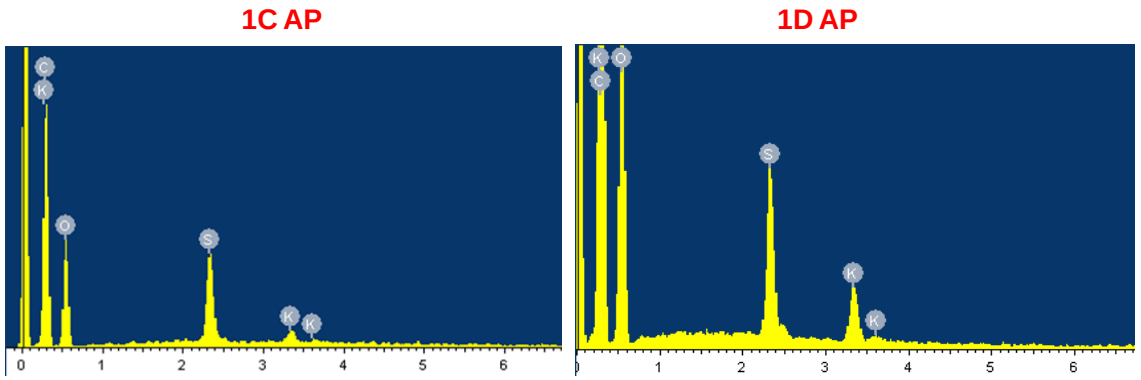

Figure 42 EDS spectra for alum poor samples

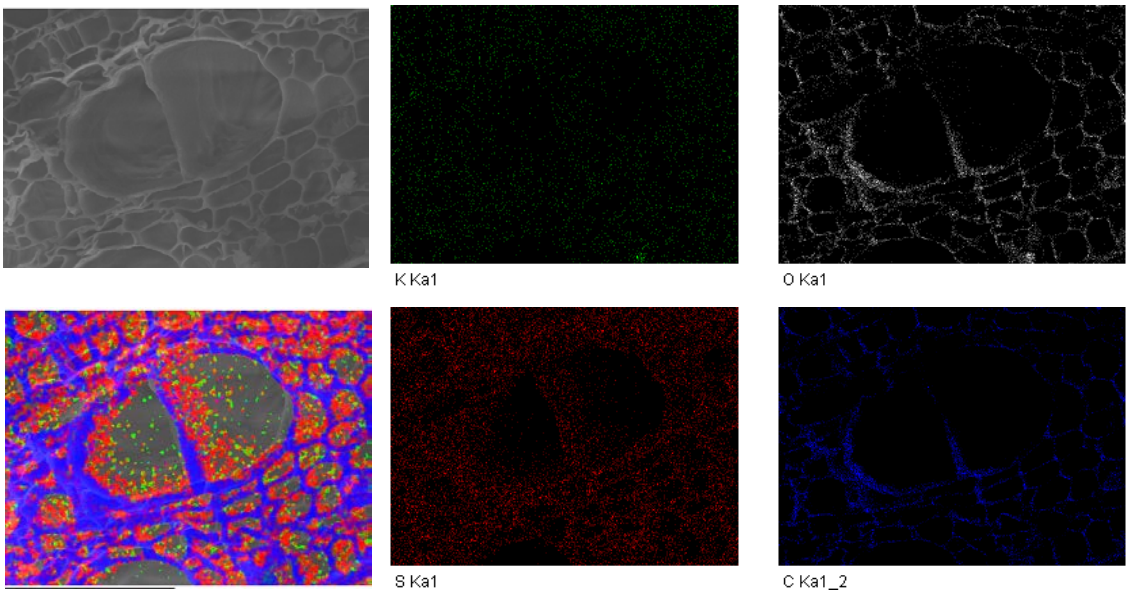

Figure 43 Elemental mapping for sample 1C-AP.

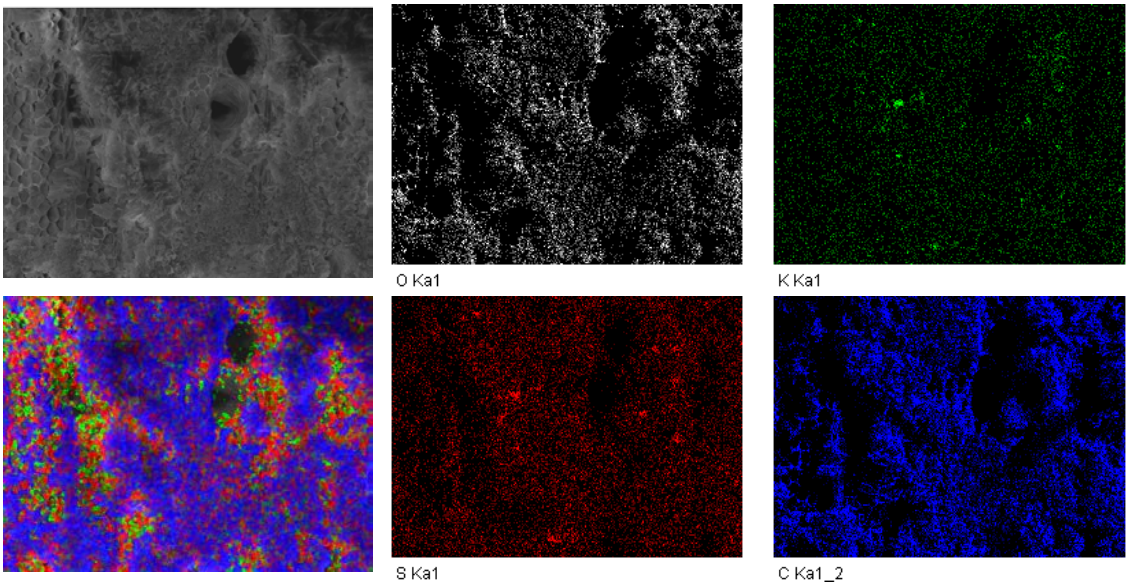

Figure 44 Elemental mapping for sample 1D-AP

For both samples **1C-AP** and **1D-AP**, K and S were distributed quite evenly, in both the cell walls and the cell lumens. It was difficult to assess if these elements were also present in the vessels because of shadowing problems. In sample **1D-AP** some intense spots were noticed in the K mapping (Figure 44), whose position corresponded to intense spots in the S mapping, indicating the presence of particles (recrystallised salts), but also in this case no Al was detected. This was likely due to a low sensitivity of the technique, but it was a clear indication of the significant differences in concentration between Al, K and S. Hutchings [55] and Braovac [56] found similar differences between Al and the other elements using SEM-EDX on Oseberg wood, suggesting that alum had undergone decomposition or that differences in penetration/diffusion had occurred.

Alum rich samples

Figure 45 shows SEM images for samples 1C and 1D from alum rich region. In sample **1C-AR** the structural integrity of cell walls appeared almost completely compromised in some areas: the detachment of cell wall was evident and some cells were completely collapsed. Spare fragments were also noticed in the cavities. In sample **1D-AR** the structure appeared in slight

better condition, and also in this case particles were noticed. Generally the wood structure was in worse condition than in samples from alum poor region. Figure 45 shows the EDS spectra of the two samples.

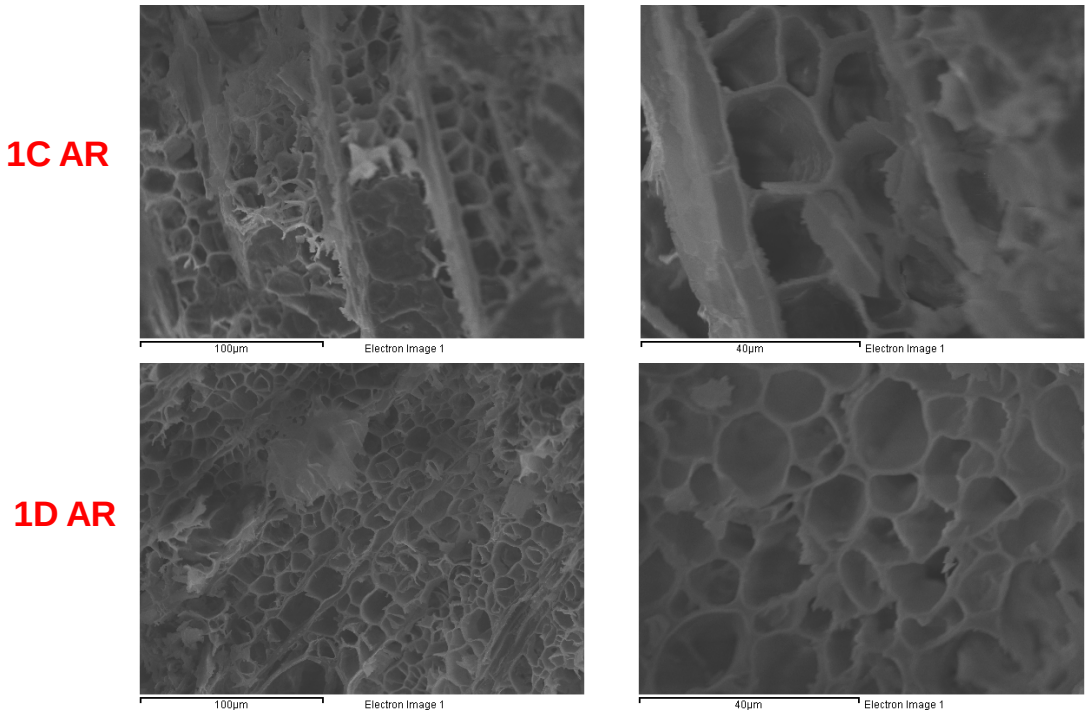

Figure 45 SEM images of alum rich samples. Left: 500x magnification, right: 1500x magnification.

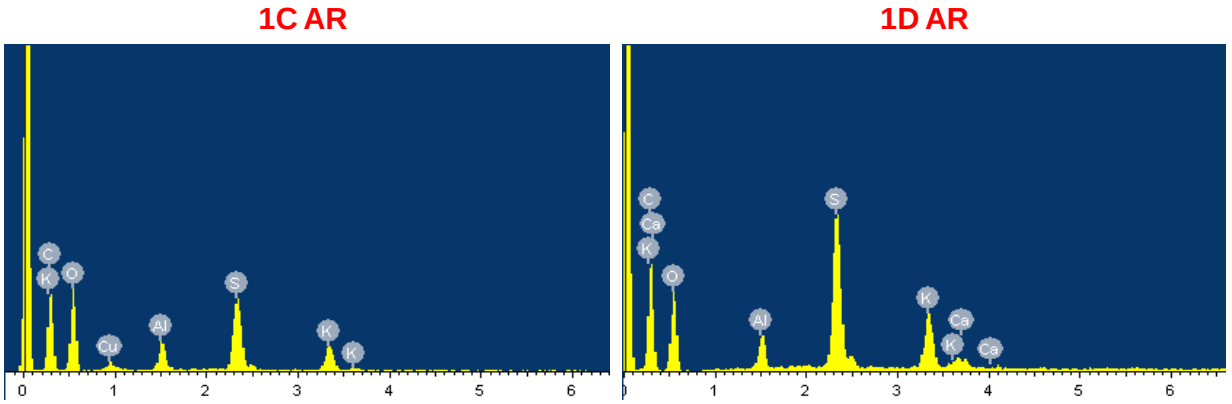

Figure 46 EDS spectra of two spots of alum rich samples.

The spectra showed the presence of Al, K and S as major elements, from the alum treatment. Also other elements were detected (Cu for sample **1C-AR** and Ca for sample **1D-AR**), indicating a higher inorganic content than in alum poor samples. Samples **1C-AR** and **1D-AR** were taken from the surface of the fragments, thus these minor elements were likely absorbed from the burial environment or during storage. Also for these samples mappings were acquired. Figures 47 and 48 show the mappings of two selected areas for the two samples.
For sample **1C-AR (**Figure 47) the co-presence of Al, K and S was clearly detected in a vessel, confirming the presence of alum or a salt with similar composition not only on the cell walls but also in the core of the cells. The presence of particles was even more evident for sample **1D AR (**Figure 48), as highlighted by the spots shown in the elemental mapping for Al, K and S. Shadowing problems could not be avoided because of the impossibility to obtain a completely flat surface for the cross sections. Nevertheless, S seemed to be more widely distributed than Al and K, indicating that probably not only alum particles were present. In addition, the distribution of the three elements was not completely homogeneous.

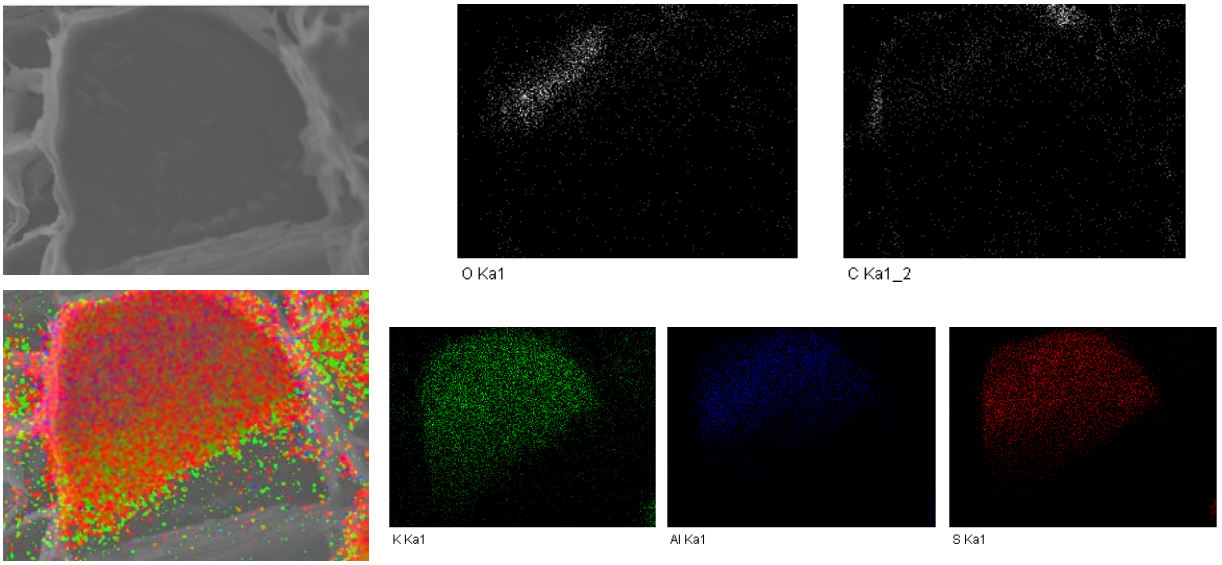

Figure 47 Elemental mapping for sample 1C-AR

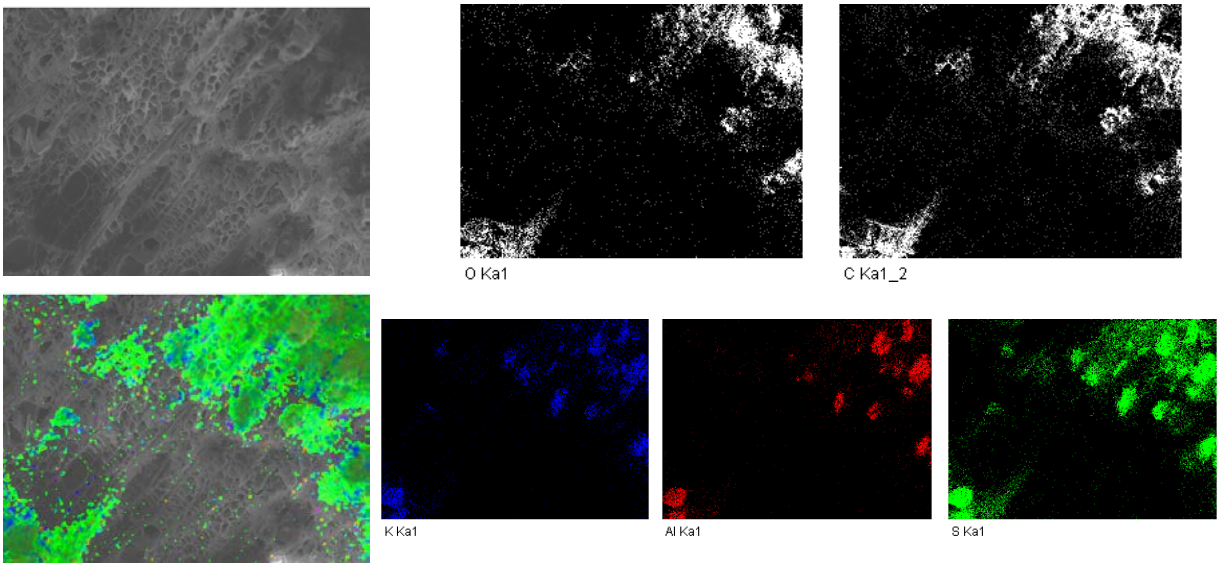

Figure 48 Elemental mapping for sample 1D AR

Observations*:* SEM-EDX highlighted that both alum poor and alum rich samples had undergone a high extent of structural deterioration. One of the most interesting result was the detection of Al only in alum rich samples. This could be due to the sensitivity of the technique, but of course it is an index of a significant difference in the concentration of this element, whereas this cannot be said for K and S, which were clearly detected in all samples, thus penetrated more deeply. This non-homogeneous distribution suggested that not only alum was present in the samples, but also some products of its partial decomposition and that differences in penetration/diffusion had occurred. The technique does not allow the certain identification of alum particles: the presence of Al, K and S in elemental form is not an univocal proof for alum presence.

ICP-OES and IC-LC conductivity analyses

As described in section 2.1 (point 2), all the samples were divided into two parts: ICP-OES analyses were performed on one part. A second subsample underwent water extraction and IC analysis was performed on the extract, whereas ICP-OES was also performed on the residue. Table 13 shows the results obtained for the alum rich and alum poor samples.

Table 13 Metals and Anions content for the samples from the Oseberg collection

	5 AP		5 AR		1B AP		1B AR		1C AP		1C AR		1D AP		1D AR	
	as it is	eluate / residue	as it is	eluate / residue	as it is	eluate / residue	as it is	eluate / residue	as it is	eluate / residue	as it is	eluate / residue	as it is	eluate / residue	as it is	eluate / residue
(mg/kg)																
ELEMENTS	**ICP-OES analysis**															
Ag	<QL	<QL	<QL	<QL	<QL	<QL	<QL	<QL	<QL	<QL	<QL	<QL	<QL	<QL	<QL	<QL
Al	18326	745	41346	86	52556	3597	53444	309	6826	608	48509	248	4473	524	28392	336
As	6	12	9	6	9	13	10	6	15	9	10	3	13	19	7	9
Sb	<QL	<QL	<QL	<QL	<QL	<QL	<QL	0	1	<QL	<QL	<QL	<QL	<QL	<LQ	<QL
Ba	6	36	5	17	3	8	3	18	30	4	6	1	24	11	12	13
Be	<QL	<QL	<QL	<QL	<QL	<QL	<QL	<QL	<QL	<QL	<QL	<QL	<QL	<QL	<QL	<QL
B	<QL	<QL	<QL	<QL	<QL	<QL	<QL	<QL	<QL	<QL	<QL	<QL	<QL	<QL	<QL	<QL
Cd	0	<QL	1	<QL	0	0	0	0	1	<QL	1	<QL	1	<QL	1	<QL
Ca	956	100	830	76	231	50	386	114	1441	46	543	31	982	108	1422	117
Cr	1	1	2	1	1	1	1	1	2	0	2	0	1	1	1	1
Co	<QL	<QL	1	<QL	<QL	<QL	0	<QL	0	<QL	0	<QL	0	<QL	0	<QL
Cu	176	238	1254	58	262	203	431	56	244	122	554	44	249	563	567	95
Fe	633	373	1931	203	396	526	1341	116	608	222	1639	60	669	791	1482	228
Li	0	1	0	<QL	0	0	0	0	0	1	<QL	<QL	0	<QL	<QL	<QL
Pb	8	4	50	1	1	2	8	1	1	3	3	1	4	10	4	3
Mg	65	16	213	8	41	16	59	8	213	5	149	3	204	16	154	14
Mn	24	1	48	0	12	0	17	0	18	<QL	18	<QL	17	1	17	1
Mo	<QL	1	1	1	<QL	1	<QL	1	3	<QL	0	<QL	1	<QL	0	<QL
Ni	<QL	<QL	3	<QL	<QL	<QL	0	<QL	1	<QL	1	<QL	1	<QL	2	<QL
Se	2	2	<QL	1	<QL	1	<QL	1	3	1	<QL	1	3	4	<QL	2
Si	9	672	159	105	23	804	78	26	41	114	419	16	260	606	131	5
Sn	4	7	3	3	3	6	3	3	4	5	3	3	10	15	2	6
V	2	3	5	2	1	2	1	2	8	<QL	3	0	5	4	4	2
Zn	1078	15	6913	15	373	15	885	11	614	7	1050	2	844	40	1573	144
K	32484	548	73856	194	65632	1774	71572	208	24976	120	71965	56	21072	336	55385	321
Na	76	256	69	118	46	131	52	84	119	140	53	79	128	337	42	179
Ti	12	37	20	5	6	28	9	9	18	12	15	5	11	52	12	10
S	92856	3241	192249	1781	195567	4633	209367	2576	79475	1044	198234	527	54594	2625	137708	2964
Hg	26	24	53	1	9	16	22	1	2	30	8	7	4	213	8	26
ANIONS	**IC-LC conductivity analysis**															
F^-		237		<QL		<QL		251		346		<QL		592		< 4,7
$HCOO^-$		0		0		0		0		0		0		0		0
CH_3COO^-		<QL		<QL		<QL		<QL		<QL		<QL		<QL		<QL
Cl^-		724		446		0		0		105		0		654		369
Br^-		<QL		<QL		<QL		5		5		<QL		<QL		<QL
NO_3^-		383		150		88		63		94		48		475		180
PO_4^{3-}		987		<QL		<QL		< 35		275		<QL		370		<QL
SO_4^{2-}		299445		565902		567122		576045		355376		630267		219639		558716

<QL = below quantification limit

For the unextracted samples the elements with the highest concentration were Al, K and S from the alum treatment. Generally, the AP samples showed lower concentrations of all elements with respect to the corresponding AR samples, as expected since they were taken from the core of the fragments. Samples **1B-AP** and **1B-AR** were an exception, since they showed a similar content of all elements, indicating that for this fragment no significant differences in the inorganic content between the surface and the core were present. Among the minor elements,

a higher content of Fe and Cu was found in the AR samples with respect to the corresponding AP samples. The concentration of Ca did not appear to follow an exact trend.
The results obtained on the residues after water extraction highlighted that generally the concentrations of major elements (Al, K and S) in wood were largely reduced, indicating that they were mostly present in the form of water-soluble salts. Sample **1B-AP** showed higher concentrations of almost all elements with respect to the others. It was interesting to notice that AP samples generally showed a higher inorganic content than AR samples, after water extraction, indicating a higher content of water-insoluble salts penetrated into the core of the fragments.
The **IC analyses** highlighted the predominant presence of sulphates in the water extracts, detected with higher concentrations in AR samples than AP samples, except for fragment 1B. Low concentrations of fluorides, chlorides, nitrates and phosphates were found for some samples with no specific trend.
In order to evaluate the stoichiometric ratios between the major elements Al, K and S, the concentrations were transformed from mg/kg to mmol/100g and the ratios between S/Al, S/K and K/Al were calculated (Table 14).

Table 14 Stoichiometric ratios between Al, K and S in the samples from the Oseberg collection.

	5 AP		5 AR		1B AP		1B AR		1C AP		1C AR		1D AP		1D AR	
	as it is	residue	as it is	residue	as it is	residue	as it is	residue	as it is	residue	as it is	residue	as it is	residue	as it is	residue
S/Al	4.3	3.7	3.9	17.4	3.1	1.1	3.3	7.0	9.8	1.4	3.4	1.8	10.3	4.2	4.1	7.4
S/K	3.5	7.2	3.2	11.2	3.6	3.2	3.6	15.1	3.9	10.6	3.4	11.5	3.2	9.5	3.0	11.3
K/Al	1.2	0.5	1.2	1.6	0.9	0.3	0.9	0.5	2.5	0.1	1.0	0.2	3.3	0.4	1.3	0.7

In the unextracted samples the K/Al ratios for samples 1C-AP and 1D-AP were 2.5 and 3.3, respectively. For the other samples the K/Al ratios were close to 1, in agreement with the alum formula $KAl(SO_4)_2 \cdot 12H_2O$. S/K and S/Al ratios showed values around 3-4, except for samples **1C-AP** and **1D-AP**, which showed values around 10. All these values were considerably different from the 2:1 ratio expected according to the alum formula. Alum modifications, differences in penetration/diffusion and presence of other sources of S are the hypotheses suggested by these results.
In the residues the stoichiometric ratios between Al, K and S drastically changed. K/Al ratios were less than 1, except for sample **5-AR**, and S/K ratios reached values around 10, suggesting a preferential removal of K in water with respect to Al and S. S/Al ratios changed after water extraction without following a clear trend. These changes were taken as a further indication that different salts with different solubility were present in the samples.

After artificial aging

The samples were analysed after artificial aging (Condition described in Chapter 2.2) and Table 15 reports the obtained results.
For the unextracted samples the main differences observed after aging concerned a general increase in Al and K concentrations and an overall decrease in S concentrations, with a consequent decrease in the S/Al and S/K ratios. However, in most of the AP samples the S content increased after ageing. These observations suggested that S may have diffused out of the AR areas of the wood, where it was most concentrated before ageing, in the form of sulphuric acid when exposed to the high RH levels, reducing the differences in the inorganic content between AP and AR samples. This was also in agreement with the IC results, because the concentration of sulphates increased for the artificially aged AP samples, though for the AR samples it was comparable with that obtained before aging.

Table 15 ICP-OES and IC conductivity results for the Oseberg samples after artificial aging

	5 AP		5 AR		1B AP		1B AR		1C AP		1C AR		1D AP		1D AR	
[mg/kg]	as it is	residue	as it is	residue	as it is	residue	as it is	residue	as it is	residue	as it is	residue	as it is	residue	as it is	residue
Element	**ICP-OES analysis**															
Ag	<QL	<QL	<QL	<QL	<QL	<QL	0	<QL	<QL	<QL	<QL	<QL	<QL	<QL	<QL	<QL
Al	88529	334	106341	226	83198	265	144834	300	112014	451	65378	744	49665	528	82009	383
As	5	4	5	4	4	3	6	4	9	8	6	4	10	7	6	4
Sb	<QL	<QL	<QL	<QL	<QL	<QL	<QL	<QL	<QL	<QL	<QL	<QL	<QL	<QL	<QL	<QL
Ba	5	3	1	<QL	3	4	4	3	12	15	6	6	13	8	5	3
Be	<QL	<QL	<QL	<QL	<QL	<QL	<QL	<QL	<QL	<QL	<QL	<QL	<QL	<QL	<QL	<QL
B	<QL	<QL	<QL	<QL	<QL	<QL	<QL	<QL	<QL	<QL	<QL	<QL	2	<QL	<QL	<QL
Cd	0	<QL	<QL	<QL	0	<QL	0	<QL	0	<QL	1	<QL	1	<QL	<QL	<QL
Ca	727	46	252	33	131	48	160	36	1234	70	1096	48	1763	49	810	79
Cr	1	0	1	0	0	<QL	1	<QL	1	0	1	0	1	0	1	1
Co	0	<QL	0	<QL	<QL	<QL	0	<QL	0	<QL	0	<QL	0	<QL	0	<QL
Cu	150	51	361	100	170	356271	184	41	233	79	409	78	192	36	300	55
Fe	588	89	789	59	291	41	425	66	566	89	937	147	474	48	805	76
Li	<QL	<QL	<QL	<QL	<QL	<QL	<QL	<QL	<QL	<QL	<QL	<QL	<QL	<QL	<QL	<QL
Pb	1	<QL	5	<QL	1	<QL	2	2	1	<QL	4	2	3	1	3	<QL
Mg	83	4	61	4	43	3	41	5	104	5	97	6	151	6	84	8
Mn	27	<QL	16	<QL	12	<QL	11	<QL	14	<QL	16	<QL	16	<QL	10	<QL
Mo	0	<QL	<QL	<QL	<QL	<QL	<QL	<QL	1	2	0	0	1	1	0	<QL
Ni	<QL	<QL	1	<QL	<QL	<QL	0	<QL	0	<QL	1	<QL	1	<QL	4	<QL
Se	<QL	<QL	<QL	<QL	<QL	<QL	<QL	<QL	<QL	<QL	<QL	<QL	<QL	<QL	<QL	1
Si	<QL	<QL	<QL	<QL	<QL	<QL	<QL	<QL	<QL	<QL	14	123	<QL	<QL	6	<QL
Sn	<QL	<QL	1	1	0	<QL	0	<QL	<QL	<QL	1	1	<QL	<QL	1	<QL
V	3	1	2	1	1	<QL	1	<QL	3	2	3	1	3	1	3	1
Zn	971	14	1255	7	411	2	579	3	459	16	706	4	762	12	694	3
K	67052	100	70383	106	86509	65	199431	62	64471	340	97109	262	52187	426	135467	108
Na	90	65	64	47	75	45	83	53	99	72	74	43	106	25	64	64
Ti	5	5	8	7	3	3	4	4	9	11	9	10	5	3	6	6
S	110210	1134	129627	825	112898	614	111879	632	105326	3458	112574	1168	97152	2358	102274	1446
Hg	9	8	15	13	2	2	4	3	3	2	4	4	2	2	3	2
ANIONS	**IC-LC conductivity analysis**															
	5 AP		**5 AR**		**1B AP**		**1B AR**		**1C AP**		**1C AR**		**1D AP**		**1D AR**	
[mg/kg]	as it is	extract	as it is	extract	as it is	extract	as it is	extract	as it is	extract	as it is	extract	as it is	extract	as it is	extract
F^-		<QL		<QL		<QL		147		<QL		<QL		<QL		<QL
$HCOO^-$		<QL		<QL		<QL		<QL		<QL		<QL		<QL		<QL
CH_3COO^-		<QL		<QL		<QL		<QL		<QL		<QL		<QL		<QL
Cl^-		<QL		<QL		<QL		361		<QL		<QL		387		<QL
Br^-		<QL		<QL		<QL		<QL		<QL		<QL		<QL		<QL
NO_3^-		<QL		<QL		<QL		<QL		<QL		<QL		<QL		<QL
PO_4^{3-}		168		156		145		341		65		121		136		168
SO_4^{2-}		567926		578377		550350		372519		516859		443945		599796		567926

Observations: The concentrations of Al, K and S showed stoichiometric ratios not corresponding to those present in the alum chemical formula $KAl(SO_4)_2 \cdot 12H_2O$. The present salts were proven to be mostly water-soluble and in the form of sulphates by IC analyses. The core of the samples contained more water-insoluble salts than the surface and higher values of S/Al ratios, confirming a non-homogeneous distribution of elements. Redistribution of inorganics was observed after ageing, most notably as an increase in S and sulfates in the AP regions of fragments.

XRD

Some XRD analyses were performed in order to assess the presence of alum and/or some crystalline products due to its decomposition. The diffraction pattern of a reference sample of alum was acquired, and it is shown in Figure 49. The diffraction patterns for samples **1B-AP** and **1B-AR** were similar. Alum was identified as well as mercallite ($KHSO_4$). Figure 50a shows the diffraction patterns for these two samples. Alum and mercallite were identified in all samples. In particular, samples **5-AP** and **5-AR** gave similar results, whereas samples **1C-AP** and **1D-AP** showed more intense signals for mercallite with respect to the corresponding AR samples. In addition, all the AP samples, with the exception of sample **1B-AP**, showed a low relative diffraction intensity and the presence of an amorphous component. Figure 50b reports the XRD patterns for samples **1C-AP** and **1C-AR**.

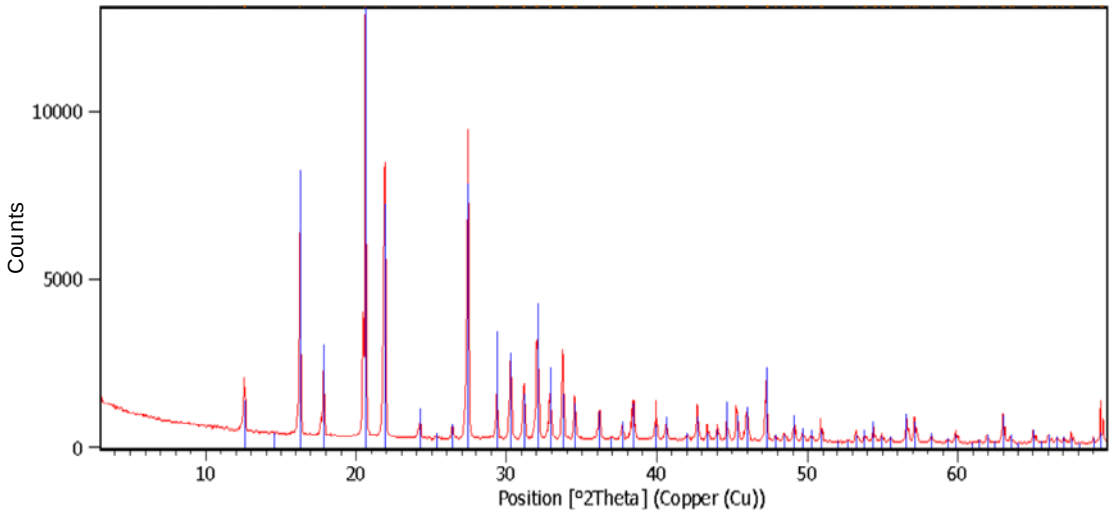

Figure 49 XRD diffraction pattern of reference alum $KAl(SO_4)_2 \cdot 12H_2O$.

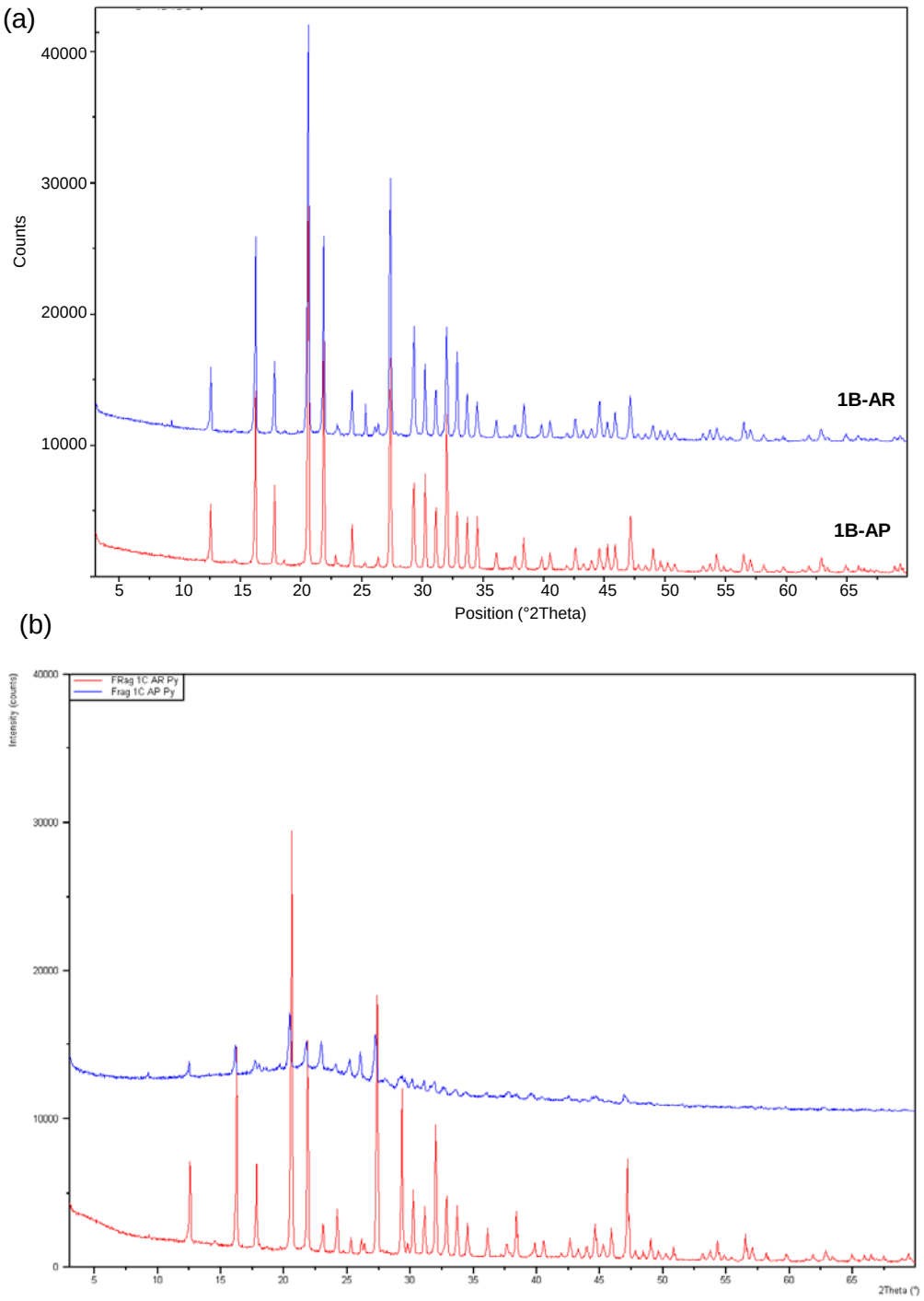

Figure 50 XRD patterns for (a) samples 1B-AP and 1B-AR and (b) samples 1C AR and 1C AP

After aging

While not much change in the proportions of alum and mercallite could be observed in the AR sample after aging, significant differences could be seen in 1C-AP and 1D-AP.1C-AP showed a significant increase in intensity of alum peaks (Figure 51a), while the intensity of mercallite peaks increased for 1D-AP (Figure 51b). In both cases the signal from the amorphous component appears to be reduced after ageing. This supports ICP and IC-LC results suggesting that sulfate compounds migrated into the AP regions of the fragments during aging.

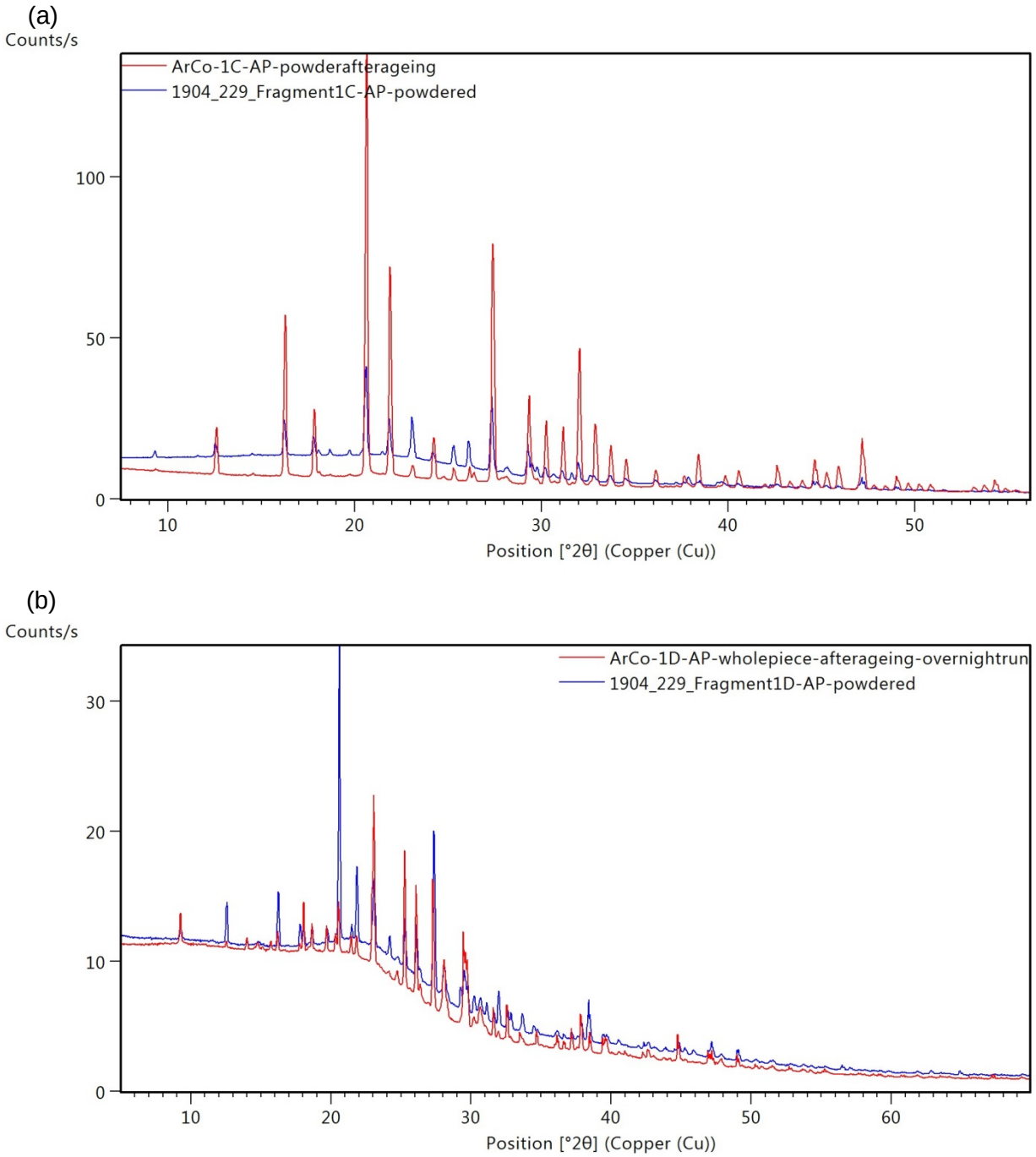

Figure 51 XRD diffraction patterns before (blue) and after (red) aging for (a) 1C-AP and (b) 1D-AP

Observations: the presence of mercallite allowed us to conclude that alum had undergone degradation reactions, and it was no longer present only in the original form. The fact that mercallite was more abundant in alum poor samples (more internal wood) is probably due to diffusion processes more effective for mercallite than for alum. The amorphous component present in the AP samples is likely due to the wood component, which is visible due to the decrease in the relative amount of crystalline compounds. Changes in distribution of alum and mercallite were evident in AP samples after aging.

FT-IR spectroscopy (ATR mode)

All the samples from the Oseberg collection were analysed by FTIR. In addition, reference alum and sound oak wood were analysed as well (Figure 52). The presented spectra are the average of three replicates.

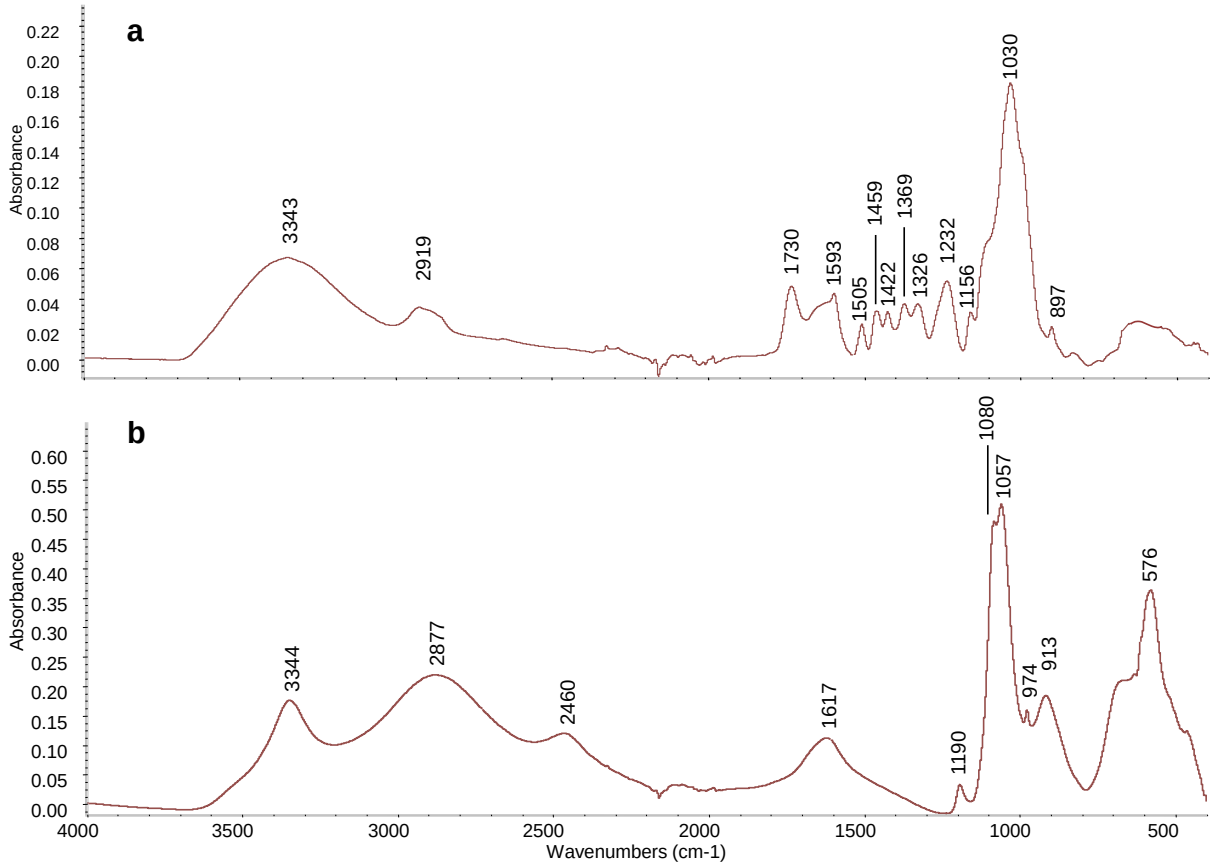

Figure 52 FTIR spectra (ATR mode) of a) sound oak wood and b) alum.

The alum spectrum showed absorption bands at 3359, 2964 and 2470 cm^{-1} attributed to crystal water. The other absorption bands in the spectrum were attributed to different stretching mode of the sulphate chemical group [57]. On the other hand, wood showed a fingerprint region between 800 and 1800 cm^{-1} with many absorption bands which can be attributed to either carbohydrates or lignin. This fingerprint region showed several overlapping of bands between alum and wood spectra, in particular in the regions 1700-1500 cm^{-1} and 1200-800 cm^{-1}. This complicates the interpretation of the spectra when alum and wood are both present in the same sample. Nevertheless, at around 576 cm^{-1} an absorption band attributable to sulphate vibrational modes was detected in the alum spectrum [57] and wood did not show any significant absorption in this region. This absorption band was used to perform an evaluation of the data based on the subtraction of the alum contribution from the spectra obtained for the Oseberg samples as follows: the spectra were all normalised with respect to the intensity of the signal at 576 cm^{-1}, thus taking into account the differences in alum concentration among the samples; after normalisation the spectrum of alum was subtracted from all the other spectra. In fact, before performing this subtraction, the FTIR spectra obtained for alum rich samples showed a strong overlapping of the alum signals with the wood ones, indicating a high concentration of alum (Figure 53). Similar results were obtained for sample **1B-AP**, confirming the results obtained by ICP-OES and XRD about the similarity of this sample to the alum rich ones. The spectra for samples **1C-AP**, **1D-AP** and **5-AP** showed alum signals with lower intensities. The spectra obtained after subtraction of the alum spectrum (Figure 54) indicated that alum interferences were mostly removed. The bands assigned to cellulose and hemicelluloses were mostly absent. The signal at 1010-1020 cm^{-1} showed a significant intensity, but this region presents an overlapping of cellulose and lignin signals, thus attribution is difficult [3, 58-60]. Nevertheless, a remarkable reduction of this band was detected with respect to sound wood. These observations allowed to assess the almost complete depletion of carbohydrates in these samples. Regarding lignin, the main observation was relative to the signal at 1713 cm^{-1}: this signal is assigned to C=O stretching in carboxylic acids [61] and it was

taken as an index for lignin oxidation. To provide semiquantitative results, the area and the height of this signal were compared to those of the signal at 1505 cm^{-1}, considered the marker signal for lignin and the one which undergoes the less changes with degradation, according to the literature [3, 62]. Table 16 reports the results of this calculation.
The obtained values highlighted that all the AR samples had a higher abundance of carboxyl functionalities, thus a higher extent of lignin oxidation compared to the corresponding AP samples.

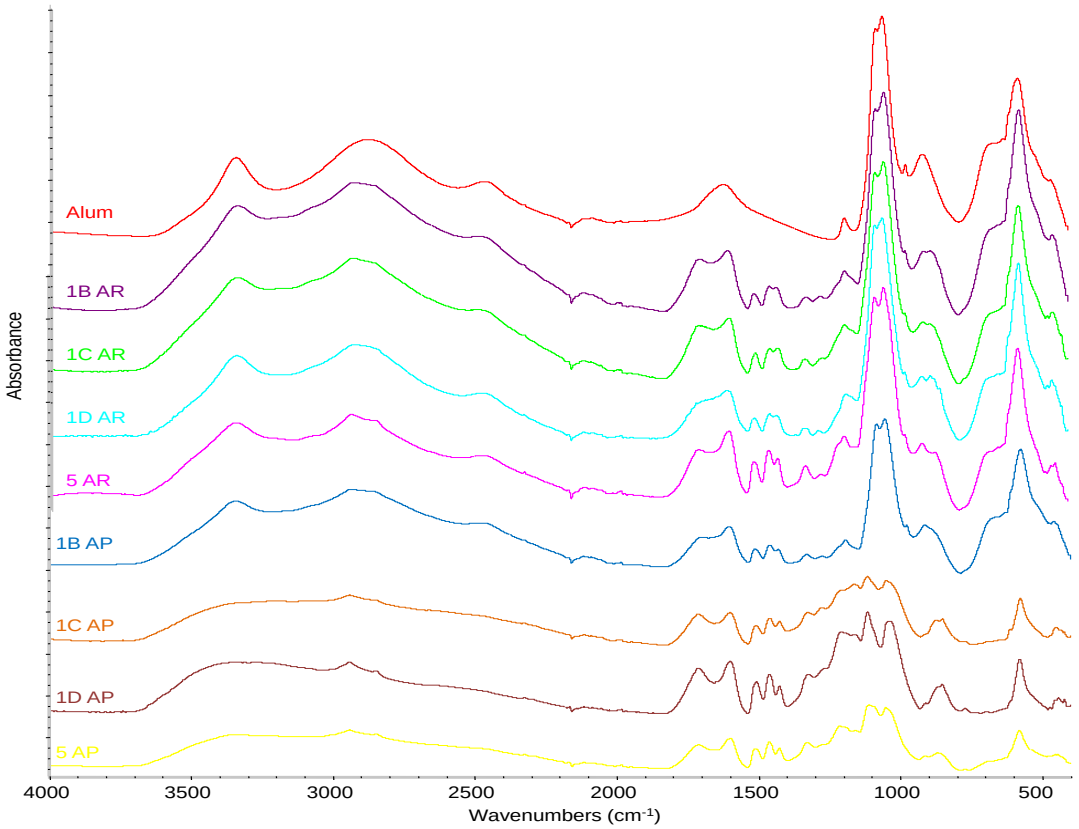

Figure 53 FTIR spectra (ATR mode) for the Oseberg samples.

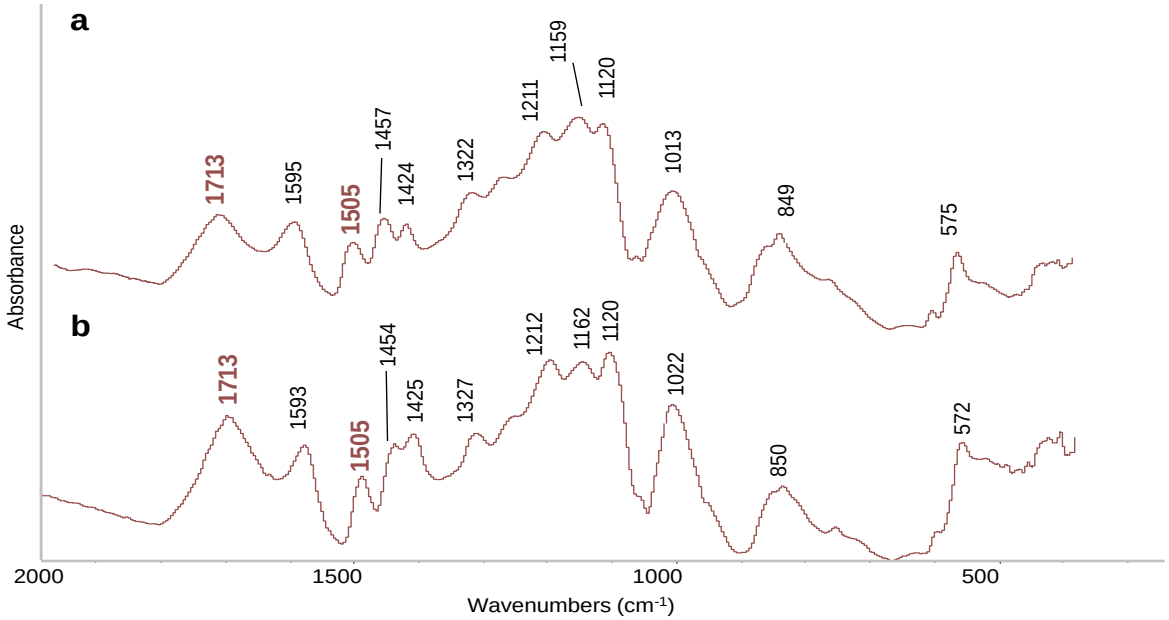

Figure 54 FTIR spectra (fingerprint region) of **a)** 1C-AP and **b)** 1C-AR from the Oseberg collection after subtraction of the alum spectrum.

Table 16 Ratios between the areas and heights of absorption bands at 1713 and 1505 cm-1 for the FTIR spectra of the Oseberg samples after subtraction of the alum spectra.

	$Area_{1713/1505}$	$Height_{1713/1505}$
1B-AP	3.6	1.3
1B-AR	6.2	2.1
1C-AP	4.2	1.5
1C-AR	5.2	1.6
1D-AP	2.9	1.1
1D-AR	3.8	1.3
5-AP	2.6	1.0
5-AR	3.2	1.5

Observations: FT-IR analysis was useful to confirm the differences in alum content among the samples. Nevertheless, alum represents an interference for evaluating wood degradation. In alternative to the washing of the samples to remove alum (with the risk to alter degraded wood composition), we adopted an approach concerning the data processing, thus subtracting the contribution of alum to the wood + alum spectra after normalization. This allowed us to obtain semi-quantitative results about the depletion of carbohydrates and lignin oxidation.

µFT-IR spectroscopy

The application of FT-IR to these samples is complicated by the simultaneous presence of alum and wood, which have many overlapping bands preventing from obtaining reliable results on wood degradation by this technique. For this reason, conventional FT-IR analysis was not performed on artificially aged samples because we didn't expect to observe significant variations.

On the hand, we exploited the advantages provided by FTIR microscopy in terms of spatial resolution, with the aim to overcome the problem. This resolution could be enhanced by use of synchtrotron radiation (SR), and during a beamtime allocated after an application from the coordinator of the project, Hartmut Kutzke, some samples from the Oseberg collection were analysed at the synchrotron Helmholtz Zentrum Berlin (Bessy II) in Berlin, Germany (Experimental research proposal 16103392; Titled: *Investigation of alum-conserved archaeological wood using various synchrotron-based analytical techniques,* 29/02/16 to 20/03/2016). The beamlines used was and **IRIS**-*IR Spectroscopy and Microscopy*. Both spot analyses and mapping were performed in order to determine the distribution of the materials into the wood matrix. A first example is the analysis of a micro-sample taken from the surface of fragment 5. The sample was squeezed between two diamond cells and analysed in transmission mode. Figure 55 shows a picture of the sample as it looked like under the microscope and a SR-FTIR spectrum representative of the spectra obtained from different spots measured in the sample.

The spectra obtained corresponded to the spectrum of alum. Absorption bands at 3359, 2964 and 2470 cm^{-1} are attributed to crystal water. The other absorption bands in the spectrum are attributed to different stretching mode of the sulphate chemical group in reference alum [57]. Even the brownish areas showed being very rich in alum, proving that the surface of wood was almost completely covered with alum.

The absorption band at 1442 cm^{-1} is not present in pure alum, and could be due to the presence of aluminium ammonium sulfate (vide infra). With the aim of obtaining information on the wood degradation state, another sample was taken 1mm under the surface. In this case, it was possible to identify some "alum regions" and some "wood regions" in the sample on the basis of the bands present in the different spectra obtained from different spots measured.

Figure 56 shows a picture of the two regions and an FTIR spectrum obtained from the wood region.

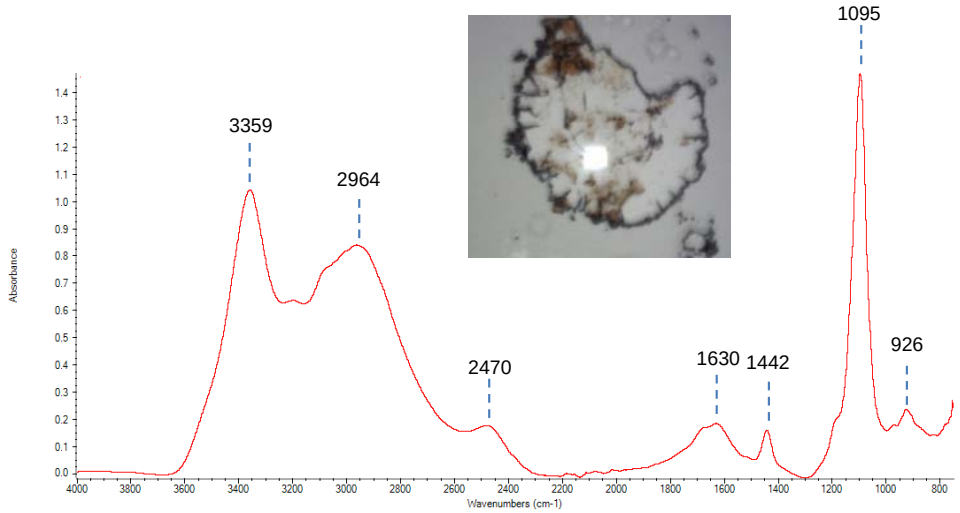

Figure 55 SR-µFTIR spectrum acquired of a sample from the surface of fragment 5 from Oseberg collection.

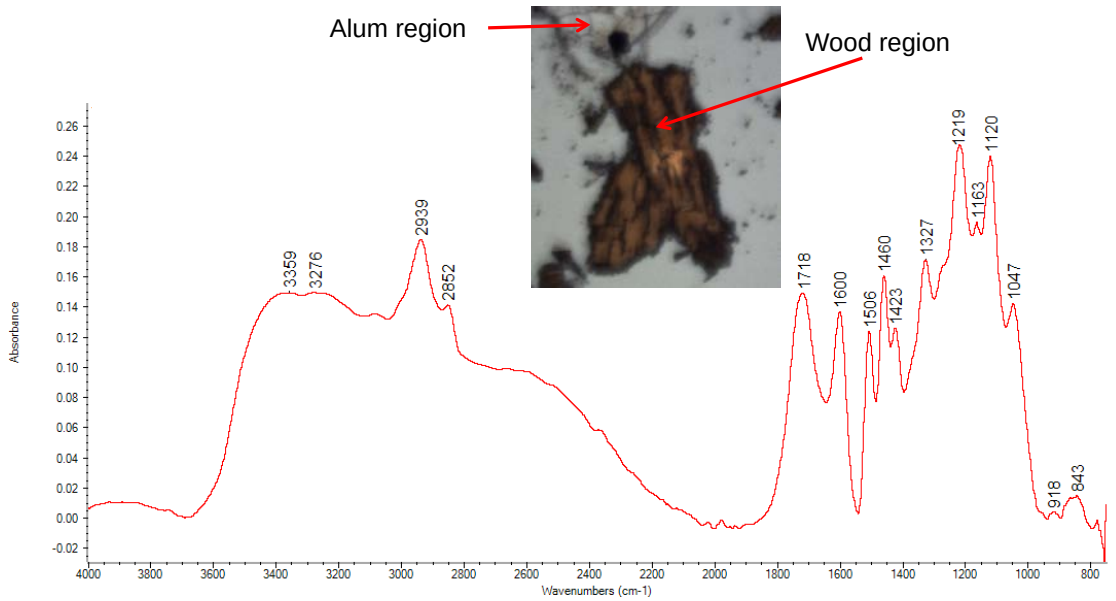

Figure 56 SR-µFTIR spectrum of a sample collected 1 mm under the surface of Oseberg fragment 5. Spectrum acquired from the wood region.

It was possible to notice that the spectrum from the wood regions was not pure: the presence of absorption bands attributed to alum, such as 3359 cm-1, as well as the impossibility to exclude that the signals in the region around 1100-1200 cm-1 derive from a combination of wood and alum absorption bands pointed to the co-presence of wood and alum in the spectra obtained. This prevented quantitative or semi-quantitative information to be obtained. Nevertheless, some qualitative observations were possible: the absorption bands attributed to cellulose and hemicelluloses were almost absent in the spectrum. In particular, the bands at 897, 1154, 1366, 1593 cm^{-1}, all related to the carbohydrate components [9, 58, 60], were not detected. All the identified absorption bands could be ascribed to lignin. One of the most interesting aspect was the intensity of the two absorption bands at 1718 and 1600 cm^{-1}. These bands are attributed to the stretching of carbonyl and carboxyl functionalities [63, 64], thus they can be related to lignin oxidation. The intensity of the bands suggested an extended oxidation of lignin, in agreement with the results obtained by the other techniques.

In order to remove the interferences from the presence of the alum salt bands in the spectra of the wood regions, a different approach from the spectral subtraction was tested. A part of fragment 5 was washed with hot bi-distilled water, dried and a µFT-IR map was acquired. The

spectra acquired in different spots after washing showed some slight differences in the relative abundances of the bands, if compared to the spectra obtained before washing. Figure 57 shows one of the spectra obtained from a central spot in the mapping, representative of the spectra obtained.

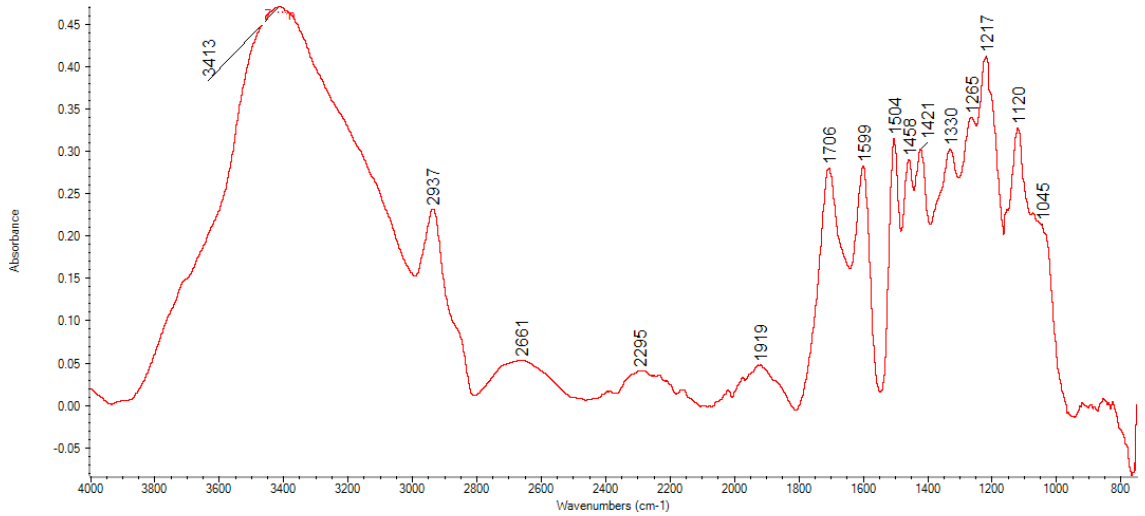

Figure 57 SR-µFTIR spectrum acquired from Fragment 5 after washing

The alum was actually removed by washing: comparing Figures 56 and 57, the bands in the region around 1120 cm^{-1}, deriving from alum, appear reduced. In the spectra obtained after washing, the position and distribution of bands seem to be in agreement with the signals deriving from wood. Residual water from the washing treatment was observed (3413 cm^{-1}). The problem of washing archaeological wood samples is the risk to remove wood degradation products, in particular the oxidation products. To investigate this aspect, three significant wavenumbers were selected: 1505 cm^{-1} attributed to aromatic skeletal vibrations in lignin, 1718 cm^{-1} attributed to C=O stretching in carboxylic acids and 2932 cm^{-1} attributed to C-H stretching in methyl and methylene groups [65, 66]. These absorption bands can be considered as indicative of the aromatic nuclei in lignin, the oxidation products and the aliphatic chains in lignin, respectively. Figure 58 shows the chemical images of the selected chemical groups obtained by mapping the absorbance at the selected wavenumbers, where the red colour means transmittance 0% and the blue colour means transmittance 100%.

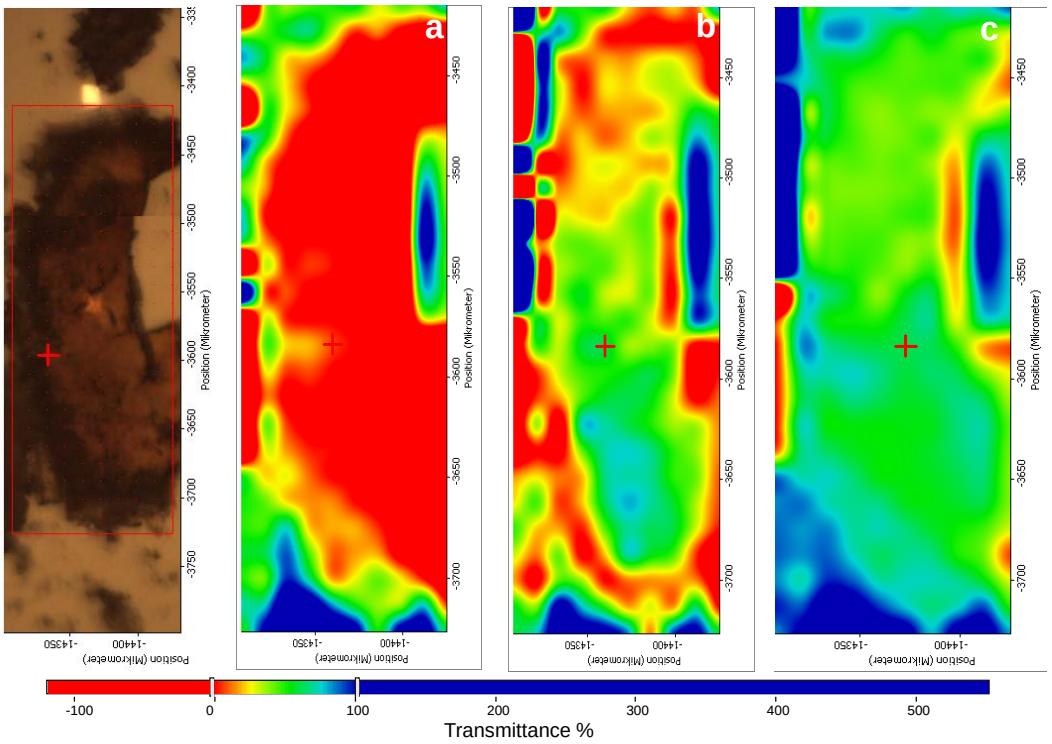

Figure 58 Mappings of IR absorption of Oseberg fragment 5 sample after washing corresponding to a) 1505 b) 2932 and c) 1718 cm^{-1}.

The distribution of lignin aromatic nuclei (Figure 58a) appeared homogenous, as expected since aromatic nuclei are so stable that they are not supposed to undergo any change in these conditions. On the other side, the intensity of the signal related to aliphatic chains was not homogeneously distributed (Figure 58b), indicating that degradation affected the lignin network, by reducing the size of the phenylpropane units present in lignin monomers. The signal for oxidation products was inhomogeneous as well (Figure 58c), suggesting that part of them was probably removed during the washing process, and that they were partially bound to low molecular weight degradation products of lignin that could be partially removed by washing. Consequently, although washing alum-treated wood allowed to remove interferences from alum, the washing process itself can lead to a loss of information on some degraded wood components, as discussed in *Alum salt interference with IR spectra* (section 3.3.2 Figure 28).

Regarding the inorganic materials in the wood samples, compounds other than alum could be observed. In the infrared map of fragment 1C-AR, mercallite was clearly observed at some points (Figure 59), confirming the results obtained by XRD measurements. This was also observed in the FTIR map spectra of 1D-AR, though the peaks were generally accompanied by significant contributions from alum or the remaining wood.

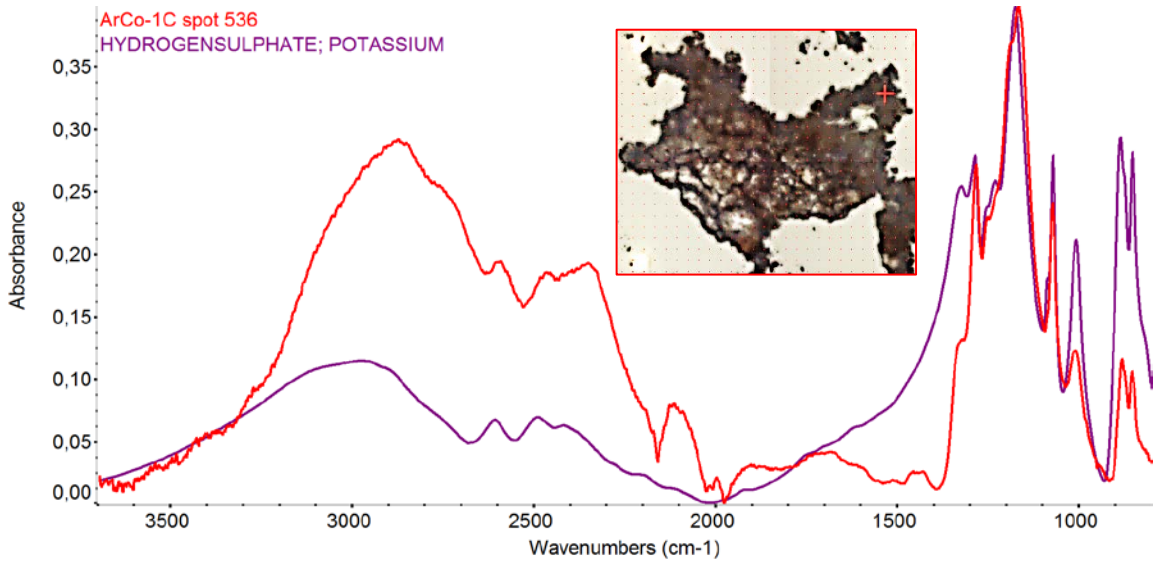

Figure 59 SR µFTIR spectrum of $KHSO_4$ from a point marked with a red cross in the map of a grain from fragment 1C-AR.

Furthermore, FTIR microscopy found some particles that gave spectra matching tschermigite, the ammonium analogue of alum, $NH_4Al(SO_4)_2 \cdot 12H_2O$ (Figure 60). The distinctive band around 1440 cm^{-1} recurred in spectra from other fragments, as noted above, though were mostly accompanied by bands from alum. The presence of ammonium salts in these samples was rather unexpected, and the source remains uncertain. However, texts from the 19th and early 20th century mention that alum was often commercially sold as a mixture of the ammonium and potassium versions [67, 68], so perhaps this compound was present in the material used for alum treatment.

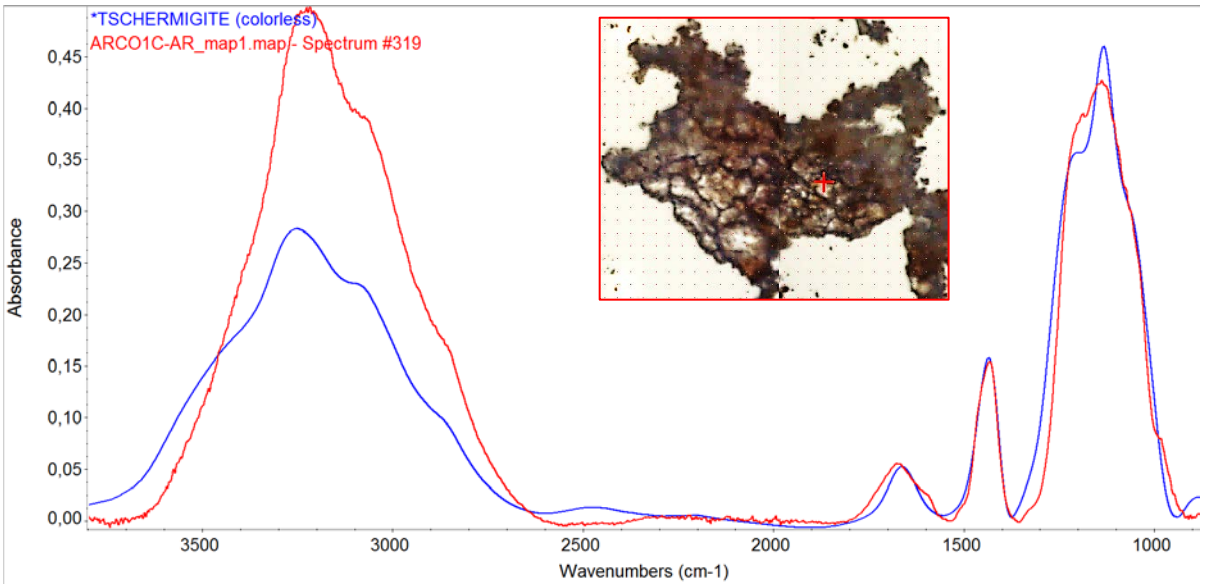

Figure 60 SR µFTIR spectrum of $NH_4Al(SO_4)_2 \cdot 12H_2O$ from point marked with red cross in map of grain from fragment 1C-AR.

After artificial aging

Fragment 1B had formed some white efflorescence on the surface during aging experiments (Figure 61). The infrared spectra of these crystals were unusual, with many absorption bands close to those found in mercallite ($KHSO_4$), but not all (Figure 62). SEM-EDS detected mainly K and S in these crystals [65, 66], and since mercallite was also detected by XRD in the wood samples, these results support that a migration of salts, in particular mercallite, occurred during the artificial aging. Other salts were also most likely present, since other unassigned absorption

bands were present in the spectra acquired. Recent results obtained from other research units show how the number of sulphur compounds increased during artificial aging [65].

Figure 61 Fragment 1B is seen after 6 days in the climate chamber with white efflorescence on the surface, and a cluster of these crystals, approximately 1 mm across, was photographed using a stereo microscope

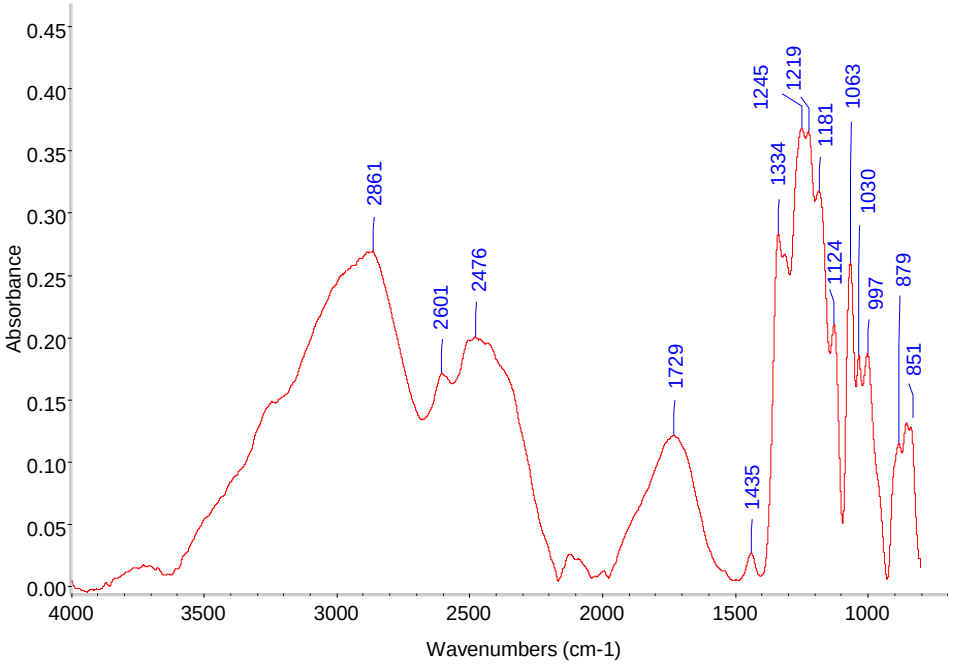

Figure 62 SR-µFTIR spectrum acquired from the white crystals formed after aging on the surface of fragment 1B

Some maps were acquired also from artificially aged samples. Figure 62 shows the results obtained for sample 1B-AR after artificial aging. The absorption band at 1442 cm^{-1} (Figure 63a) indicated that ammonium alum was present almost in all the sample, with some slight differences in abundance. The low intensity of the absorption band at 1505 cm^{-1} (Figure 63b) allowed to confirm again the high inorganic content of the Oseberg samples: this absorption band is typical of lignin and the map showed that in some areas of the surface wood is pratically not present. On the other hand, the absorption band at 1095 cm-1 (Figure 63c), typical of alum, revealed that alum was present everywhere in the sample.

Observations: the spatial resolution achieved by FTIR microscopy allowed us to identify some alum-rich and alum-free areas in the samples. Some absorption bands, such as 1442 cm^{-1}, were related to the presence of inorganic salts different from potassium alum. In fact, ammonium aluminium sulphate and mercallite (potassium bisulfate) were detected. It was also shown that washing alum out of the samples removes some parts of alum, however rinsing allows for better comparisons with spectra of archaeological woods. The maps provided information on the distribution of the compounds, and the examination of the artificially aged samples suggested a migration of inorganic species and the formation of a larger variety of alum degradation products.

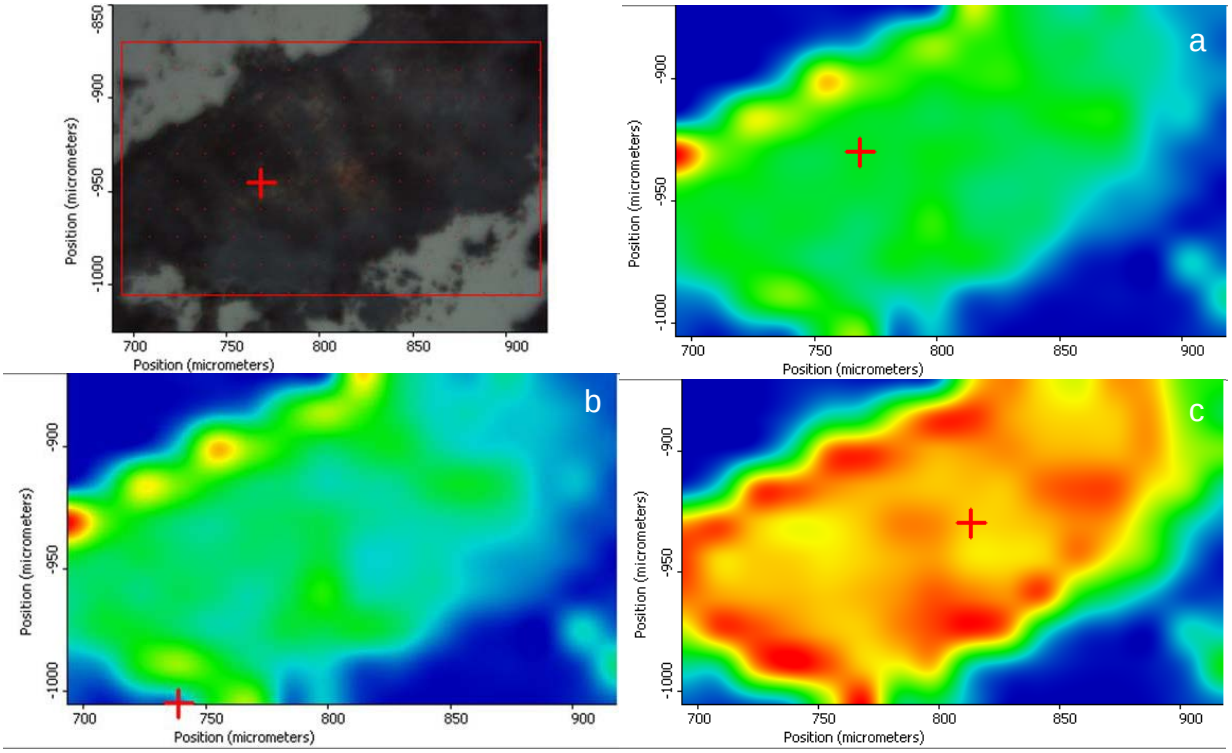

Figure 63 Mappings of IR absorption of Oseberg sample 1B-AR after artificial aging washing corresponding to a) 1442, b) 1505 and c) 1095 cm^{-1}.

Py-GC/MS analysis

The pyrolysis products of holocellulose and lignin are reported in Table 8. The areas of the peaks were determined, normalised and expressed as percentages of the sum of all the pyrolysis products. Figure 64 shows the pyrograms for both alum poor and alum rich regions of fragment 1C. The semi-quantitative results about relative amounts of wood components are shown in Table 17. H/L is ratio between the amounts of holocellulose and lignin pyrolysis products; S/G is the ratio between the amounts of syringyl and guaiacyl lignin pyrolysis products.

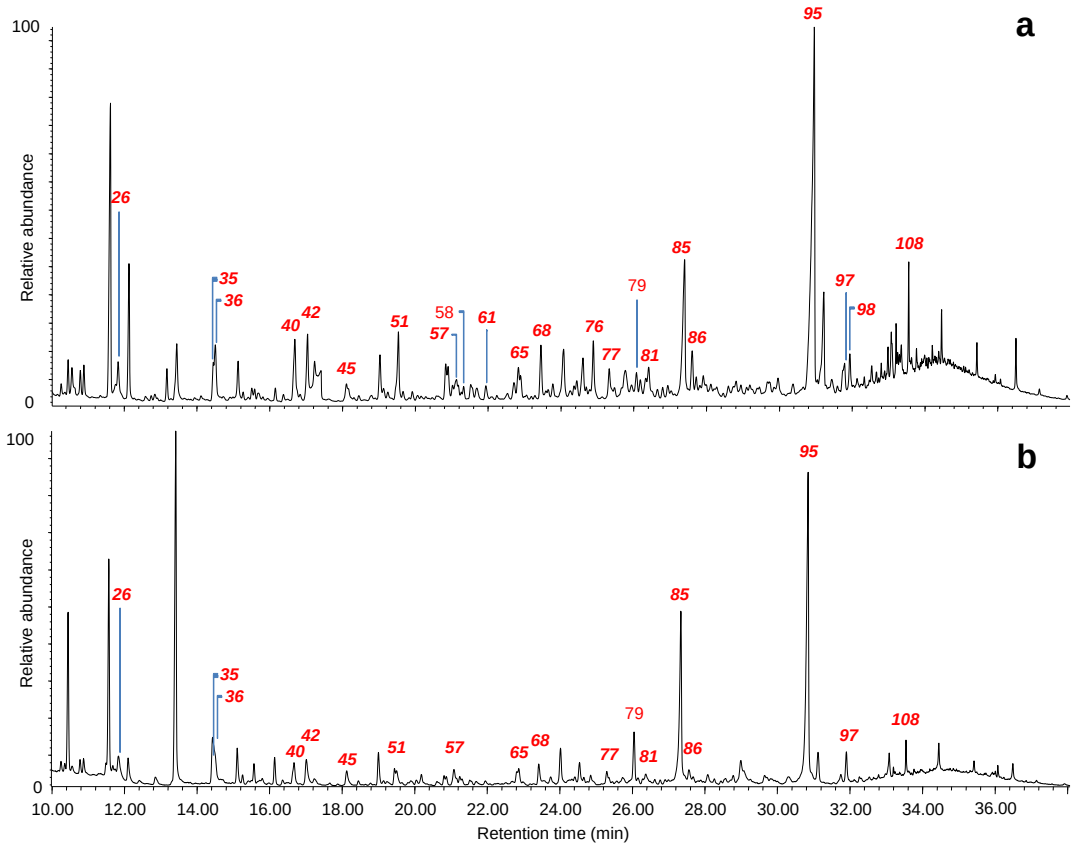

Figure 64 Py-GC/MS profiles for samples **a)** 1C-AP; **b)** 1C-AR. Peak labeling refers to compounds in Table 8. In Italic: lignin pyrolysis products.

Table 17 Relative percentage of wood components, H/L and S/G ratios calculated for the archaeological samples from the Oseberg collection. %sd: percentage standard deviation.

	1B-AP	1B-AR	1C-AP	1C-AR	1D-AP	1D-AR	5-AP	5-AR
Sum H	2.0	2.3	4.0	7.0	8.3	4.3	3.4	4.6
Sum L	98.0	97.7	96.0	93.0	95.7	91.7	96.6	95.4
H/L	**0.02**	**0.02**	**0.04**	**0.08**	**0.09**	**0.05**	**0.03**	**0.05**
%sd	-	0.01	0.00	0.02	0.00	0.01	0.02	0.01
S/G	**2.00**	**1.00**	**1.90**	**1.50**	**1.79**	**2.30**	**2.90**	**3.00**
%sd	-	0.06	0.20	0.10	0.08	0.10	0.10	0.50

The Py-GC/MS profiles were similar for all the samples. Vanillic and syringic acids (#85, 95, Table 8) were the most abundant pyrolysis products, and all the others have very low abundances. In particular a very low amount of holocellulose pyrolysis products was observed (2-8%). All the H/L ratios were very low (<0.10). Such low values did not allow to highlight significant differences among the samples, but only to assess an almost complete loss of the carbohydrate components, also in agreement with FTIR results. S/G ratios were higher for AP samples with respect to the corresponding AR samples, with the exception of fragment 1D, suggesting a preferential alteration of syringyl lignin. Because of their low amount, the carbohydrates pyrolysis products did not provide significant information, thus the molecular profiles of lignin pyrolysis products were carefully inspected.

Generally in a fresh (undegraded) wood the lignin pyrolysis products are composed of almost 50% of monomeric structures (coniferyl and sinapyl alcohols). The rest is composed of guaiacyl and syringyl units *p*-substituted by “short” (up to 2 carbon atoms) and “long” (3 carbon atoms) alkyl chains (about 20%), carbonyl compounds (10-15%) and demethylated/demethoxylated compounds (15-20%). A very little amount of acidic pyrolysis products is usually present in sound wood (3-5%).

Lignin pyrolysis products were thus divided into categories: **acidic** pyrolysis products (vanillic acid, syringic acid, etc.), **carbonyl** (aldehyde/ketone) pyrolysis products (vanillin, sinapyl-aldehyde, acetovanillone, acetosyringone, etc.), **monomers** pyrolysis products (coniferyl alcohol, sinapyl alcohol, etc.), "**short**" and "**long**" chain pyrolysis products based on number of carbon atoms of the side chain (short: guaiacol (G), methyl-G, ethyl-G, vinyl-G, syringol (S), methyl-S, ethyl-S, vinyl-S ; long: eugenol, *Z*-isoeugenol, *E*-isoeugenol, propenyl-S, *Z*-isopropenyl-S, *E*-isopropenyl-S, vanillylpropanol, syringylpropanol) and **demethylated** syringyl and guaiacyl derivatives (catechols, methoxy-benzenediols, etc.). The sum of the pyrolysis products of each category can be expressed as percentages relative to the total amount of lignin. Figure 65 summarizes the results obtained by Py-GC/MS analysis of the samples in terms of lignin composition.

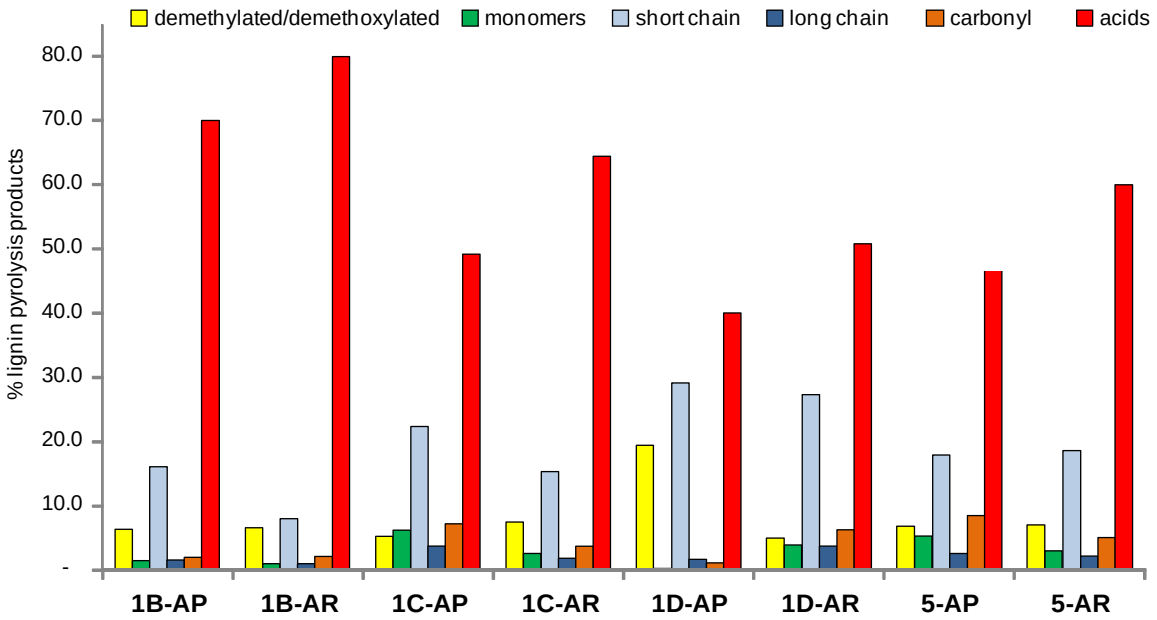

Figure 65 Distribution of categories of lignin pyrolysis products expressed as percentages in the samples analysed from the Oseberg collection.

The relative abundances of acid lignin pyrolysis products were particularly high (40-80%). Samples from fragment **1B** showed the highest relative abundance of acid lignin pyrolysis products, thus these samples had undergone the highest extent of lignin oxidation. For all fragments lignin oxidation was higher in AR samples than in the corresponding AP samples. Fragment **1D-AP** showed higher relative abundances of demethylated and short chain pyrolysis products, suggesting that oxidation reactions were less advanced. Monomers and long chain lignin pyrolysis generally showed very low relative abundances, indicating an almost complete alteration/fragmentation of lignin propanoid side chains. *P*-hydroxy benzoic acid, which can be considered a final oxidation product of lignin units, resulting from oxidation coupled with chain scission and demethoxylation of guaiacyl and syringyl compounds, was detected in fragment **1B**, thus indicating a further lignin oxidation in this fragment.

After artificial aging

The analyses were repeated after artificial aging and Figure 66 reports the distribution of lignin pyrolysis products divided into categories.

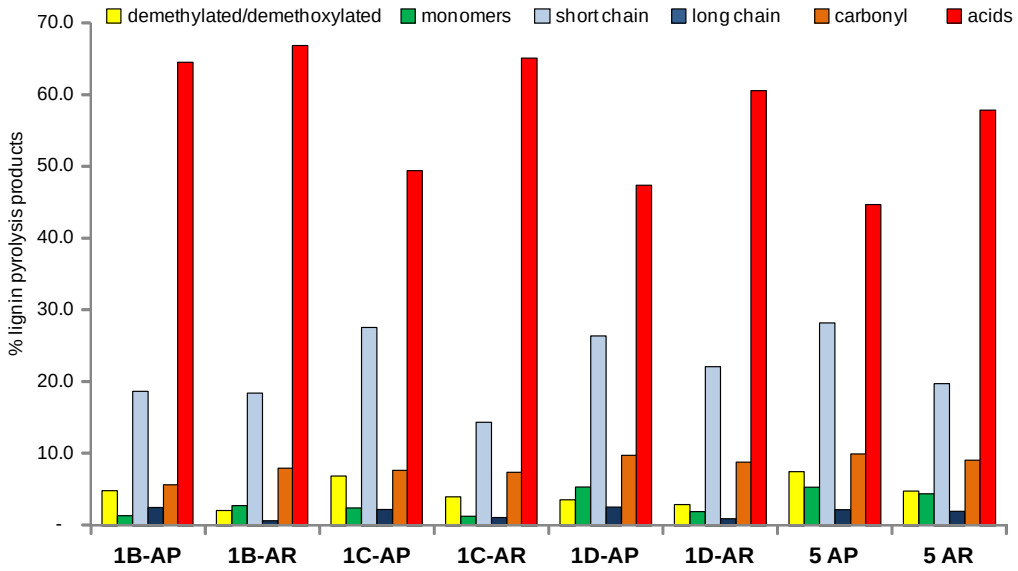

Figure 66 Distribution of categories of lignin pyrolysis products expressed as percentages in the samples from the Oseberg collection analysed after artificial aging.

The results for samples from fragment 1B were similar to those obtained before aging and p-hydroxybenzoic acid was detected. For the other samples a higher relative abundance of acid pyrolysis products was detected in the AR samples with respect to the AP samples, similarly to the results obtained before aging. The samples from fragment 1D, which had the lowest relative abundances of acid pyrolysis products before aging, showed results similar to samples from fragments 1C and 5 after aging. These observations suggested a slight increase in lignin oxidation after aging and the general maintenance of the differences between AP and AR samples.

Observations: an almost complete degradation of carbohydrates and significant oxidation of lignin was observed. *P*-hydroxy benzoic acid, which can be considered a final oxidation product of lignin units, was present only in fragment 1B. Slight differences were noticed between the alum poor and alum rich samples. The alum treatment played a role in this extensive oxidation phenomenona.

EGA-MS analysis

The samples before and after artificial aging were analysed by mean of evolved gas analysis coupled with mass spectrometry. This pyrolysis based analytical approach exploits the differences in thermal degradation between wood and conservation materials to separate them for mass spectrometric analysis. This is the first time that this technique is applied to consolidated archaeological wood samples. Before analysing consolidated wood samples, the thermograms of pure consolidating materials were acquired.
Alum showed its thermal decomposition between 600 and 800°C and all the mass spectra recorded in this temperature range corresponded to sulphur dioxide SO_2 (m/z=64), which was identified as the thermal degradation product of alum in these conditions (Figure 67).

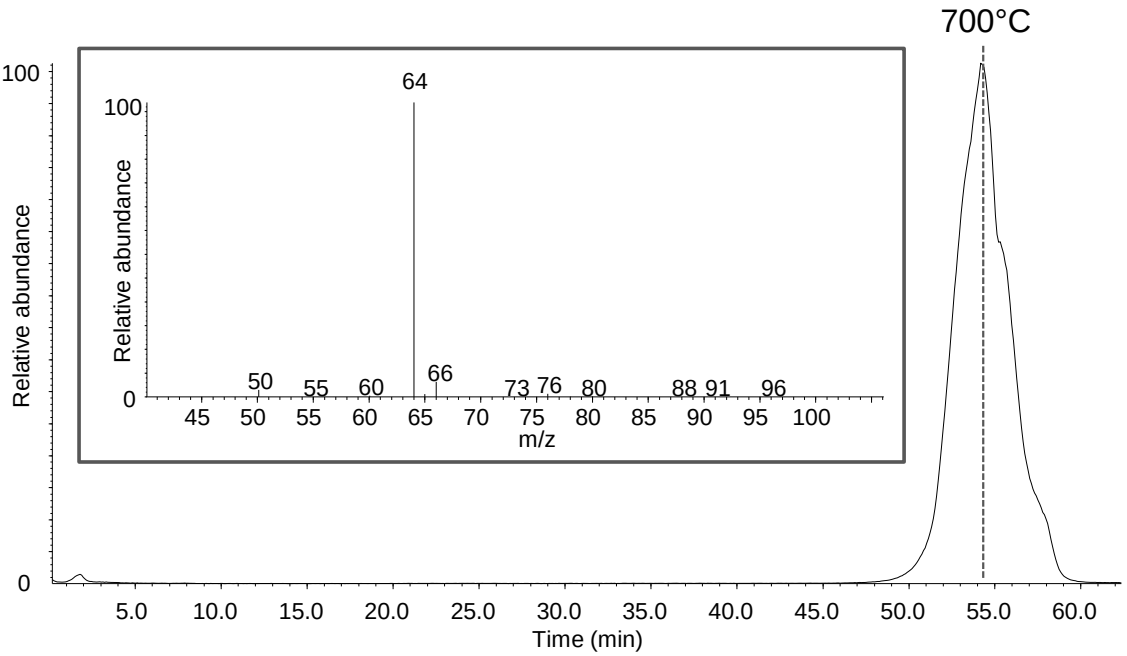

Figure 67 Total ion thermogram obtained by EGA-MS analysis of alum $Al(SO_4)_2 \cdot 12H_2O$. Insert: overall mass spectrum obtained in the thermal degradation region.

The wood samples from the Oseberg collection showed a thermal degradation dominated by alum decomposition, which heavily interferes with obtaining information on the wood fraction. Nevertheless, significant differences were obtained between the AP and the AR samples. Figure 68 shows the total ion thermograms obtained for samples 1C-AP and 1C-AR.
The mass spectra of sample 1C-AR mainly showed the evolution of SO_2 (*m/z* 64), similarly to the alum reference, thus reflecting the high concentration of alum with respect to other materials present in the sample and covering all other signals. On the other hand, the spectra for sample 1C-AP, despite a high relative abundance of *m/z* 64, revealed also fragment ions indicative of wood pyrolysis products. In particular, *m/z* 110 is attributed to catecholic structures, *m/z* 124 and 154 correspond to the molecular mass of guaiacol and syringol, respectively. These lignin pyrolysis products have no side chain, thus they are indicative of a high level of lignin depolymerisation and alteration of the propanoid side chains originally present in the monomers. In addition, *m/z* 151 and 181 are produced by all the p-substituted guaiacyl and syringyl units, respectively, with a carbonyl group at the benzylic position. *m/z* 168 and 198 correspond to the molecular mass of vanillic and syringic acid, respectively. All these pyrolysis products highlighted a high lignin oxidation in the samples, proving the technique to be suitable

to provide information on wood degradation when the interference from alum is not excessive.

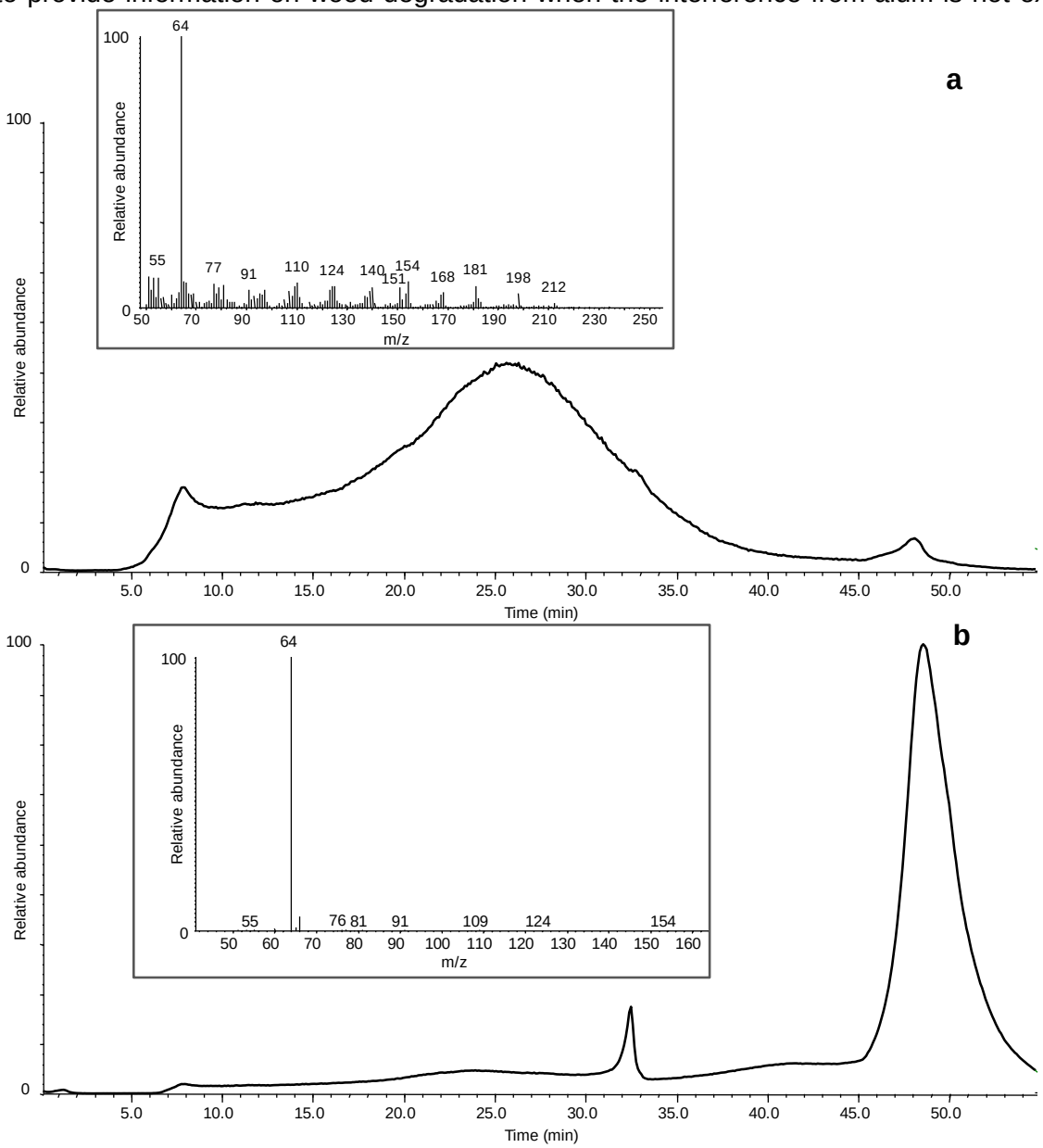

Figure 68 Total ion thermograms obtained by EGA-MS analysis of samples a) 1C-AP and b) 1C-AR from the Oseberg collection. The overall mass spectra for each thermogram are reported in the inserts.

Similarities were observed for all the other samples from the Oseberg collection, with the exception of those taken from fragment 1B, which both showed a high alum content, in agreement with the previous results. No significant differences were observed by EGA-MS analysis before and after artificial aging treatment.

Observations: The thermal degradation of alum was predominant in the thermograms of Oseberg samples. Nevertheless, some of the alum-poor samples showed *m/z* peaks from wood in the mass spectra. In particular, it was possible to highlight the high extent of oxidation and depolymerization of lignin in these samples, as well as the absence of carbohydrates.

Correlations between Py(HMDS)-GC/MS and ICP/IC results for "as it is" samples

In order to highlight interactions between organic and inorganic components, some correlations between the percentage sum of the acid pyrolysis products and the concentrations of significant elements were investigated for both non-aged and aged samples.

An interesting correlation was found between the sum of the percentage areas of acidic pyrolysis products (p-hydroxybenzoic acid, vanillic acid and syringic acid) and Al concentration in the non-aged samples analysed, as shown in Figure 69.

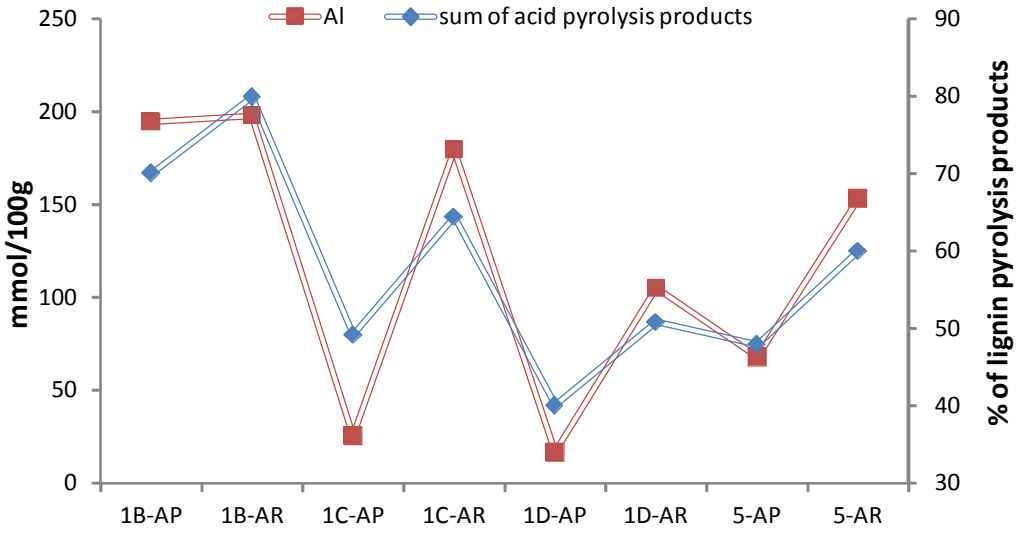

Figure 69 Correlation between the sum of acid lignin pyrolysis products and Al content in the non-aged Oseberg samples.

The Pearson's *r* correlation index of the two variables -sum of acidic lignin pyrolysis expressed as percentage and Al content was 0.92, indicating a strong correlation between the two variables. Similar results were obtained comparing the sum of acid pyrolysis products with K and S and sulphates. The Pearson's *r* correlation indexes were 0.83, 0.91 and 0.79, respectively. This supports the previous hypothesis that the extent of lignin oxidation is related to the alum treatment. The correlations with Al and K contents were more evident for the 229 fragments than for the 185 series, while S was not included in the previous analysis. In addition to expected lower contents of Al, K and S in the AP samples with respect to the AR samples, the ICP results also revealed that the stoichiometric ratios between Al, K and S (Table 15) were variable across the samples. In particular, hight values of K/Al and S/Al in 1C-AP and 1D-AP samples supported the higher proportion of $KHSO_4$ observed by XRD.

The S/Al and S/K values were all higher than the value for alum in the samples suggesting that sources of sulphur other than alum are present in the samples. At the same time, IC-LC results suggested that most of the sulphur was present in the form of sulphates. This is consistent with a high level of sulphuric acid being released into the wood during alum treatment, which results from hydrolysis of Al species and is accompanied by the precipitation of aluminium-hydroxide containing compounds, such as alunite ($KAl_3(SO_4)_2(OH)_6$) [43], the presence of which could account for Al/K ratios higher than 1.

$$3KAl(SO_4)_2 + 6H_20 \rightarrow KAl_3(SO_4)_2(OH)_{6\downarrow} + K_2SO_{4(aq)} + 3H_2SO_{4(aq)}$$ [43]

The concentrations of iron and copper were lower with respect to Al, K and S. However, the fact that Fe and Cu can act as catalysts in Fenton degradation of wood in well-known [46, 47]
No convincing correlation was found considering the Fe content (Pearson's *r* correlation index 0.30), whereas a Pearson's *r* correlation index 0.78 was found considering the subtraction between the concentrations of Fe and Ca (Figure 70).

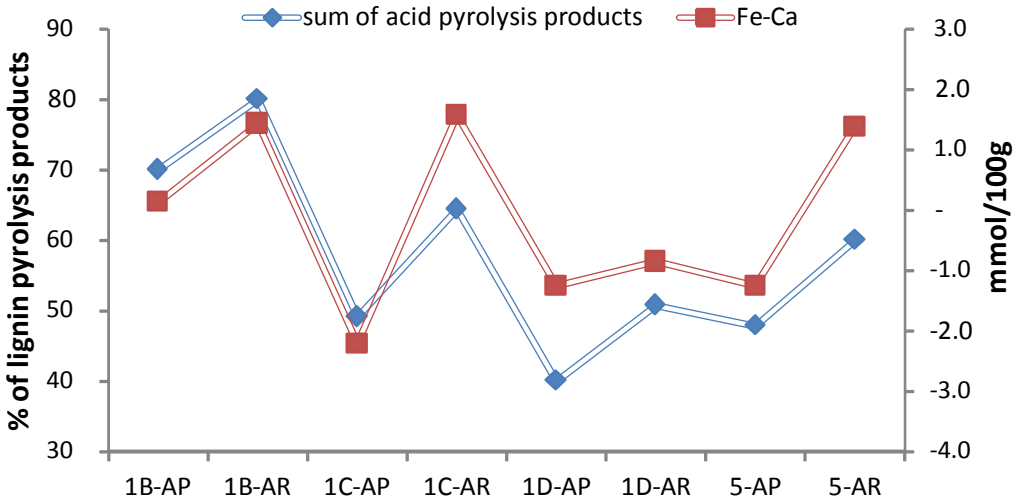

Figure 70 Comparison of the sum of acid lignin pyrolysis products to Fe content minus Ca content in the Oseberg samples.

These results highlighted that lignin oxidation was directly related to the alum treatment (Al, K and S), but also minor elements, such as Fe and Ca, could play a role in wood degradation, as described in section before regarding series 185 and supporting the results previously obtained. Regarding the results obtained after artificial aging, good correlations were observed between the sum of acid pyrolysis products and the concentrations of K and sulphates, obtaining Pearson's *r* correlation indexes 0.70 and 0.62, respectively. No significant correlations were found considering the concentrations of Al and S, mainly because sample 1C-AP had a higher concentration of Al with respect to sample 1C-AR, unlike the samples taken from the other fragments, and the concentrations of S just showed slight differences among the samples. The subtraction between the concentrations of Fe and Ca correlated with the sum of acid pyrolysis products with a Pearson's *r* correlation index 0.63.
These results confirmed that some changes involving the inorganic components had occurred, but it is not yet possible, at the present state of the art, to draw conclusions on the impact of these changes on the organic component. XRD analyses on the samples after aging, planned in the final period of the Arco project, will help to better investigate this subject.

^{1}H NMR relaxation experiments

For these experiments a selection of 8 samples was analysed: pure alum, a fresh birch sample, an archaeological aspen sample, samples **1D-AP** and **1D-AR**, samples **5-AP** and **5-AR** and a sample taken from fragment 5 after washing (5-washed). The interpretation of these results is complex and the following paragraphs present the work done so far in collaboration with Prof. Eddy Hansen form the Department of Chemistry, University of Oslo.
Three pulse sequences were adopted to perform three measurements, in order to obtain information on the water contained in the samples and its state:

- Solid echo → FID analysis
- Inversion recovery → T1 relaxation times
- CPMG → T2 relaxation times

Solid echo

The solid echo curves were acquired for different value of τ (echo time). Figure 71 reports the solid echo curves with τ = 14 μs for all samples except pure alum and alum rich samples.

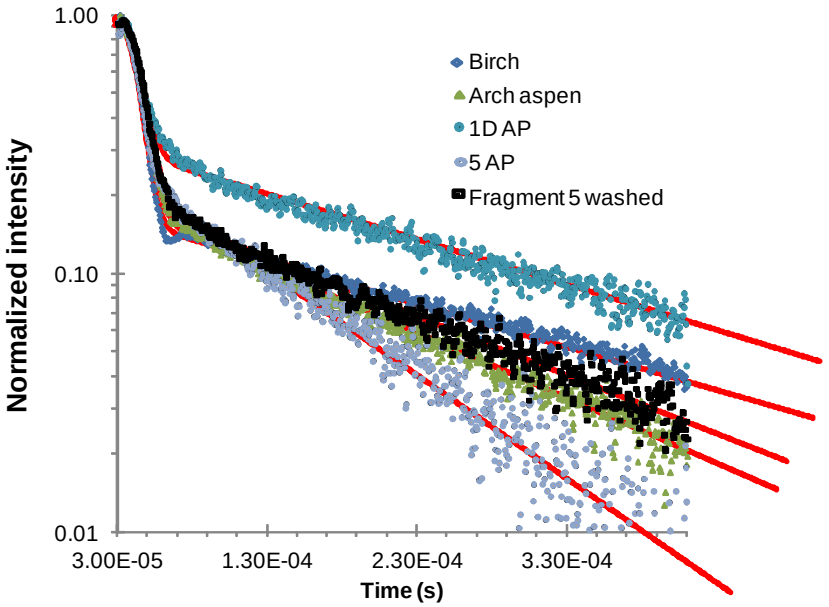

Figure 71 Comparison of solid echo curves with τ = 14 µs

The solid echo curves can be well approximated by a sum of two characteristic functions: a Gaussian function, representing the non-mobile fraction of protons from the wood matrix, and a Lorentzian function, characteristic of the mobile fraction of protons (water, etc).
Two characteristic T_2-times derived from the fitting of the Gaussian function and they were associated with the solid matrix and another T_2-time derives from the fitting of the Lorentzian function:
a) T_{2rigid}, as derived from the initial decay of the curve;
b) T_{2DD} (dipole-dipole spin-spin relaxation time), derived from the envelope of a series of solid-echo experiments using various echo times (τ); it characterizes the interaction strength between protons and depends on the distance between the protons and the internal dynamics of the protons;
c) $T_{2Mobile}$ characterizes the dynamics of the mobile proton fraction (water and/or segmental motion of small "polymer"-fragments within the wood).
In addition the percentage of the mobile proton fraction (Mob. Protons %) relative to all the proton present in the samples can be calculated.
Within experimental error, the motional features (T_{2rigid} and T_{2DD}) of the rigid fraction did not vary within the various samples. In contrast, the relative amount of the mobile fraction differed significantly between the samples, although it remained relatively small, of the order of 2 – 15%. Moreover, the motional characteristics ($T_{2Mobile}$) of this component seemed to vary somewhat between samples. The origin of this mobile component (water, -OH, etc.) has to be further investigated. Table 18 summarizes these results. Preliminary experiments suggested that the molecular motional features within the alum rich samples are significantly different, becoming much slower compared to corresponding motion within AP samples (*work in progress*).

Table 18 Parameters obtained from Solid-Echo experiments

	Birch	**Arch aspen**	**1D-AP**	**5-AP**	**5 washed**
T_{2rigid} (s)	$11 \cdot 10^{-6}$	$12 \cdot 10^{-6}$	$12 \cdot 10^{-6}$	$11 \cdot 10^{-6}$	$13 \cdot 10^{-6}$
$T_{2Mobile}$ (s)	$2.6 \cdot 10^{-4}$	$1.7 \cdot 10^{-4}$	$2.5 \cdot 10^{-4}$	$1.1 \cdot 10^{-4}$	$1.9 \cdot 10^{-4}$
Mob. protons(%)*	8.3	1.9	6.2	6.8	14.1
T_{2DD} (ms)	16 ± 01	19 ± 1	18 ± 2	19 ± 2	18 ± 2

Inversion recovery

This sequence is used to calculate the T1 spin-lattice relaxation time, characteristic of the interactions between protons and their chemical environment. The obtained relaxation curves can be fitted according to a sum of exponential functions. Figure 72 shows the obtained curves for the analyzed samples.

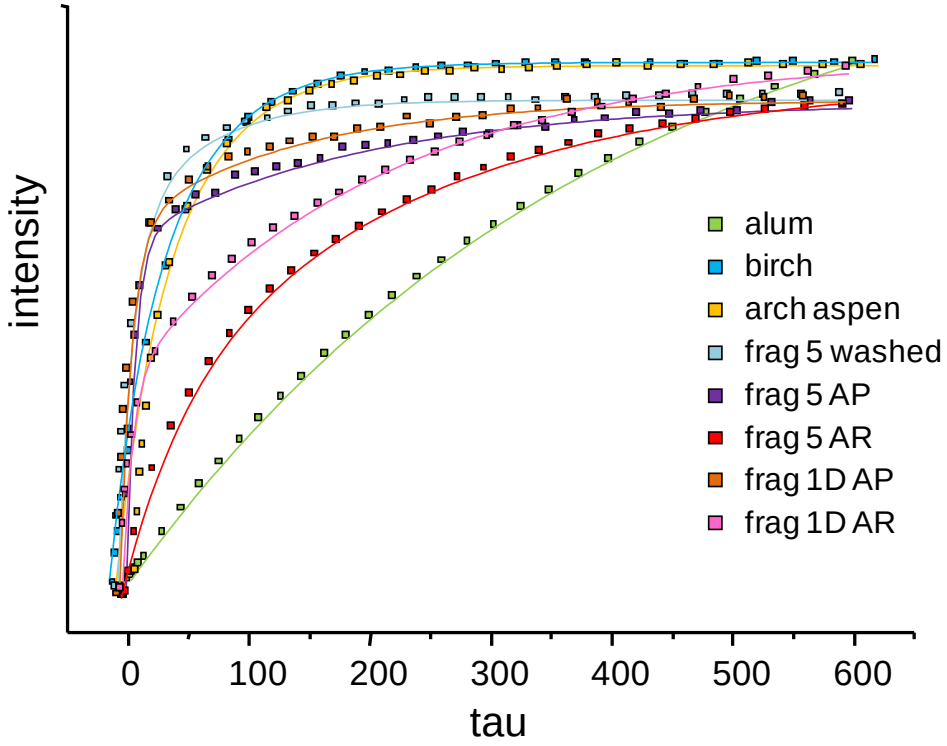

Figure 72 Inversion recovery fitted curves.

From these curves T1 relaxation times were obtained and the results are shown in Table 19. For alum sample and sound birch wood sample just one component of T1 ($T1_1$) was obtained. For alum the T1 was very long, indicating a slow relaxation time. Actually Figure 72 shows that the spin-lattice relaxation process is not concluded in the range of analysis, because the curve does not reach the plateau, thus T1 for alum was likely even longer. For fresh birch T1 was shorter. For all the other samples two components of T1 ($T1_1$ and $T1_2$) were calculated. Archaeological aspen and fragment 5 washed gave similar results, showing $T1_1$ similar to fresh birch and a very short $T1_2$. Alum poor samples showed the same low value of $T1_2$ and a longer value of $T1_1$, attributable to alum presence. In fact Alum rich samples had a $T1_1$ even longer.

Table 19 T1 relaxation times

	$T1_1$(ms)	**$T1_2$ (ms)**
alum	395 ± 2	0
birch	46 ± 1	0
arch aspen	55 ± 2	9 ± 1
frag 5 washed	62 ± 5	12 ± 1
frag 5 AP	191 ± 16	7 ± 1
frag 5 AR	232 ± 15	51 ± 10
frag 1D AP	139 ± 12	9 ± 1
frag 1D AR	215 ± 9	8 ± 1

CPMG

This sequence is used to calculate the T2 spin-spin relaxation time, characteristic of the interactions between protons. The obtained relaxation curves can be fitted according to an exponential function. Figure 73 shows the obtained curve for the **5-AP** sample. The other curves were very similar. From these curves T2 relaxation times were obtained and the results are shown in Table 20.

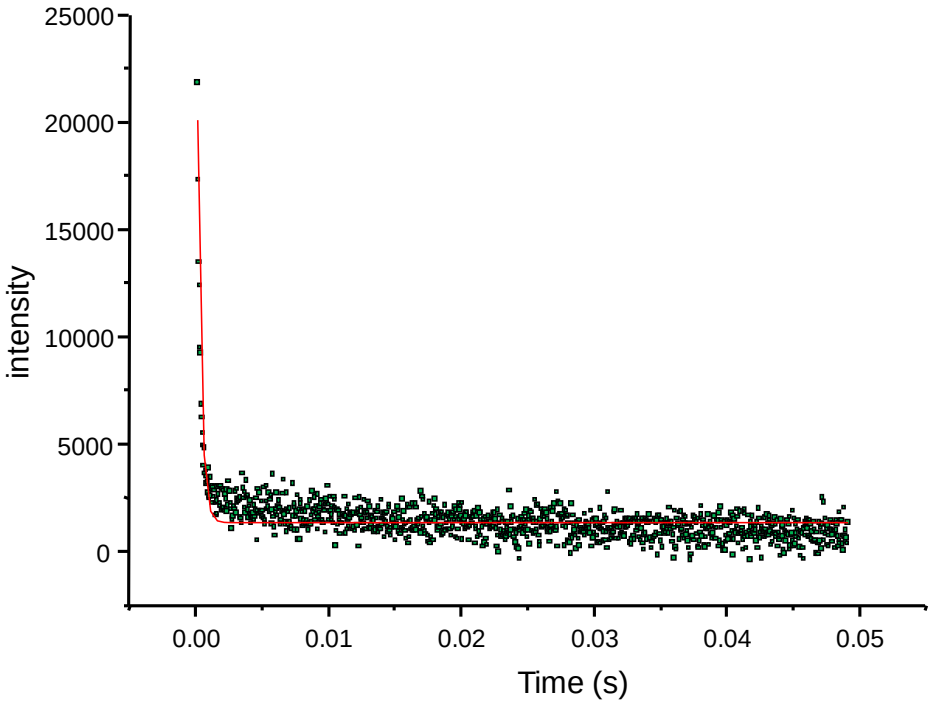

Figure 73 CPMG fitted curve for sample 5-AP and echo time 25 ms

Table 20 T2 relaxation times

	T2($\cdot 10^{-4}$ s)
alum	1.20 ± 0.20
birch	4.14 ± 0.07
arch aspen	2.59 ± 0.07
frag 5 washed	2.65 ± 0.08
frag 5 AP	2.70 ± 0.10
frag 5 AR	2.16 ± 0.09
frag 1D AP	3.85 ± 0.14
frag 1D AR	2.41 ± 0.06

For alum T2 was the shortest and for fresh birch it was the longest. The alum rich samples showed a T2 value lower than alum poor samples, probably due to the presence of alum. For the other samples the values are similar, except for sample **1D-AP**, which showed a long T2 time.

Observations: there is not much literature about the application of these techniques on archaeological wood, and the interpretation of these results is complex and still in progress. We can say that differences were evident among the samples, but the real reason of this behavior needs to be further investigated, and correlations between the results obtained by other techniques have to be found. Nevertheless this technique can provide information about the

distribution of water, and this is potentially useful to understand the environment in which degradation processes have taken place.

Discussion of ArCo results

The results obtained by all the techniques highlighted that the samples named “alum rich”, taken from the surface of the fragments, actually had a higher inorganic content and a higher extent of wood degradation with respect to the corresponding “alum poor” samples, taken from the core of the samples, with the exception of fragment 1B, which showed similar results from both the surface and the core. We note that since the alum rich zone is the outer surface of the fragment, it is also more accessible to external conditions and inorganic impurities from soil during burial, which can affect the level of degradation.

SEM-EDX allowed us to highlight very poor preservation conditions of wood morphological structure. EDX spectra and mapping showed Al, K and S from the alum treatment being the most abundant elements and having a non-homogeneous distribution. These results suggested that not only alum was present in the samples, but also some products of its partial decomposition and that differences in penetration/diffusion had occurred.

These results were confirmed by ICP-OES and XRD. The concentrations of Al, K and S showed stoichiometric ratios not corresponding to those present in the alum chemical formula $KAl(SO_4)_2 \cdot 12H_2O$. The present salts were proven to be mostly water-soluble and in the form of sulphates by IC analyses. The core of the samples contained more water-insoluble salts than the surface and higher values of S/Al ratios, confirming a non-homogeneous distribution of compounds. In fact, alum and mercallite ($KHSO_4$) were both identified in the samples and mercallite was generally more abundant in the AP samples relative to alum than in the AR samples, indicating a more effective diffusion than alum.

SR-µFTIR confirmed the non-homogeneous distribution of compounds and highlighted the difficulty of obtaining information on wood degradation because of the strong overlapping between alum and wood absorption bands. Results obtained after washing out the alum from the samples suggested that the process of washing could remove some wood degradation products, preventing from precisely assessing the wood degradation state from a chemical point of view. The subtraction of the alum spectrum from the samples spectra after normalisation using the 576 cm^{-1} absorption band (sulphate stretching) appeared to be a more convincing strategy to remove alum contamination. However the disadvantage is that it is difficult to compare these spectra to those of untreated archaeological wood. A high depletion of carbohydrates was highlighted, and lignin in “alum rich”, samples was found to be more oxidised than in “alum poor”, samples.

Differences in oxidation were confirmed by Py(HMDS)-GC/MS. The relative abundances of acid lignin pyrolysis products ranged from 40 to 80% in the analysed samples, according also to the results obtained for the **series 185**. *P*-hydroxybenzoic acid, considered as a marker of wood degradation in extreme acidic environment, was detected only in samples from fragment 1B.

The differences in wood degradation correlated with those observed considering the inorganic content. In particular, the percentage sum of acid lignin pyrolysis products showed good correlation with the content of Al, K, S and sulphates (Pearson’s correlation indexes 0.92, 0.83, 0.91 and 0.79, respectively), supporting a direct relationship between wood degradation and the alum treatment. A good correlation was also found considering the subtraction between the concentrations of Fe and Ca, supporting the suggestion that a potential modulating effect of calcium compounds on iron-promoted degradation might be worth investigating.

The artificial aging treatment didn’t produce significant changes in the wood components of the samples in study, as expected being the lignocellulosic polymers already very degraded. Nevertheless, some of the observations from both EGA-MS analysis and Py-(HMDS)-GC/MS suggested a slight increase in lignin oxidation during the climatic chamber treatment in presence of alum, and the general maintenance of the differences between AP and AR samples.

From the point of view of the changes before and after artificial aging the significant difference that has been observed is that relating to the inorganic components introduced into the wood.

The relative concentrations of Al, K and S, identified by ICP-OES and IC, changed significantly after artificial aging and the changes were mainly related to a relative decrease in S concentration, though an increase for most AP samples, with respect to the non-aged samples. Migration of sulphuric acid and other sulphate-containing compounds out of the AR areas was hypothesised, as well as the formation of minerals with different composition than alum. IC results showed that the concentration of sulphates increased for the artificially aged AP samples, whereas for the AR samples it was comparable with that obtained before aging. Consequently, the differences in the inorganic content between AP and AR samples were reduced.
Redistribution of minerals during aging was confirmed by XRD, which showed notable changes in relative intensities of alum and mercallite in the alum-poor regions. Furthermore, some white crystals were formed during the time spent in the climate chamber on the surface of some fragments. The analysis of the crystals by FTIR suggests that these may contain mercallite ($KHSO_4$) and other sulfates, though this was not conclusive. Nonetheless, this supports that a migration of salts, such as mercallite, occurred during the artificial aging.

3.4 Moisture adsorption studies

*See details in Braovac, S., **Alum-treated wood, Material characterization, A case study of the Oseberg finds**, Doctoral thesis, 2015*

The aim of the RH experiments was to determine the hygroscopic properties of alum-treated woods from the Oseberg find by measuring the weight of water gained and lost during adsorption and desorption, respectively, in the range of 20% to 95% RH (20C). This would serve as a basis against which to evaluate the moisture response of samples retreated with different polymers. However, the experiments had to be stopped after adsorption to 75% RH. Thus, the calculated moisture content (MC) in these experiments does not represent the true MC, as it was normalized to the start weight and not the dry mass. Nonetheless, the data showed similar sinusoidal moisture uptake patterns as observed in standard curves for wood and thus was considered valid regarding general trends, within a reasonable degree of certainty.

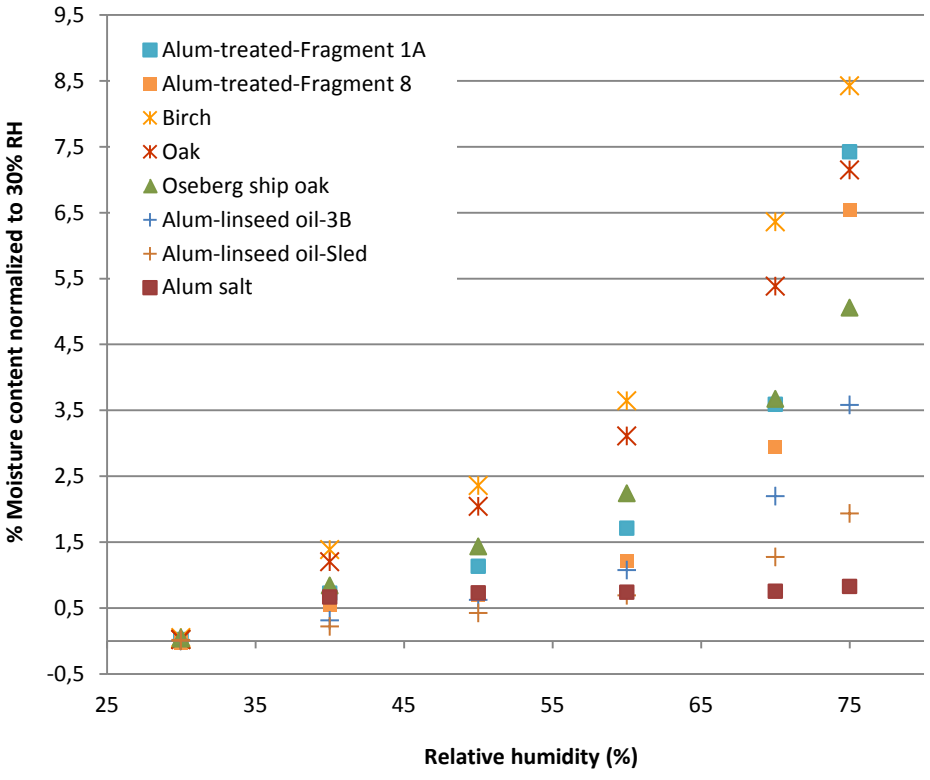

Figure 74 Moisture uptake of wood samples representing different treatment types in the Oseberg as explained in the Experimental section.

Figure 74 shows the plot of % MC against RH for samples representing the different treatment types found in the Oseberg collection, as well as fresh woods (birch and oak) and fresh alum powder. The Oseberg samples included two samples of alum-treated wood (Fragment 1A and Fragment 8), two samples of alum-treated wood containing linseed oil (Sled and 3B), and the untreated Oseberg ship oak.
It is clear that alum salts did not absorb significant amounts of water with increasing RH. All wood samples in Figure 74 showed a marked increase in moisture content at 70% RH and above. The fresh woods had the greatest moisture uptake, except at 75% RH where the MC of the alum-treated samples was similar to oak. The (untreated) Oseberg ship oak had the greatest MC of the archaeological samples except at 75% RH, at which point the two alum-treated samples retained significantly more water. At 70% RH Oseberg ship oak was similar to Fragment-1A.
The differences in MC observed between the fresh woods and Oseberg ship oak may be related to the reduced hemicellulose content of the latter [32], as the hygroscopic properties of fresh woods are mainly associated with its hemicellulose fractions [69]. Archaeological woods often have reduced hemicellulose content due to biological deterioration in the burial environment [70].
The differences in moisture uptake between the relatively well-preserved untreated samples and the alum-treated samples are likely mainly due to the alum-content of the latter, which appears to dampen moisture uptake. The two alum-treated samples, Fragments-1A and -8 also differed slightly: Fragment 8 consistently had a lower MC in the RH range tested, possibly due to a higher content of alum salt. Both samples of alum and linseed oil-treated woods were the least responsive woods in the series tested. Sample 3B absorbed more water above 70% RH than the Sled sample, possibly due to a greater amount of linseed oil in the latter.

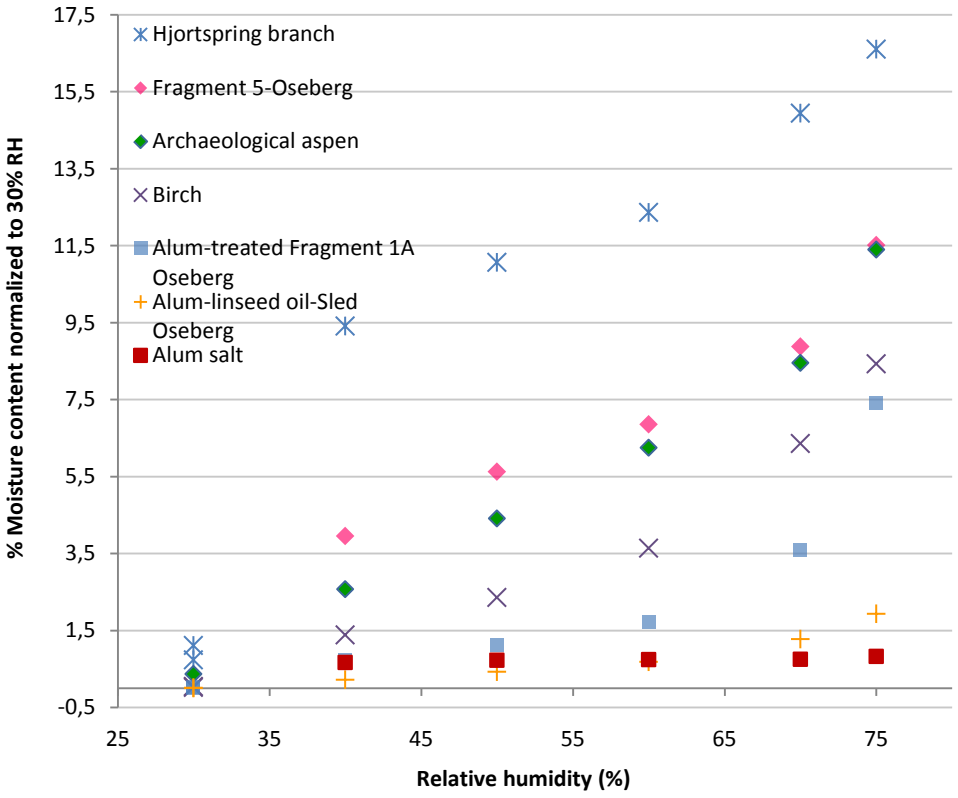

Figure 75 Moisture uptake of alum-treated and alum/linseed oil-treated wood samples, from Oseberg compared with other archaeological woods, treated and untreated. The 'moisture contents' have been normalized to the weight at 30% RH, as explained in the Experimental section.

Figure 75 compares the moisture uptake of some of the same samples from the previous figure with alum/glycerol-linseed oil-treated wood from the Hjortspring find (Hjortspring branch), as well as archaeological wood without alum (a sample of Oseberg wood which had been washed

free of alum and freeze dried (Fragment 5) and a recently excavated archaeological sample (aspen) which had only been freeze dried).
The graph demonstrates that the most reactive sample to moisture – across the entire RH range – was by far the Hjortspring branch, which contained glycerol. Thus the hygroscopic properties of alum/glycerol-linseed-oil treated woods are most strongly influenced by the glycerol. The alum/linseed oil-treated sample (Sled) and the alum powder had lowest moisture contents. Across the entire RH range tested, the unimpregnated woods (Fragment 5 and arch.aspen) had significantly higher MC than the remaining samples, even fresh birch.
The removal of alum salts opened up the wood structure in Fragment 5, increasing its surface area and hence its capacity to adsorb more water molecules. Similar moisture adsorption patterns of untreated archaeological woods have been observed by other researchers [71, 72]. Foston and Ragauskas [73] attributed the higher MC measured for acid-degraded aspen (compared to untreated aspen) to the greater porosity in the fibres formed by the acid treatment. However, in heavily deteriorated archaeological woods, an increase in polarity due to oxidation of polymers may also be a significant factor to consider as it can influence the wood's moisture response. Therefore the high moisture uptake observed for the archaeological aspen and Fragment 5 are likely related to two main factors of deterioration: 1) increased polarity of the lignin fraction and 2) increased porosity. From the data, it was not possible to ascertain which of the two factors influenced the wood behavior most.
Alum-treated Fragment 1A had far lower moisture contents than the other woods across the RH range measured. This clearly indicated that alum in fact dampens the wood's response to RH: it is less hygroscopic than the wood substrate, thus when it fills pores in the wood, it decreases the surface area available to interact with water.
These experiments have shown that moisture cycling within the range normally encountered in the museum environment will lead to shrinkage and swelling of the wood structure, while the alum salts remain relatively unchanged. This will likely lead to eventual damage in the wood, as its movement is constrained by the more rigid alum salts. With increasing chemical deterioration, the wood will not withstand the mechanical forces due to swelling and shrinkage, which eventually will lead to its pulverization. It is possible that if salts besides alum were formed in the wood during treatment (such as potassium hydrogen sulphate) they may also affect the observed responses to RH, as different salts vary in their responses to RH [74]. However, this effect is likely minor as alum is, overall, the major crystalline compound that has been detected in wood samples.

3.5 Model studies

*See details in Braovac, S., **Alum-treated wood, Material characterization, A case study of the Oseberg finds**, Doctoral thesis, 2015*

3.5.1 Alum solutions and alum treatments in the laboratory

Effect of heat on solutions of alum salts

Alum solutions, 2 parts alum to 1 part water by weight, were heated to investigate the reactions at 90°C, the approximate temperature used to conserve the Osberg finds. At room temperature, the alum solution had a pH of 3.5 which decreased after approximately 2 hours of heating to pH 2. A white precipitate also formed during heating, which was identified as potassium aluminum sulfate hydroxide (alunite), $KAl_3(SO_4)_2(OH)_6$ (Figure 76) In addition to the hydrolysis of water molecules, protons are also released during the formation of this precipitate at higher temperatures, which likely partly explains the drop in pH of heated solutions.

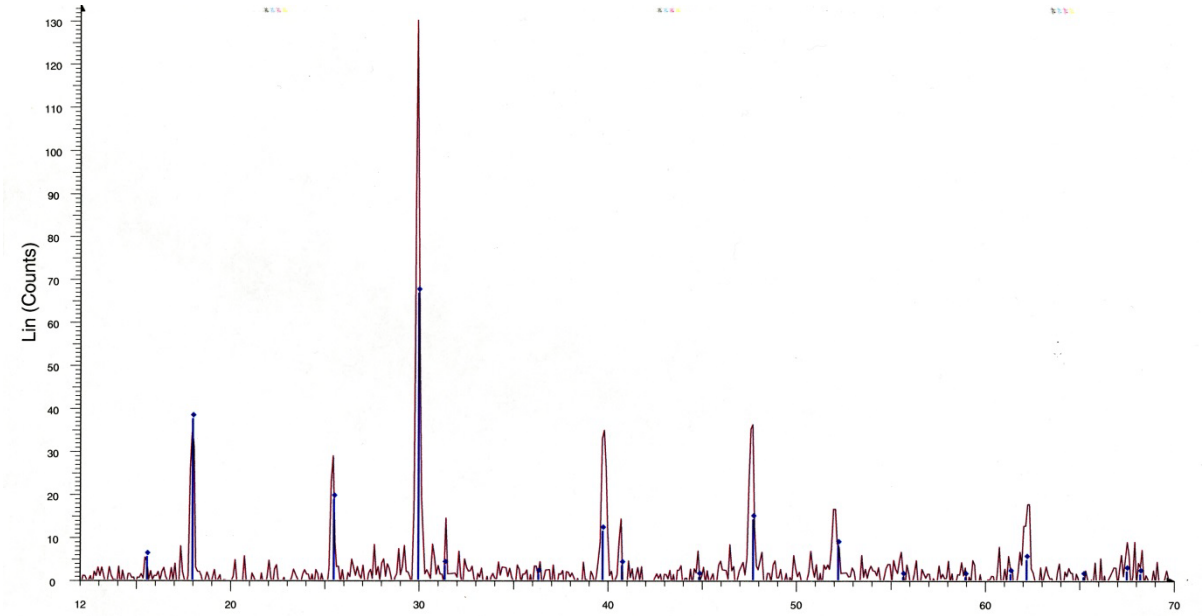

Figure 76 XRD powder spectrum of the precipitate which formed upon heating alum solutions. It was identified as alunite. **RED CURVE:** Alum solution heated, precipitate. **BLUE CURVE:** Reference 00-047-1885 potassium aluminum sulfate hydroxide (alunite).

Reaction [1] summarizes the reactions in the solution phase, while reaction [2] suggests a probable reaction forming the precipitate.

At RT, pH 3.5:

[1] $KAl(SO_4)_2 + 2\ H_2O \rightleftharpoons 2K^+ + Al(OH)^{2+} + H_3O^+ + 3\ SO_4^{2-}$

At 90°C, pH 2:

[2] $3KAl(SO_4)_2 + 12\ H_2O \rightarrow KAl_3(SO_4)_2(OH)_{6\ (ppt)} + 2K_{(aq)}^+ + 4SO_4^{2-}{}_{(aq)} + 6H_3O^+$

Aspen (*populus* spp.) treated with alum and sulphuric acid solutions in the lab

Recall the experimental conditions described in Section 2.2: alum concentrations used 2:1 and 4:1 parts alum:water by weight and sulphuric acid solutions of pH 0, 1, 2, 3. Treated 24 hours at 90°C. Sample overview is given in Table 2 which also show pH of woods before and after treatment. A brief summary of Py-GC/MS results for sample 4B-2009 were mentioned in Section 3.3.1. Infrared analyses were carried out on the Perkin Elmer instrument (range: 4000-650 cm^{-1}).

The alum treatment applied to archaeological woods clearly gave good results in terms of preventing extensive shrinkage and acceptable colour. The experiments also demonstrated the drawbacks of the treatment, such as brittleness and relatively high acidity, especially in the archaeological samples (pH 3). All sulphuric acid treatments at 90°C caused immediate darkening of fresh aspen after treatment, while only the solution at pH 0 caused noticeable darkening of the archaeological aspen based on visual examination.

Microscopic investigations of the alum-treated wood revealed an uneven distribution of alum salts in both fresh and archaeological woods. More alum penetrated the archaeological samples than that observed in the fresh aspen. SEM-EDX analyses (not shown) confirmed that the major inorganic product retained by the wood was indeed alum salt. X-ray tomographic images in Figures 77 and 78 showed alum salts had a uniform density, unlike that observed for the Oseberg samples (Section 3.3.2). Therefore the presence of denser alum-derived compounds in X-ray tomographic images of aged alum-treated woods may indicate that alum salts are not stable and may be actively involved in wood-degrading reactions. Further investigation is required.

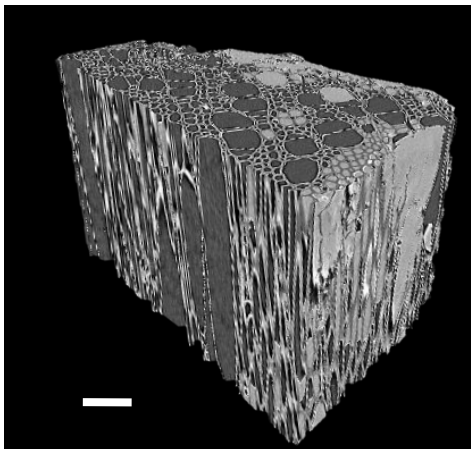

Figure 77 X-ray tomographic image of fresh aspen treated with 2 parts alum to 1 part water at 90°C, 24 hours.

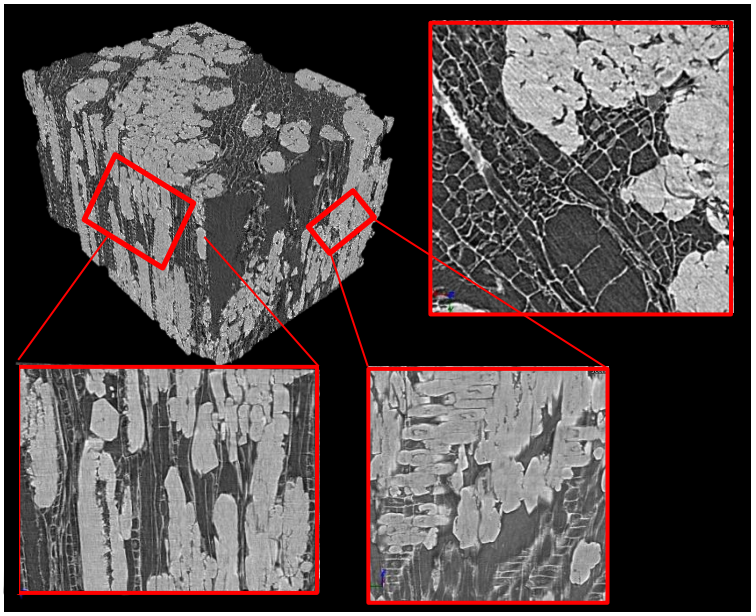

Figure 78 Archaeological aspen (sample 6B) treated with 2 parts alum and 1 part water at 90°C, 24 hours.

RH experiments showed that impregnation with alum at 90ºC reduces water uptake by wood (Figure 79). No differences in moisture uptake were observed for the different treatment concentrations of alum salt at 90ºC, likely as the samples were well-impregnated with alum. Experiments also showed that at lower RH levels (especially below 50% RH), water uptake increased with increasing deterioration of wood: compare Archaeological aspen (less degraded) and Oseberg alum washed out (much more degraded), Figure 80.

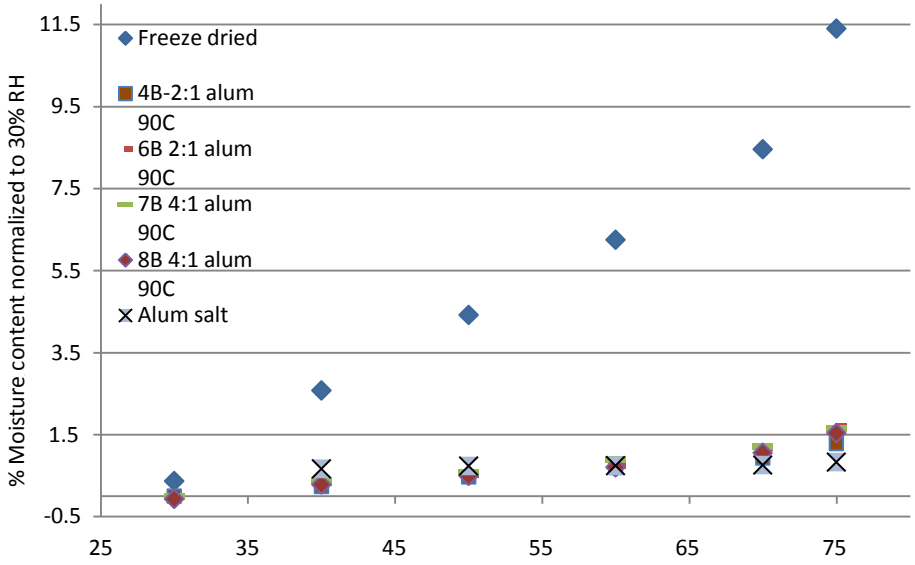

Figure 79 Moisture uptake of alum-treated archaeological aspen (treated at 90°C), untreated (freeze-dried) archaeological aspen, fresh alum powder.

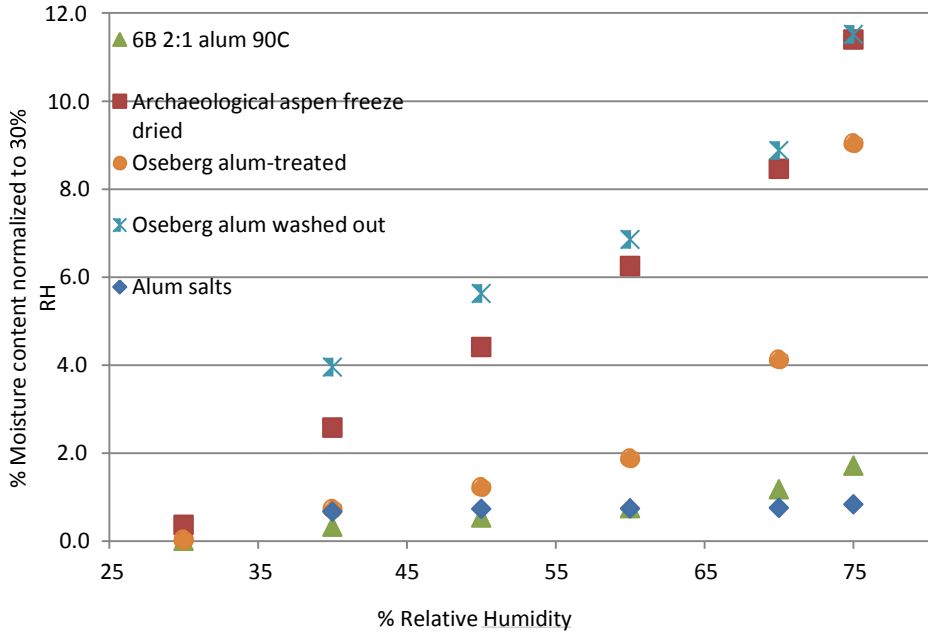

Figure 80 Moisture uptake of sample 6B (2:1 alum 90°C) compared to alum-treated wood from Oseberg, alum-treated wood from Oseberg where the alum has been washed out and the sample freeze dried, and fresh alum powder.

In fresh wood, alum treatment solutions regardless of temperature or concentration did not cause observable changes in IR spectra. However fresh wood treated with sulphuric acid solutions at pH 0 (at both RT and 90ºC) and at pH 1 at 90ºC had reduced IR signals for hemicellulose (at 1734 and at 1240 cm^{-1}) (Figure 81).
Infrared spectra for all treated archaeological samples (both alum concentrations and acid) showed slightly more degradation at 90°C than at RT, based on slightly higher band height ratios 1122/1026 at 90°C and no differences were observable between samples treated with 2:1 and 4:1 alum solutions (not shown). Spectra also showed that the chemical changes caused by alum at 90^0C were closest to that caused by sulphuric acid at pH2 at 90^0C (Figure 82). However, the rinsing step carried out before infrared analyses (to remove interferences from alum) also removed important information from the carbonyl-containing region, such that it was not possible to observe degradation trends.

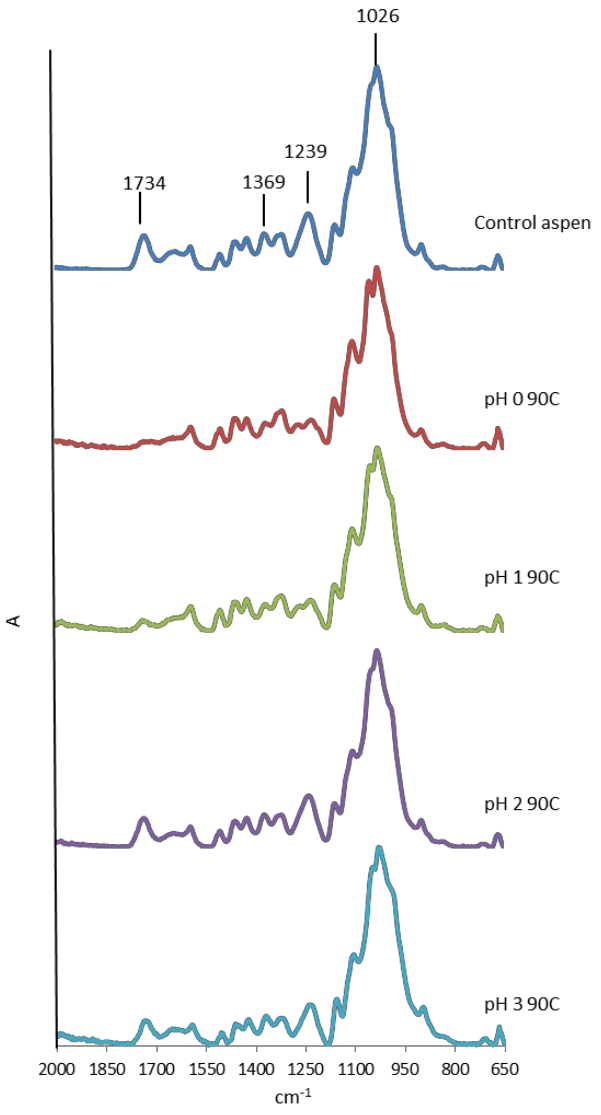

Figure 81 Infrared spectra of fresh aspen treated with sulfuric acid solutions at 90°C, compared to untreated aspen. Bands with significant changes are labelled.

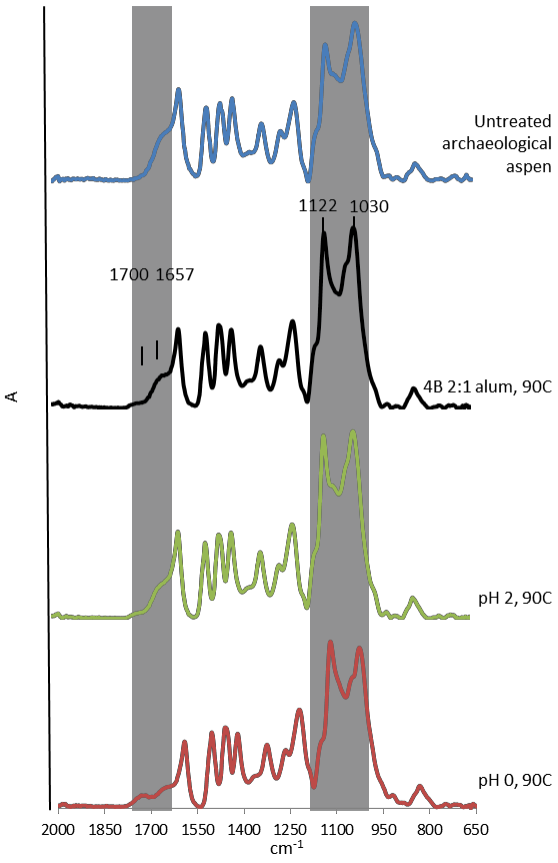

Figure 82 Infrared spectra of archaeological aspen treated with alum and sulfuric acid solutions pH 0 and pH 2 at 90°C, compared to untreated aspen. Shaded and labelled regions indicate where band heights were measured.

3.5.2 Aging studies on birch recently treated with alum and sulphuric acid, pH 2

Recall from the experimental information given in Section 2.2: fresh birch and archaeological birch were treated with 2:1 parts alum:water by weight and by sulphuric acid at pH 2 at 90°C for 24 hours (and for 40 hours for alum treatments on archaeological birch). Freeze dried samples of both fresh and archaeological woods served as controls[3]. The sample overview given in Table 3 shows measured densities. After treatment all samples were divided into 2 groups: Aging (kept at 50°C, 60% RH for 370 days) and Ambient (control group, kept at RT, 60% RH for 370 days). Colour measurements and infrared spectra were taken of samples at regular intervals (using the Perkin Elmer instrument, with range 4000-650 cm^{-1}). Two archaeological samples were analysed by ICP-OES in Germany (procedure 1). Samples were also examined by SEM before and after aging.

Both chemical analyses and visual inspection have shown that alum-treated Oseberg woods showed a far greater extent of deterioration than those samples which had remained untreated, indicating that the deterioration observed is related to the alum- treatment and that it was relatively slow[4]. Colour measurements of the 185-series (Oseberg) were taken and ΔE* was calculated relative to the freeze-dried fresh birch sample. These values are compared with extent of oxidation by the band height ratio of 1700/1030 (carboxylic acids) and the relative abundance of oxidized lignin determined from Py-GC/MS (Figure 83).

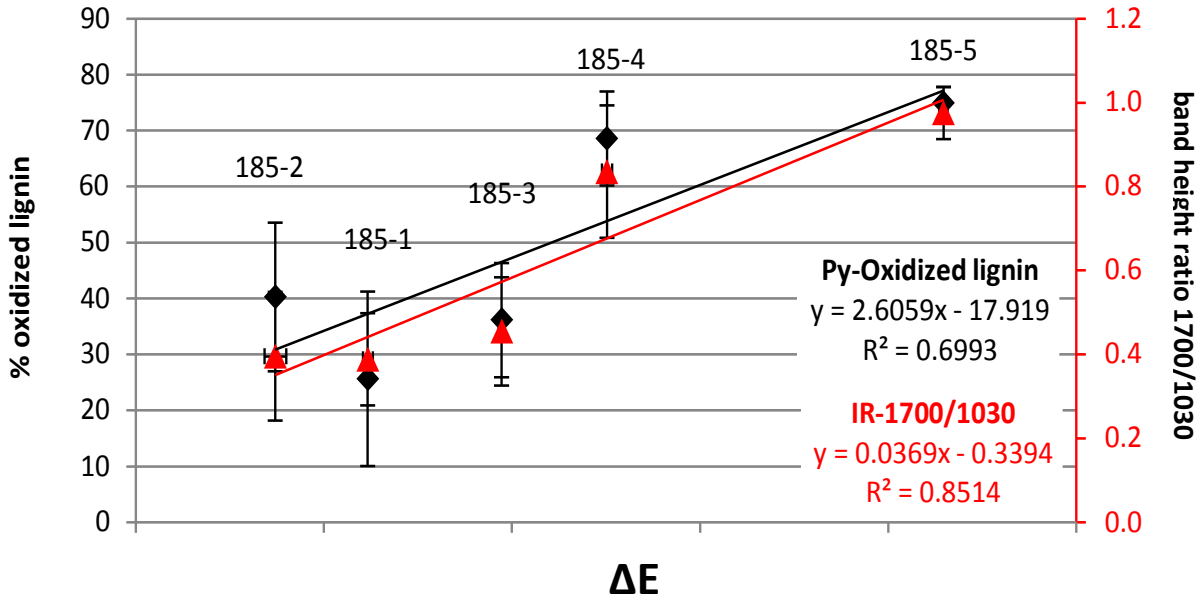

Figure 83 Scatter plot of the colour differences, ΔE*, (relative to fresh birch) of Oseberg woods compared to oxidized lignin relative abundance calculated from Py-GC/MS and band height ratio 1700/1030 calculated from infrared spectra. Both methods show a relatively good correlation between colour and extent of oxidation. The values used in the plot are shown in the table.

Here, aging experiments were set up to measure the changes which would occur over 1 year using colour measurements, SEM and infrared analyses. Aging conditions (50°C, 60% RH) were deliberately set to be mild to avoid potential temperature-induced reactions in alum salts that would normally not occur at room temperature.
Comparing **colour change (ΔE*)** of aged sample sets to the ambient sets of fresh and archaeological birch after 370 days, it is clear that the aging conditions had an effect on the alum-treated samples' colour, which increased significantly relative to samples kept at RT

[3] A more correct reference sample in these experiments would have been birch treated with pure water at 90°C for 24 hours, as was carried out for the 'treated' samples. Under these conditions the wood would lose a part of extractives, which is not the same as after freeze drying.

[4] The alum treatment, despite its drawbacks of producing wood which was extremely pale and brittle, was in use for almost 100 years. This indicates that the immediate results from the alum treatment must have been considered to be favourable by conservators. It would likely not have been in use for so long had it produced brown, powdery wood within the first few decades. However, it remains a mystery as to why they insisted on using glycerol in the alum treatment even when it proved to be so problematic.

(Figures 84, 85). Thus, the aging conditions caused colour change, but it is still uncertain whether or not this was due to unintended reactions in alum salts (that would not otherwise occur at RT).
Within the aged set, the increase in ΔE* after 370 days for alum-treated fresh birch and most archaeological birch samples were greater than that for the freeze dried and sulphuric acid treated samples, both of which had similar magnitudes of colour change (Figures 84, 85). As increase in colour change is related to increase in oxidation of the wood polymers, this indicates that alum caused a greater extent of oxidation than sulphuric acid solutions at the same pH after aging.

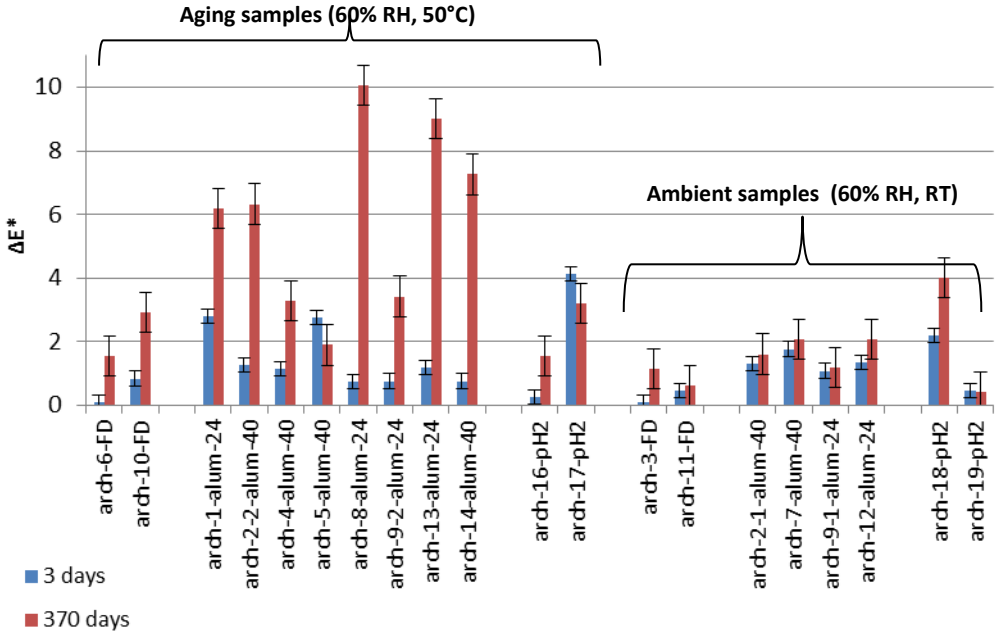

Figure 84 Archaeological woods after 3 days and 370 days of storage at aging and ambient conditions. The colour change is compared for all samples.

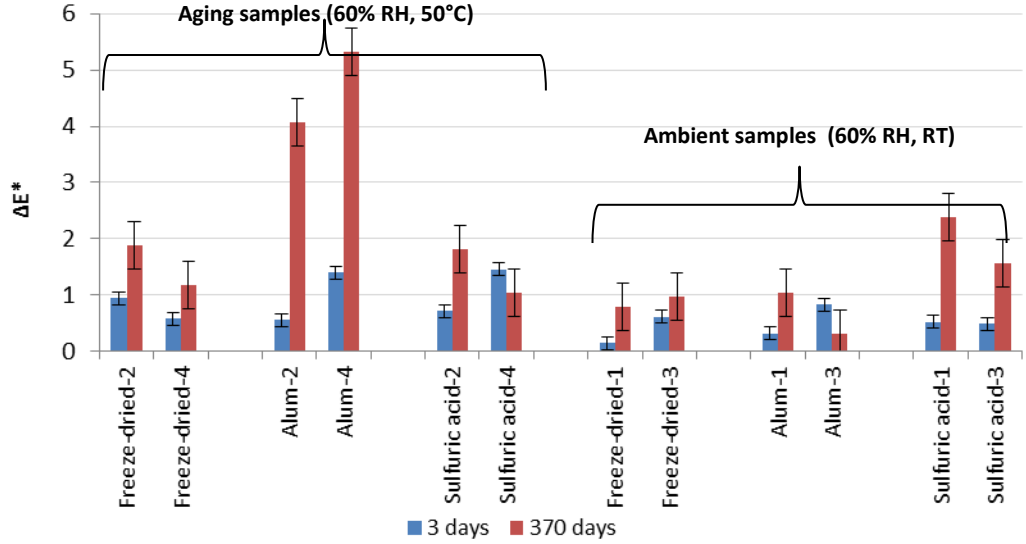

Figure 85 Fresh woods after 3 days and 370 days of storage at aging and ambient conditions. The colour change is compared for all samples.

SEM analyses before and after aging for 370 days did not distinguish major changes under the magnifications used (Figure 86). X-ray tomographic microscopy was not carried out for these samples, but it may have revealed morphological difference

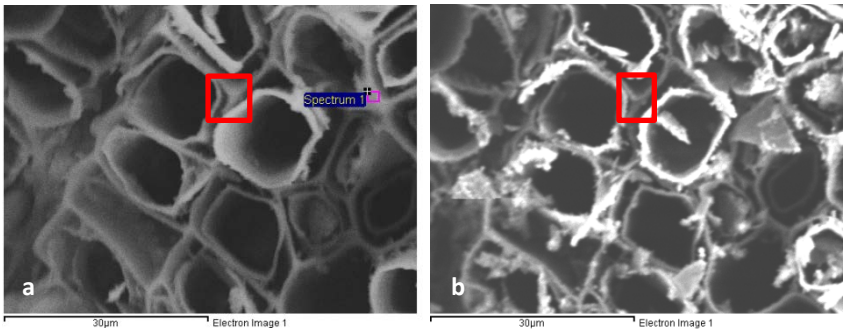

Figure 86 SEM analysis of arch-1 before (a) and after aging (b) for 370 days. The two figures represent the same region. The red frames show potential changes in the cell wall corners.

Infrared analyses (ATR-FTIR) showed some changes before and after aging (Figures 81 and 82). In fresh woods greatest change occurre in the hemicelluloses, where signals occur at 1734 and 1230 cm^{-1} (Figure 87). For archaeological woods (Figure 88), greatest change occurred in the 1650-1715 cm^{-1} region, which represents signals from different types of carbonyl groups and at 1122 and 1030 cm^{-1}, each of which represents signals from both lignin and holocellulose (see Table 6 for more detailed assignments). In these experiments, IR spectra were also compared by ratios of the band height at 1660 cm^{-1} (conjugated carbonyl stretch in lignin) over that at 1030 cm^{-1} (Figures 89 and 90). An increase in the 1660/1030 ratio would indicate increased oxidation. Here there was less correlation of a correlation between aged and unaged sample sets, as well as between the different pre-treatments (freeze-dried (control), alum and sulphuric acid). This may have something to do with the rinsing step used to remove the alum salts before IR analyses which can remove signals from this region (as previously discussed in Section 3.3.2). Thus whether or not the alum treatment was more aggressive than that using sulphuric acid under aging conditions (measured by increase in level of oxidation) is still uncertain. Future experiments may benefit from more sensitive analytical techniques (such as NMR or Py-GC/MS) to analyze the chemical changes during aging, complemented by both ICP-AES and XRD.

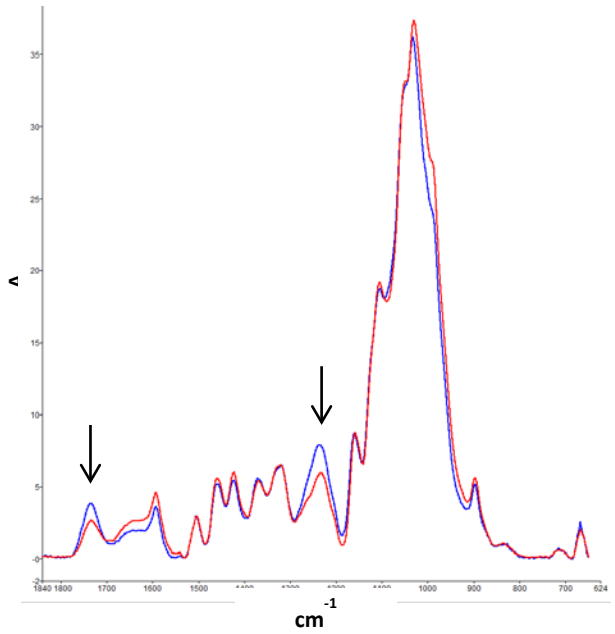

Figure 87 Infrared spectra of alum-treated fresh wood (Fresh birch-alum-2) after 3 days (blue curve) and 370 days (red curve) of aging at 50°C and 60% RH. Areas with hemicellulose degradation are indicated by arrows (1734

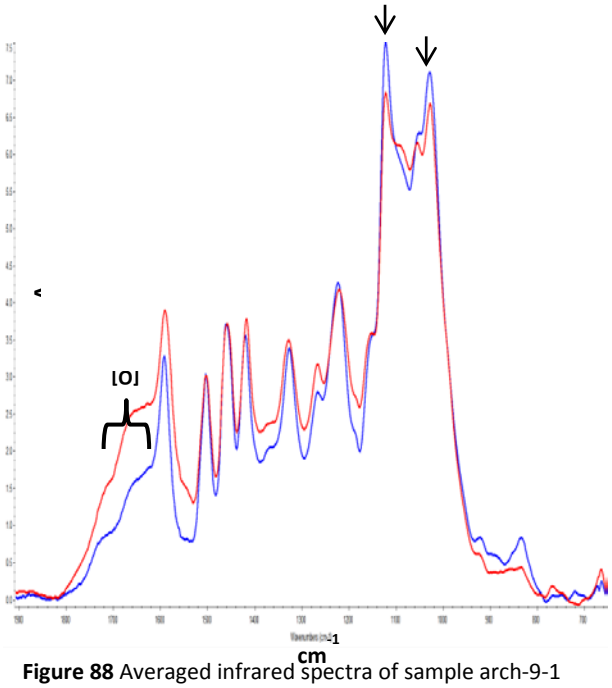

Figure 88 Averaged infrared spectra of sample arch-9-1 (blue curve) and arch-9-2 (red curve) after 370 days. Arch-9-1 was stored at RT, while arch-9-2 was kept at 50°C. Both samples were maintained at 60%RH. The most significant differences are also evident at 1122 and 1030 cm^{-1} (black arrows). The oxidized region [O] at 1650-1715 cm^{-1} increased after 370 days for arch-9-2.

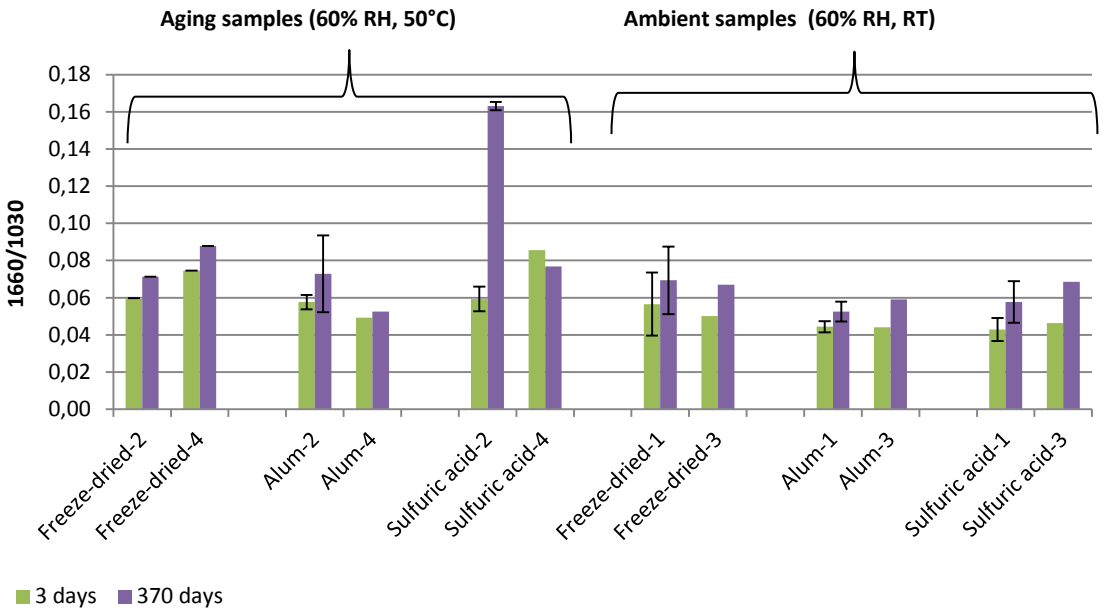

Figure 89 Fresh woods after 3 days and 370 days of storage at aging and ambient conditions. The band height ratio 1660/1030 is compared for all samples.

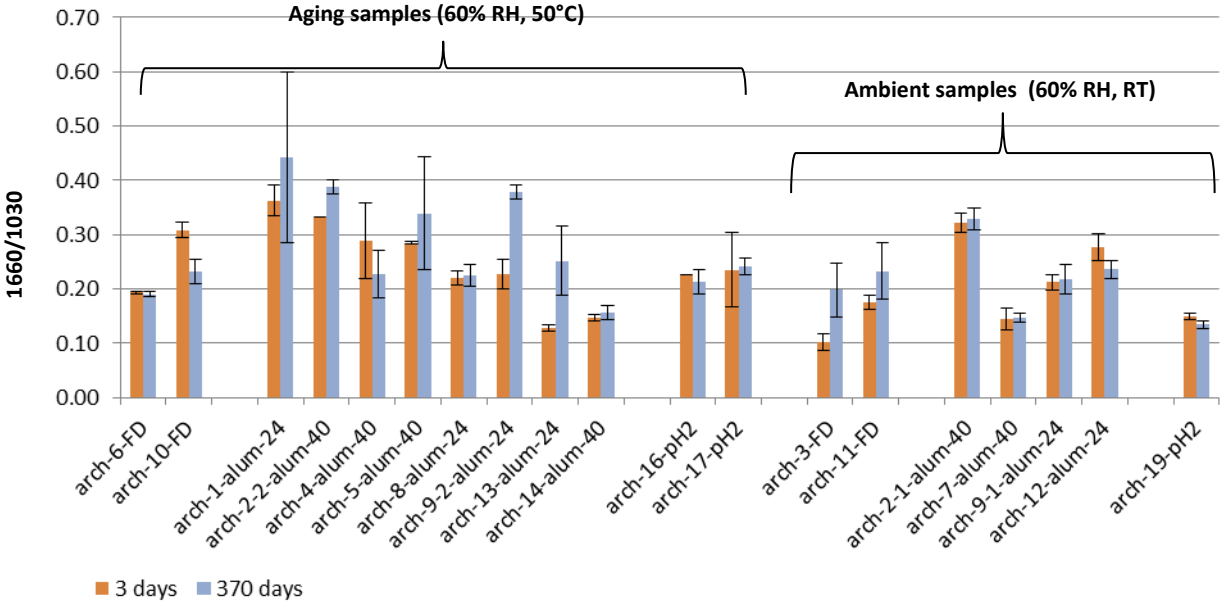

Figure 90 Archaeological woods after 3 days and 370 days of storage at aging and ambient conditions. The band height ratio 1660/1030 is compared for all samples.

In these experiments, **sources of uncertainty** include the chemical and anatomical / morphological variabilities within the sample material – especially in the archaeological woods, due to degradation and uptake of impurities during burial. The ICP-OES analyses of two samples (Table 21) show relatively large differences in for example Fe, which may affect how the woods age. What should have been done was that each sample, especially for the archaeological woods, should have been cut in half after treatment, with one half to undergo aging while the other half kept in a control set. This would have reduced the variability of aging changes, such that the samples would be more directly comparable.

Table 21 Elements analyzed by ICP-OES in two recently alum-treated samples subjected to aging at 50°C and 60%RH.

	mmol/100g							
	Al	**K**	**Ca**	**Mg**	**Fe**	**Cu**	**Mn**	**Zn**
Arch-1 2012-24	30.98	105.24	0.02	0.00	0.43	0.00	≤ 0.021	0.00
Arch-4-2012-40	58.66	115.71	0.85	0.00	0.14	0.01	≤ 0.010	0.00
Fresh birch	-	-	0.97	0.58	0.00	0.00	≤ 0.071	0.04

None of the samples treated in these experiments were as highly oxidized as those observed for the Oseberg woods, indicating that deterioration of alum-treated woods would take more time. However it is important to also emphasize that the rate of degradation (and the actual shape of this curve) is not yet fully understood. Harsher aging conditions are not recommended in artificial aging experiments to speed up rate of decay for alum-treated woods as alum salts are known to be more reactive at temperatures above 50˚C (personal communication, Hartmut Kutzke). On the other hand, a higher aging temperature may give an indication of the *potential* for a wood to degrade, but the problem of translating the degradation observed at higher temperatures to RT remains. For the highly degraded 185-series there is a better correlation between colour difference and oxidized lignin or acid content than that which had been found in artificially aged samples, suggesting that alum-treated samples would, over time, likely establish more definite trends with further deterioration.

3.6 Investigating survey indicators – preliminary results

Background for this study

- Variable condition and extent of restoration of the alum-treated objects will require that they are sorted for different types of retreatment
- Previously on a smaller sample set:
  - correlation between increasing darkness and reduced state of preservation.
  - darker woods generally more acidic wood and had more iron
- Do these relationships hold on a wider set of samples?

AIM: Want to see if simple and/or non-destructive analytical techniques can aid visual interpretation:

- Does darkening really correlate to increased degradation? Or do some paler woods also exhibit high degradation?
- Is the darkening due to higher concentration of reactive metal ions? (such as Fe, Cu)?

Methods

- pH (strips)
- Infrared analyses (ATR-FTIR): compared acid content, and compared spectra by PCA (not shown)
- Color difference (ΔE^*) was calculated relative to the averaged fresh diffuse porous wood types (birch, maple, aspen, alder)
- SEM: estimation of iron and other elements

Samples (Table 4)

- 54 fragments from 19 objects
- 34 alum-treated
- 20 alum + linseed oil-treated (or with varnish)
- Almost all samples are diffuse porous hardwoods. Two ring porous samples (C55000/299 and 210).
- chose those with existing breaks

Summary

- pH is generally higher in the lighter coloured woods (Figure 91)
- *Generally* more oxidized / acidic groups in darker woods (via IR) (Figure 92)
- Reason for variable degree of darkness is not closely related to Fe-content (Figure 93)
- Alum+linseed –treated fragments oil appear to be better preserved than fragments with only alum (colour, IR, pH) (Figure 91 for ex.)

Thus, colour appears to be a significant indicator for the state of preservation of the wood. It may be worthwhile to undertake colour measurements / or establish colour categories during future surveys and note them. Work is continuing in SO-II.

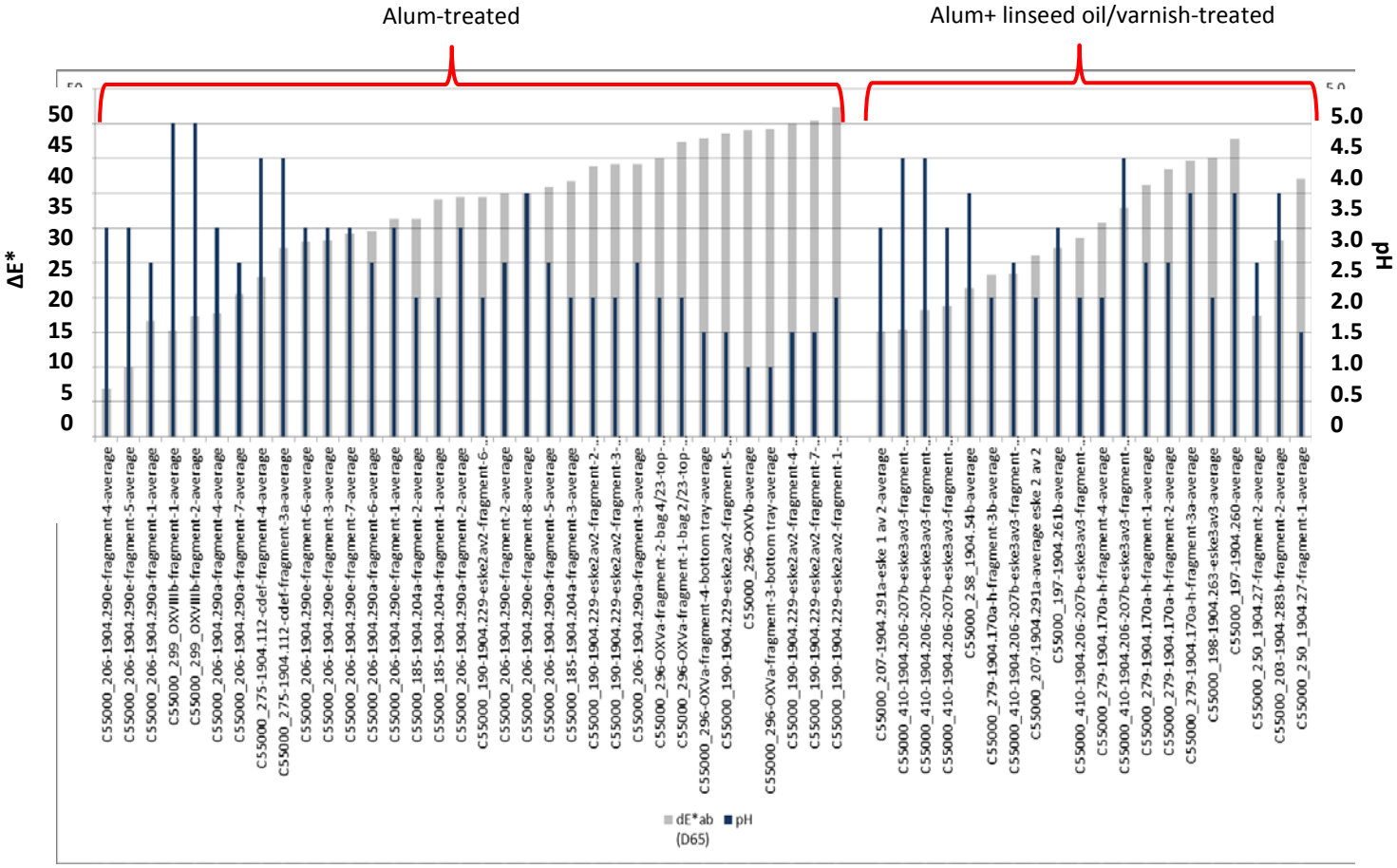

Figure 91 Colour difference (left vertical axis, grey bars) compared with pH (right vertical axis, blue bars).

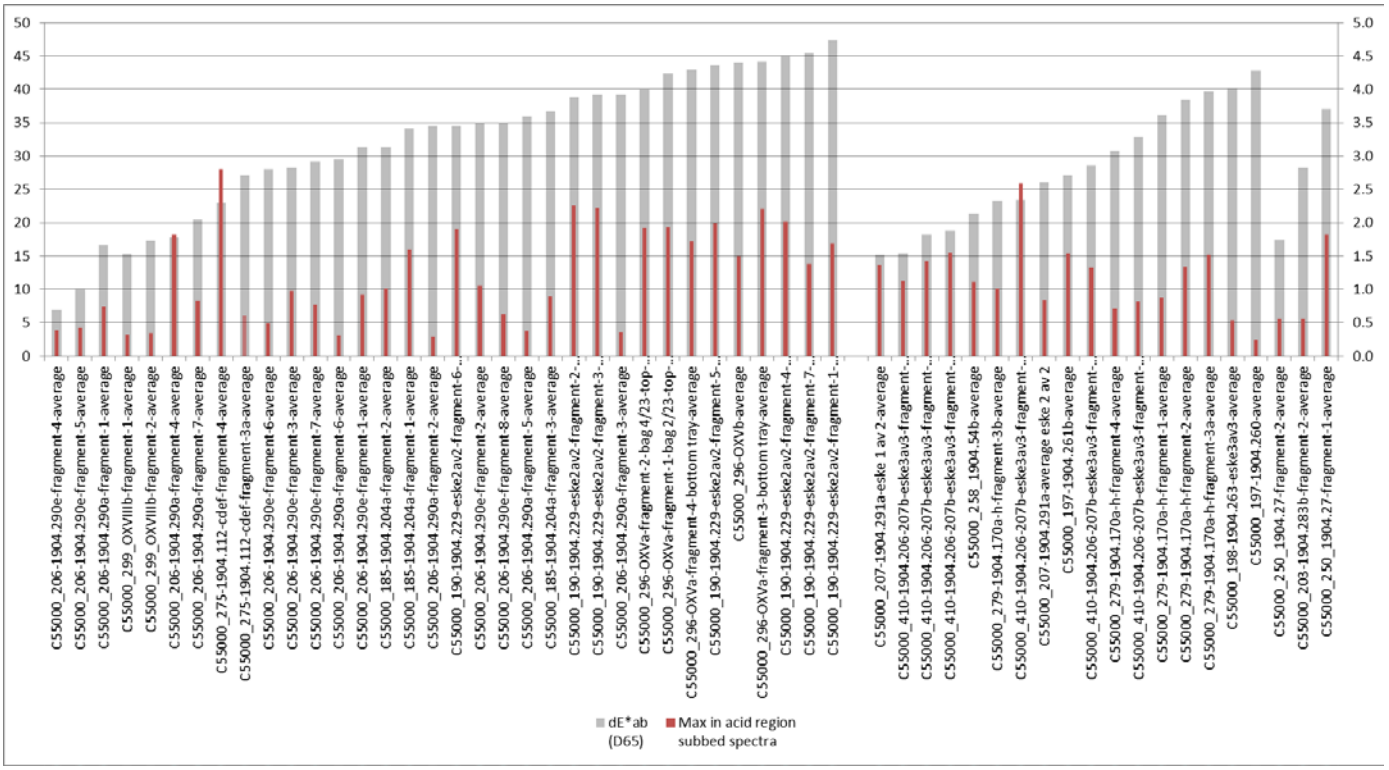

Figure 92 Colour difference (left vertical axis, grey bars) compared with maximum intensity in acidic region of infrared spectra (right vertical axis, red bars).

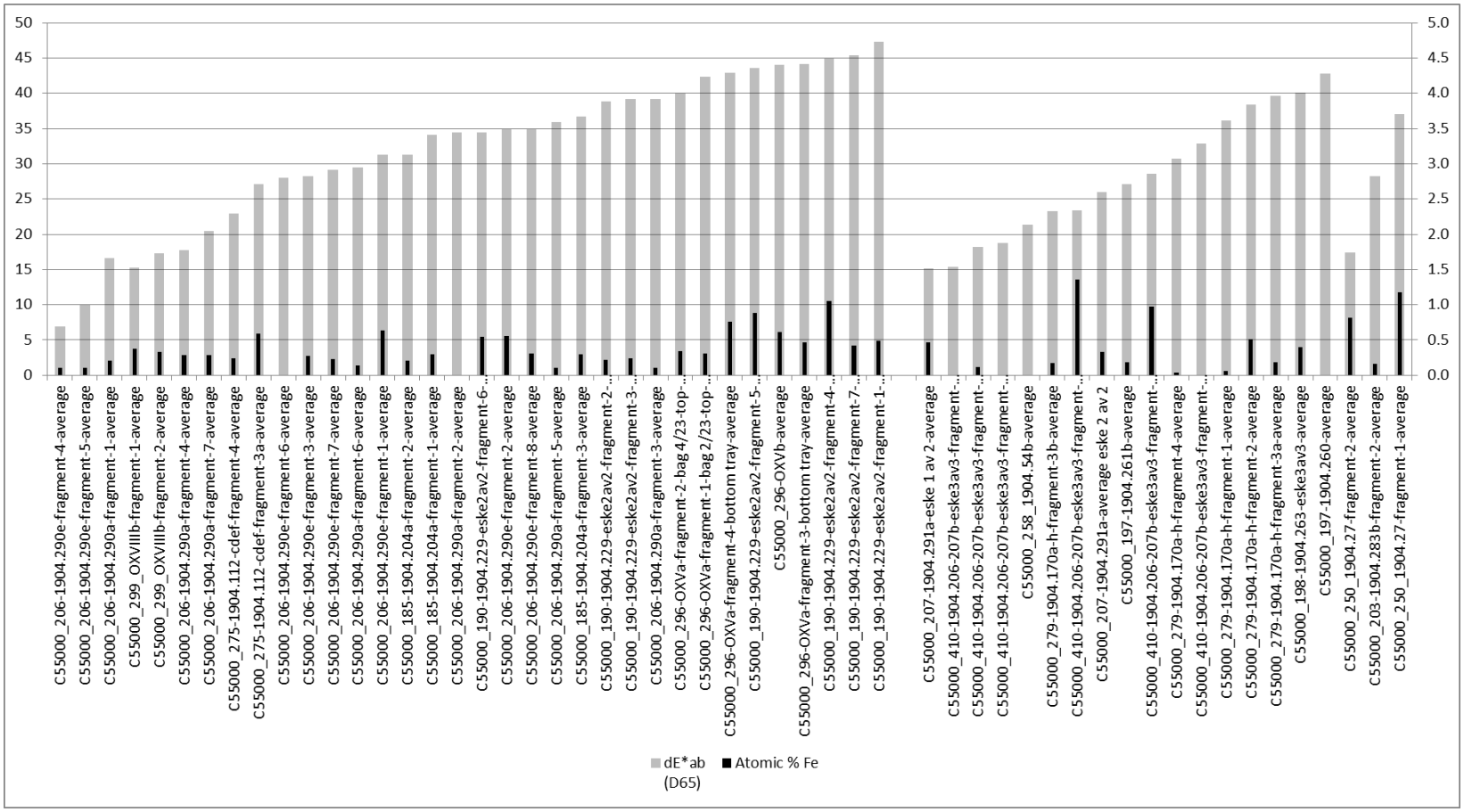

Figure 93 Colour difference (left vertical axis, grey bars) compared to atomic % of iron, found by SEM-EDS (right vertical axis, black bars).

3.7 Advantages and limitations of methods used

The applied analytical techniques were successful in characterising the inorganic components and the lignocellulosic materials in the analysed objects.

In particular, analytical pyrolysis-based techniques Py(HMDS)-GC/MS permitted to evaluate the degradation state of composite archaeological wooden artefacts in terms of loss of polysaccharides and alteration of lignocellulosic polymers at molecular level. The categorisation of a high number of wood pyrolysis products and the evaluation of their distribution allowed to obtain a high molecular detail, going beyond the simple estimation of the H/L ratio and highlighting new potentialities of analytical pyrolysis in the analysis of archaeological wood.

FTIR, Py(HMDS)-GC/MS and ICP analyses were found to be useful complementary tools for studying trends in wood degradation and inorganic content. GPC and NMR spectroscopy (HSQC) also provided information about the condition of the wood, but are less readily available techniques and do not provide significantly more useful information that the FTIR/Py-GC/MS combination at this stage of our investigations. XRD, FTIR-microscopy and SEM-EDS were useful for identifying specific inorganic compounds and providing information about their distribution. Synchrotron techniques such as X-ray and neutron imaging gave structural information that was not possible to obtain otherwise.

However, challenges in analyzing and examining wood components of alum-treated samples arose from interference by alum salts (FTIR, EGA-MS) and the large inorganic component (potential interference in Py(HMDS)-GC/MS). But using complementary techniques such as FTIR with Py(HMDS)-GC/MS could allow us to distinguish actual trends from those caused by method. Removal of the alum interference from FTIR spectra remains an issue, as both rinsing and subtraction have advantages and drawbacks, and further work is required to improve this (e.g. involving deconvolution of spectra). In addition, alum often overshadows other inorganic compounds in XRD patterns and FTIR spectra, though microscopic mapping often helps in the latter case.

Conventional microscopy (SEM, light microscopy) is also difficult for the alum-treated wood, requiring lengthy sample preparations due to its powdery nature. This means detailed, high magnification studies of cellular structure, or ID of the wood, are not possible. We recently had some success with embedding some samples before microscopic study. However this requires more sample than sometimes can be taken, so not all samples could be examined in such great detail.

4. Overall Conclusions

This report summarizes the experimental work undertaken during most of SO-I on alum-treated wood, without other additives, using a wide range of analytical techniques and experimental setups. Here we investigated alum-treated woods in a range of states of preservation, as well as the different zones existing in larger fragments (alum rich and alum poor). We compared alum-treated samples to both fresh and untreated archaeological woods. Archaeological woods included samples from both recent excavations and from the Oseberg collection.

The condition of the alum-treated wood

Relative to untreated archaeological woods, all alum-treated woods from Oseberg are much more degraded. In general, extensive degradation of holocellulose and oxidation of lignin were observed by both Py(HMDS)-GC/MS and FTIR techniques, and morphological studies revealed extreme deterioration of the cell walls. GPC and HQSC NMR analyses also confirmed that extreme depolymerization of alum-treated woods from Oseberg had occurred.
We could nonetheless distinguish levels of degradation among alum-treated woods as illustrated by the 185-series. In terms of inorganic components, alum was accompanied by varying amounts of its decomposition product $KHSO_4$ in almost all analysed samples from objects 185 and 229.

The alum treatment is the source of alum-treated woods' high acidity (pH ≤ 2). The ICP, EDX and IC-LC analyses indicated that there is a large amount of sulphates in all samples not bound as alum or $KHSO_4$, reflecting a high level of sulphuric acid released by hydrolysis of alum during treatment. This would imply that the wood would suffer from extreme hydrolysis. Indeed, the alum-treated woods are characterized by low holocellulose levels. More degraded wood was shown by Py(HMDS)-GC/MS to also have higher levels of anhydrosugars, and higher levels of derivatization of these sugars. Anhydrosugars were present in the tri-TMS, di-TMS and mono-TMS forms, and levoglucosan was the most abundant compound in this category. This phenomenon can be correlated with the degree of degradation: more degraded polymer networks, which present a more open and incoherent structure, are more reactive towards HMDS because steric hindrance is reduced. Thus the relative amount of persilylated (tri-TMS) anhydrosugars was higher for those samples that showed a higher degradation of carbohydrates, indicating higher depolymerization. This will be looked into further during SO-II.

However, the visually observable damage in Oseberg samples was mainly related to oxidation of lignin, the main remaining wood polymer (there was almost a complete absence of polysaccharides). Increasing visual deterioration (i.e. increase in darkening and decrease in the wood's visual structural integrity) was highly correlated to increasing lignin oxidation: as observed, for instance in samples 185-1, -2, -3, which had much less oxidized lignin than 185-4, -5, -6 (see Figure 23). The extent of lignin oxidation was observed in both Py(HMDS)-GC/MS and FTIR analyses results. Colour differences in the 185-series (relative to fresh birch) correlated well with acid lignin pyrolysis products and with bands corresponding to lignin oxidation products in FTIR spectra, indicating that increasing colour change (darkening) corresponded to increasing degradation (and an increase in acid lignin content) (see Figure 83).

Moisture uptake experiments showed that alum is not hygroscopic, but that the deteriorated wood is. Oseberg samples which had been washed to remove alum and freeze dried had higher moisture uptakes than even fresh woods. Further work on this topic using time-resolved NMR will be undertaken in SO-II.

Distribution and effects of inorganic compounds

Alum salts are spread unevenly throughout wood, at both cellular level (as seen by X-ray tomographic microscopy) and at the macroscopic level, resulting in alum-rich and alum-poor zones in larger fragments.

The ArCo project investigated chemical differences between alum-rich and alum-poor zones in the 229-samples. Alum-rich surface samples had a higher extent of wood degradation and a higher inorganic content than the corresponding alum-poor core samples. However we noted that since the alum rich zone is the outer surface of the fragment, it is also more accessible to external conditions and inorganic impurities from soil during burial, which can affect the level of degradation. The extent of wood degradation correlated more strongly with the Al, K and S levels in these samples than any other inorganic elements, as did an estimation of the acid content. This supports a direct relationship between wood degradation and alum treatment/ release of sulphuric acid from alum treatment.

Good correlations between the subtraction Ca from Fe concentrations and acid lignin pyrolysis products in both the 185 and 229 samples could suggest that iron-promoted degradation is a factor in the condition of the wood and that it is modulated by calcium compounds. However, such a relationship is not yet conclusive, and in these woods the concentrations of these elements are relatively low. Further investigations into samples with higher iron concentrations as well as model experiments with iron and calcium impregnated fresh wood have begun and will be concluded in Phase II.

ICP-OES and SEM-EDX also indicated that K- and S- containing ions had migrated more effectively than Al-ions into the core of the fragments 1C and 1D, which was supported by a larger proportion of $KHSO_4$ relative to alum seen by XRD. Elemental analyses before and after water extraction of wood samples indicated that, while the major elements were mostly present as water-soluble salts, more water-insoluble salts were present in the alum-poor regions than the alum-rich regions.

In addition, evidence of ammonium compounds, ammonium alum in particular, was detected in several samples by FTIR. This source of this remains uncertain, but could reflect the presence of ammonium-alum in the original treatment material. Further investigations into this, including quantification of ammonium and the implications of its presence, are underway and will be continued in Phase II.

The ArCo project also investigated differences in the wood fragments before and after artificial aging (extreme RH cycling at 30°C). This did not result in significant changes in the wood components, though the concentrations and distributions of inorganic components varied significantly. Changes in Al, K and S concentrations indicated migration of salts and other compounds, and in particular that sulfur-containing compounds, had migrated out of the alum-rich areas and into alum-poor regions. Redistribution of alum and $KHSO_4$ in alum-poor samples was also observed by XRD, and migration of salts was also supported by formation of K and S-containing crystals on the surface of some fragments.

Model experiments

Aging experiments using model woods treated with alum and sulphuric acid pH 2 showed that alum caused greater colour change than sulfuric acid at 50°C after 370 days. Whether this colour change implies greater oxidation was not confirmed since the samples were only analysed by FTIR, which required a rinsing step which likely affected information about level of oxidation. Thus whether the alum treatment generally causes a greater extent of both oxidation and hydrolysis (after some aging) than sulphuric acid is uncertain. This will be looked into further in SO-II.

Further questions to be investigated in SO II

There remain several aspects of alum-treated wood chemistry that are not yet well understood and have a direct impact on decisions about reconservation. One major question is about the rate of decay of alum-treated wood. What is the present rate of decay? Is it slow enough to no longer cause concern and therefore makes it unnecessary to reconserve some objects? Additionally, the chemical stability of alum crystals in the wood must be better understood, in order to decide whether efforts should be aimed at their removal or not. Although preliminary work on survey indicators has been presented here, the trends are not yet very clear, so further work should be devoted to improving trend-analyses in order to address which visual traits can be connected to information about the state of preservation of the wood.

5. Related publications

Chemical analyses of extremely degraded wood using analytical pyrolysis and inductively coupled plasma atomic emission spectroscopy
S. Braovac, D. Tamburini, J. J. Łucejko, C. McQueen, H. Kutzke, M. P. Colombini, Microchemical Journal, 124, (2016), 368

New insights into the degradation processes and influence of the conservation treatment in alum-treated wood from the Oseberg collection
C. M. A. McQueen, D. Tamburini, J. J. Łucejko, S. Braovac, F. Gambineri, F. Modugno, M. P. Colombini, H. Kutzke, Microchemical Journal, 132, (2017), 119

Chemical analysis of degraded wood by analytical pyrolysis-gas chromatography/mass spectrometry and infrared spectroscopy,
Braovac S., Tamburini D., Łucejko J. J., Kutzke H., Colombini M. P., in: Conference Proceedings of CONDITION 2015 Conservation and Digitalization, Narodowe Muzeum Morskie w Gdansku, Gdansk 2015, p. 49-52, ISBN 978-83-64150-10-4

6. Related contributions at conferences

Integrated approach for the chemical characterization of whole wall cell materials: application to archaeological woods, *L. Zoia, M. Orlandi, A. Salanti, E.-L. Tolppa, J. J. Łucejko, D. Tamburini, F. Modugno, M. P. Colombini Sustainability In Cultural Heritage, CNR, Rome 11th-12th of January **2016** – oral contribution*

The dramatic effect of the alum treatment on the Oseberg wood collection: a Py-GC/MS and ICP-OES study, *D. Tamburini, J. J. Lucejko, F. Modugno, M. P. Colombini, F. Gambineri, H. Kutzke, 21st International Symposium on Analytical and Applied Pyrolysis, 9-12 May **2016** in Nancy, France – poster contribution*

The combination of pyrolysis-based techniques to evaluate the state of preservation of archaeological wood in the presence of consolidating agents, D. Tamburini, J.J. Łucejko, F. Modugno, M.P. Colombini, *21st International Symposium on Analytical and Applied Pyrolysis, 9-12 May **2016** in Nancy, France – oral contribution*

Identification of metal compounds in alum-treated wood from the Oseberg collection, McQueen, Caitlin; Kutzke, Hartmut; Braovac, Susan, *13th ICOM-CC Wet Organic Archaeological Materials Conference (WOAM); 16-21 May **2016**, Florence, Italy – oral contribution*

Application of Ionic Liquids for the Chemical Characterization of Archaeological Woods from Oseberg, Zoia, L., A. Salanti, and M. Orlandi in *18th ISWFPC, International Symposium*

on Wood, Fiber and Pulping Chemistry. **2015**. Vienna, Austria: BOKU, Dept of Chemistry-poster contribution

Investigation of treated composite archaeological wood artifacts using synchrotron radiation infrared spectroscopy, *D. Tamburini, J. J. Lucejko, .F Modugno, M. P. Colombini, "Year of Light 2015: the chemical point of view", Pisa, 9-10 February **2015** – oral contribution*

Chemical analysis of degraded wood by Py-GC/MS and ICP-AES, *Diego Tamburini, Susan Braovac, Jeannette Łucejko, Francesca Modugno, Caitlin McQueen, Hartmut Kutzke, Maria Perla Colombini "Technart 2015 − Catania, April 27-30, **2015** – oral contribution*

Py-GC-MS with in situ silylation to the analysis of treated composite archaeological wood artefacts - The ArCo Project, *D. Tamburini, J. J. Lucejko, F. Modugno, M. P. Colombini, H. Kutzke, S. Braovac, M. Mortensen, G. Chaumat, F. Gambineri, The Art Institute of Chicago, Northwestern University, the Field Museum, and Agilent Technologies, Chicago, Illinois, USA, 17 – 22 May **2015** – poster contribution*

The ArCo Project - Aging Study of Treated Composite Archaeological Waterlogged Artefacts - preliminary results, *D. Tamburini, J. J. Lucejko, F. Modugno, M. P. Colombini, H. Kutzke, S. Braovac, M. Mortensen, G. Chaumat, F. Gambineri, Condition 2015, National Maritime Museum in Gdansk, Poland 19th – 22nd May **2015** - oral contribution*

Chemical analysis of degraded wood by Py-GC/MS, and FTIR, *S. Braovac, D. Tamburini, J. J. Lucejko, H. Kutzke, M. P. Colombini, Condition 2015, National Maritime Museum in Gdańsk, Poland 19th – 22nd May **2015** - oral contribution*

Synchroton Based Infrared Microscopy as a Powerful Tool to Investigate Cultural Heritage Objects, *H. Kutzke, D. Tamburini, J. J. Lucejko, .F Modugno, F. di Girolamo, A. Lluveras Tenorio, M. Christensen, C. Bisulca, F. Andriulo, S. Braovac, K. Kausland, U. Schade, E. Aziz, Norwegian Synchrotron - and Neutron User Meeting 2015, Stavanger 19-20 January **2015** – oral contribution*

ArCo Project and Saving Oseberg Project: chemical investigations to preserve archaeological wooden objects, *F. Modugno, D. Tamburini, J. J. Lucejko, H. Kutzke, S. Braovac, M. P. Colombini XXV National Congress of the Italian Chemical Society "SCI2014", Arcavarcata 7-12 September **2014** – poster contribution*

Saving Oseberg – a new research project to stabilize actively deteriorating archaeological wooden objects *S. Braovac, J. J. Lucejko, D. Tamburini, H. Kutzke, M. P. Colombini, 2nd International Conference on Biodeterioration of Wood and Wood Products, Tartu (Estonia) April 24-27, **2013** – poster contribution*

7. References

1. Bardet, M., et al., *Dynamics property recovery of archaeological-wood fibers treated with polyethylene glycol demonstrated by high-resolution solid-state NMR.* Cellulose, 2012. **19**(5): p. 1537-1545.
2. Walsh, Z., et al., *Multifunctional supramolecular polymer networks as next-generation consolidants for archaeological wood conservation.* Proceedings of the National Academy of Sciences of the United States of America, 2014. **111**(50): p. 17743-17748.
3. Faix , O., *Classification of Lignins from Different Botanical Origins by FT-IR Spectroscopy.* Holzforschung 1991. **45**(s1): p. 21-28.
4. Zoia, L., A. Salanti, and M. Orlandi. *Application of Ionic Liquids for the Chemical Characterization of Archaeological Woods from Oseberg*. in *18th ISWFPC, International Symposium on Wood, Fiber and Pulping Chemistry*. 2015. Vienna, Austria: BOKU, Dept of Chemistry.

5. Schwanninger, M., et al., *Effects of short-time vibratory ball milling on the shape of FT-IR spectra of wood and cellulose.* Vibrational Spectroscopy, 2004. **36**(1): p. 23-40.
6. Best, S.P., R.S. Armstrong, and J.K. Beattie, *Infrared Metal-Ligand Vibrations of Hexaaquametal (III) Ions in Alums.* Inorganic Chemistry, 1980. **19**(7): p. 1958-1961.
7. Faix, O., et al., *Monitoring of chemical changes in white-rot degraded beech wood by pyrolysis—gas chromatography and Fourier-transform infrared spectroscopy.* Journal of Analytical and Applied Pyrolysis, 1991. **21**(1–2): p. 147-162.
8. Barbour, R.J., *Treatments for waterlogged and dry archeological wood*, in *Archaeological Wood: Properties, Chemistry, and Preservation*

R.M. Rowell and R.J. Barbour, Editors. 1990, American Chemical Society: Washington. p. 177-192.

9. Bjarnestad, S. and O. Dahlman, *Chemical Compositions of Hardwood and Softwood Pulps Employing Photoacoustic Fourier Transform Infrared Spectroscopy in Combination with Partial Least-Squares Analysis.* Analytical Chemistry, 2002. **74**(22): p. 5851-5858.
10. Mohebby, B., *Attenuated total reflection infrared spectroscopy of white-rot decayed beech wood.* International Biodeterioration & Biodegradation, 2005. **55**(4): p. 247-251.
11. Faix, O., *Classification of Lignins from Different Botanical Origins by FT-IR Spectroscopy.* Holzforschung, 1991. **45**(s1): p. 21-28.
12. Meier, D. and O. Faix, *Pyrolysis-Gas Chromatography-Mass Spectrometry*, in *Methods in Lignin chemistry*, S. Lin and C. Dence, Editors. 1992, Springer-Verlag: Berlin. p. 177-199.
13. Fabbri, D. and G. Chiavari, *Analytical pyrolysis of carbohydrates in the presence of hexamethyldisilazane.* Analytica Chimica Acta, 2001. **449**(1-2): p. 271-280.
14. Łucejko, J.J., *Wet archaeological wood: chemical study of degradation and evaluation of consolidation treatments*, in *Department of Chemistry and Industrial Chemistry*2010, University of Pisa: Pisa. p. 178.
15. Tamburini, D., et al., *Snapshots of lignin oxidation and depolymerization in archaeological wood: an EGA-MS study.* Journal of Mass Spectrometry, 2015. **50**(10): p. 1103-1113.
16. Pouwels, A.D., G.B. Eijkel, and J.J. Boon, *Curie-point pyrolysis-capillary gas chromatography-high-resolution mass spectrometry of microcrystalline cellulose.* Journal of Analytical and Applied Pyrolysis, 1989. **14**(4): p. 237-280.
17. Ralph, J. and R.D. Hatfield, *Pyrolysis-GC-MS characterization of forage materials.* J. Agric. Food Chem., 1991. **39**(8): p. 1426-1437.
18. Galletti, G.C. and P. Bocchini, *Pyrolysis/gas chromatography/mass spectrometry of lignocellulose.* Rapid Communications in Mass Spectrometry, 1995. **9**(9): p. 815-826.
19. Łucejko, J.J., et al., *Characterisation of archaeological waterlogged wood by pyrolytic and mass spectrometric techniques.* Analytica Chimica Acta, 2009. **654**: p. 26-34.
20. van der Hage, E.R.E., M.M. Mulder, and J.J. Boon, *Structural characterization of lignin polymers by temperature-resolved in-source pyrolysis—mass spectrometry and Curie-point pyrolysis—gas chromatography/mass spectrometry.* Journal of Analytical and Applied Pyrolysis, 1993. **25**: p. 149-183.
21. Modugno, F., et al., *Analysis of lignin from archaeological waterlogged wood by direct exposure mass spectrometry (DE-MS) and PCA evaluation of mass spectral data.* Microchemical Journal, 2008. **88**(2): p. 186-193
22. Shiraishi, N. and D.N.S. Hon, *Wood and cellulosic chemistry*. 2001, New York: Marcel Dekker. VIII, 914 s. : ill.
23. Łucejko, J.J., et al., *Analytical pyrolysis vs. classical wet chemical analysis to assess the decay of archaeological waterlogged wood.* Analytica Chimica Acta, 2012. **745**: p. 70-77.
24. Łucejko, J.J., et al., *Analytical instrumental techniques to study archaeological wood degradation.* Applied Spectroscopy Reviews, 2015. **50**(7): p. 584-625.
25. Tamburini, D., et al., *Archaeological wood degradation at the site of Biskupin (Poland): wet chemical analysis and evaluation of specific Py-GC/MS profiles.* Journal of Analytical and Applied Pyrolysis, 2015. **115**: p. 7-15.

26. Kotake, T., H. Kawamoto, and S. Saka, *Mechanisms for the formation of monomers and oligomers during the pyrolysis of a softwood lignin.* Journal of Analytical and Applied Pyrolysis, 2014. **105**(0): p. 309-316.
27. Kotake, T., H. Kawamoto, and S. Saka, *Pyrolysis reactions of coniferyl alcohol as a model of the primary structure formed during lignin pyrolysis.* Journal of Analytical and Applied Pyrolysis, 2013. **104**(0): p. 573-584.
28. Kawamoto, H., M. Ryoritani, and S. Saka, *Different pyrolytic cleavage mechanisms of β-ether bond depending on the side-chain structure of lignin dimers.* Journal of Analytical and Applied Pyrolysis, 2008. **81**(1): p. 88-94.
29. Huang, J., et al., *Density functional theory studies on pyrolysis mechanism of β-O-4 type lignin dimer model compound.* Journal of Analytical and Applied Pyrolysis, 2014. **109**: p. 98-108.
30. Hørte, T., et al., *Teknisk rapport Styrkeanalyse av Osebergskipet, Rapport Nr. 2005-1615, Revisjon nr. 02.*, 2006, Det Norske Veritas.: Høvik, Norge.
31. Brøgger, A.W., et al., *Osebergfundet: utgit av den Norske stat*. 1917, Oslo: Kristiania: Distribuert ved Universitetet oldsaksamling.
32. Tamburini, D., et al., *Characterisation of archaeological waterlogged wood from Herculaneum by pyrolysis and mass spectrometry.* International Biodeterioration & Biodegradation, 2014. **86, Part B**: p. 142-149.
33. Popescu, C.-M., M.-C. Popescu, and C. Vasile, *Structural changes in biodegraded lime wood.* Carbohydrate Polymers, 2010. **79**(2): p. 362-372.
34. Martínez, A.T., et al., *Studies on wheat lignin degradation by Pleurotus species using analytical pyrolysis.* Journal of Analytical and Applied Pyrolysis, 2001. **58-59**: p. 401-411.
35. Lu R., Y. Kamiya, and T. Miyakoshi, *Applied analysis of lacquer films based on pyrolysis-gas chromatography/mass spectrometry.* Talanta, 2006. **70**: p. 370-376.
36. Wang, Z., et al., *Fractionation and characterization of saccharides and lignin components in wood prehydrolysis liquor from dissolving pulp production.* Carbohydrate Polymers, 2015. **126**(0): p. 185-191.
37. Bardet, M. and D. Robert, *On the reactions and degradation of the lignin during steam hydrolysis of aspen wood.* Svensk Papperstidning, 1985. **88**: p. R61-R67.
38. Rahimi, A., et al., *Formic-acid-induced depolymerization of oxidized lignin to aromatics.* Nature, 2014. **515**(7526): p. 249-252.
39. Tabassum, S., et al., *Removal of chemically hazardous p-hydroxybenzoic acid during total chlorine free bleaching process of Hevea Brasiliensis.* Journal of Cleaner Production, 2012. **25**(0): p. 68-72.
40. Araújo, J.D.P., C.A. Grande, and A.E. Rodrigues, *Vanillin production from lignin oxidation in a batch reactor.* Chemical Engineering Research and Design, 2010. **88**(8): p. 1024-1032.
41. Ohra-Aho, T., M. Tenkanen, and T. Tamminen, *Direct analysis of lignin and lignin-like components from softwood kraft pulp by Py-GC/MS techniques.* Journal of Analytical and Applied Pyrolysis, 2005. **74**(1-2): p. 123-128.
42. Bertsch, P.M., & Parker, D. R. , *Aqueous polynuclear aluminum species*, in *The environmental chemistry of aluminum*, G. Sposito, Editor. 1996, CRC Press, Inc. Boca Raton, FL. p. 117-168.
43. Braovac, S. and H. Kutzke, *The presence of sulfuric acid in alum-conserved wood - Origin and consequences.* Journal of Cultural Heritage, 2012. **13**(3): p. S203–S208.
44. Baty, J., W. Minter, and S.Y. Lee, *The role of electrophilic metal ions aluminium(III) and magnesium(II) in paper degradation and deacidification.* The Book and Paper Group Annual, 2010. **29**: p. 113-120.
45. Baty, J. and M.L. Sinnott, *Efficient electrophilic catalysis of 1,5-anhydrocellobiitol hydrolysis by AlIII; implications for the conservation of "rosin-alum" sized paper.* Chemical Communications (Cambridge, United Kingdom), 2004(7): p. 866-867.
46. Fors, Y. and S. Magnus, *Sulfur and iron in shipwrecks cause conservation concerns.* Chemical Society Reviews, 2006. **35**: p. 399 - 415.
47. Sandström, M., et al., *Deterioration of the seventeenth-century warship Vasa by internal formation of sulphuric acid.* Nature 2002. **415**: p. 893-897.

48. Bokare, A.D. and W. Choi, *Review of iron-free Fenton-like systems for activating H2O2 in advanced oxidation processes.* Journal of Hazardous Materials, 2014. **275**(0): p. 121-135.
49. Schilling, J.S., *Effects of calcium-based materials and iron impurities on wood degradation by the brown rot fungus Serpula lacrymans.* Holzforschung, 2010. **64**(1): p. 93-99.
50. Almkvist, G. and I. Persson, *Analysis of acids and degradation products related to iron and sulfur in the Swedish warship Vasa.* Holzforschung, 2008. **62**(694-703).
51. Norbakhsh, S., I. Bjurhager, and G. Almkvist, *Impact of iron(II) and oxygen on degradation of oak – modeling of the Vasa wood.* Holzforschung, 2014. **68**: p. 649-655.
52. Schwanninger, M. and B. Hinterstoisser, *Klason Lignin: Modifications to Improve the Precision of the Standardized Determination.* Holzforschung, 2005. **56**(2): p. 161-166.
53. Stewart, D., et al., *Fourier-Transform Infrared and Raman Spectroscopic Study of Biochemical and Chemical Treatments of Oak Wood (Quercus rubra) and Barley (Hordeum vulgare) Straw.* Journal of Agricultural and Food Chemistry, 1995. **43**(8): p. 2219-2225.
54. Lai, Y.Z. and K.V. Sarkanen, *Isolation and Structural Studies*, in *Lignins Occurrence, Formation, Structure and Reactions*, K.V. Sarkanen and C.H. Ludwig, Editors. 1971, Wiley-Interscience: New York. p. 165-240.
55. Hutchings, J. *The properties of Alum*. in *Proceedings of the 10th ICOM Group on Wet Organic Archaeological Materials* 2007. Amsterdam: Rijksdienst voor Archeologie, Cultuurlandschap en Monumenten.
56. Braovac, S., *Alum-treated wood. Material characterization. A case study of the Oseberg find.*, in *The Royal Danish Academy of Fine Arts, Schools of Architecture, Design and Conservation.* 2015, University of Oslo.
57. Best, S.P., R.S. Armstrong, and J.K. Beattie, *Infrared metal-ligand vibrations of hexaaquametal (III) ions in alums.* Inorganic Chemistry, 1980. **19**(7): p. 1958-1961.
58. Schwanninger, M., et al., *Effects of short-time vibratory ball milling on the shape of FT-IR spectra of wood and cellulose.* Vibrational Spectroscopy, 2004. **36**: p. 23–40.
59. Pandey, K.K., *A study of chemical structure of soft and hardwood and wood polymers by FTIR spectroscopy.* Journal of Applied Polymer Science, 1999. **71**(12): p. 1097-4628.
60. Mohebby, B., *Attenuated total reflection infrared spectroscopy of white-rot decayed beech wood.* International Biodeterioration & Biodegradation, 2005. **55**: p. 247–251.
61. Silverstein, R.M., et al., *Spectrometric Identification of Organic Compounds*. 8th Edition ed. 2014: Wiley.
62. Pandey, K.K. and A.J. Pitman, *FTIR studies of the changes in wood chemistry following decay by brown-rot and white-rot fungi.* International Biodeterioration & Biodegradation, 2003. **52**(3): p. 151-160.
63. Colombini, M.P., et al., *Analytical Strategies for Characterizing Organic Paint Media Using Gas Chromatography/Mass Spectrometry.* Accounts of Chemical Research, 2010. **43**(6): p. 715-727.
64. Colombini, M.P. and F. Modugno, *Organic Materials in Art an Archeology*, in *Organi Mass Spectrometry in Art and Archeology*, M.P. Colombini and F. Modugno, Editors. 2009, Wiley: Pisa, Italy. p. 3-36.
65. Mortensen, M.N. and M. Taube. *Climate dependent degradation processes in conserved archaeological wood*. in *13th ICOM-CC Wet Organic Archaeological Materials* 2016. Florence, Italy.
66. McQueen, C., H. Kutzke, and S. Braovac. *Identification of metal compounds in alum treated wood from the Oseberg collection*. in *13th ICOM-CC Wet Organic Archaeological Materials* 2016. Florence, Italy.
67. *Encyclopaedia Britannica*, 1823, Archibald Constable: Edinburgh.
68. Thorpe, E., *A Dictionary of Applied Chemistry*, 1918, Longmans, Green and Co.: London.
69. Fengel, D. and G. Wegener, *Wood: Chemistry, Ultrastructure Reactions*. 1989, Berlin; New York: Walter de Gruyter. 613.
70. Blanchette, R.A., *A review of microbial deterioration found in archaeological wood from different environments.* International Biodeterioration & Biodegradation, 2000. **46**(3): p. 189-204.

71. Grattan, D.W., *A Practical Comparative Study of Several Treatments for Waterlogged Wood.* Studies in Conservation, 1982. **27**(3): p. 124-136.
72. Giachi, G., et al., *New trials in the consolidation of waterlogged archaeological wood with different acetone-carried products.* Journal of Archaeological Science, 2011. **38**(11): p. 2957-2967.
73. Foston, M. and A.J. Ragauskas, *Changes in the Structure of the Cellulose Fiber Wall during Dilute Acid Pretreatment in Populus Studied by ^{1}H and ^{2}H NMR.* Energy & Fuels, 2010. **24**(10): p. 5677-5685.
74. Price, C. and P. Brimblecombe, *Preventing salt damage in porous materials.* Studies in Conservation, 1994. **39** (Supplement-2): p. 90-93.